THE UNIVERSITY OF WARWICK

University of Warwick institutional repository: http://go.warwick.ac.uk/wrap

A Thesis Submitted for the Degree of PhD at the University of Warwick

http://go.warwick.ac.uk/wrap/73652

This thesis is made available online and is protected by original copyright.

Please scroll down to view the document itself.

Please refer to the repository record for this item for information to help you to cite it. Our policy information is available from the repository home page.

WAVE PROPAGATION IN NEGATIVE RESISTANCE MEDIA

A thesis submitted by

A. C. Baynham, B.Sc.

for the Degree of Doctor of Philosophy

at the University of Warwick, Coventry.

November 1971

Preface

The work described in this thesis was carried out at the Royal Radar Establishment, Malvern, between early 1969 to early 1971. Supervision during this period was shared by Professor P. N. Butcher at the University of Warwick and Dr. E. G. S. Paige at the Royal Radar Establishment.

Three papers have been published by the author upon the work described here, and a further paper is in the course of preparation. Those already published are :

Wave Propagation in Negative Differential Conductivity Media : n-Ge
A.C. Baynham, I.B.M. Jnl.Res. and Dev. 13, No.5, 568-572, (Sept.1969)

Emission of T.E.M. Waves Generated within an n-Ge Cavity
A. C. Baynham, Elect.Lett. 6, No.10, (4 May 1970)

A New Mode of Microwave Emission from GaAs
A. C. Baynham, D. J. Colliver, Elect. Lett. 6, No.16 (6 August 1970)

The latter paper is the only article published or to be published with a joint authorship. Mr. Colliver's contribution to the work described in that paper was a valuable assistance in fabrication of alloy contacts upon GaAs. The remaining work described here is also original with the exception of that reviewed in Section 1 and those portions in subsequent sections where acknowledgments to other workers are specifically included.

The author would like to thank both Professor Butcher and Dr. Paige for their constant interest and numerous helpful discussions. He would also like to thank the Ministry of Technology for their financial support during the course of this work, and Mrs. Bartlett for her careful typing of the thesis.

Published by kind permission of the Controller, H. M. S. O.

ABSTRACT

Wave Propagation in Negative Resistance Media

When an electromagnetic wave enters a medium having an effective negative resistance, it may be expected to grow spatially. The conditions under which such growth may be observed are examined, and an experimental regime chosen where it should be possible to observe these effects. Such observations can throw light not only upon the negative resistance travelling wave amplification process, but also upon the transport process giving rise to the host negative resistance. The experimental work is therefore divided between a study of a new negative differential conductivity process recently discovered in n-Ge and a study of the negative resistance travelling wave amplification process in GaAs.

The diagnostic measurements upon n-Ge provide new data relating to the negative resistance process in that material; data such as the maximum negative slope mobility of 300 $cm^2/V.sec.$ at $77^{\circ}K$ ($E \,//\, <100>$) the threshold electric field for N.D.C. of 2.95 KV/cm. ($E \,//\, <100>$), and the ceiling frequency of 5 GHz beyond which N.D.C. dissappears, all of which have been subsequently corroberated by other workers.

Observations of the emission spectrum from GaAs, when the amplified electromagnetic wave begins to experience round trip gain within the specimen cavity, have allowed some fairly detailed discussion to be undertaken concerning the nature of the emission process, which rely upon careful measurements of the spectral power and line width. Although the maximum pulse power observed of 4 mW is low, such observations of emission do provide a new mechanism by which microwave power may be extracted from a suitably biased material having a negative differential conductivity.

Finally, attention is directed towards some potentially profitable areas for future work.

Index

1. HISTORICAL SURVEY : The Concept of Wave Propagation in Negative Resistance Media, and a Description of Suitable Media

In this section both the background information and the direction of thought which has stimulated the present work is reviewed. During the course of this discussion we range over three fields of work which are, at first sight, only linked by the loosest of bonds. These are : firstly, the quest for a solid state analogue of the travelling wave tube; secondly, the relevant portion of a huge body of work upon the strong negative differential conductivity existing in Ga-As; finally, we review the microwave emission from n-Ge which was discovered at about the time of the commencement of this work.

1.1 The Quest for Solid State Travelling Wave Amplification

For a number of years now there has been a preoccupation amongst many workers with the hope that it might fall to them to discover the high frequency solid state amplifier which would finally replace the travelling wave tube (TWT). Not unnaturally, most of the thinking has been along the lines of a direct analogue to the TWT. Attention has been focused upon semiconductors because of the high electron drift velocities which can be achieved whilst maintaining the accompanying power dissipation within acceptable bounds. The host of waves known to propagate in semiconductors have each, it would seem, been subjected to high electric fields in the search for amplification. Helicon waves,[1] Alfven waves[2], helical waves[3], space charge[4] and dipolar space charge waves[5], spin waves[6], acoustic[7] and optic phonons[8], have all been studied during this search. Success has however been minimal; the only real success being with the acoustic amplifier, and even here upper frequency limits are so low that transistor amplifiers still offer superior performance.

In some cases the reason for this lack of success can be hinted at. Most of the drift/wave interactions have a gain threshold which is determined by the relative magnitude of the electron drift velocity and the phase velocity of the wave as in the TWT. However many of the waves cited (plasma waves in particular) accelerate in the presence of a biasing electric field. Consequently any attempt to achieve synchronism between drifting electrons and an accompanying wave may be unexpectedly difficult, necessitating very high power dissipation within the semiconductor sample. Even if, at this stage, synchronism is achieved, the free carriers have usually entered the hot electron regime, and the

VELOCITY FIELD DIAGRAM FOR NEGATIVE CONDUCTIVITY (UPPER) AND NEGATIVE DIFFERENTIAL CONDUCTIVITY (LOWER) MEDIA

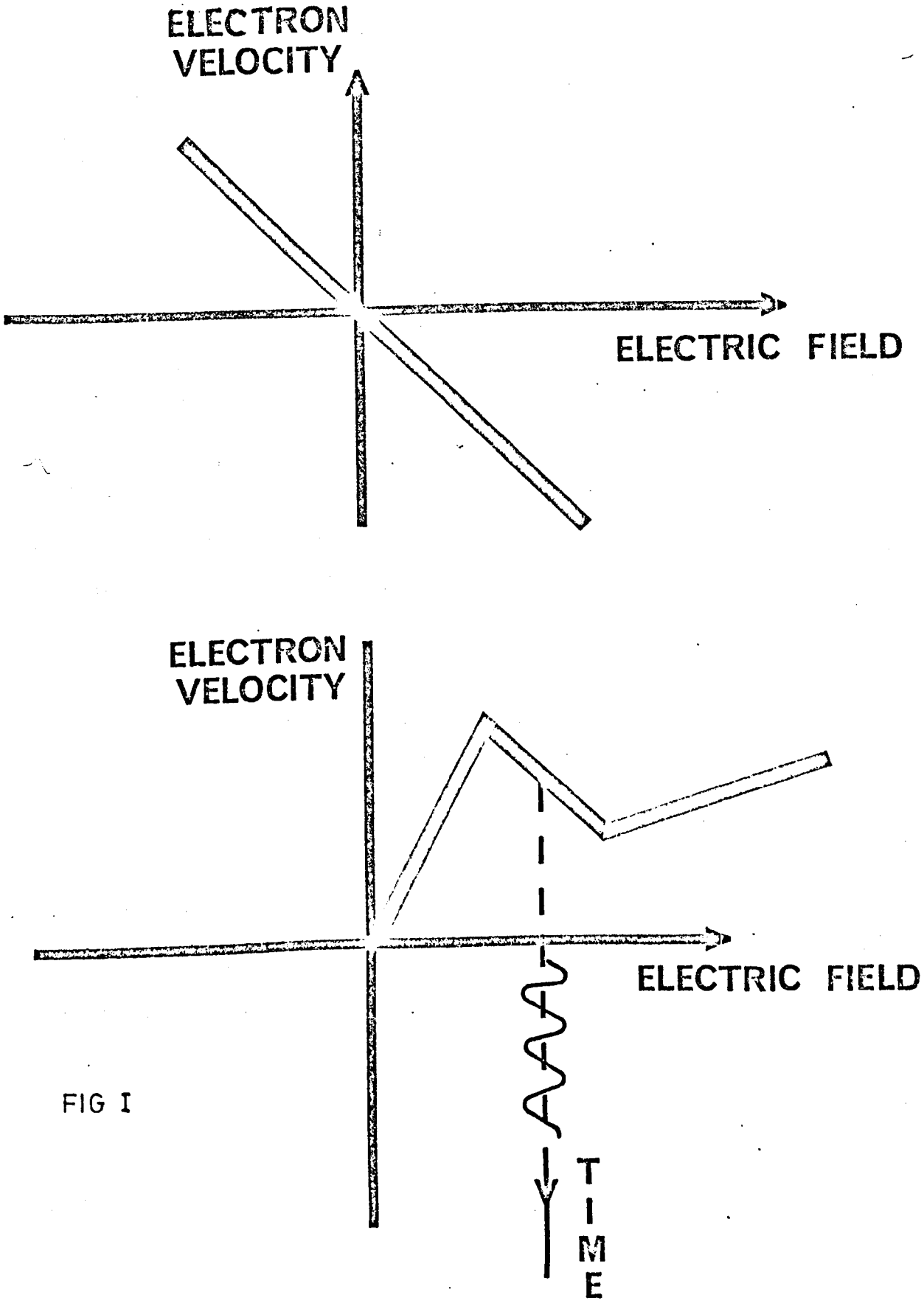

FIG I

simple cold electron model, so often employed in this work, is invalid.

It was within this context of dissillusionment with synchronous instability that the present work commenced. One was forced to ask if an alternative class of instability could be conceived of, and immediately the possibility of wave propagation in a negative resistance medium was introduced. It is this intuitively obvious amplification mechanism with which we shall be concerned here. A fundamental difficulty is, of course, encountered when a suitable total negative resistance medium is sought. (See upper diagram in Figure 1). So far as the present author is aware, the only such mechanism, proposed by Stocker[9], has only recently been demonstrated experimentally[9a]. However, a number of materials are now known which exhibit negative <u>differential</u> conductivity. (Lower diagram in Figure 1). It was therefore proposed that one of these materials be biased into their region of negative differential conductivity, when an incident wave will behave as if entering a material having a total negative conductivity. (This statement is examined in detail in Section 2). The lower portion of Figure 1 shows schematically how a suitably polarised oscillating field may be viewed as superimposed upon the biasing field.

Similar lines of thought have been pursued by other workers. For example, Midford and Bowers[10] have launched a transverse electromagnetic wave through a silicon Impatt device, and Robinson and Kino[11] have launched space charge waves in a Gunn device which was stable against domain formation. Each of these sets of workers have achieved gain, and the space charge wave amplifier has now been studied extensively[12,13,14].

The present work has followed an intermediate path, focussing attention upon the propagation of a transverse electric wave within two

USED ON
APP'D 4. < 2 system
TRACED J.PITCHFORD
R.R.E.
ISSUE 1. 20·9·71

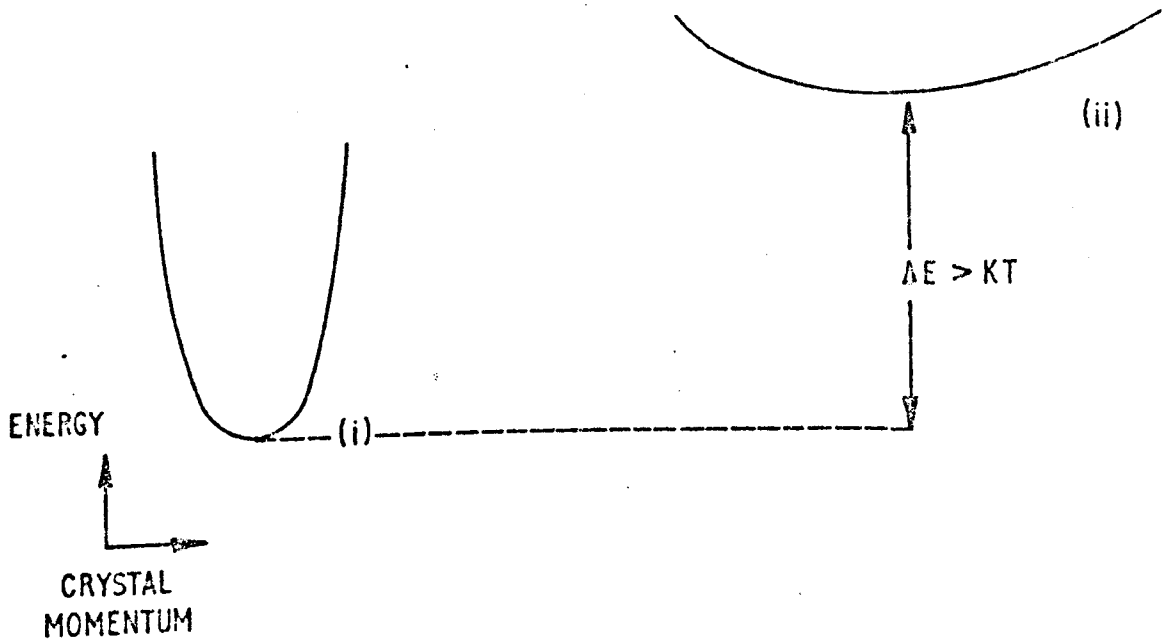

FIG. 2a
CONDUCTION BAND ENERGY MINIMA

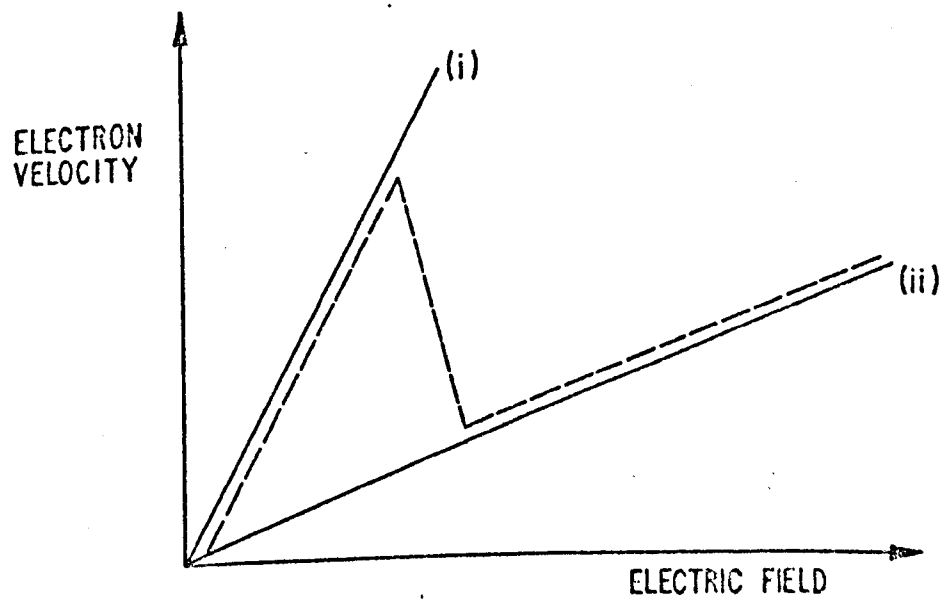

FIG. 2b
ELECTRON VELOCITY – FIELD CURVES CHARACTERISTIC OF ELECTRON IN MINIMA (i) AND (ii) TOGETHER WITH A DOTTED COMPOSITE CHARATERISTIC

different materials (n-Ge and GaAs) which both exhibit a negative differential conductivity. It is shown in subsequent sections that wave amplification can be obtained in both materials. In addition oscillation is demonstrated under suitable feed-back conditions, and it is shown that the propagating transverse electromagnetic wave may be employed as a diagnostic tool with which to study the negative differential conductivity phenomenon.

1.2 Negative Differential Conductivity in Gallium Arsenide

In 1961 Ridley and Watkins[15] first discussed the possibility of negative resistance effects occurring in semiconductors. The thoughts of these two authors together with those of Hilsum[16] concerning the application of such effects laid the foundation for observations of microwave emission to be made by Gunn[17] a few years later.

The proposed negative resistance mechanism was based upon a combination of features of the electronic energy band structure which can occur in semiconducting materials. Attention was focused upon the details of the behaviour of electrons in a material having a light mass conduction band edge and close to it, but a little higher in energy, a heavy mass minimum ((ii) in Figure 2A). Electrons in the lower light mass minimum ((i) in Figure 2A), are then expected to exhibit a large mobility in comparison to any in the upper heavy mass minimum. However, the energy separation of the lower and the upper minima ($\Delta\mathcal{E}$) is to be such that at room temperature there are few if any electrons in the upper minimum. Thus at room temperature the observed velocity field curve is expected to be characterised by electrons exclusively confined to the band edge (Figure 2B).

As the applied electric field is increased, the light electrons gain energy rapidly from the electric field owing to their high mobility,

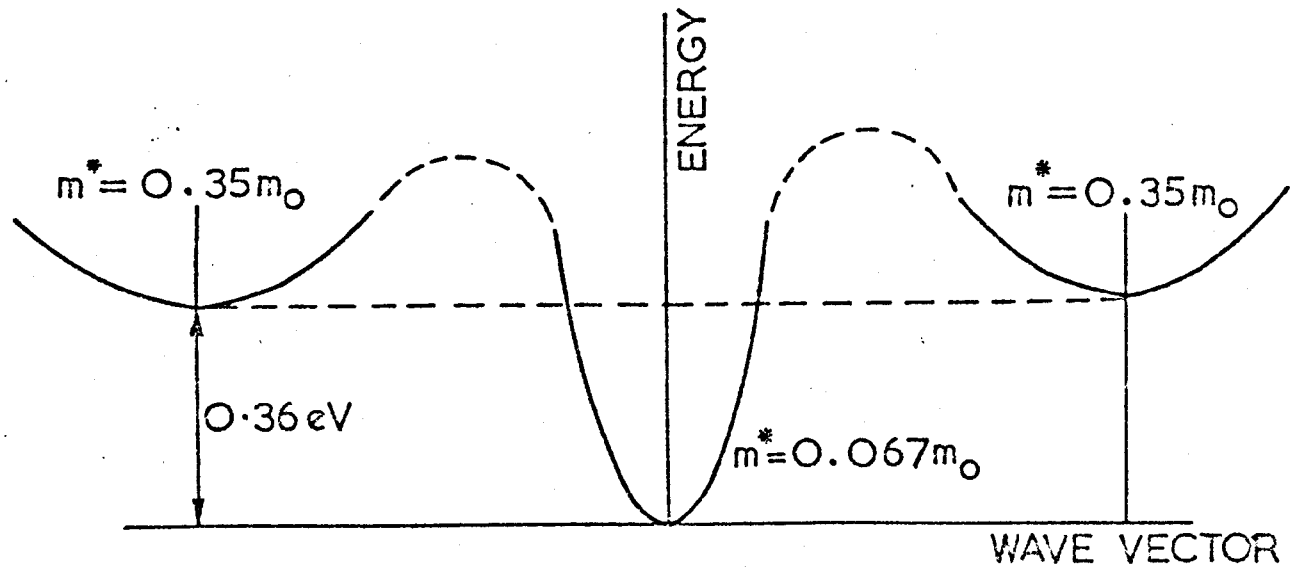

GALLIUM ARSENIDE CONDUCTION BAND

FIG 3

(energy/carrier/ sec = μE^2) and at quite modest electric fields it is possible for the electrons to assume a very high mean energy. (1500°K)[18] so that, although $\Delta \mathcal{E} >> kT$, the electrons may never-the-less begin to transfer to the upper minimum. Let us assume that at some defined field strength a catastrophic total electron transfer occurs. Then the observed external velocity field curve must change from that characteristic of the light mass minimum ((i) in Figure 2B) to one characteristic of the heavy mass minimum ((ii) in Figure 2B). The average velocity-field characteristic resulting from such a transfer is shown dotted in Figure 2B and is seen to demand a reduction in current density and therefore a region of finite negative differential conductivity (NDC) beyond a threshold field E_T. This, then,is the immediate intuitive explanation of the negative differential conductivity to be exploited here, and is seen to be based upon a non-equivalent intervalley scattering mechanism; the transferred electron mechanism.

Gallium Arsenide is one of a number of materials* which may be expected to have a suitable conduction band structure for observation of the Ridley-Watkins-Hilsum negative differential resistance. As shown in Figure 3, at the centre of the Brillouin zone we encounter the band edge with a small effective mass of 0.067 m_o[19] where m_o is the free electron mass. At the edges of the Brillouin zone in the <100> direction there are three further conduction band minima, about 0.35 eV [20] above the conduction band edge. These are thought to have a mass of 0.35 m_o by

---

* Other materials in which the Gunn effect has been observed are InSb[22a] InP [22], CdTe [23], GaAsP [24] alloys and InAs under sufficient uniaxial strain to prevent impact ionisation[25]. In the case of InP it is now proposed that the mechanism is in fact a "three level" variant upon the Gunn effect[26]. Never-the-less it remains an electron transfer phenomenon.

comparison with GaP which is a similar material but has the (100) minima at the band edge where they may be readily studied.

When Gunn first observed[17] microwave emission from GaAs it was not immediately attributed to the transferred electron mechanism. However, there is now no doubt that Gunn's observations are due to the Ridley-Watkins-Hilsum mechanism. Overwhelming justification for this identification are for example, in the variations of the threshold field with strain, temperature and alloying, and the class of materials from which precisely similar emission[18] is to be observed.

1.2.1 The Electronic Transport Process

Rather than follow further the historical development of the transferred electron mechanism we set out a more detailed account of the relevant principles which underly it. We begin by describing the transport process giving rise to the instability.

It is common to write the drift velocity (v) in terms of an average over the contributions from various valleys, thus

$$v(E) = \frac{E}{n} \sum_i n_i(E)\mu_i(E)$$

where μ_i is the mobility in the i^{th} valley containing n_i free electrons, and E is the applied electric field intensity.

It is the behaviour of the electron system within the i^{th} valley which fixes $\mu_i = v_i/E$. Their behaviour is summarized by the Boltzmann equation. In a multi-valley system this is conveniently written as

$$\frac{\partial f_i(k)}{\partial t} = \left(\frac{\partial f_i(k)}{\partial t}\right)_E + \left(\frac{\partial f_i(k)}{\partial t}\right)_{Scatt_{ii}} + \left(\frac{\partial f_i(k)}{\partial t}\right)_{Scatt_{ij}}$$

$$= \frac{e}{\hbar} \underset{\sim}{E} \cdot \nabla_k f_i(\underset{\sim}{k}) + \left(\frac{\partial f_i(k)}{\partial t}\right)_{Scatt_{ii}} + \left(\frac{\partial f_i(k)}{\partial t}\right)_{Scatt_{ij}}$$

where $f(\underline{k})$ is the electron distribution function in valley i, $\underline{k}$ being the electron wave vector. The second and third terms here describe the effects of intra-valley and intervalley scattering events respectively, and these remain to be described. We consider scattering by phonons first of all. The contribution to $\frac{\partial f_i(k)}{\partial t}$ due to electron scattering from a state at k to states at all k' for which $\underline{k} - \underline{k}'$ is equal to the phonon wave-vector is

$$\frac{\partial f_i(k)}{\partial t} = -\frac{2\pi}{\hbar} \sum_{k'} f(\underline{k}) (1 - f(\underline{k}') B(\underline{k},\underline{k}') N \delta(\epsilon(k') - \epsilon(\underline{k}) - \hbar\omega(\underline{k} - \underline{k}'))$$

$$+ \frac{2\pi}{\hbar} \sum_{k'} f(\underline{k}') (1 - f(\underline{k}) B(\underline{k}, \underline{k}') (N + 1) \delta(\epsilon(\underline{k}') - \epsilon(\underline{k}) - \hbar\omega(\underline{k} - \underline{k}'))$$

$$- \frac{2\pi}{\hbar} \sum_{k'} f(\underline{k}) (1 - f(\underline{k}')) B(\underline{k},\underline{k}') (N + 1) \delta(\epsilon(\underline{k}) - \epsilon(\underline{k}') - \hbar\omega(\underline{k} - \underline{k}'))$$

$$+ \frac{2\pi}{\hbar} \sum_{k'} f(\underline{k}') (1 - f(\underline{k})) B(\underline{k}, \underline{k}') N \delta(\epsilon(\underline{k}) - \epsilon(\underline{k}') - \hbar\omega(\underline{k} - \underline{k}'))$$

In these expressions $f(\underline{k})$ the electron distribution function is normalised so that $\int f_i(\underline{k})\, d\underline{k} = n_i$, number of electrons per unit volume of the crystal in the i^{th} valley. $B(\underline{k}, \underline{k}')$ is a parameter which specifies the strength of scattering between the states at k and k'. The first term on the right hand side describes electron transfer to a higher energy state by absorption of a phonon, the second describes electron transfer from a higher energy state by stimulated and spontaneous phonon emission, the third describes electron transfer to a lower energy state by stimulated and

spontaneous phonon emission and the fourth describes electron transfer from a lower energy state by absorption.

The expression can be approximated to

$$\left[\frac{\partial f_i(k)}{\partial t}\right] = \frac{2\pi}{\hbar}\sum_{k'} B(\underline{k}, \underline{k}') \left[\left\{ f(k')\,(N+1) - f(\underline{k})\,N \right\} \delta\left(\epsilon(\underline{k}') - \epsilon(\underline{k}) - \hbar\omega(\underline{k} - \underline{k}')\right) + \left\{ f(\underline{k}')\,N - f(\underline{k})\,(N+1) \right\} \delta\left(\epsilon(\underline{k}) - \epsilon(\underline{k}') - \hbar\omega(\underline{k} - \underline{k}')\right)\right]$$

In the case of inter-valley scattering all states k' lie in a valley which is not equivalent to the one in which the state k is found, whilst in the case of intra-valley scattering k and k' lie in the same valley.

Intra-valley scattering is dominated in pure material by polar optic modes at low fields[27] and by acoustic phonons at higher fields, the polar mode scattering having become weak owing to the large $(\underline{k} - \underline{k}')$ range of $\underline{k}$ vectors now encountered. Phonons which may provide $\underline{k}$ conservation in intra-valley scattering processes are of course those lying near the centre of the Brillouin zone where the optical mode energy is approximately independent of the $\underline{k}$ vector and $B_{ii}(\underline{k}\,\underline{k}')$ is known in this approximation[21]. Similarly the scattering term for acoustic phonon scattering is known under simplifying assumptions of isotropic valleys[28].

Inter-valley scattering can be neglected at low fields, the intra-valley scattering within the central minimum being dominant. At higher fields it becomes important, of necessity. The phonon

involved in this process is determined by the symmetry of the initial and final states[27a]. If the satellite minima are at the edge of the zone (as is believed to be the case) then the L.O. phonon is involved, whilst, if the satellite valleys lie within the Brillouin Zone both L.O. and L.A. phonon may participate in the scattering. A similar symmetry argument is involved in determining the dominant equivalent intervalley scattering process. Ionised impurity scattering is weak for inter-valley scattering where the change of k vector is large but may be important for intra-valley scattering. It is however commonly neglected unless the material is exceptionally impure.

Once the various scattering terms are known, it remains to solve the Boltzmann equation in the steady state situation where $(\partial f/\partial t) = 0$. It is at this point that the problem becomes really difficult. The most common simplifying assumption has been that electron-electron scattering is dominant, establishing a displaced Maxwellian distribution function[29]. One then simply solves the equations for the parameters of the distribution function. More recently it has become possible to carry out exact numerical solutions of the Boltzmann equation by the Monte Carlo technique[30]. Here the path of a single electron is followed through k space over many scattering events. By careful "book keeping" of the time spent in each elemental volume of k space, the electron distribution function and thence the mean electron velocity is thus obtained.

Suffice it to say, that it is possible to obtain the electron distribution function, and the electron drift velocity as a function of electric field strength, by a number of methods. Such calculations have provided a variety of results. The most recent

COMPARISON OF EXPERIMENTAL AND THEORETICAL VELOCITY FIELD CURVES
FOR GaAs AT 300°K

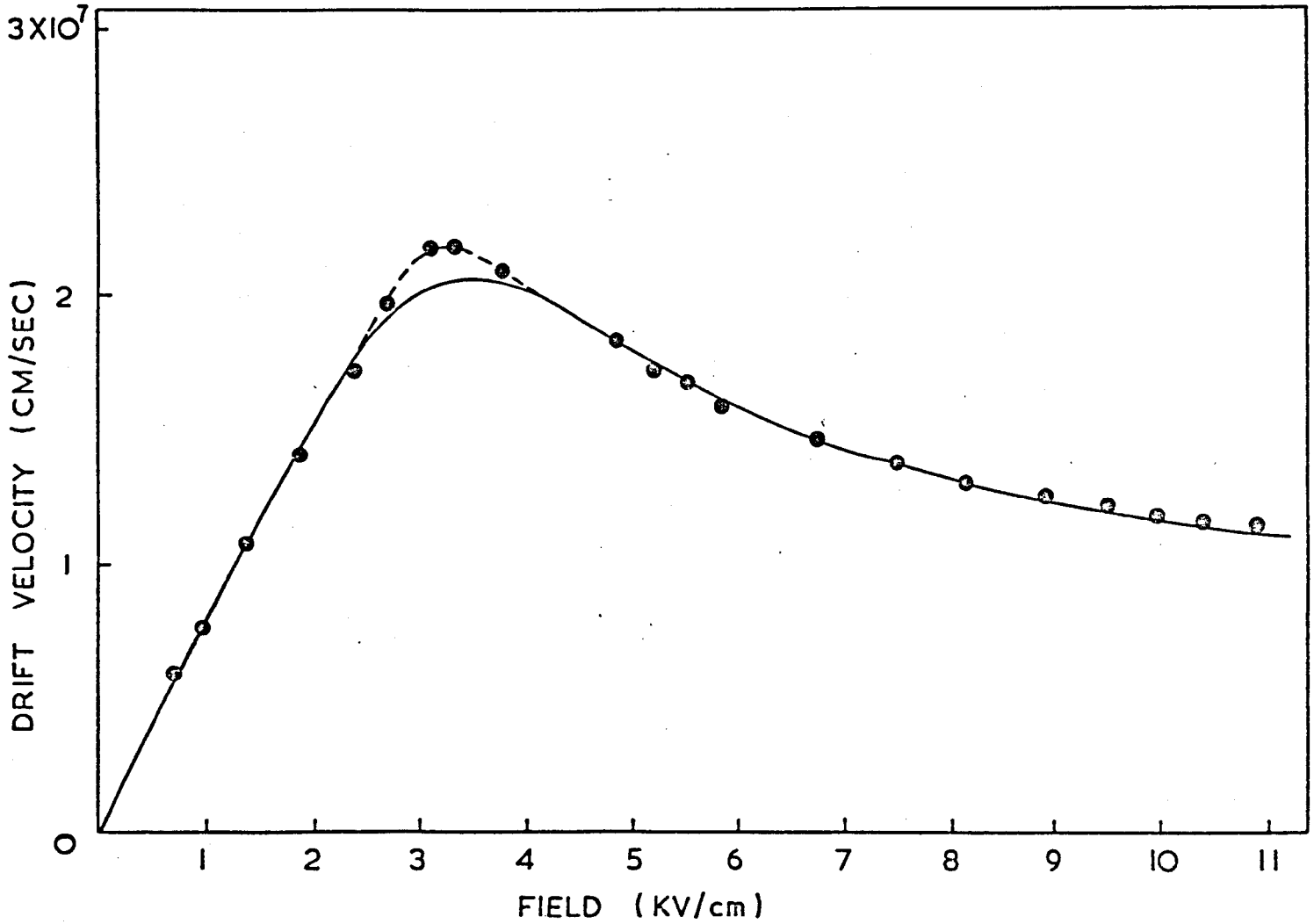

FIG 4

is that of Fawcett et al[31] which bears a close similarity to the experimentally determined velocity field curve as shown in Figure 4. The experimental results shown in Figure 4 were obtained by a time of flight technique[32]. This requires very high resistivity material. (10^6 - 10^8 Ω cm). The negative specimen contact was of gold but separated from the specimen by a thin film of SiO, whilst the anode was a straight forward N+ tin contact. A short pulse of electrons ejected by an electron beam at the cathode was then timed as it travelled to the anode under various biasing electric field intensities. In this way the electron velocity was obtained as a function of electric field intensity. These results are probably more reliable than those of a variety of other workers owing to their freedom from interpretative problems. For example, Gunn and Elliott[33] have made a measurement of sample impedance in a time short compared with the dielectric relaxation time. One is however, concerned to know the response of the highly conducting contact region in such an experiment. Furthermore, if the theoretical estimates of the negative mobility are correct the measurement was already too slow by a factor of ten. Thus it is not surprising that this measurement provided a low apparent negative slope mobility.

In conclusion then, theoretical estimates of the static velocity field characteristics have been made which have, by and large, a common starting point, but differ in the means adopted for elucidating a final solution. Experimental work, on the other hand, has also been performed which furnishes information concerning this vital N.D.C. characteristic. The best results of the two disciplines, theoretical and experimental, are seen to be in good agreement.

1.2.2 The Macroscopic Consequences of N.D.C.

Our objective in this section is to review contemporary understanding of the macroscopic behaviour of a specimen which has the microscopic differential conductivity discussed in the previous section.

a) Spatial Non Uniformity in Stable Specimens

In one dimension Poisson's equation gives

$$\frac{\partial E}{\partial x} = \frac{\rho}{\epsilon_L} = \frac{(n - n_o)e}{\epsilon_L} \qquad \ldots (1)$$

for n type material. Here n is the local free electron concentration, e the electronic charge, ϵ_L the lattice dielectric constant, and n_o is the density of ionized donors.

Looking for a time-independent solution we obtain from the current continuity equation, $\partial J/\partial x = 0$, the result

$$J = nev(E) = \text{constant} \qquad \ldots (2)$$

Now, clearly, if at all points $n = n_o$ in equation (1), n, E, μ and consequently J all become spatially independent to satisfy equation (2). However, we know that at the contact the field is considerably below its value in the centre of the specimen. Thus it emerges that, because of the contacts, n cannot equal n_o at all points in the specimen and that the boundary conditions therefore play a vital role in determining the behaviour of any specimen. This was pointed out long ago by Shockley[34] and has been emphasised more recently by Kroemer[35].

We discuss first of all a sample biased so that at all points within the specimen $E < E_T$. Let us consider a point "A" (Figure 5a) immediately inside the cathode where the electric field

ISSUE 1. 20·9·71 | R.R.E. | TRACED J.PITCHFORD | APP'D. A. C. Bowsham | USED ON

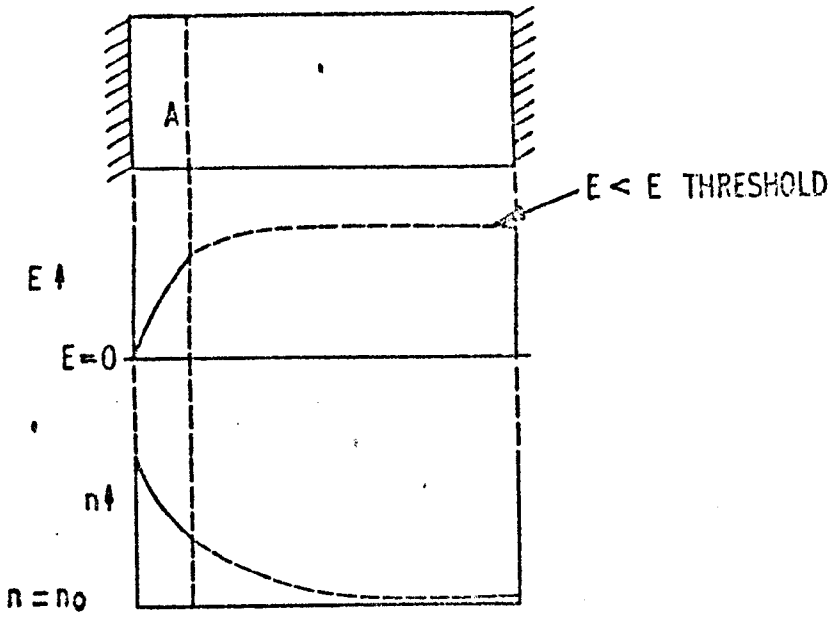

FIG. 5a
ELECTRIC FIELD AND FREE CARRIER DISTRIBUTIONS IN A SAMPLE BIASED BELOW THRESHOLD

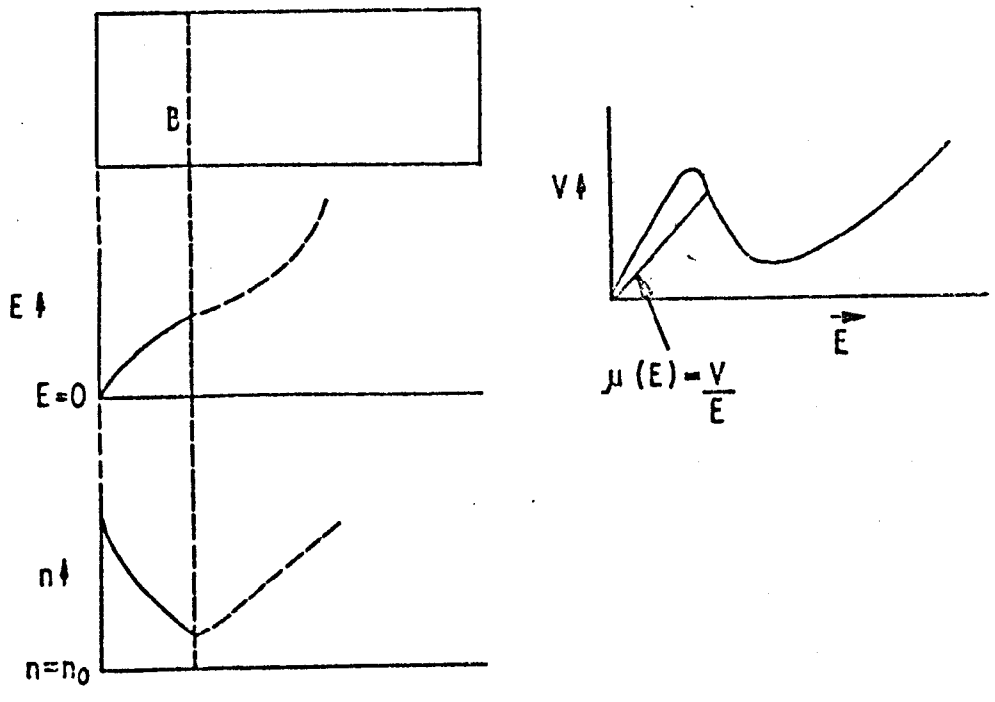

FIG. 5b
ELECTRIC FIELD AND FREE CARRIER DISTRIBUTIONS IN A SAMPLE BIASED BEYOND THRESHOLD FOR N.D.C.

is still increasing in intensity away from the cathode. At this point $\frac{dE}{dx}$ in + ve , and thus from equation (1) $n > n_o$. In equation (2) we see that this is an acceptable solution.

Substituting (1) into (2) we see that

$$J = \left(\epsilon_L \frac{\partial E}{\partial x} + n_o e\right) v(E) \qquad \ldots (3)$$

Thus as E increases with distance from the cathode, $\frac{dE}{dx}$ decreases, and the system rapidly tends to a spatial uniform field distribution with $E = E_J < E_T$, where E_J is determined by $J = n_o e V(E_J)$.

We turn our attention now to a sample biased so that a part of the specimen has a field in excess of the threshold field E_T . Consider a point "B" (Figure 5b) where $E > E_T$. Here the field, we suppose, is still increasing spatially towards the mean applied field, for it remains necessary that

$$\int \underline{E} \cdot \underline{dx} = \text{Total Applied Voltage} .$$

However, in this case, increase of E necessarily now produces a falling V(E), and the tendency to equilibrium with $\frac{dE}{dx} \rightarrow o$ is no longer found. In order that J remain constant n must rise indicating, with the aid of equation (1), not a tendency to a uniform field distribution, but a "run away" situation, in which the field increases ever more rapidly spatially. This system is only brought under control when the field enters a positive slope resistance region of the velocity field characteristic at even higher electric field strengths.

This discussion has shown that a stable electric field distribution within a sample having a N.D.C. cannot be of the familiar uniform nature with a droop at each contact; this is only found in positive conductivity media. McCumber and Chynoweth[36]

and Mahrous and Robson[37] have both calculated the spatial field distribution. Both of these authors neglect diffusion and the first authors verify it to be unimportant to the conclusion. At a later stage in this work (See Section 3.2.2), it will be necessary to pursue this calculation for both GaAs and n-Ge in order to evaluate the spatial distribution of the free carrier concentration within the specimen; neither of the foregoing authors having evaluated this term.

b) The Development of Instability

In the foregoing discussion a time-independent solution of the current continuity equation was specifically sought. However, this steady-state distribution will be unstable if a small space charge fluctuation, generated either by noise within the specimen or switching transients outside the specimen grows in time. A number of estimates of the "amount of negative resistance" which can be tolerated whilst retaining stability have been made. Perhaps the most attractive is that of McCumber and Chynoweth[36]. These authors calculate the sample impedance using the foregoing equations and find the system unstable if

i) There is a negative resistance region within the sample i.e. the dielectric relaxation time at the biasing field is negative and

ii) The product of the free carrier concentration N and sample length L exceeds a critical value $(NL \geqslant C_{osc})$.

The critical N L product which defines the threshold of temporal instability is now well confirmed by experiment[18], though empirical values of the product tend to be somewhat larger than theory would suggest.

A further rather interesting aspect of the approach adopted by McCumber and Chynoweth[36] is related to a stable sample's

ISSUE 1. 20·9·71 | R.R.E. | TRACED J.PITCHFORD | APP'D. A.C. Bingham | USED ON

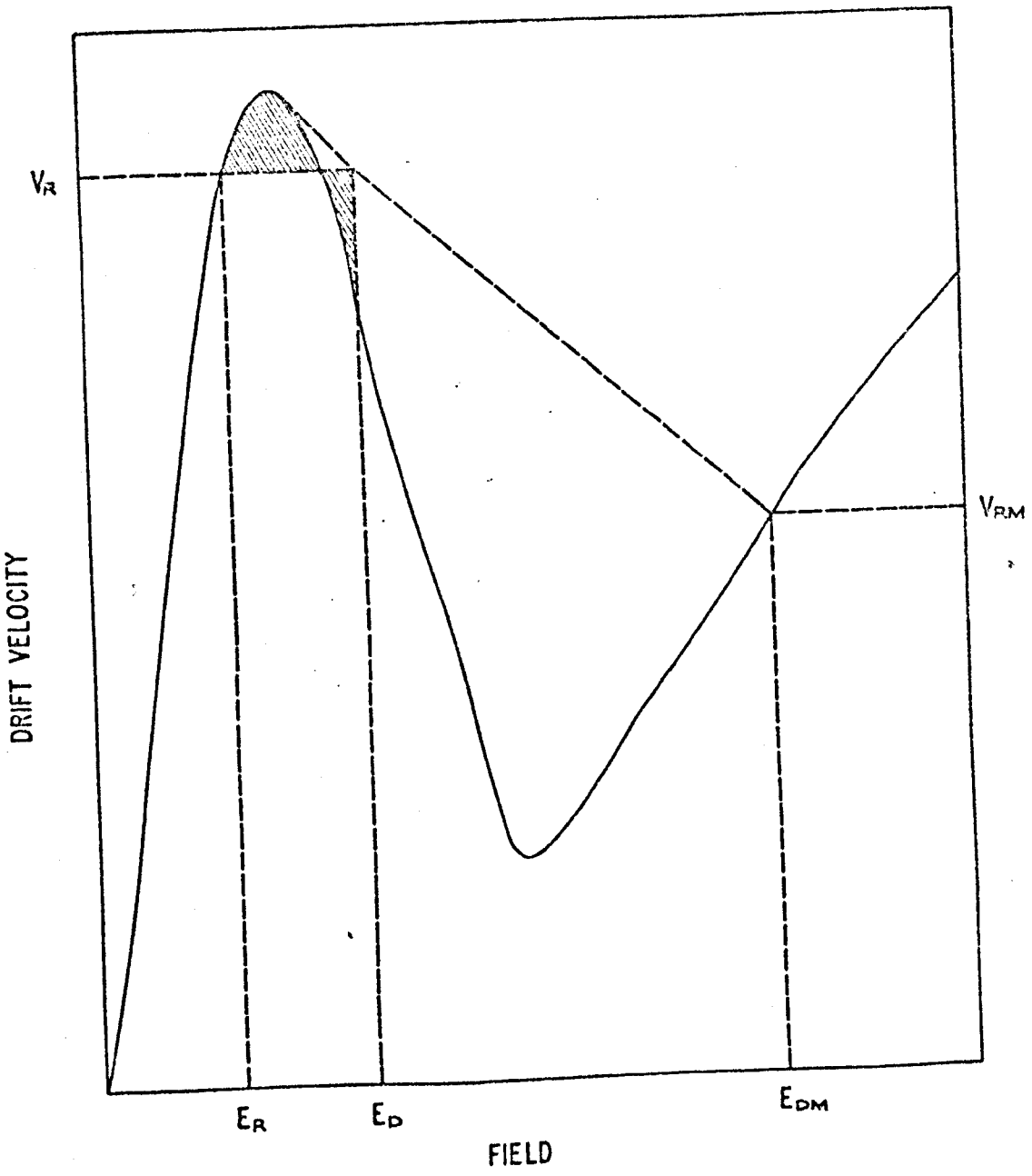

FIG. 6
CONSTRUCTION OF THE DYNAMIC CHARACTERISTIC FOR STABLE DOMAINS

terminal impedance. They find that a stable sample, may exhibit terminal negative differential resistance over a small range of frequencies centred upon the inverse of the electron transit time through the sample. This fact has been exploited by Thim[43] in making a low N L product amplifier.

c) Large Signal Instability

In unstable samples space charge fluctuations grow up from noise to assume a characteristic large-signal form. Ridley[38], who first proposed that the final form is a travelling high-field domain, and Kroemer[39] have both contributed greatly to the development of our understanding of domains. We confine our attention, however, to the final picture which has emerged.

The problem is once again one of solving Poisson's equation together with the current continuity equation. Since the objective is to find the large signal stable solution of these equations we look for a solution in which the profile of Ridley's domain is constant during propagation i.e. such that the high field and the accompanying space charge profiles are functions only of $(x - v_o t) = y$. A suitable change of variable in the two starting equations then allows the new variable y to be eliminated yielding a differential equation relating the field and free carrier concentration. This equation has been solved by Butcher[40] under the assumption of a field-independent diffusion constant. It emerges that the velocity of the domain must equal the velocity of the electrons outside the domain, and that the peak domain field is defined by a simple geometrical construction illustrated in Figure 6. The two shaded areas have to be equal in order that an integral appearing in Butcher's solution should vanish as required.

ISSUE 1. 17·9·71 | R.R.E. | TRACED J.PITCHFORD | APP'D. | USED ON

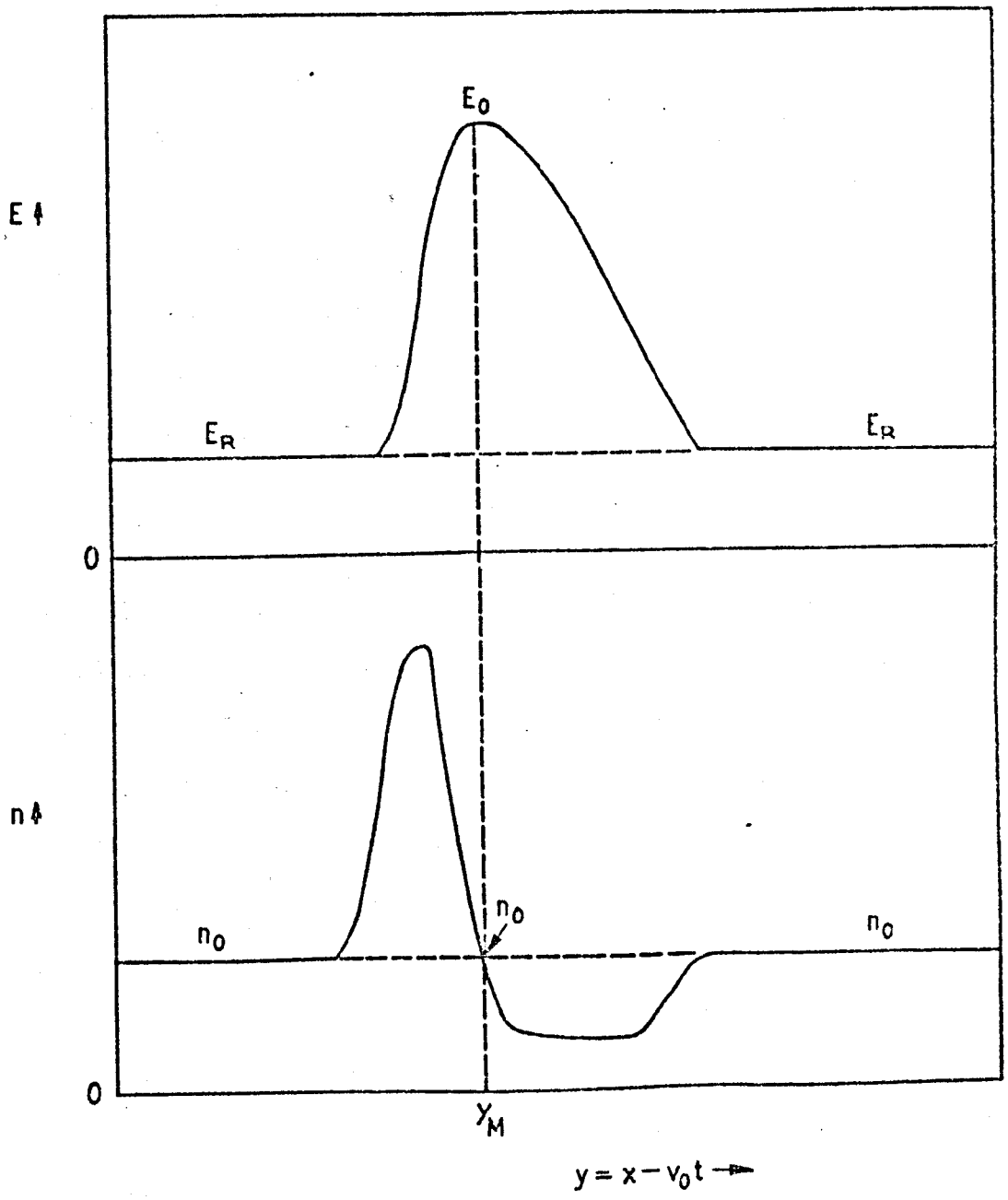

FIG. 7
STABLE DOMAIN PROFILE

This latter condition clearly defines a "dynamic" characteristic of peak domain field versus drift velocity, which is shown dotted in Figure 6.

The picture which we have of the stable domain is therefore of a high field region propagating through a specimen at the same velocity as the electron system at each side of it. Its peak field is defined in relation to the electron drift velocity and field outside the domain. The profile of the domain is shown in Figure 7. Poisson's equation clearly demands that the accompanying space charge modulation should be of the form shown which is the origin of the common terminology: "dipole" domain.

Domains which approximate to this shape have been seen by Gunn[41] and Heeks[42] using minature capacitative probe techniques. Less direct evidence of the existence of domains is of course to be found in the very existence of the transit mode of operation of unstable samples. In this mode of operation a "spikey" current wave form is observed under conditions of constant voltage supply, these spikes corresponding to initiation and collapse of domains at cathode and anode. The separation of the spikes is very closely related to the length of the specimen indicating a transit effect.

We include one further consequence of domain propagation. It will be noticed from figure six that when the current through a specimen biased beyond threshold is increased, the domain field falls. Detailed calculations show that the domain potential also falls, when the specimen current is increased, and that this effect can be stronger than the positive resistance effect of the remainder of the specimen yielding a terminal negative resistance[21]. The ensuing broad-band negative resistance has been exploited by Thim[43] as the basis for an amplifier. In that work the Gunn sample was however a local negative resistance circuit element unlike the work to be described here at a later stage.

1.3 N.D.C. in n - Ge

In this section we describe those features of the N.D.C. of n - Ge which were known at the time of the commencement of this work. Since that time some further publications[52, 53] have appeared which include those of the present author. Discussion of this later work is postponed until the final sections of Chapters 3 and 4 in order that the contemporary work may be treated in context.

The first observations of current instabilities in n - Ge were made by McGroddy and Nathan[44]. These authors found instability under the following experimental conditions

a) Lattice temperature below 150K.

b) Electric field parallel <100> or <110> in the zero stress regime.

In the <110> orientation it was possible to change the threshold field by applying a uniaxial stress also in the <110> direction. Oscillation frequencies ranged from a few hundred MHz to 2.8 GHz, and were characterised by a threshold NL product for oscillation of 2×10^{13} cm^{-2}. Subsequent work by McGroddy has shown that the N.L. product is "Well in excess of $2 - 10^{13}$ cm^{-2} " (Private communication).

In seeking the source of these instabilities, Elliott et al[45] conducted a series of fast pulse and potential probing experiments. The fast pulse experiments were designed to make an observation of the sample current and applied voltage before the electric field non-uniformity and associated space charge was able to establish itself; that is before a dielectric relaxation time had elapsed. They revealed a terminal N type negative differential resistance, at 27°K and 77°K for electric fields in excess of 3 KV/cm, and parallel to a <100> crystalographic axis. However, owing to limited response of the circuitry employed, this data cannot be regarded as a quantitative measurement of the electric field dependence

of the electron drift velocity*. Thus, this measurement establishes the existence of N.D.C., with a threshold electric field strength of 3 KV/cm, but does not yield the value of the negative slope mobility.

Probing experiments[45], were used to study the spatial field distribution within the sample as a function of time. These indicated the existence of dipole domains at 27°K which nucleated near to the cathode and propagated at a velocity of $1.3 - 10^7$ cm sec^{-1} towards the anode. This observation is also consistent with the existence of a bulk N.D.C. in n - Ge at 27°K. (electric field parallel $<100>$) though of unknown origin or magnitude. Measurements of the velocity field characteristic in n - Ge were made by Chang and Ruch[46] using the "time of flight technique"[47]. In this method the response of a reverse biased Schottky barrier/intrinsic/n - Ge structure to a 0.1×10^{-9} sec pulse is studied as a function of time. The pulse introduces a sheet of electrons within the intrinsic layer and as this traverses it, a terminal current flow is observed. The duration of this current pulse is a measure of the electron drift velocity within the intrinsic layer. Knowing the field strength within the I layer, the velocity field relationship is thus obtained.

An N - type N.D.C. was observed for lattice temperatures between 33°K and 130°K and for current flow in the $<100>$ direction in the crystal. At 33°K a slope mobility of 300 $cm^2/V.sec$ was evaluated with a threshold field of 1.5 KV/cm, in contrast to the threshold of 3 KV/cm observed by

---

* A similar experiment was performed in Gallium Arsenide by Gunn and Elliott[45a]. They found a velocity field characteristic which is at considerable variance with more recent work of, for example, Ruch and Kino[45b].

BAND STRUCTURE OF N-Ge

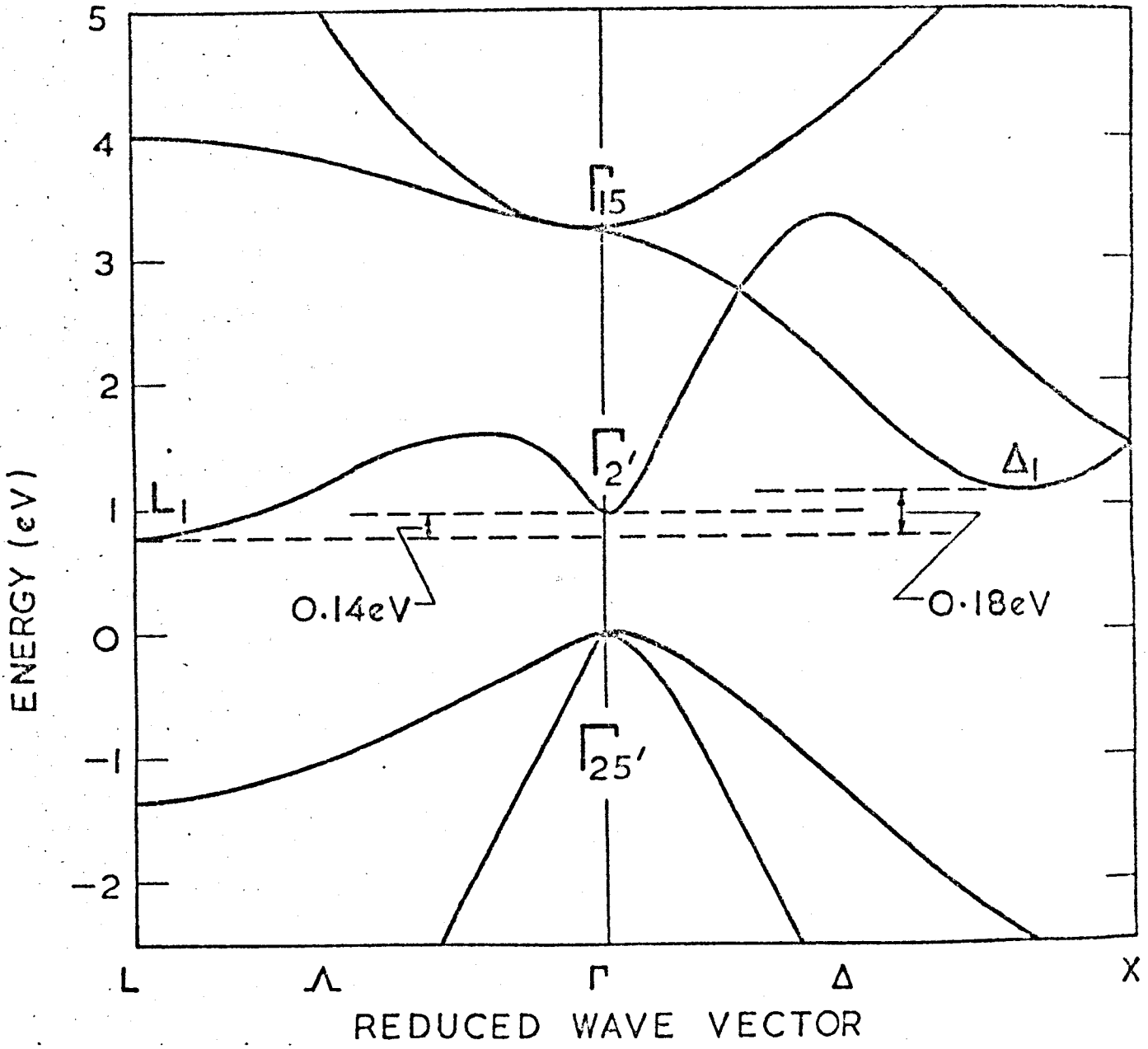

FIG. 8

Elliott et al[45]. At 79°K a "measured slope mobility of - 80cm^2/Vsec" was obtained for electric fields between 2.2 KV/cm and 4.3 KV/cm. However, experimental uncertainties lead the authors to state that they "cannot ascertain that a negative differential mobility exists around 79°K." Again threshold electric fields obtained by these authors are considerably lower than those of Elliott et al[45].

The conduction band structure of n - Ge is shown in Figure 8. A uniaxial stress applied to Ge in any direction other than <100> causes splitting of the <111> conduction band minima, which are degenerate in the absence of strain. Similarly, the degeneracy of the higher energy <100> silicon like minima may be lifted by uniaxial stress applied in other than a <111> direction. Measurements of the transport properties of n - Ge under stress may therefore be used to further elucidate the distinctive features of the N.D.C. process. Following this philosophy Smith, McGroddy and Nathan have studied the current voltage characteristics of a number of specimens under a variety of orientations of current and uniaxial stress[8]. With current flow in the <211> direction and stress along the <111> direction, for example, the threshold field reduces from an infinite value at zero stress, to a minimum value of 0.45 KV/cm and then subsequently increases as the uniaxial stress is steadily increased.

The effect of hydrostatic pressure upon the electronic energy band structure is clearly isotropic, bringing all the <100> silicon like minima down towards the <111> minima. Measurements of the effects of hydrostatic pressure upon the threshold field in a <100> direction at 77°K revealed that it increased with increasing pressure[49].

The source of the N.D.C. in n- Ge has been the subject of some debate. In their initial paper reporting observation of micro-wave emission from n - Ge, McGroddy et al[44] and subsequently Chang and Ruch[46] and Fawcett and Paige[50] consider the possibility of electron transfer

between <111> and <100> minima as the source of the N.D.C. Later work by Meltz and McGroddy[49] would seem to undermine this model since their hydrostatic pressure measurements indicated that, as the <100> and <111> minima approach each other, the threshold electric field increases. A simple model of the transferred electron effect would suggest a decrease of threshold electric field as the valleys approach each other.

An alternative model suggested by Dumke[51] relies only upon non-parabolicity of the individual <111> minima. In this calculation electrons were allowed to rise to quite high energies within the <111> minima, as a consequence of the omission of the <100> minima which provide an energy ceiling. Dumke finds that non-parabolicity alone can provide an N.D.C. which arises from the increase of the effective mass with energy.

The introduction of an N.D.C. by application of a uniaxial stress in Smith's[48] work, on the other hand, is attributed to transfer between the now non-equivalent <111> minima. Clearly, however, since an N.D.C. is known to exist in the absence of uniaxial stress for current flow in a <100> direction, this latter model is a gross simplification of a very complex situation.

In a very recent Monte Carlo calculation, Fawcett and Paige[52] have been able to account for nearly all the observed behaviour by suitable choice of the various disposable parameters. However, because the final behaviour is a consequence of the interplay of a number of similarly small effects a detailed intuitive explanation remains complex. The electron transfer mechanism is however of paramount importance.

Thus, in summary, in 1969 N.D.C. was known to exist in n - Ge for current flow parallel to the <100> direction, and for temperatures below 150°K. The magnitude of the negative slope mobility had, however, not been measured at 77°K[44] * and the threshold field was variously reported as 2.2 KV/cm and 3 KV/cm [45].

---

* It has already been pointed out that the measurement by Chang and Ruch has been discounted by the authors, for in presenting their result at this temperature they point out that the measured negative mobility is much smaller than the experimental error.

References

1. J. Bok and P. Nozieres

   J. Phys.Chem.Sol. 24, 707-714 (1963)

   or

   A. C. Baynham and P. W. Braddock

   Sol.Stat.Comm. 4, 377 (1966)

2. D. J. Bartelink

   Phys.Rev.Lett. 16, 510-513 (1966)

   or

   Phys.Rev. B1, 1107-1124 (1970)

3. O. Holter

   Phys.Rev. 129, No.6, 2548-2553 (15 March 63)

4. D. Bohm, E. P. Gross

   Phys.Rev. 75, No.12, 1851-1864 and 1864-1876(June 15, 1949)

5. G. A. Swartz and B. B. Robinson

   Appl.Phys.Lett. 9, 232-235 (1966)

   B. B. Robinson and G. A. Swartz, IBM.

   J. Res. and Dev.13, 601-606 (1969)

6. E. Schlömann

   J.A.P. 40, No.3, 1422-1424 (March 69)

7. A. R. Hutson, J. M. McFee and D. L. White

   Phys.Rev.Lett. 7, 237-239 (1961)

8. J. B. Gunn

   Phys.Rev.138, 6A, 1721-6 (June 65)

9. H. J. Stocker

   18, No.26, Phys.Rev.Lett. (26 June 1967)

9a. P. N. Butcher - Private Communication

10. T. A. Midford and H. C. Bowers

Proc.Inst.Elect.Electron.Engrs. 36, 1724-1725 (1968)

11. P. N. Robinson, G. S. Kino and B. Fay

IEEE Trans.El.Dev. 612-615 (Sept 1967)

12. W. Frey, R. W. H. Engelmann and B. G. Basch

Proc. MOGA Conf. (1970)

13. P. Kozdon and P. N. Robson

Proc.Moga. Conf. (1970)

14. J. Koyamo, S. O'Hara, S. Kawazura and K. Mumabe

S.S.Device Conference Boulder (1968)

15. B. K. Ridley and T. B. Watkins

Proc.Phys.Soc. 78, 293-304 (1961)

16. C. Hilsum

Proc.I.R.E. 50, 185-189 (1962)

17. J. B. Gunn

I.B.M. J.Res.Devel. 8, 141-159 (1964)

18. I. B. Bott and W. Fawcett

Advances in Microwaves, 3, 223-299 (1968)

19. C. Hilsum,

Proc.7th Intern.Conf.Phys.Semicond. Paris,

1127-1139, Donod, Paris 1964.

20. As 19, or

A. R. Hutson, A. Jayaraman and A. S. Cariell

Phys.Rev. 155, 786-796 (1967)

21. As 18.

22. As 17, or

A. G. Foyt and A. L. McWhorter

ED-13, 79-87 (1966)

22a S. Paranski W. Paul I. C. McGroddy H. E. Nathan J. E. Smith Jr Sol. State comm I 705 (1969)

23. As 17.

24. J. W. Allen, M. Shyam, Y. S. Chen, G. L. Pearson
Appl.Phys.Lett. 7, 78-80 (1965)

25. J. W. Allen, M. Shyam and G. L. Pearson,
Appl. Phys.Letters, 9, 39-41 (1966)

26. C. Hilsum and H. D. Rees
Elect.Lett. 6, 277-278 (1970)

27. As 19. and 20.

27a. J. L. Birman, M. Lax and R. Loudon
Phys.Rev. 145, 620-622 (1966)

28. E. G. S. Paige
Prog. in Semiconductors, 8, (1964)

29. H. Frohlich and V. B. Paranjape
Proc.Phys. Soc. B69, 21-32 (1957)

30. T. Kurosawa
Proc.Int.Conf.Phys.Semicond. Kyoto (1966) or
J.Phys.Soc.Jap.Suppl. 21, 424 (1966)

31. W. Fawcett, A. D. Boardman and S. Swain
J.Phys.Chem.Sol. 31, 1963-1990 (1970)

32. J. G. Ruch and G. S. Kino
Appl.Phys.Letters 10, 40-42 (1967)

33. J. B. Gunn and B. J. Elliott
Phys.Letters 22, 369-372 (1966)

34. W. Shockley
Bell System Tech. Int. 33, 799-826 (1954)

35. H. Kroemor
Proc. IEEE 53, 1246 (1965)

36. D. E. McCumber and A. G. Chynoweth
IEEE Trans.El.Devices ED-13, 4-21 (1966)

37. S. M. Mahrous and P. N. Robson
Electron.Letters 2, 107-108 (1966)

38. B. K. Ridley

Proc.Phys.Soc. 82, 954-966 (1963)

39. H. Kroemer

IEEE Trans. el. Dev. ED-13, 27-40 (1966)

40. P. N. Butcher

Phys.Lett. 19, 546-547 (1965)

41. J. B. Gunn

Proc.7th Int.Conf.Phys.Semicond. (Plasma effects)

Paris 1964, 199-207 Dunod 1964.

42. J. S. Heeks

IEEE Trans.el.Dev. ED-13, 68-79 (1966)

43. H. W. Thim

Proc.IEEE 55, 446-447 (1967)

44. J. C. McGroddy and M. I. Nathan

IBM, Jnl. of Res. and Dev. 11, 337 (1967)

45. B. J. Elliott, J. B. Gunn, J. C. McGroddy

Appl.Phys.Lett. 11, No.8, 253-255 (15 Oct 1967)

45a. J. B. Gunn and B. J. Elliott

Phys.Lett. 22, No.4, 369 (1 Sept 1966)

45b. J. G. Ruch and G. S. Kino

Appl.Phys.Lett. 10, 40 (1967)

46. D. M. Chang and J. G. Ruch

Appl.Phys.Lett. 12, 111-112 (1968)

47. As 45b.

48. J. E. Smith (Jr.), J. C. McGroddy and M.I. Nathan

Electron.Device Conference Boulder, 1968

49. P. J. Melz and J. C. McGroddy

IBM. Report, Rc 1013 (Feb 14, 1968)

50. W. Fawcett and E. G. S. Paige

Electronics Letters 3, No.11 (Nov.1967)

51. W. P. Dumke

Phys.Rev. B2, 987-996 (1970)

52. W. Fawcett and E. G. S. Paige

J. of Phys. C. 4, 1801 (Sept.1971)

53. A. P. Neukerman and G. S. Kino

10th Int.Conf.Phys. of Semicond. 40-45 (1970)

E. G. S. Paige

I.B.M. Jul. of Res. and Dev. 13, No.5, 562-567 (1969)

A. C. Baynham,

I.B.M. Jul. of Res. and Dev. 13, No.5, 568-572 (1969)

A. C. Baynham

Electronics Letters, 6, No.10 (1970)

2. Wave Propagation in Conducting Media

It was proposed in Section 1 that amplification may be achieved by launching a (quasi) T.E.M. wave through a negative resistance medium. In the absence of any materials having a total negative resistance, it was suggested that materials which exhibit negative differential conductivity could possibly be employed, if biased into the region of N.D.C. as shown schematically in Figure 1 of Section 1.

In this section we examine this proposed amplification process and the ideas developed here form a basis for the remainder of the work to be described. We deal first with wave propagation in an infinite uniform medium, then introduce successively, complexities arising from finite specimen geometry, non-uniformity, anisotropy, and frequency dependence of the negative resistance process. Each of these features will be seen to place its own constraints upon any experimental system designed to observe wave amplification in a N.D.C. medium. Consequently whenever a new observational system is introduced, in subsequent sections, the conditions established here will be relied upon in the choice of the experimental parameters.

2.1 T.E.M. Wave Propagation in an Infinite Uniform Medium

From Maxwell's equations we have

$$\underline{\nabla}\wedge(\underline{\nabla}\wedge\underline{E}) = -\mu_o \frac{\partial}{\partial t}(\underline{\nabla}\wedge\underline{H}) = -\mu_o \frac{\partial}{\partial t}\left(\underline{J} + \frac{\partial \underline{D}}{\partial t}\right)$$

where electric and magnetic field vectors are $\underline{E}$ and $\underline{H}$ respectively, $\underline{J}$ is the current density μ_o the permeability of free space (which is relevant in all cases of present interest) and t is time. $\underline{\nabla}\wedge$ and $\underline{\nabla}\cdot$ are the vector operators curl and div. respectively.

Assuming that the wave is transverse electric, i.e. that the electric vector lies in, for example, the x direction, which is orthogonal to the direction of wave propagation, z, we obtain*

$$\frac{\partial^2 \underline{E}}{\partial z^2} = \mu_o \frac{\partial}{\partial t}\left(\underline{J} + \frac{\partial \underline{D}}{\partial t}\right) = \mu_o \frac{\partial}{\partial t}\left(\underline{\underline{\sigma}}\,\underline{E} + \underline{\underline{\epsilon}}_L \epsilon_o \frac{\partial \underline{E}}{\partial t}\right)$$

where $\underline{\underline{\sigma}}$ and $\underline{\underline{\epsilon}}_L$ are the conductivity and lattice dielectric constant tensors. These will be assumed to be diagonal and time independent*.

If the wave has the form

$$\underline{E} = \underline{E}_o \exp\left[i(\omega t - kz)\right]$$

then

$$-k^2 = \mu_o (i\sigma\omega - \omega^2 \epsilon_L \epsilon_o)$$

i.e.
$$\frac{c^2 k^2}{\omega^2} = \epsilon_L \left(1 - \frac{i\sigma}{\omega \epsilon_L \epsilon_o}\right) \quad \ldots (1)$$

Now, both the conductivity σ, and the wave number k are in

---

* These assumptions imply that $\underline{\nabla}\cdot\underline{D} = \rho = 0$. The material is thus implicitly assumed to be free from space charge accumulation.

general complex, allowing respectively for a current which lags the electric field, and damping of the wave. By writing

$$\left.\begin{aligned} \sigma &= \sigma_R + i\,\sigma_i \\ k &= k_R + i\,k_i \end{aligned}\right\} \qquad \ldots \quad (2)$$

In (1) and separating real and imaginary parts we find that, from the real parts,

$$k_R = \frac{1}{\sqrt{2}} \left\{ \frac{\epsilon_L \omega^2}{c^2} + \frac{\sigma_i \omega}{\epsilon_o c^2} \pm \sqrt{\left(\left(\frac{\epsilon_L \omega^2}{c^2} + \frac{\sigma_i \omega}{\epsilon_o c^2} \right)^2 + \frac{\sigma_R^2 \omega^2}{\epsilon_o c^4} \right)} \right\}^{1/2}$$

The positive sign must be taken so that

$$k_R = \frac{k_{LR}}{\sqrt{2}} \left\{ 1 + \frac{\sigma_i}{\epsilon_L \epsilon_o \omega} + \sqrt{\left(\left(1 + \frac{\sigma_i}{\epsilon_L \epsilon_o \omega} \right)^2 + \frac{\sigma_R^2}{\epsilon_L^2 \epsilon_o^2 \omega^2} \right)} \right\}^{1/2} \qquad \ldots \quad (3)$$

where k_{LR} is the real wave vector arising in the absence of all the free carriers, i.e. $k_{LR} = \epsilon_L^{1/2} \frac{\omega}{c}$

Using the imaginary part of equation (1) we also have

$$k_i = \frac{-\sigma_R}{2\omega\epsilon_o} \cdot \frac{\omega^2}{c^2 k_R} = \frac{-\sigma_R k_o^2}{2\epsilon_o \omega k_R} \qquad \ldots \quad (4)$$

Hence, using (3),

$$k_i = \frac{-k_o^2 \epsilon_L \left(\frac{\sigma_R^2}{\epsilon_L^2 \epsilon_o^2 \omega^2} \right)^{1/2}}{k_{LR} \sqrt{2} \left\{ 1 + \frac{\sigma_i}{\epsilon_L \epsilon_o \omega} + \sqrt{\left(\left(1 + \frac{\sigma_i}{\epsilon_L \epsilon_o \omega} \right)^2 + \frac{\sigma_R^2}{\epsilon_L^2 \epsilon_o^2 \omega^2} \right)} \right\}^{1/2}}$$

Use of the following identity

$$\frac{\sigma_R^2}{\epsilon_L^2\epsilon_o^2\omega^2} = \left(1 + \frac{\sigma_i}{\epsilon_L\epsilon_o\omega} + \sqrt{\left(\left(1 + \frac{\sigma_i}{\epsilon_L\epsilon_o\omega}\right)^2 + \frac{\sigma_R^2}{\epsilon_L^2\epsilon_o^2\omega^2}\right)}\right)\left(\pm 1\right.$$

$$\left. \pm \frac{\sigma_i}{\epsilon_L\epsilon_o\omega} \mp \sqrt{\left(\left(1 + \frac{\sigma_i}{\epsilon_L\epsilon_o\omega}\right)^2 + \frac{\sigma_R^2}{\epsilon_L^2\epsilon_o^2\omega^2}\right)}\right)$$

allows us to write

$$k_i = \frac{k_{LR}}{\sqrt{2}}\left\{\pm 1 \pm \frac{\sigma_i}{\epsilon_L\epsilon_o\omega} \mp \sqrt{\left(\left(1 + \frac{\sigma_i}{\epsilon_L\epsilon_o\omega}\right)^2 + \frac{\sigma_R^2}{\epsilon_L^2\epsilon_o^2\omega^2}\right)}\right\}^{1/2} \quad \ldots (5)$$

The lower sign must be taken here

The basic characteristic of T.E. wave propagation in an infinite uniform medium are specified by equations (3) and (5) for the complex wave number, and equation (4) which relates the signs of k_R and k_i. It is the latter equation which provides the basis for the gain process. We see that, as the real conductivity goes from positive to negative, the relative signs of k_R and k_i change. Since loss is known to occur in the everyday world of positive resistance media, gain must be associated with a negative conductivity; a conclusion which is borne out by equation (4), for if $k_R > o$, $\sigma_R < o$ then $k_i > o$ and the wave assumes the form

$$\underline{E} = \underline{E}_o \exp i\,(\omega t - (k_R + i\,k_i)\,z) = \underline{E}_o \exp i\,(\omega t - k_R z)\exp(+\,|k_i|\,z)$$

We note further that there is no damping of the wave when there is zero real conductivity, whilst the real part of the wave vector tends to the lattice limited value.

ISSUE 1 20·9·71 | R.R.E. | TRACED J.PITCHFORD | APP'D. A.C. Bayliss | USED ON

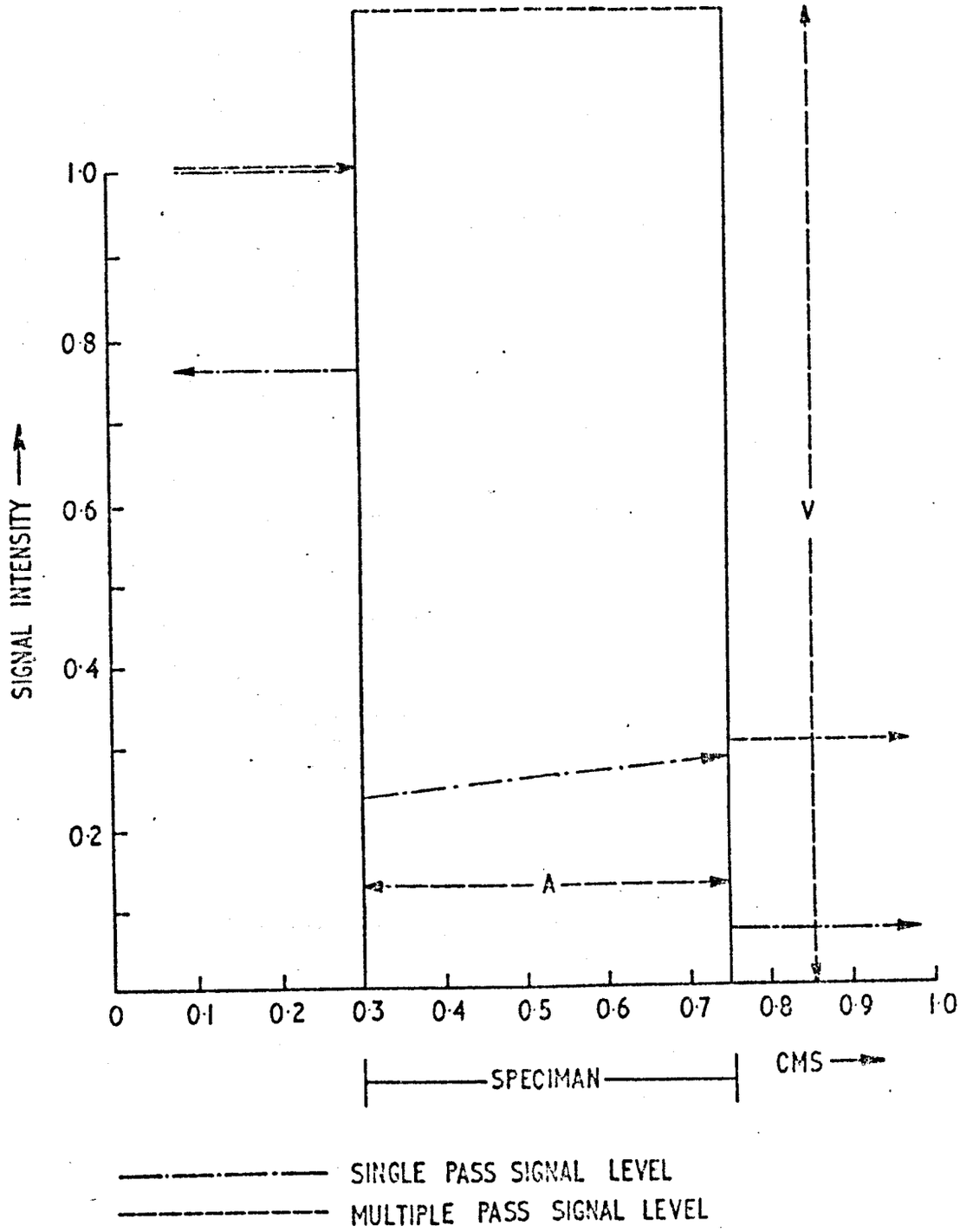

FIG. 1

SCHEMATIC DIAGRAM OF RADIATION INCIDENT UPON A FABRY PÉROT COMPOSED OF NEGATIVE RESISTANCE MATERIAL.

829982 500 8 70

2.2 Finite Specimen Geometry

2.2.1 Finite Specimen Geometry in the Direction of Wave Propagation

In this section we introduce a finite specimen geometry in the propagation direction, as shown schematically in Figure 1. It is immediately clear that in the absence of gain we have a Fabry Pérot structure.

The amplitude of radiation, transmitted through a Fabry Pérot etalon thickness A is

$$L_t = L_o e^{k_i A} T^2 (1 + r^2 e^{2k_i A} \text{Cos} (2 k_R A) \ldots)$$

where L_o is the incident amplitude from the cavity's environmental noise spectrum, for example and T and r the surface transmission and reflection coefficients. We now distinguish a number of distinct operational regimes for such a structure with potential internal gain.

(i) $r^2 e^{2k_i A} < 1$

If $r^2 e^{2k_i A} < 1$, that is, there is no round trip gain in the cavity

$$L_t = \frac{L_o T^2 e^{k_i A}}{(1 - r^2 e^{2k_i A} \text{Cos} (2 k_R A))} \qquad \ldots (6)$$

and transmitted signals remain finite, though under some circumstances they may be larger than the incident signal. The threshold for this insertion gain is clearly defined by

$$\frac{L_t}{L_o} = 1 = \frac{T^2 e^{k_i A}}{1 - r^2 e^{2 k_i A}}$$

at the frequency of peak gain. Insertion gain occurs then if

$$k_i A > \log_e \left\{ \frac{-T^2 + \sqrt{T^4 + 4r^2}}{2r^2} \right\} \quad \ldots (7)$$

This "$k_i A$ product" which defines the threshold for insertion gain is more usefully expressed as an "NA product" using equation (5) when the complex conductivity

$$\sigma = ne(\mu_R + i\mu_i)$$

of the host negative resistance material is known. The (free carrier concentration x A) product (NA product) is employed in describing the stability of a specimen, and will be used extensively throughout the remainder of this work *.

The surface reflection and transmission coefficients may, of course, be expressed in terms of the free space wave - vector k_o and the complex wave - vector within the material of the Fabry Pérot using Fresnel's equations. Thus the exact insertion gain $L_T L^*_T / L_o L_o^*$ is derived with the aid of equation (6) and becomes

$$\frac{L_T L_T^*}{L_o L_o^*} = 16 k_o^2 (k_R^2 + k_i^2) e^{-2 k_i A} \Big/ \Big\{ (1+\alpha^2)(A_1^2 + B^2 + C^2 + D^2) + 2(1-\alpha^2)(A_1 B + CD) + 2\alpha \Big[(B^2 - A_1^2 + D^2 - C^2)\cos\varphi + 2 \sin\varphi \; (BC - A_1 D) \Big] \Big\} \quad \ldots (8)$$

---

* It should be pointed out that owing to the free carrier contribution to the surface reflection, and transmission coefficients the $k_i A$ and NA products defined by equation (7) are not truly constants. They show a dependence upon the free carrier concentration which is negligible for lightly doped material. However, in more heavily doped material, owing to the large free carrier contribution to r and T the NA product must be treated with caution.

after some manipulation

where

$$\delta = 2 (k_R + i k_i) A$$

$$\alpha = e^{-2 k_i A}$$

$$A_1 = k_R^2 - k_i^2 + k_o^2$$

$$B = 2 k_R k_o$$

$$C = 2 k_i k_R$$

$$D = 2 k_o k_i$$

The transmitted power is therefore determined by the parameters k_R k_i, k_o and A. Through equations (3) and (5), it can be expressed in terms of k_o, A, the free carrier concentration and complex mobility.

At a later stage the insertion gain is computed for both n - Ge and GaAs as a function of free carrier concentration using these equations. The programme written for this purpose is given in Appendix 1.

We have seen that when there is no round trip gain within the cavity, the device may exhibit either insertion loss or insertion gain. In the latter case, the bandwidth of the amplifier is determined by the magnitude of the internal reflection coefficient, or, in other words by the strength of the feedback process.

Equation (6) indicates that the transmitted signal falls to $1/\sqrt{2}$ of its peak amplitude when

$$k_r \doteq \frac{1}{2A} \cos^{-1} \left\{ \frac{\sqrt{2}\, r^2 e^{2 k_i A} - 0.4}{r^2 e^{2 k_i A}} \right\}$$

Hence, remembering that at present we specify no round trip gain within the cavity, the bandwidth is, (in terms of the real wave vector)

$$\Delta k_r \doteq \frac{2}{A}\left\{\pi - \frac{1}{2}\cos^{-1}\left(\frac{\sqrt{2}\, r^2 e^{2 k_i A} - 0.4}{r^2 e^{2 k_i A}}\right)\right\}$$

(ii) $\underline{r^2 \quad 2k_i A = 1}$

If $r^2 e^{2 k_i A} = 1$ then equation (6) becomes invalid whenever $\cos(2 k_R A) = 1$ as a sum of the multiply reflected waves within the Fabry Perot etalon. The sum has in fact become infinite, indicating the commencement of oscillation. The threshold for oscillation is thus given by

$$k_i A = \frac{1}{2}\log_e\left(\frac{1}{r^2}\right) \qquad \ldots \quad (8)$$

Using equation (5) this $k_i A$ product can again be expressed as an NA product for a material of known complex mobility. Thus a second NA product is defined which determines the threshold for oscillation; $NA \geqslant k_{osc}$. The analogy to the NL product widely used to define the threshold of domain mode oscillation ($NL \geqslant C_{osc}$) is clear: The NA product defines the threshold of electromagnetic instability transverse to the applied electric field, whilst the conventional NL product defines the threshold of space charge instability parallel to the applied electric field. Once again we point out that this second NA product defined in equation (8) is only approximately a constant, owing to the free carrier contribution to r.

Assuming that the system does not saturate, then at the frequencies for which the phase angle $k_R A = n\pi$, we see from (6) that infinite output is predicted. However an infinitessimally removed frequency for which $\cos(2 k_R A)$ is marginally smaller than

unity has a finite transmitted amplitude. The width of the predicted spectral emission signal is then infinitely small, and it is centred upon a normal mode of the Fabrey Pérot cavity.

(iii) $\underline{r^2 e^{2 k_i A} > 1}$

When $r^2 e^{2 k_i A} > 1$, assuming that the system again does not saturate, for all those frequencies for which the product $r^2 e^{2 k_i A} \cos (2 k_R A) \geq 1$ infinite transmission occurs. The edges of this broad power spectrum will occur, as before, when $r^2 e^{2 k_i A} \cos (2 k_R A) = 1$.

Any real system must of course reach an equilibrium situation through some nonlinear process. In this situation, the rate of supply and loss of microwave energy will have become equal. Assuming that the rate of generation of power is still a maximum where the small signal condition $\cos (2 k_R A) = 1$ is satisfied, then the system reverts to that behaviour already ascribed to such a regime; that is to an infinitely narrow emission spectrum which is centred upon a cavity mode or modes.

In this section the conclusions have been drawn that a negative resistance amplifying medium having boundaries in the direction of wave propagation may behave as

a) a circuit element having net insertion loss

b) an amplifier having a bandwidth determined by the product $r^2 e^{2 k_i A}$, and a threshold defined by an NA product.

c) an oscillator which has an infinitely narrow spectral emission line centred upon a normal mode of the cavity, and having a threshold defined by an NA product.

It is the object of the present work to observe each of these classes of electromagnetic instability.

$nl < 5.10^{11}$	$na < 3.10^{13}$	Stable
$nl > 5.10^{11}$	$na < 3.10^{13}$	Space charge instability
$nl < 5.10^{11}$	$na > 3.10^{13}$	Electro-magnetic instability
$nl > 5.10^{11}$	$na > 3.10^{13}$	Hybrid instability

CLASSES OF INSTABILITY

FIG 2

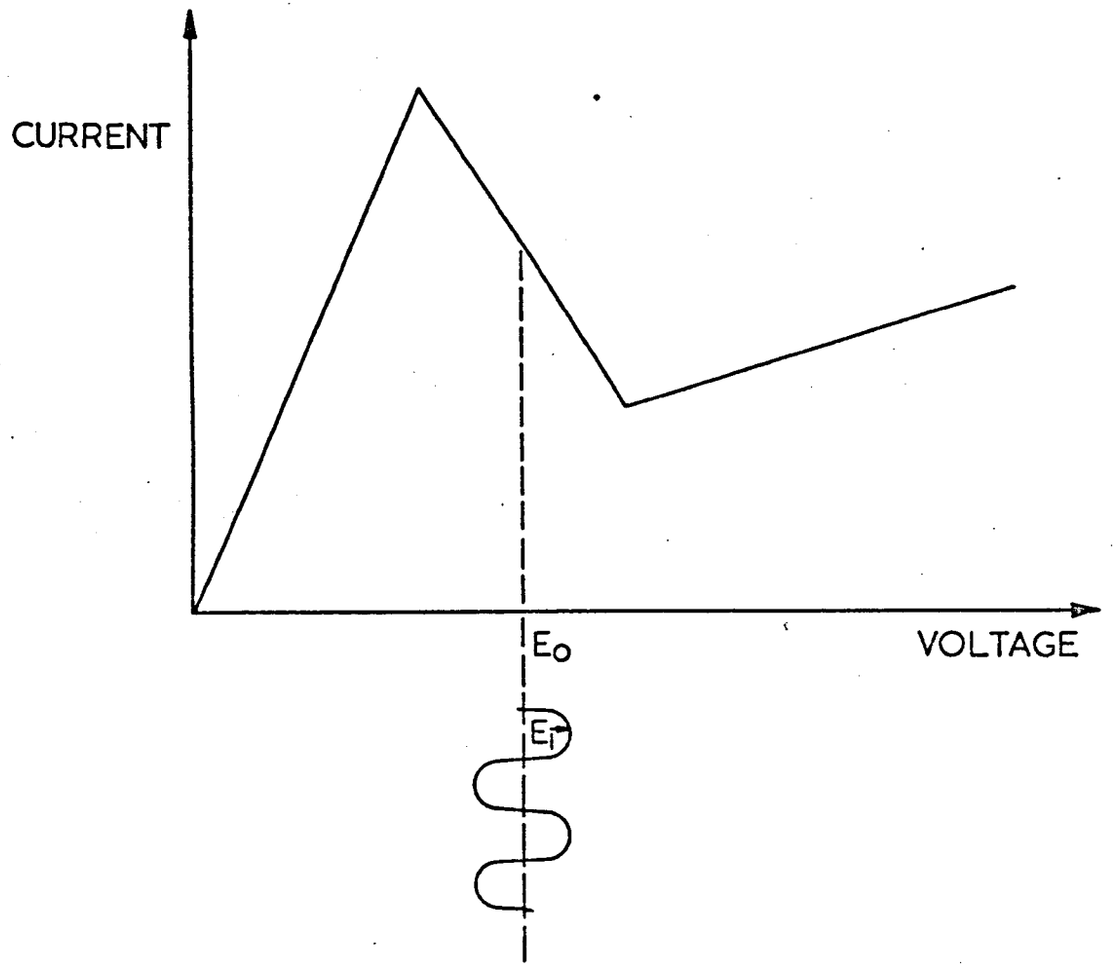

FIG. 3

A CURRENT – VOLTAGE CHARACTERISTIC FOR AN IDEALISED MATERIAL HAVING NEGATIVE DIFFERENTIAL CONDUCTIVITY. THE SPECIMEN HAS A MEAN BIASING FIELD OF E_o, AND SUPPORTS MICROWAVE RADIATION OF AMPLITUDE E_1.

2.2.2 Finite Specimen Geometry, in the Direction of the Applied Electric Field

The conclusions which have been reached in this section have, thus far, been of a general nature. However, it is now necessary to draw conclusions which refer to the specific type of negative resistance process to be used. In section 1, the transferred electron effect was introduced as a mechanism providing a suitable negative differential conductivity (N.D.C.) for the present experiments. We envisage a system in which a DC electric field biases a sample into a region of N.D.C. Incident electromagnetic waves then sense the negative slope conductivity and behave as if incident upon a material having a total negative resistance as indicated in Figure 3.

In Section 1, however, it was pointed out that a sample which has a bulk N.D.C. became unstable to space charge fluctuations when biased into the N.D.C. range. This is clearly a complication which is to be avoided if possible, in order that experimental observations of the electromagnetic instability may be clear cut. This choice of experimental regime stands in marked contrast to the large body of work which has already been devoted to the N.D.C. process in GaAs (see Figure 2); we choose to impose space charge STABILITY by making NL smaller than critical value for domain formation, and to extract microwave power from the bulk N.D.C. by allowing electromagnetic instability in its place i.e. by making NA greater than the critical value for electromagnetic instability. In addition to the two foregoing regimes in which microwave power may be extracted from a sample having a bulk N.D.C. there is, of course, a third one in which both space charge and electromagnetic instability are simultaneously present. Two of these regimes, regimes in which electromagnetic instability is operative, are now examined in more detail.

a) Space Charge Stable Case

Space charge stability is achieved most readily by imposing a low NL product upon the specimen. Under these circumstances, the specimen does not, however, assume a uniform spatial distribution of the biasing electric field[1]. Moreover, owing to both the electric field dependence of the free carrier contribution to the total dielectric constant[2] and the associated accumulation and depletion layers, any such non uniformity of biasing electric field is reflected in a correspondingly non uniform "microwave path length" within the Fabry Pérot cavity. Thus, this spatially non-uniform biasing electric field is of clear importance to the present work.

We calculate the spatial distribution of electric field and free carrier concentration neglecting diffusion. The omission of this term is justified ~~both~~ on the grounds that, in similar calculations, McCumber and Chynoweth[3] found it to be unimportant everywhere except in regions of very rapid discontinuities, and ~~because of~~ the uncertainty which surrounds the precise form which this term should take[4].

The iterative procedure which we adopt commences at a point adjacent to the metallic cathode contact. Here the semiconductor has an electron concentration which is approximately equal to that existing within the metal. For a chosen specimen current density J_c, an electron drift velocity V, and field E_1, may therefore be deduced. An arbitrarily small increment in electron drift velocity δV is then chosen in order to initiate the iterative procedure. We look for a stationary solution for which

$$\nabla \cdot \underline{J} = -\frac{\partial \rho}{\partial t} = 0$$

The appropriate increment of free carrier concentration corresponding to this increment of electron drift velocity is therefore established through the current continuity equation. The average value of the initial and final free carrier concentrations is used to define an average field gradient within this drift velocity increment using Poisson's equation.

$$\epsilon \nabla \cdot \underline{E} = (n - n_o)\, e$$

where n_o is the doping level which is assumed uniform. The magnitude of the spatial increment over which these steps occur is then established using the electron velocity - field characteristic;

The velocity at the end of the spatial increment is clearly

$$V_2 = V_1 + \delta V$$

Using the velocity field characteristic, an appropriate electric field at the end of the spatial increment is established E_2. Now it is necessary that

$$E_2 = E_1 + \frac{dE}{dx} \cdot \delta x = E_1 + (n - n_o) \frac{e}{\epsilon} \cdot \delta x$$

Hence the magnitude of the spatial increment is established, and all parameters E_1, n_1, V_1 at this point within the specimen are assigned.

A similar procedure allows further steps down the specimen to be taken successively. Reference to the computer programme which is included as Appendix II will show that a few additional safety measures were necessary, in order that increments neither became too large near threshold, or too small as the free carrier concentration tended to the equilibrium level.

This approach to the calculation of the spatial distribution of electric field, and space charge within the specimen makes no attempt to exploit the second boundary condition offered by the anode. (In this and some other respects, this calculation resembles the work of, for example, Mahrous and Robson[5]). However, the effect of the anode is not felt by an electron until it enters its vicinity, at which time a new variable is introduced; namely the geometry of the anode region. In the case of a step function anode contact, at this point the electron concentration falls well below the equilibrium metallic contribution, $\nabla \cdot \underline{D} = (n - n_o)e$ becomes large and positive, and the field is very rapidly returned to low proportions. Results obtained using this computational proceedure are to be found in Sections 3.2.1 and 5.1.1.

b) Combined Space Charge and Electromagnetic Instability

In this section we consider a transit, domain mode, Gunn specimen which has one large dimension normal to the biasing electric field. The dynamics of domain formation and propagation have already been reviewed in Section 1.2.2. Thus we are already aware of the spatially nonuniform electric field and free electron concentration profile within the specimen.

It remains to point out that in this, more complex, case a simple alternative view of the gain process is possible. In the introductory section we have mentioned that owing to the dynamics of the domain within a Gunn sample, it is possible to observe terminal negative resistance over a broad band of frequencies. It is therefore sufficient to consider a T.E.M. wave propagating within a composite dielectric which exhibits a terminal negative resistance at the transmission line electrodes. These conditions alone indicate that gain must occur. A similar argument has been used by

Midford and Bowers[6] in their work upon T.E.M. wave propagation in an extended Impatt device. Here again the detailed behaviour of the silicon loading the transmission line is complex, but gain is implied because of the terminal negative resistance which it is known to exhibit.

In concluding this section it is necessary to emphasise the gross simplification which has been pursued here. The "space charge stable" case would, for example, support a growing space charge fluctuation as shown by Robson and Kino[7] immediately an electromagnetic wave was incident upon it. Space charge and electromagnetic instabilities can clearly not be rigorously regarded as alternative separate mechanisms by which the negative resistance process can relax. They are all part of the same composite problem and a rigorous solution would have to treat them as such. Such a solution was attempted, but proved prohibitively difficult because of the sheer complexity of the spatial non-uniformity existing within the sample.

The conclusions of this section are never-the-less intuitively reasonable. They are that the finite specimen geometry in the direction of T.E.M. wave propagation introduces the possibility of obtaining either amplification or oscillation depending on the magnitude of an NA product. In the latter case oscillation occurs at a frequency defined by the 'A' dimension of the sample rather than the 'L' dimension as in conventional Gunn samples. On the other hand the geometry of the sample parallel to the applied electric field is very complex owing to spatially non-uniform electric field (which arises as a direct consequence of employing materials having an N.D.C.) It also gives rise to two limiting regimes of operation, one in which the space charge system is strongly unstable and one in which

it tends to stability. Any combination of the transverse and longitudinal regimes is clearly admissable. The studies of previous workers have been confined to specimens with low NA products and transverse dimensions which were very much smaller than one wavelength at the frequency of operation. The Gunn specimen may then be correctly regarded as a local microwave circuit element. In contrast, in the present work, we look upon the specimen as a distributed transmission system.

2.3 Wave Polarisation

We have thus far considered T.E.M. wave propagation in an infinite negative resistance medium, and have introduced the considerable complexities which arise with a finite specimen geometry. We now introduce a further constraint upon the experimental system which stems from the use of a N.D.C. rather than a total negative resistance. Comment has already been made concerning the necessity of biasing a sample having N.D.C. into the appropriate region of the velocity-field characteristic as illustrated in Figure 3. It is clear from this diagram that an electromagnetic wave will only sense the negative slope conductivity if the electric vector of the wave is parallel to the biasing electric field. Thus, there is an added polarisation requirement placed upon the experimental system which stems from the anisotropy of the slope conductivity which is introduced by the biasing electric field. (Further anisotropy occurs for example in n-Ge where the N.D.C. is only operative in some crystallographic directions. However, this complexity is not referred to at this point).

It is of interest to consider the effect of misalignment of the electric vector of the wave and the biasing electric field. Such a situation is clearly of more than passing interest, for the transverse wave solution of Section 2.1 was only obtained under the assumption of spatial uniformity. However, in Section 2.2 gross non-uniformity in the

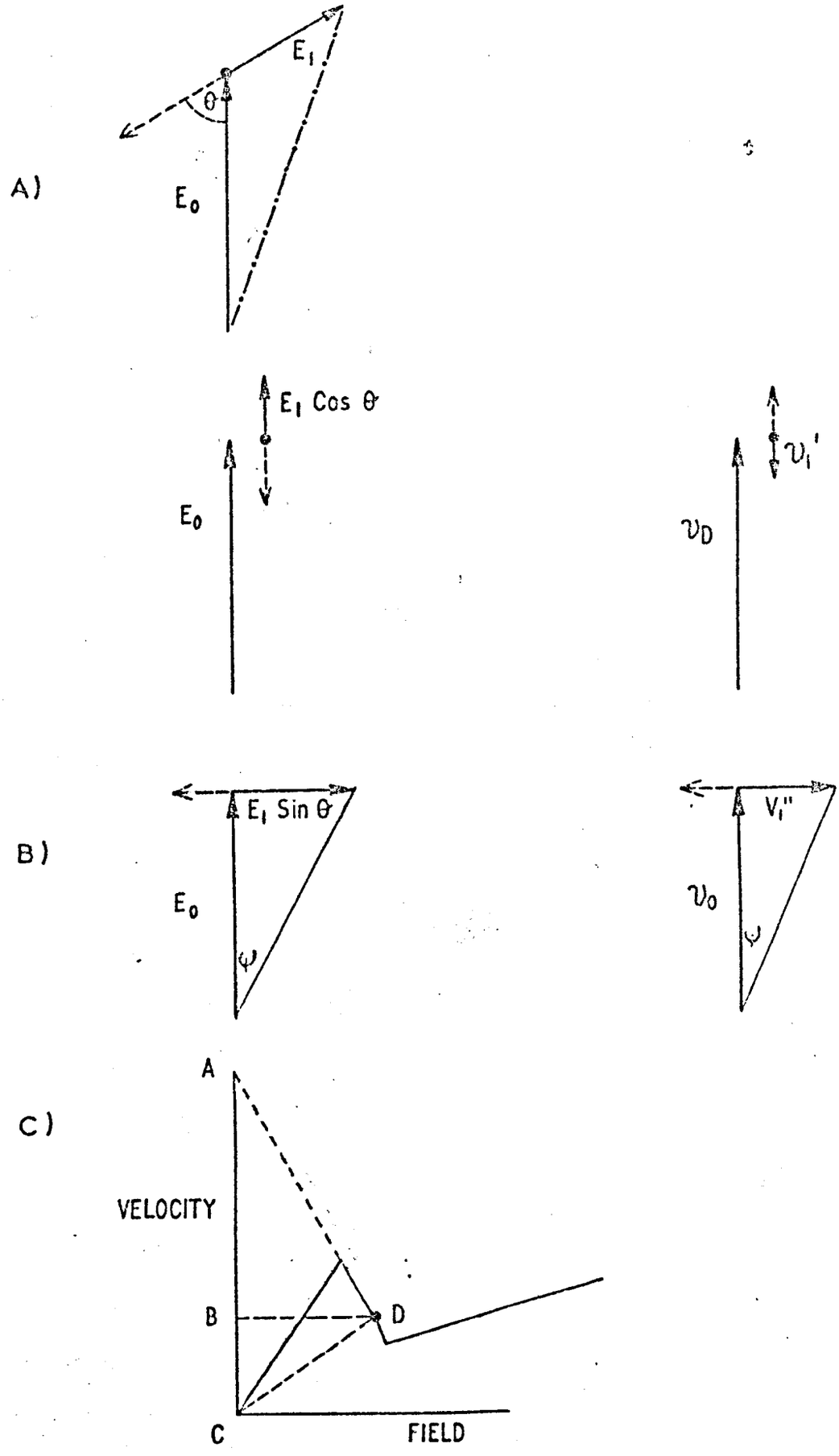

SCHEMATIC FIELD AND ELECTRON VELOCITY VECTOR DIAGRAMS

FIG 4

direction parallel to the biasing electric field was discovered. Thus the profile of the wave, and in particular, the local orientation of the electric vector may well not be in accord with a simple model.

In Figure 4a the relative orientation of a D.C. biasing electric field E_o and an oscillatory field E_1 are shown. E_o produces a velocity V_o according to the relation $V_o = \mu_{CHORD}\ E_o$, μ_{CHORD} being the slope of the chord on the velocity field diagram joining the point (V_o, E_o) to the origin. $E_1 \text{ Cos } \theta$, the component parallel to the biasing electric field produces an out of phase velocity V_1 also parallel to the biasing electric field. $V_1 = \mu_- E_1 \text{ Cos } \theta$ where μ_- is the negative slope mobility.

It remains to discover the effect of $E_1 \text{ Sin } \theta$. Other workers[8] have pointed out that this merely amounts to a re-orientation of the biasing electric field, AND A SUITABLE DRIFT VELOCITY ALONG IT. (Providing the N.D.C. process is not a function of crystallographic orientation).

Thus, referring to Figure 4b

$$E_o \text{ Tan} \psi = E_1 \text{ Sin } \theta$$

and equally

$$V_o \text{ Tan} \psi = V_1''$$

thus

$$E_o \frac{V_1''}{V_o} = E_1 \text{ Sin } \theta$$

$$V_1'' = \mu_{CHORD} E_1 \text{ Sin } \theta$$

The effectiveness of the net mobility at some angle θ for amplification of the oscillatory field is then readily established by summing the two energy exchanges,

$$\mu_- (E_1 \cos\theta)^2 + \mu_{CHORD} (E_1 \sin\theta)^2$$

Thus gain ensues so long as

$$|\mu_-| \cos^2\theta > \mu_{CHORD} \sin^2\theta$$

$$\frac{|\mu_-|}{\mu_{CHORD}} > \tan^2\theta$$

This places a condition upon the orientation of an oscillatory electric field relative to the biasing field, in order that energy may be extracted from the D.C. field and supplied to the R.F. field. It can be re-expressed in terms of the velocity field curve, for referring to figure 4c it is seen that

$$|\mu_-| = \frac{AB}{BD} \quad , \quad \mu_{CHORD} = \frac{BC}{BD}$$

Thus we require $\frac{AB}{BC} > \tan^2\theta$, and it appears that θ may be increased, for example, by increasing the biasing electric field strength. Equally, it appears that θ is minimal at the threshold field strength.

2.4 Choice of Frequency of Operation

Throughout the discussion thus far, it has been assumed that an oscillatory microwave field will interact with a suitably biased sample having an N.D.C. in a manner described by the (negative) slope mobility.

The problem of the interaction of a microwave field with a biased sample has already been considered by Gibson et al[9]. In their work they introduced phenomenological relaxation times τ_m and τ_ϵ describing the momentum and energy relaxation times respectively. An immediate conclusion which is intuitively satisfying may then be drawn that, providing $\omega\tau_M < 1$, the momentum of the free carriers can respond to the oscillatory accelerative field whilst, if $\omega\tau_\epsilon < 1$, the mean energy of the electron distribution function will not lag behind the oscillatory

field which of course also supplies energy.

These concepts allowed measurements of microwave conductivity to be readily interpreted; for example, at high frequencies (35 GHz) and low temperatures the microwave conductivity can be much smaller than the low frequency slope conductivity in n - Ge but tends to the correct value as a biasing electric field is increased. This is attributable to the fact that $\omega\tau_M > 1$ at low field whilst as the electric field is increased the reduction in τ_M which customarily accompanies hot carrier effects finally brings $\omega\tau_M$ below unity and D.C. and A.C. slope conductivities into agreement.

The free carrier system will of course in general lag behind the oscillatory electric field, that is, behave inductively, reducing the apparent lattice dielectric constant. If $\omega\tau_M$ is large and falls with increasing electric field, so too will the inductive free carrier contribution to the lattice dielectric constant fall with increasing electric field.

When $\omega\tau_\varepsilon > 1$ the free carrier "temperature" tends to lag behind the oscillatory field, giving rise to two further effects. The distribution function can be cool when the microwave field is large and hot when the microwave field is small. Thus the microwave mobility may appear anomalously large if $\omega\tau_\varepsilon > 1$ and the dominant momentum scattering process increases in probability with increasing free carrier energy: The microwave velocity is anomalously high for the applied microwave field, the distribution function not yet having heated up to its equilibrium value at which momentum scattering would be much stronger. It is also clear from this argument that the peak electron velocity occurs at a point in time which is now governed by BOTH the microwave field and the lagging mean energy of the free electrons. In consequence, the dielectric constant

must also be remarkably field dependent in such circumstances, and can in fact change sign and become capacitative.

Measurements have been made of the free carrier distribution function[10] in the presence of high electric field in p - Ge which indicate that it is not only not a displaced Maxwellian[11], but has additional complexities[12]. The subsequent discovery of the N.D.C. in GaAs and InP introduced a strong incentive towards the removal of the assumption of a displaced Maxwellian from theoretical descriptions of the transport process. A number of improved computational techniques emerged in answer to this problem: first a parameterised[14] solution which exploited certain features of the experimentally measured distribution function. Following this the Monte Carlo[15] and iterative techniques[16] were developed. The latter technique has been used to calculate the high frequency response of the N.D.C. process in GaAs without the assumption of relaxation times[17]. However, impressive though this technique certainly is, the same qualitative conclusions emerge. Namely, that there is a frequency ceiling beyond which frequency dependent effects occur, reducing the N.D.C. to a positive differential conductivity.

We conclude then that the operational frequency must be chosen sufficiently low for the negative differential mobility to be a true description of the conductivity presented to an incident microwave signal.

In this section we have shown how a T.E.M. wave incident upon a material having negative resistance may be expected to grow spatially. Introducing boundaries, we discover that this mechanism may be exploited to produce either amplification or oscillation. The behaviour is to be distinguished from the work already carried out by many researchers in which the sample forms a local circuit element rather than a distributed transmission system which contains the T.E.M. wave.

Consideration of the consequences of employing a N.D.C. material which is biased into the region of negative slope mobility, reveal that a further distinction can be drawn between samples in which travelling domain formation is strong and those in which it is weak. The former situation is regarded as one of hybrid or combined instability, and the latter as one of electromagnetic instability. A further consequence of using a N.D.C. rather than a total negative resistance phenomenon is that polarisation of the wave is seen to be of consequence, since it is essential that the electric vector of the wave falls within a certain angular inclination to the biasing electric field. Finally, we have seen that, in so far as any negative resistance process is a transport process involving electrons having a finite response time, an upper frequency limit to negative conductivity is to be expected.

References

1. W. Shockley

   Bell Sys.Tech.J. 33, 799-826 (July 1954)

2. A. F. Gibson, J. W. Granville and E. G. S. Paige

   J.Phys.Chem.Sol. 19, 198 (1961)

3. D. E. McCumber and D. G. Chynoweth

   IE^3 Trans.El.Dev. ED-13, No.1, 4-21

4. I. B. Bott and W. Fawcett

   Advances in Microwaves, 3, (1968)

5. S. M. Mahrous and P. N. Robson

   Electronics Lett. 2, 107-108 (1966)

6. T. A. Midford and H. C. Bowers

   Proc.Inst.Elect.Electron. Engrs. 36, 1724-1725 (1968)

7. P. N. Robinson, G. S. Kino and B. Fay

   IE^3 Trans.el.dev. 612-615 (Sept 1967)

8. P. N. Butcher

   Private Communication

9. As Ref.2

10. M. A. C. S. Brown, E. G. S. Paige and L. N. Simcox

    Proc.Int.Conf.Semicond.Phys.Exeter 111 (1962)

11. A. C. Baynham and E. G. S. Paige

    Phys.Lett. 6, 7-10 (Aug 1963)

12. A. C. Baynham

    Sol.State Comm. 3, 253-255 (1965)

13. J. B. Gunn

    IBM. J.Res.Dev. 8, 141-459 (1964)

14. G. Perksy and D. J. Bartelink

Phys.Lett. 28A, 749 (1969)

or

IBM. Jnl.Res.Dev. 13, No.5, 607-610 (1969)

15. H. Budd

Proc.Int.Conf.Phys.Semicond., Kyoto (1966):

J.Phys.Soc.Jap.Suppl. 21, 420 (1966)

T. Kurosawa

Proc.Int.Conf.Phys.Semicond., Kyoto (1966)

J.Phys.Soc.Jap. Suppl. 21, 424 (1966)

16. H. D. Rees

Phys.Lett. 26A, 416 (1968)

J.Phys.Chem.Sol. 30, 643 (1969)

Sol.Stat. Comm. 7, 267 (1969)

17. H. D. Rees

IBM, Jnl. of Res. Dev. 13, (1969)

3. Measurement of Negative Mobility by a Bridge Technique

In Sections 3 and 4 experimental work is described which is intended to exploit the diagnostic potential of T.E.M. wave propagation in negative resistance media. (See Section 1 and 2). Accordingly, the work is carried out in n - Ge; the most recent addition to the list of materials known to possess a bulk N.D.C.

3.1 n-Type Germanium

The discussion in Section 1 has already indicated that very little was known about the source of N.D.C. in n-Ge at the time of commencement of the work to be described here. Subsequently it has become fairly widely accepted as an intervalley transfer process. The strength of the process was also unknown, (although it was clearly weak) as was its frequency dependence. These were the major factors which motivated the initial choice of this material; the fact that the origin of the process, and in particular its strength, was largely unknown indicated that there was scope for experimental work of an exploratory or diagnostic nature, whilst its weakness indicated that the spatially non-uniform electric fields encountered in media with such a N.D.C. (see Section 2.3) may be rendered less severe.

In Section 3.2 constraints which govern the choice of experimental regime are discussed and in Section 3.3 the experimental system is described. In the final Section, 3.4, the results gained using this technique are discussed, with particular reference to the consequences of the non-uniform D.C. field distribution within samples, and to subsequently published data relating to this N.D.C. process.

3.2 Concept and Planning of the Experimental Regime

In Section 2 the real and imaginary parts of the wave-vector of a T.E.M. wave propagating in a negative conductivity medium were derived in terms of the complex conductivity. Thus the electric field dependence of the transport process in n-Ge may be studied by measuring the propagation constant for T.E.M. waves within this material, as a function of biasing electric field. Moreover, by measuring both real and imaginary parts of the propagation vector, both the in phase and

the out of phase components of the conductivity may be evaluated. Thus attention is directed towards a bridge measurement in which measurements of transmitted phase and amplitude of an incident signal may be used to obtain the complete propagation vector, and hence the complex conductivity.*

The choice of many of the experimental features is dictated by the rather severe, but vital, constraints enumerated in Section 2. We therefore deal with these first.

3.2.1 Stability of Specimen

It is clearly necessary that the specimen should not oscillate during the course of the bridge measurement. Thus it is necessary to maintain

$N.A. < K_{osc} = 2.2 \quad 10^{14}$ electromagnetic stability

$N.L. < C_{osc} = 2 \quad 10^{13}$ spacecharge stability

The symbols have the same significance as in earlier sections, and we use the value of C_{osc} obtained by McGroddy and Nathan[2]. (See Section 1.3).

K_{osc} is an estimated value obtained by using the equations of Section 2, and assuming that (a) the reflection at the specimen surface is determined only by its permittivity relative to free space, i.e. assuming that there is no specimen surface coating or equivalent microwave environmental mismatch, and (b) the negative mobility is $-300\ cm^2/Vsec$.

---

* It is of interest to notice that extensive measurements of the transport properties in n-Ge have already been made using a bridge technique by Gibson et al[10]. These will be introduced at a later stage in this Section.

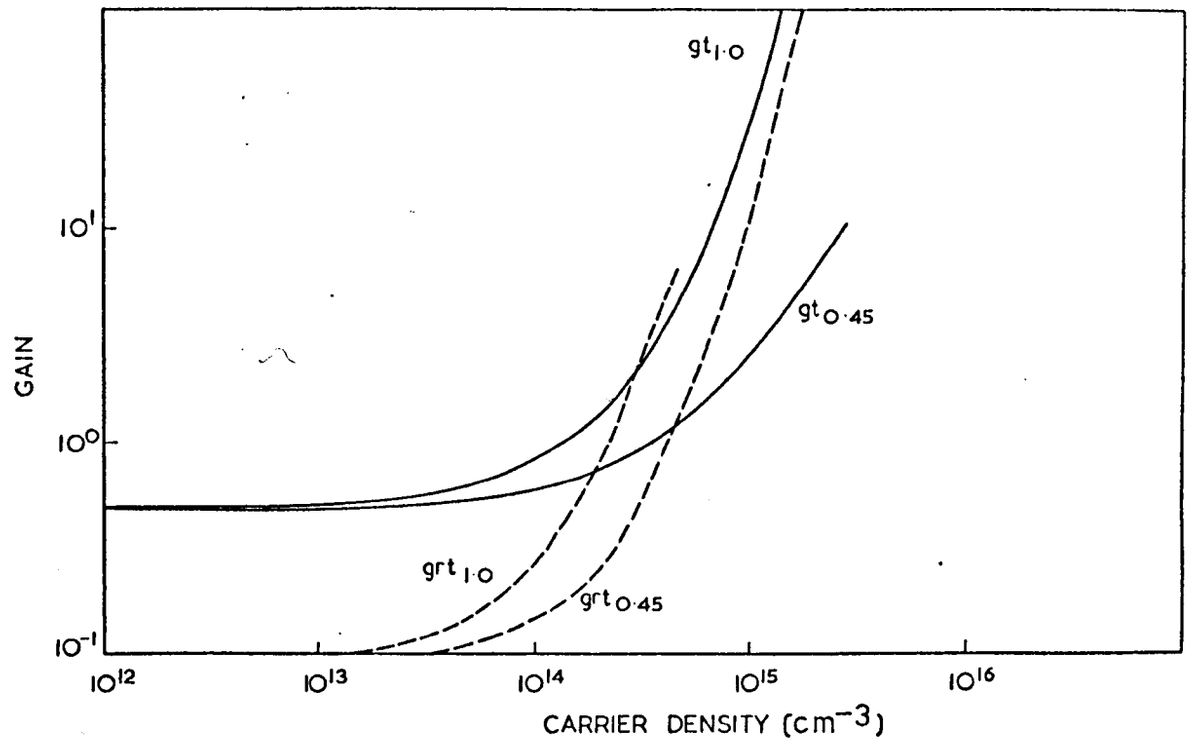

COMPUTED TRANSMISSION GAIN (gt) AND ROUND TRIP GAIN (grt) IN Ge AT 77°K AS A FUNCTION OF FREE CARRIER CONCENTRATION USING THE FOLLOWING DATA.

LATTICE DIELECTRIC CONSTANT 16

MOBILITY = -300 +0·i

FREQUENCY = $3 \cdot 10^{10}$ rad / sec

THE SUFFIXES ON (gt) AND (grt) REFER TO THE LENGTH OF THE SPECIMAN IN THE PROPAGATION DIRECTION (CMS)

FIG 1

In point of fact K_{osc} is defined for a 1 cm long specimen. Specimens of other lengths would have somewhat different values of K_{osc}. This feature has been pointed out in Section 2; it arises because, although the product "N.A." certainly defines a well defined gain for a specimen of given mobility and at a given frequency, the boundary reflection loss from the cavity is itself also free carrier concentration dependent. (Owing to the free carrier contribution to the total effective dielectric constant of the material). Thus "N.A." defines a discrete gain, but the gain necessary to establish round trip gain itself varies with free carrier concentration. Hence, the necessary value of N.A. for oscillation to occur is a weak function of free carrier concentration. This feature is demonstrated in Figure 1, where theoretical gain is plotted against free carrier concentration for samples of two different lengths, but otherwise similar characteristics, which appear in the legend. The curves are obtained using the equations developed in Section 2. It will be observed that the curve "g r t", which is a plot of the round trip gain within the cavity, passes through unity gain, which is of course the oscillation threshold, at a free carrier concentration which when multiplied by the specimen length is not constant from specimen to specimen. The curve "g t" in these figures demonstrates that similar length dependence is found in the N.A. product necessary for insertion amplification. In view of the foregoing remarks, it is clear that the N.A. product can only be used as a convenient approximate guide in selecting an experimental regime.

The stability requirements serve to define an aspect ratio of the specimen $\frac{A}{L} \gtrsim 10$, which contrasts sharply with the geometry of normal Gunn devices. The aspect ratio of conventional Gunn devices is very much closer to 0.2 - 2.0,

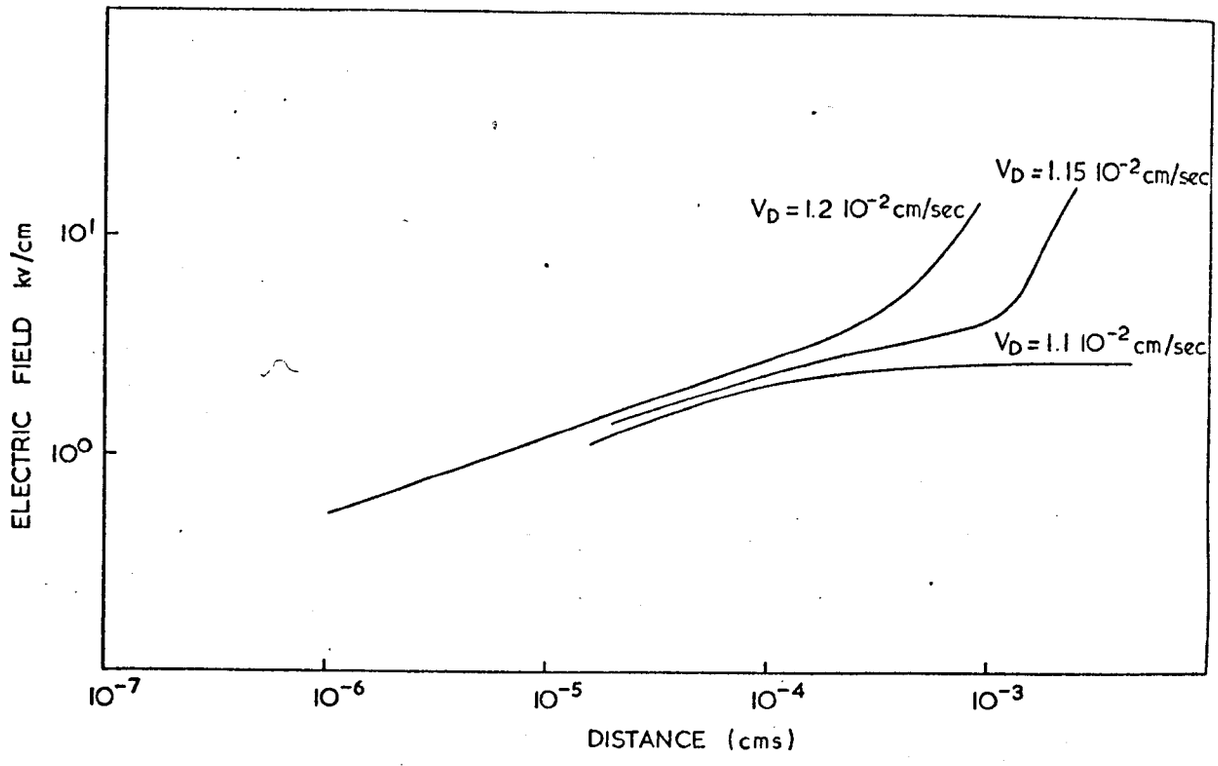

SPATIAL DISTRIBUTION OF ELECTRIC FIELD IN Ge AT 77°K CALCULATED USING THE VELOCITY FIELD CURVE OF FAWCETT et al AND THE FOLLOWING DATA:

FREE ELECTRON CONCENTRATION = $8{\cdot}0\ 10^{14}/cm^{-3}$
(ZERO APPLIED FIELD)
LATTICE DIELECTRIC CONSTANT = 16

RESULTS ARE SHOWN FOR TWO DIFFERENT ELECTRON DRIFT VELOCITIES (CURRENT DENSITY IN ARBITARY UNITS) AT THE CONTACT

FIG 2

as indeed it should be since it exploits space charge rather than electromagnetic instability.

This large aspect ratio of $\frac{A}{L} \gtrsim 10$ is responsible for a recurrent problem associated with the low specimen impedance, and in particular the difficulty of matching it to a high voltage pulse generator. Any attempt to increase specimen impedance by making N.A. very much less than K_{osc} will reduce the size of the desired free carrier modulation of the microwave signal. Equally L must be maintained as large as possible, consistent with stability, in order that specimen impedance is maintained high.

3.2.2 Non-uniformity of Biasing Electric Field

Having inhibited space charge instability by choice of a suitably low N.L. product, the discussion of Section 2 indicates that a spatially non-uniform biasing electric field distribution is to be expected within the sample. Using the procedures described in Section 2, this electric field distribution has been computed for n-Ge using data which is tabulated in the legend of Figure 2.

In Figure 2 the theoretical results are presented. The characteristic rise of the electric field to a uniform value within about one micron of the metallic contact is seen for low current densities, where even the highest fields lie in the positive conductivity region of the velocity field characteristic. At higher current densities, the behaviour at low fields near to the contact remains qualitatively unchanged, whilst the behaviour once the electric field exceeds the threshold value is quite different.

The figure demonstrates that the non-uniformity of the biasing electric field is severe. Its consequences for the diagnostic potential of the proposed bridge measurement are immediate. At low fields, such that no part of the specimen is in the N.D.C. region the

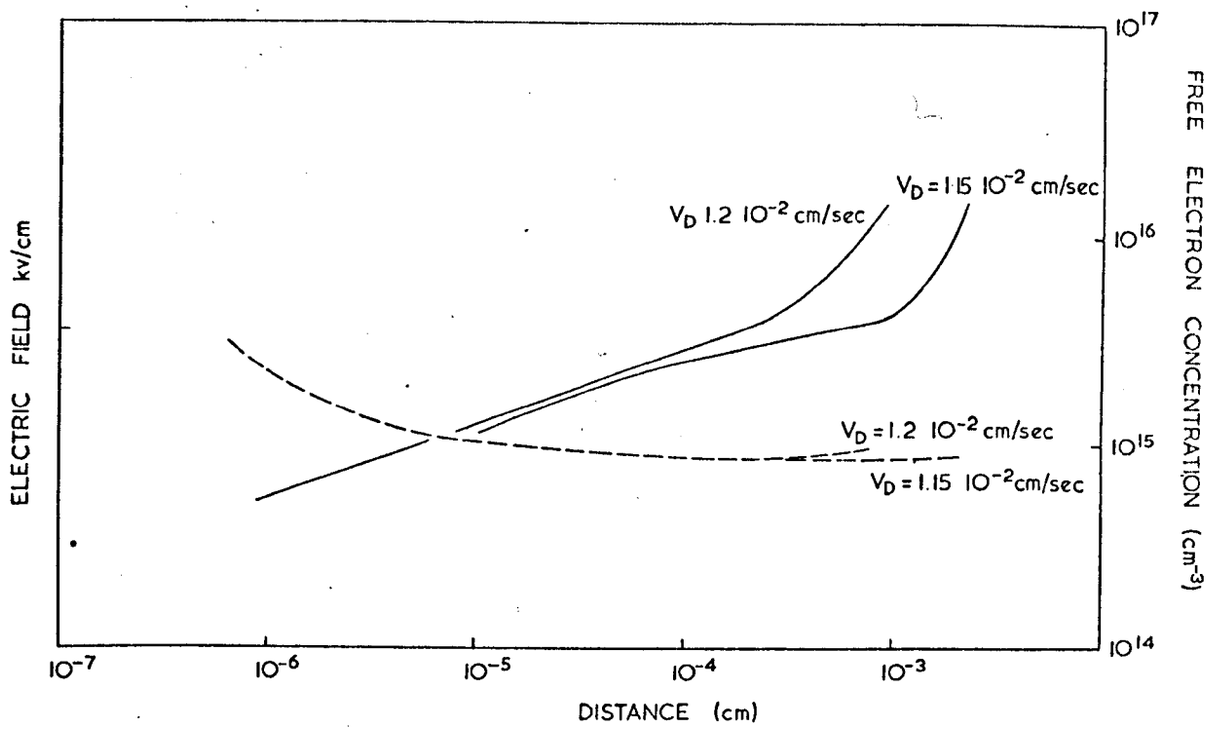

SPATIAL DISTRIBUTION OF ELECTRIC FIELD (SOLID LINE) AND FREE ELECTRON CONCENTRATION (BROKEN LINE) IN Ge AT 77°K CALCULATED USING THE VELOCITY FIELD CURVE OF FAWCETT et al AND THE FOLLOWING DATA

FREE ELECTRON CONCENTRATION = 8 10^{14}/cc FOR ZERO APPLIED ELECTRIC FIELD

LATTICE DIELECTRIC CONSTANT 16

THRESHOLD FIELD = 3·5 kv/cm

FIG 3

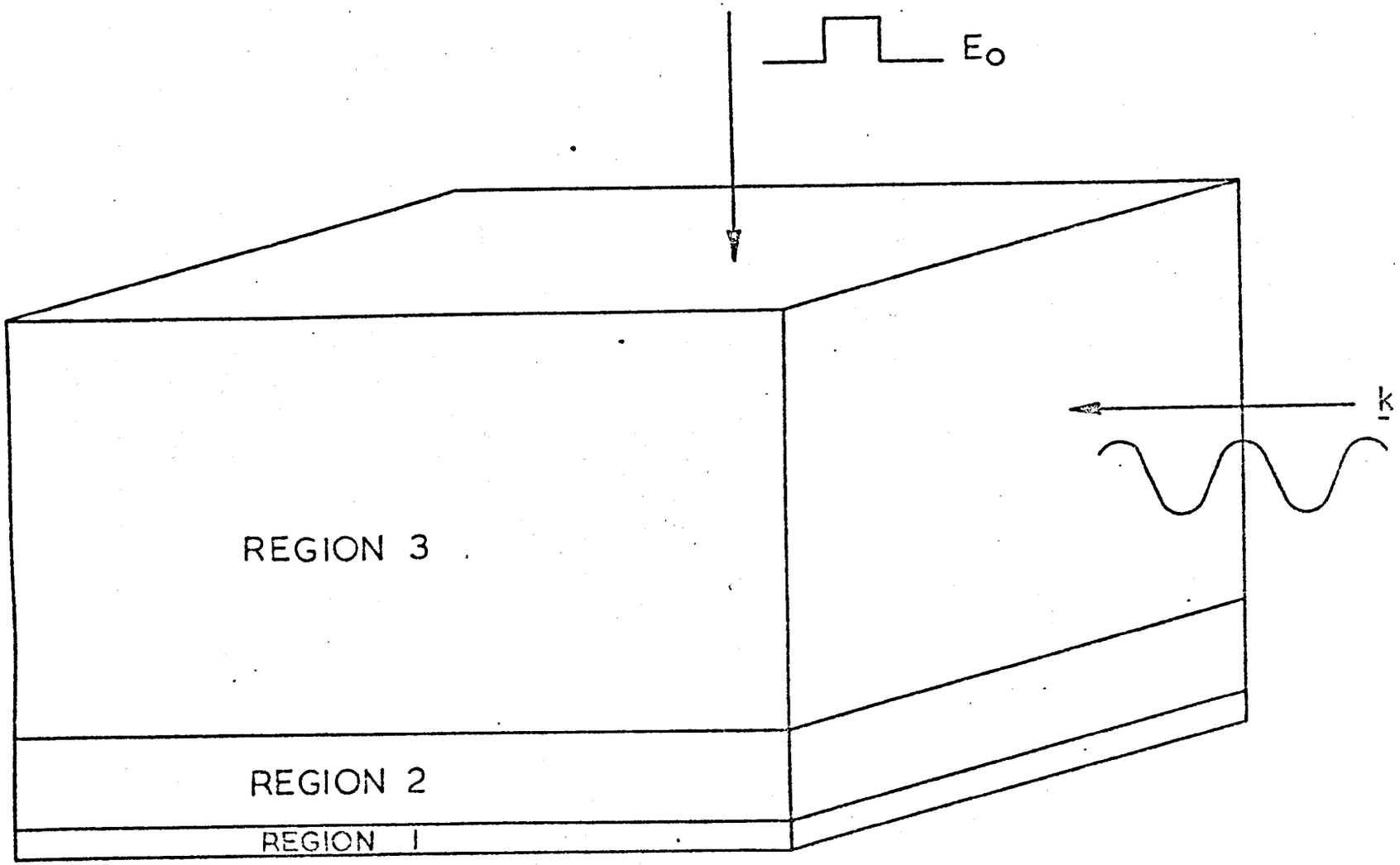

SCHEMATIC DIAGRAM OF THE REGIONS OF DIFFERENT RESISTIVITY WITHIN A SPECIMEN BIASED BEYOND THE THRESHOLD FOR N.D.C.

FIG 4

measurement remains valid. At higher fields, the microwave energy is effectively distributed within a stratified medium; as shown in Figure 4. In this figure we distinguish three major strata. Region one, near to the cathode, has positive conductivity and is therefore lossy. It is, however, a small region according to the data shown in Figure 2, being about one micron in total thickness.

Region two is one of strong non-uniformity of the electric field, and, in consequence, of the free carrier concentration and the effective permittivity. Figure 3 shows the distribution of the free electron concentration through the specimen. (In Section 5 we shall see that the concentration non-uniformity is much larger in GaAs specimens in consequence of the larger magnitude of the N.D.C.) Region two is a region in which energy is supplied to the wave rather than being extracted from it as is the case in region one.

Region three is of considerable interest owing to its size. In this region the velocity field curve may be saturated, or have a slight positive conductivity. Thus conductive losses in this very large region are either zero or very small.

It is thus clear that once the threshold field for N.D.C. is exceeded, the striation of the specimen will introduce an averaging effect into the measurement made by the microwave probe. Any negative mobility observed is, therefore, a minimum value, in contrast to measurements below threshold, which are, in principle, directly meaningful. (In the latter case we ensure that field gradients near to the contacts are unimportant by having specimens very much thicker than the micron or so over which contact effects extend).

3.2.3 Frequency Limit

We turn now to the complexities of the transport process comprised within the terms σ_r and σ_i. The microwave electric fields are small in comparison to the bias field in the present experiment, and therefore an incremental conductivity, appropriate to a particular bias field, may be used in the equations of section two for the complex wave-vector. It is well known that this conductivity will not necessarily be equal to the "slope" conductivity, as defined by the gradient of the velocity-field characteristic. Indeed, the present experiment resembles the work of Gibson et al[1] in which the microwave conductivity of a positive resistance sample was studied. Following the philosophy of that work, we conclude that in order that the T.E.M. wave may follow the N.D.C. both $\omega\tau_M < 1$ and $\omega\tau_\epsilon < 1$ are necessary. (Here τ_M and τ_ϵ are the momentum and energy relaxation times respectively). However, there is currently little doubt that the N.D.C. in n-Ge is a transferred electron effect[3], and recent work on the N.D.C. in GaAs has shown that the frequency limitation[4] for observation of an N.D.C. lies well below that suggested by a simple relaxation time approximation. Thus, whilst an upper frequency limit for observation of growing waves clearly exists, it is dangerous to imply its value from a simple model of the transport in n-Ge. Guidance in the choice of angular frequency of the wave is therefore sought from other experimental data.

A number of workers have shown that in the warm electron regime, n-Ge shows significant "$\omega\tau$ effects" at 9 GHz [6] with a lattice temperature of 77°K. In the hot electron, regime the work of Koenig[7] suggests, (and we now believe) that non-equivalent intervalley scattering becomes an important process.

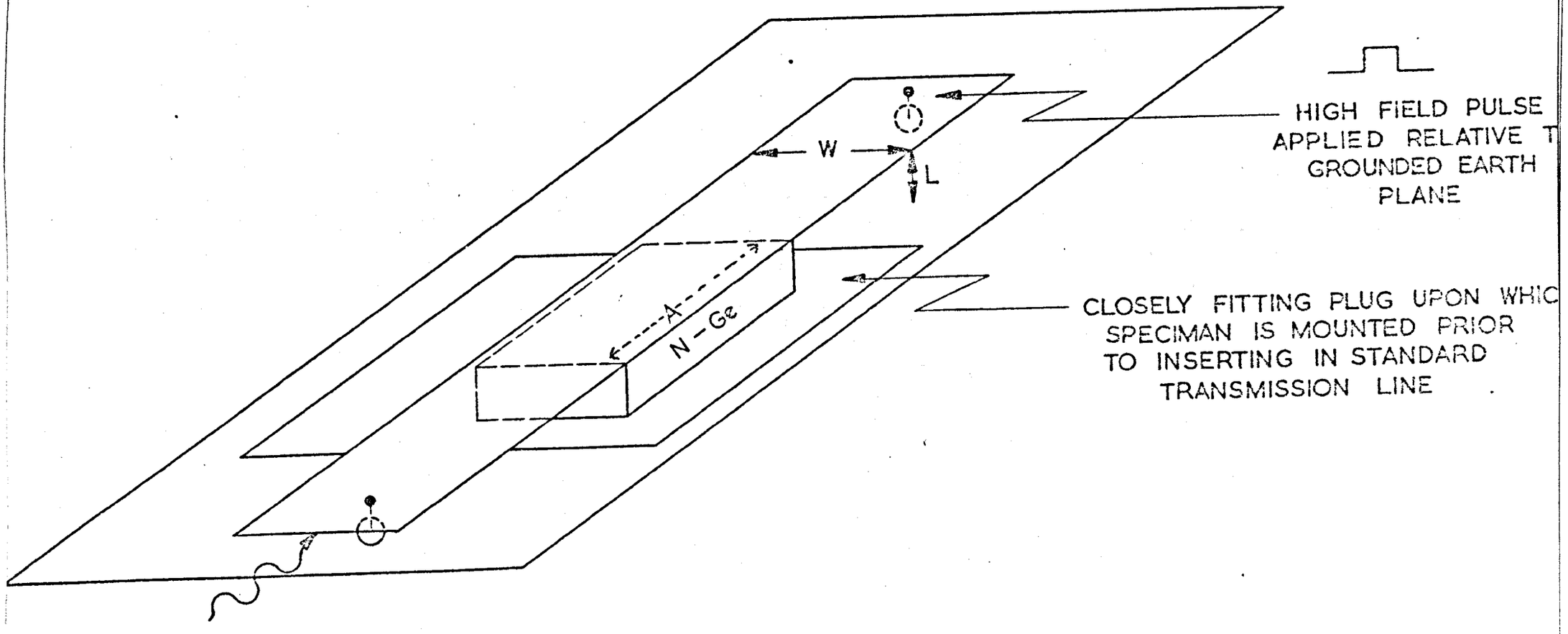

SPECIMAN MOUNT IN MICRO-STRIP TRANSMISSION LINE

FIG 5

Thus the foregoing data may not be relevant to the N.D.C. regime. However, using Morgan's [5, 6] technique, Zuker et al[8] have shown that with a frequency of 2.85 GHz the microwave and slope conductivities are in agreement throughout the warm and hot carrier regions. Therefore, in the light of this data, a frequency of of 3 GHz or less is desirable in the present work, in order that the measurement may be valid for all bias fields between zero and the threshold for N.D.C.

3.3 Summary of Experimental Constraints, Leading to a Finalised Experimental Scheme

The foregoing discussion has served to focus attention upon a bridge measurement to be performed at 77°K, in order that important diagnostic measurements may be made upon the weak N.D.C. existing in n-Ge at this temperature. Under these conditions the problems of non uniformity are minimal. The frequency is to be 3 GHz or less, N.A. $< 2.2 \times 10^{14}$ cm^{-2} and N.L. $< 2 \times 10^{13}$ cm^{-2} are required, and the specimen aspect ratio in two of its dimensions is to be of the order of ten.

Further constraints are applied by :

i) the necessity of retaining a reasonably high specimen impedance in order that high field pulses may be applied to it.

ii) problems of making the specimen "load" any chosen microwave circuit.

iii) the necessity of having microwave and biasing electric fields parallel to each other, and the <100> crystallographic direction.

Microstrip transmission line is chosen as the most convenient microwave environment for the specimen, which is compatible with the foregoing restrictions. (see Figure 5) Waveguide is too large at these frequencies, whilst coaxial line cannot be used owing to the crystallographically directional properties of the N.D.C. in n-Ge.

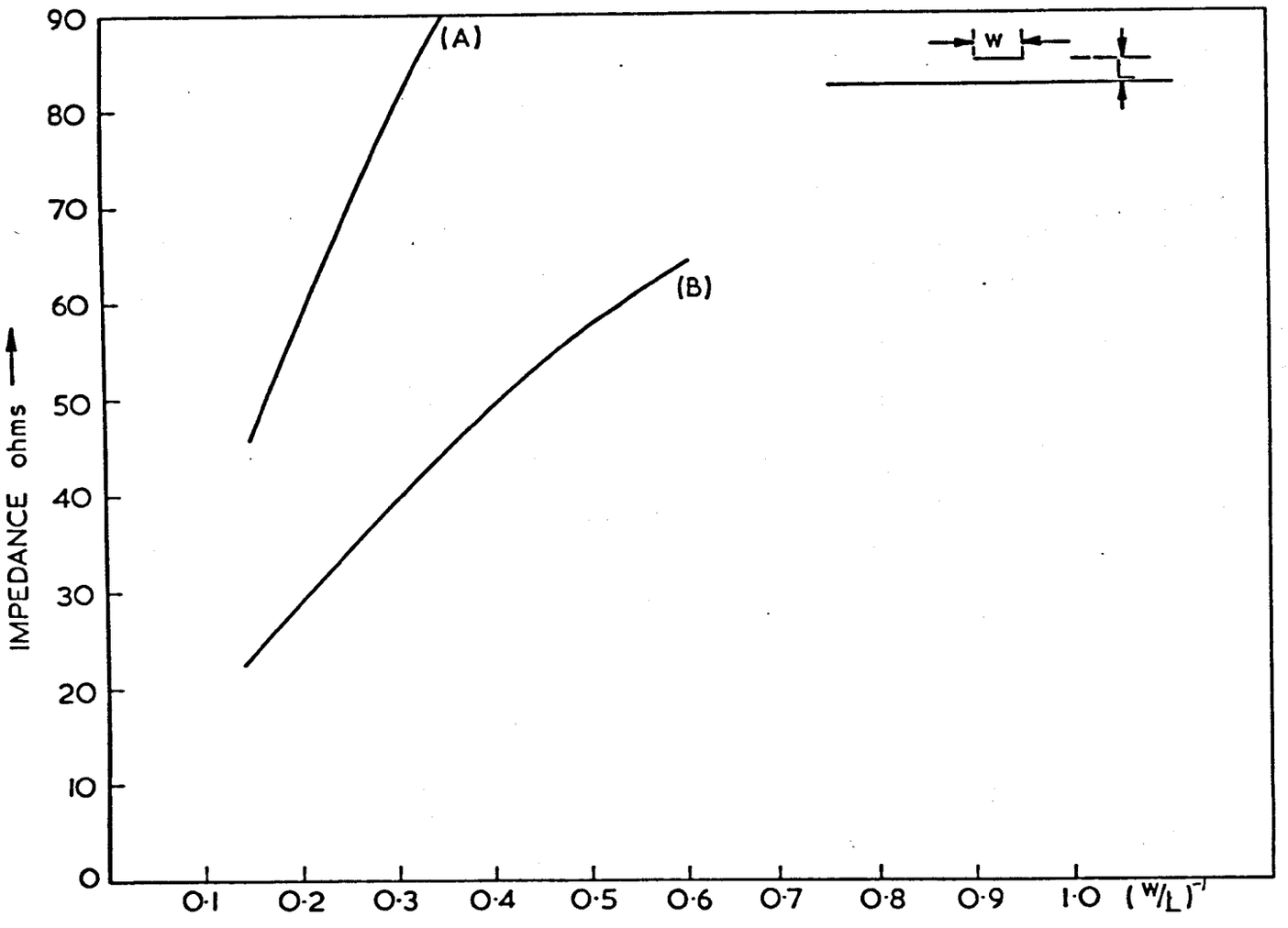

THEORETICAL MICROSTRIP IMPEDANCE AS A FUNCTION OF TRANSMISSION LINE ASPECT RATIO $(W/L)^{-1}$ FOR A UNIFORM AIR DIELECTRIC IN CASE 'A' AND A SILICONE FIBRE-GLASS DIELECTRIC ($\epsilon = 4.18$) IN CASE 'B'

FIG 6

3.3.1 Microstrip Transmission Line

The properties of simple configurations of microstrip transmission line are by now well understood[9]. This transmission line supports a T.E.M. wave, thus satisfying the polarisation requirement, for the oscillatory microwave field is necessarily parallel to a biasing field applied between live and ground planes. It has no cut-off wavelength, so that the W dimension, in Figure 5, can be made small. In consequence, the remaining unspecified specimen dimension (that dimension normal to both the biasing field and the propagation direction) becomes small. We shall now demonstrate that this renders it possible to match the high field pulse source into the specimen whilst still allowing the specimen to offer a good filling factor to the transmission line.

The calculated relationship between the microstrip impedance and W/L is shown in Figure 6 for the case when the whole of the half space above the earth plane is filled with a uniform dielectric medium. Approximately 75% of the microwave flux is concentrated in the region between live and ground planes[10], and we therefore propose filling only this region of the transmission line with Ge. The high dielectric constant of Ge will of course increase the fraction of microwave energy confined within the specimen volume.

Using the approximate aspect ratio of 10 already introduced, we note that the specimen resistance is (see Figure 5)

$$R_{spec} = \frac{\rho L}{A.W.} = \frac{1}{n A} \cdot \frac{L}{W} \cdot \frac{1}{e \mu}$$

$$= \frac{1}{n L} \cdot \frac{1}{10} \cdot \frac{L}{W} \cdot \frac{1}{e \mu}$$

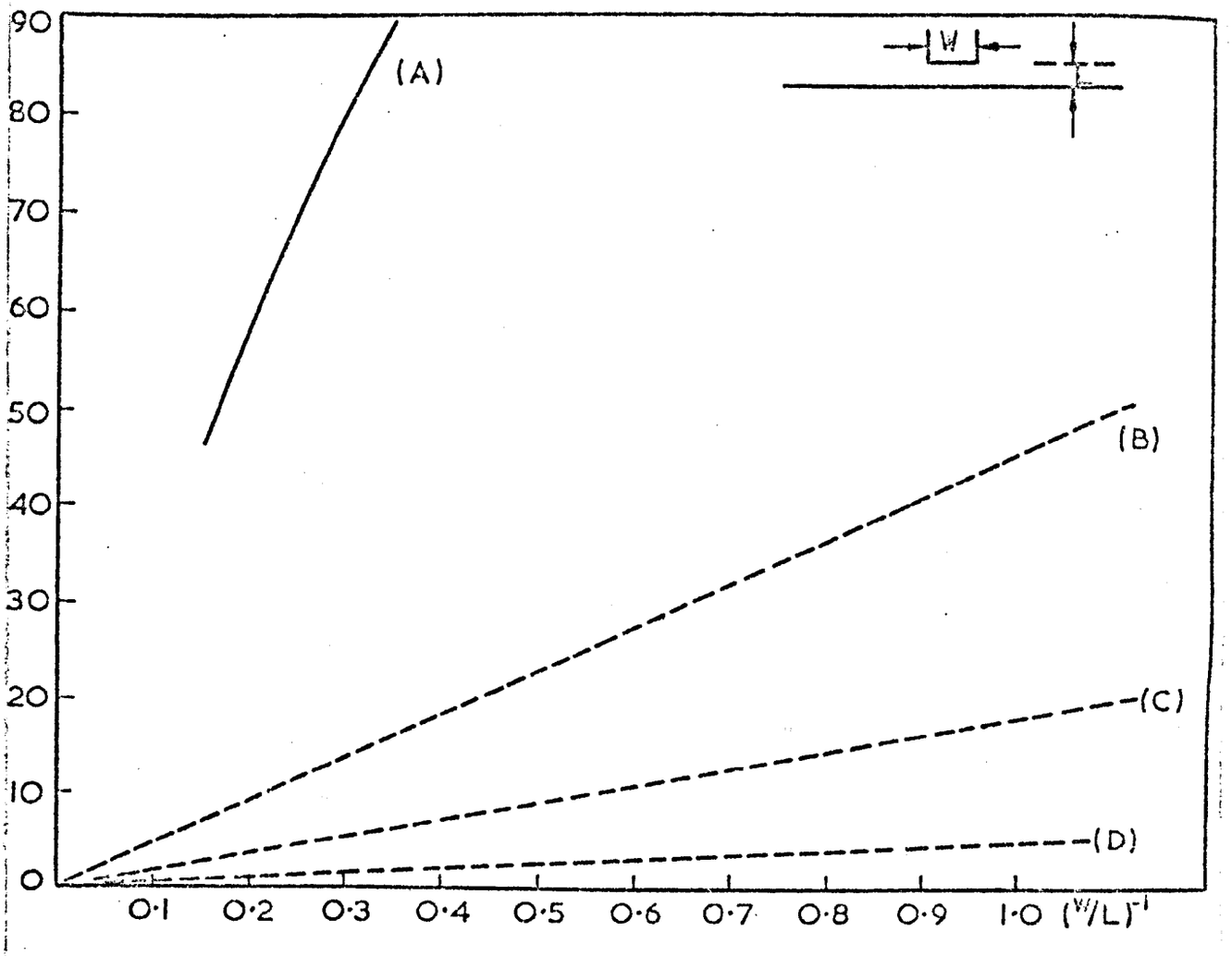

THEORETICAL MICROSTRIP IMPEDANCE FOR AIR DIELECTRIC AS A FUNCTION OF MICROSTRIP ASPECT RATIO $(W/L)^{-1}$ IS SHOWN AS CURVE A CURVES B, C AND D OF SPECIMEN IMPEDANCE WITH $na = 0 \cdot 4K_{osc}$, K_{osc} AND $4 \cdot K_{osc}$ RESPECTIVELY. IN EACH CASE THE SPECIMEN OCCUPIES THE SPACE BELOW THE LIVE PLANE ONLY. (THE CHORD MOBILITY AT THE THRESHOLD FIELD IS USED IN DERIVING THE PRESENT DATA).

FIG. 7

SCHEMATIC DIAGRAM OF MICROWAVE BRIDGE

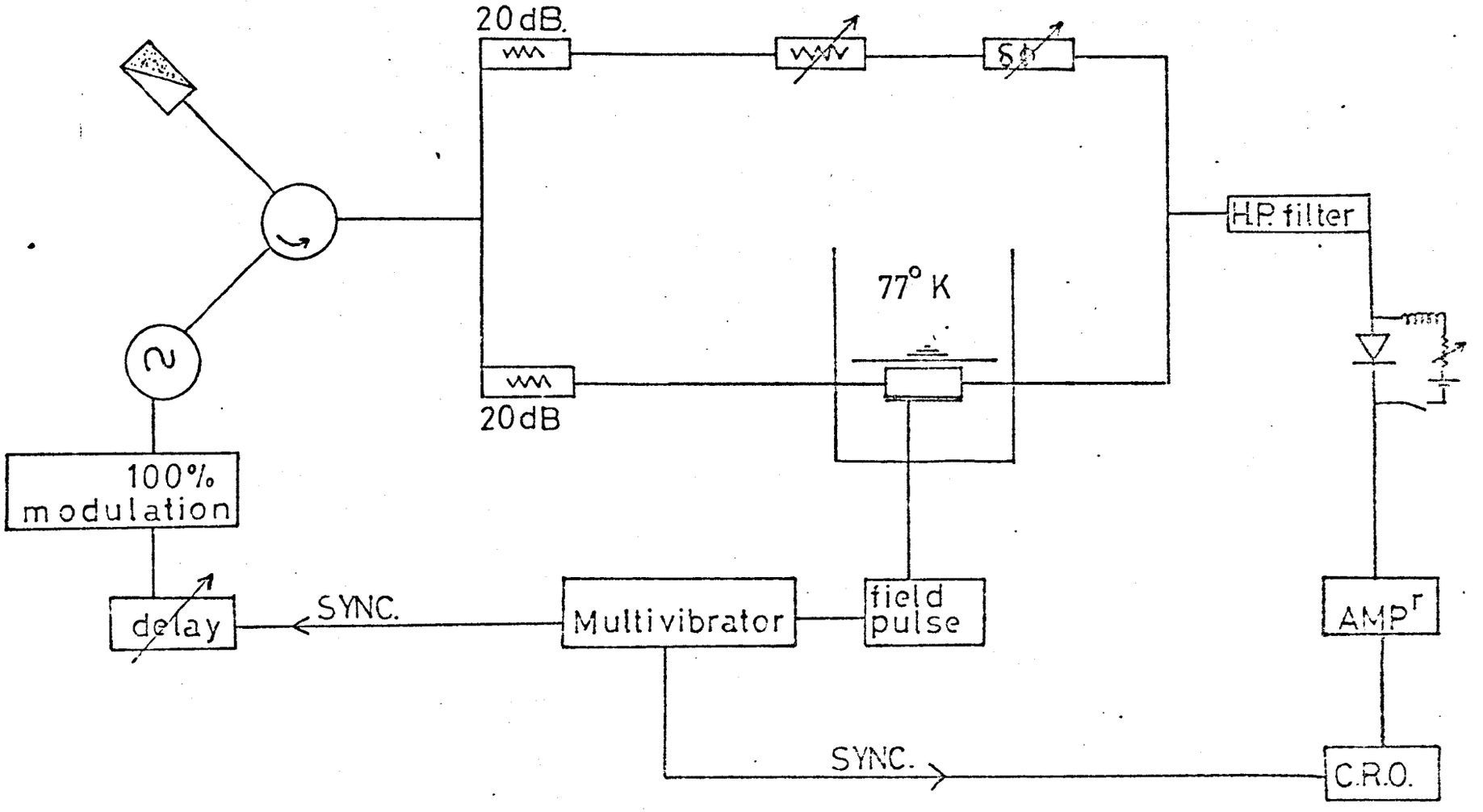

FIG 8

Where the resistivity $= \frac{1}{n e \mu}$, and the specimen width is W since it fills the area below the live plane.

Thus the specimen resistance is readily superimposed upon the impedance data of Figure 6 for a variety of N.L./N.A. products, as in Figure 7. It is clear from this data that a quite reasonable specimen impedance, ($3\frac{1}{2}$ ohms) a microstrip impedance of 50 ohms, and a large microwave filling factor, in excess of 75% with N.A. = K_{osc} (i.e. at the point of insertion gain) can all be achieved simultaneously in this geometry. This contrasts with experience in waveguide where other workers have found difficulty in maintaining simultaneously high filling factors and specimen impedances[1].

3.3.2 The Experimental System

The complete experimental system is shown schematically in Figure 8. With the exception of the specimen mounted in microstrip, all of the elements are coaxial transmission line units, these being the only ones available at this frequency. The phase shifter is in fact a line stretcher, phase measurements being obtained by simply measuring the overall physical length of the stretcher, and relating this to the wave-length in this air cored coaxial line.

The transformation from coaxial to microstrip transmission line is of course of some importance since this is an interface between a balanced and unbalanced transmission line. The "Balun" is made, following the prescription used successfully by other workers[9]. However, it was found that this device could give rise to mismatch reflections. In order to minimise the importance of any such reflections, 20 dB attenuators were placed within the bridge in such a way as to optimise the single transit signal in relation to any signal multiply reflected within the bridge circuit. Similarly,

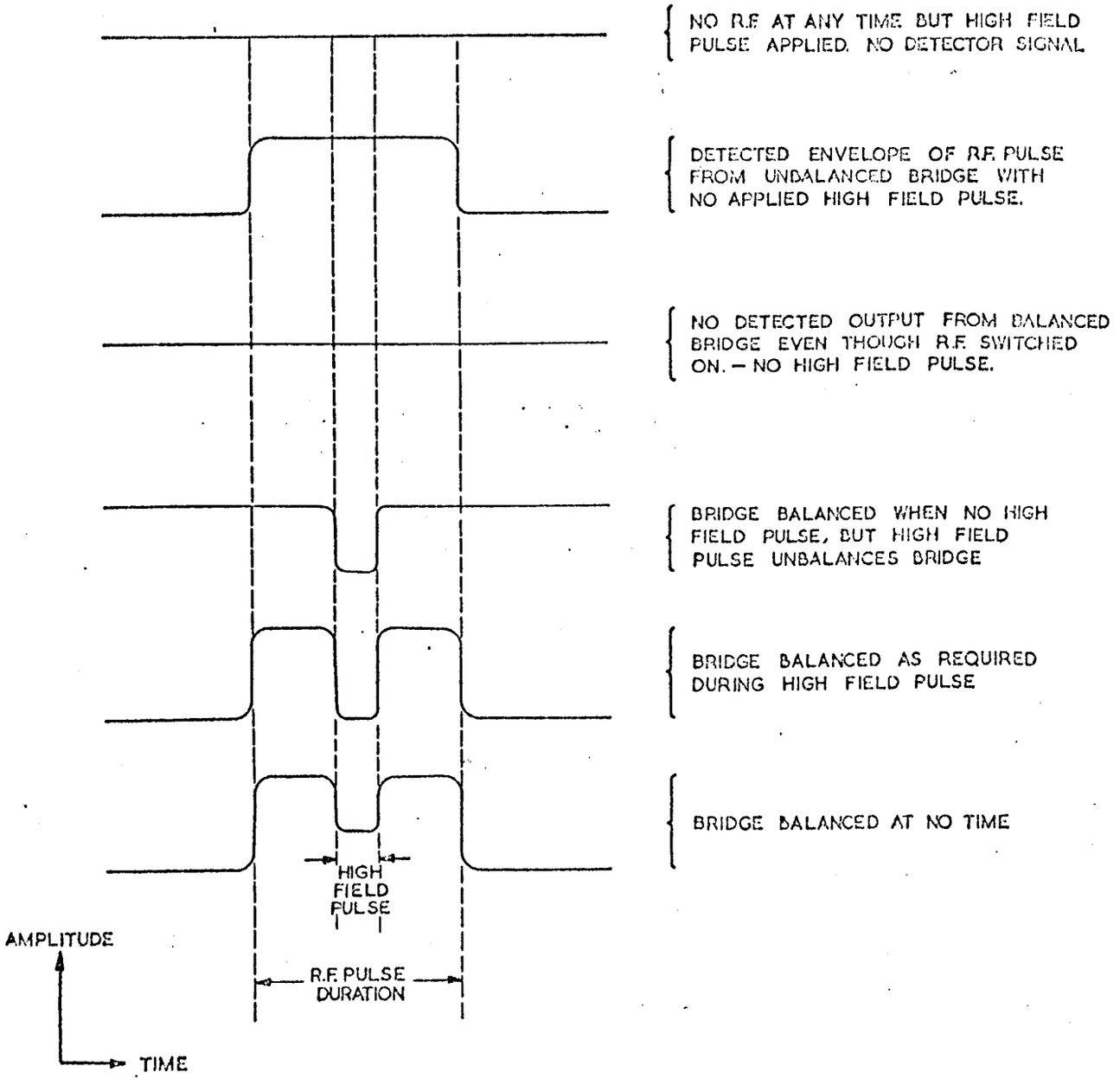

WAVE-FORMS ENCOUNTERED IN BALANCING MICRO-WAVE BRIDGE

Fig 9

inclusion of the circulator to isolate the bridge and R.F. source proved essential for reliable measurements.

The high pass filter (600 MHz) allows the microwave power to reach the detector diode and succeeding equipment, whilst preventing the high field biasing pulse reaching the detector. Thus any spurious effects, owing to the high field pulse accidentally biasing the detector diode and thus changing its sensitivity, are avoided. An intentional biasing facility which allows the diode sensitivity to be optimised during the balancing of the bridge is however included.

Having detected the envelope of the microwave radiation, and then imposed subsequent stages of A.C. gain, there is clearly some uncertainty concerning the D.C. level which corresponds to zero microwave power, emergent from the balanced bridge. This problem is overcome by the synchronising loop which locks a 100% modulation of the microwave signal to the high field pulse in the manner shown schematically in Figure 9. (An identical technique was used by Gibson et al[1] in their bridge measurements).

3.3.3 Specimen Problems

Fabrication of the specimen and maintaining it at 77°K was expected to provide no problem. The latter requirement was, in fact, readily satisfied, by immersing the complete microstrip assembly in liquid nitrogen slowly, in order to avoid thermal shocks to the specimen. (When the bridge was balanced with no specimen in the microstrip line, immersion of the microstrip line in a liquid nitrogen bath did not disturb the bridge's balance). However, in spite of careful cooling, considerable difficulty was experienced in forming contacts which were capable of withstanding the cooling cycle.

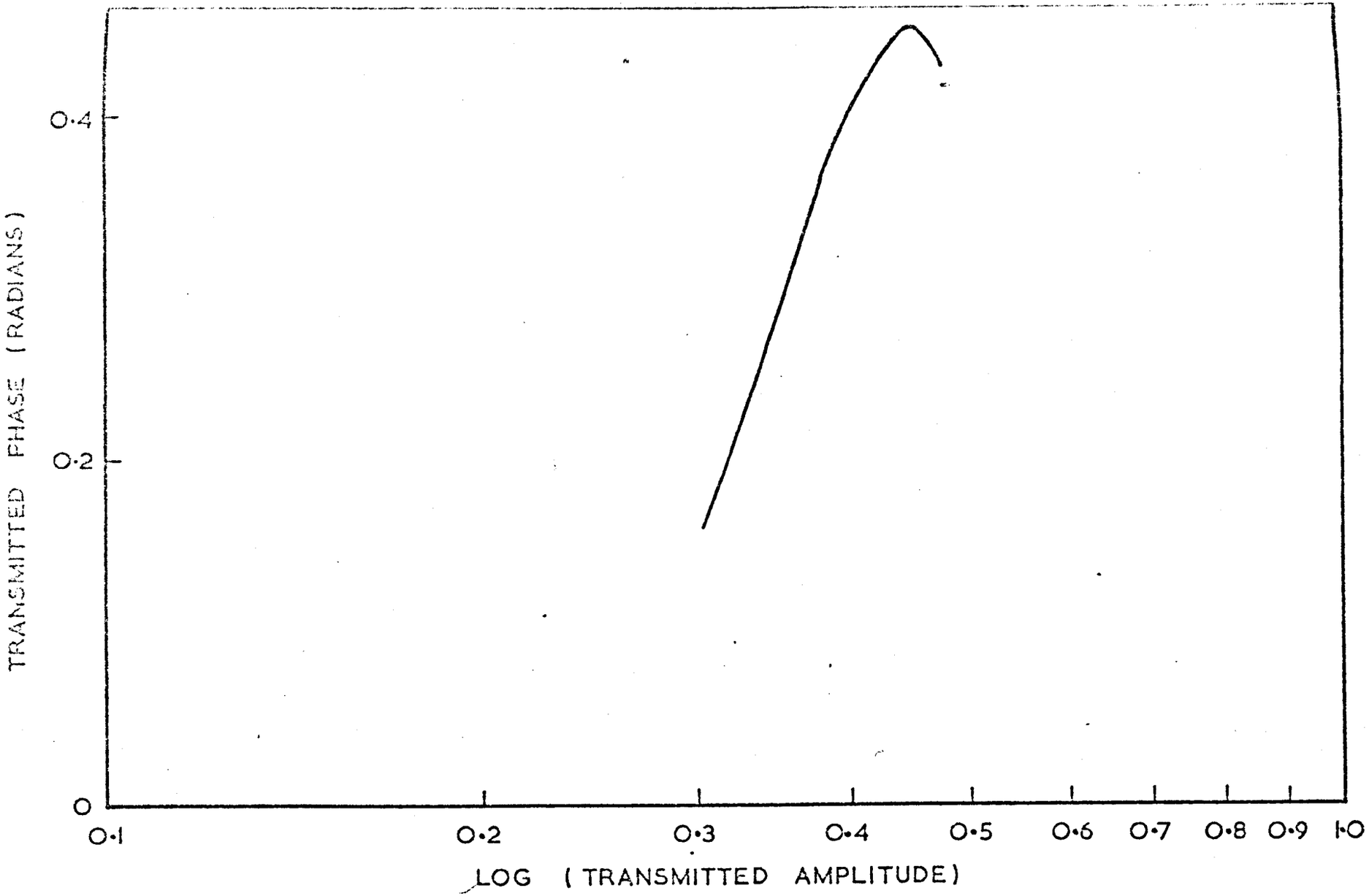

FIG.10. PHASE AND AMPLITUDE OF TRANSMITTED SIGNAL FOR A SPECIMEN OF 5·7Ω CM Ge AT 77°K ELECTRIC FIELD APPLIED ALONG <100> DIRECTION

It was found that the problems arose from the unusually large contact area employed in the present experiment (0.5cm by 0.5 cm) and the thermal mismatch between specimen and contact plate. The problem was finally solved only when it was found that gold plated Kovar could provide a good thermal match to Ge. When this was used as contact material, in a normal gold/germanium eutectic junction, it provided an entirely satisfactory bond, capable of withstanding numerous thermal cycling events.

3.3.4 Measurement

Measurements of the phase and amplitude settings required to produce a balance during a high field pulse were made as a function of applied electric field on a range of more than thirty samples.

3.4 Analysis of Results

In analysing these results, it is clearly necessary to take account of the immediate microwave environment in which the sample is placed. The theory of microstrip transmission line in an infinite dielectric medium has already been mentioned, and is fairly well established. Some work has also been done in which the dielectric is restricted to an infinite sheet of thickness L and positioned between live and earth planes. No work is known of, in which the microstrip is loaded in the manner now proposed and shown in Figure 5. It has therefore been necessary to treat this configuration theoretically, in order that results may be analysed. This work is relegated to Appendix III in order to maintain continuity in the present discussion.

The experimental results are conveniently plotted on a phase/amplitude plane, each point upon this plane then corresponding to an observation at a known electric field strength. Typical results are shown in Figure 10. The origin of this phase amplitude plane is clearly arbitrary in as much as the length of the arms of the bridge is arbitrary.

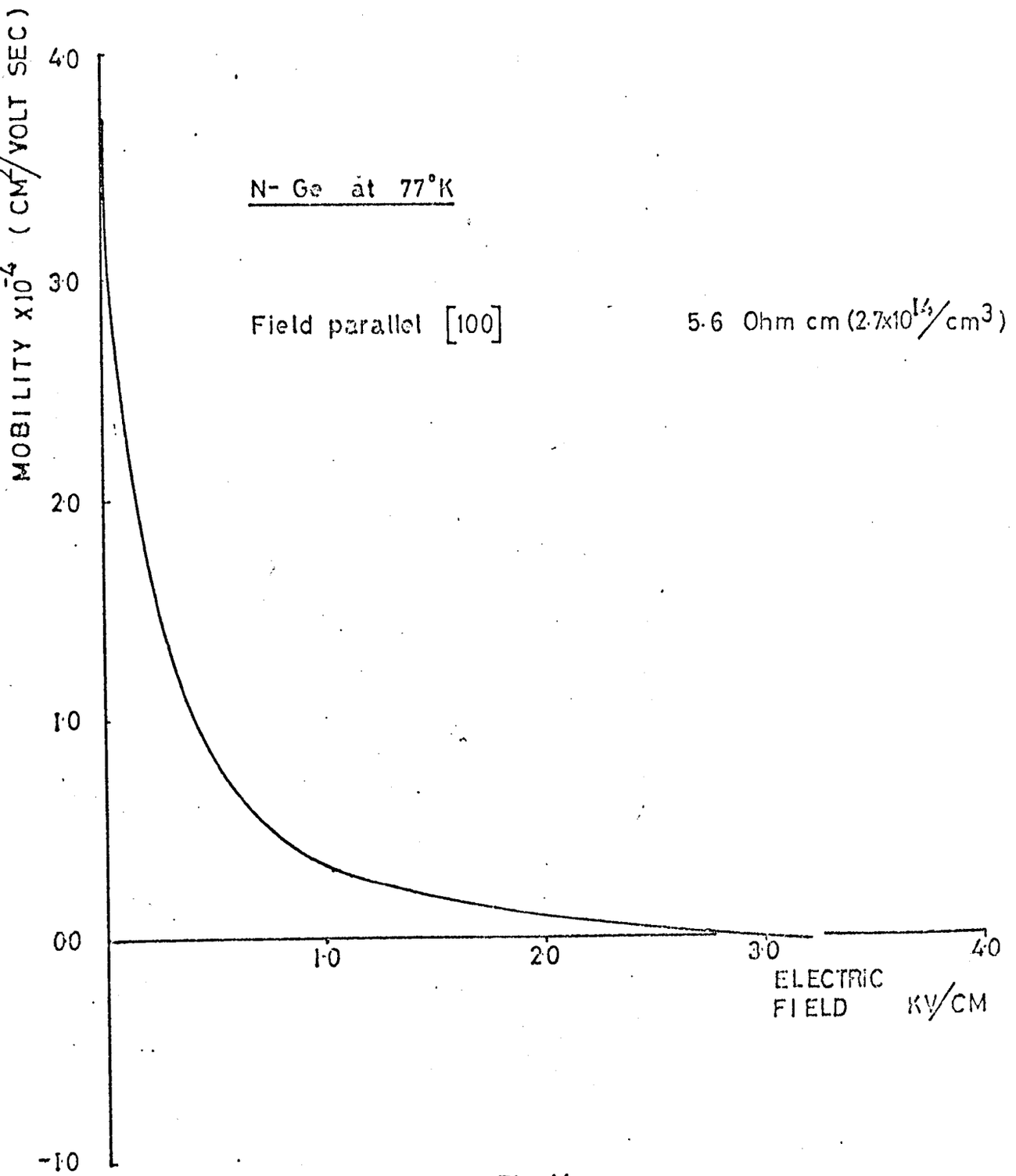

Fig 11

Electronic mobility as a function of applied electric field

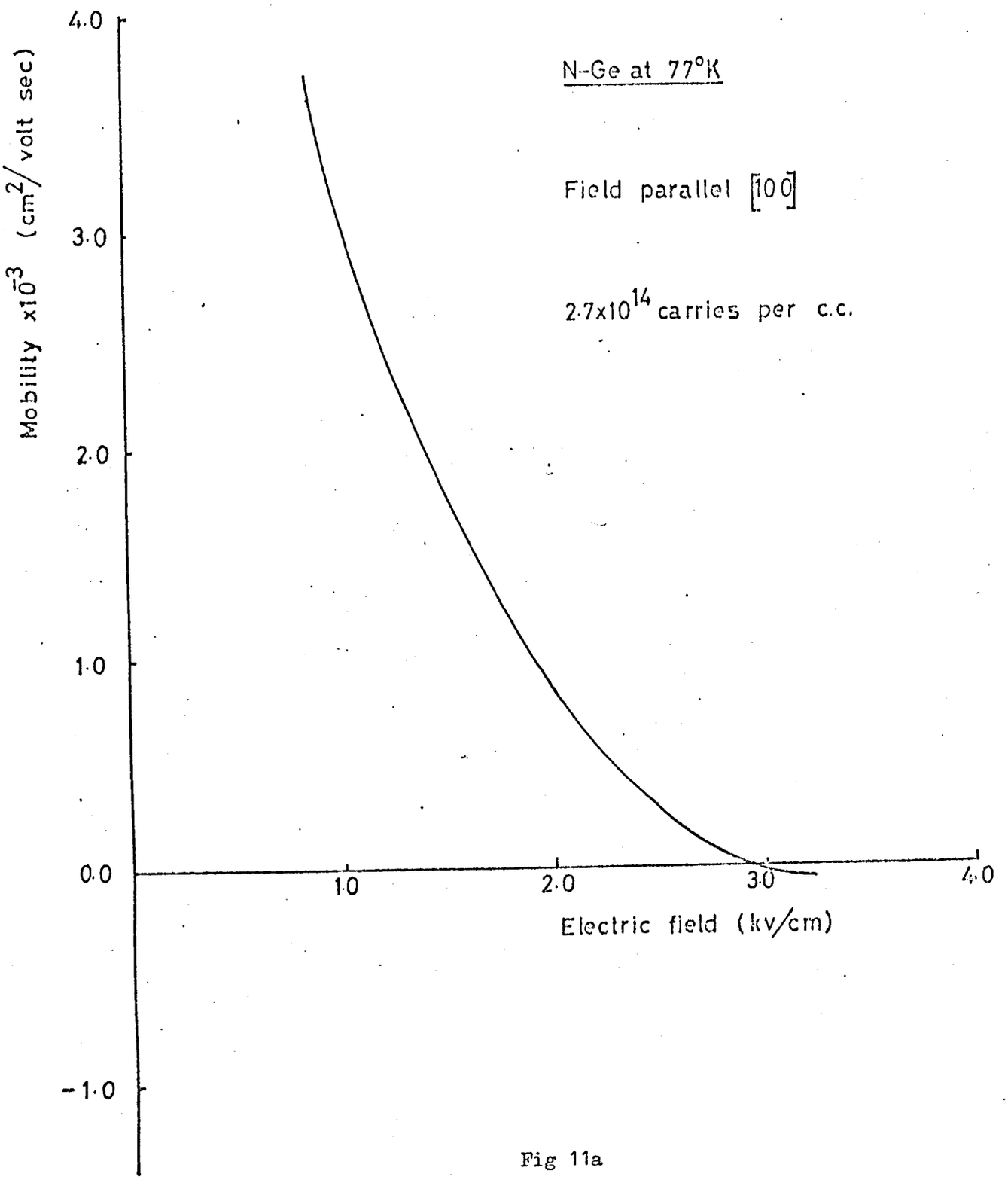

Fig 11a

Expanded plot of electron mobility as a function of applied electric field

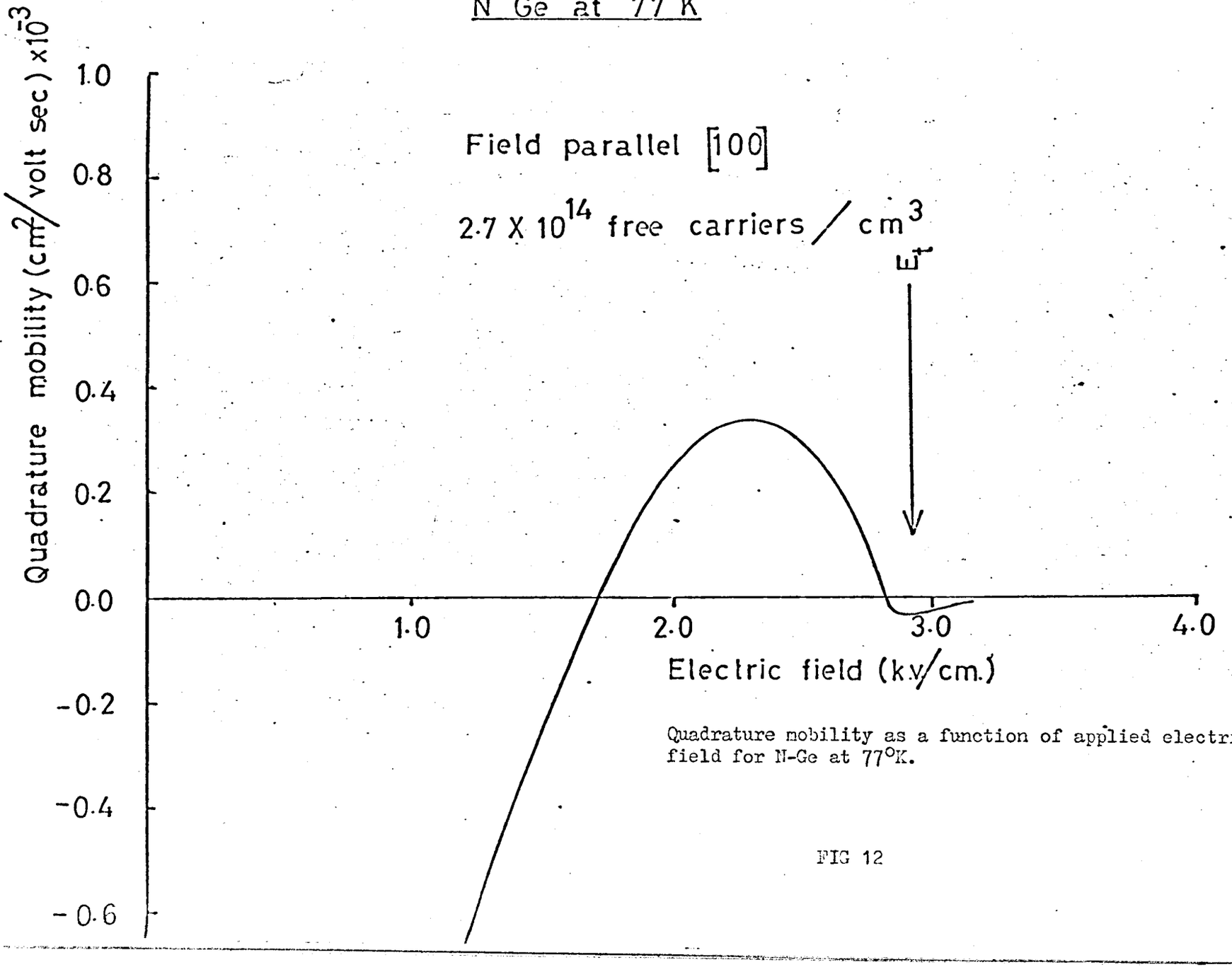

Quadrature mobility as a function of applied electric field for N-Ge at 77°K.

FIG 12

However, the zero field mobility is well known and may therefore be used as a reference point for analysis of the experimental results.

Appendix III provides an expression for the microstrip impendance in terms of the specimen dimensions and its (complex) mobility. Thus having a known specimen geometry, the phase and amplitude of a signal transmitted through the specimen may be evaluated for any assumed mobility. (The correction required to bring the origin of the theoretical and experimental phase/amplitude planes into coincidence is simply evaluated using the zero field mobility.) It is therefore possible to analyse the foregoing experimental results merely by guessing an initial mobility and subsequent successive approximation onto the observed signal phase and amplitude at each field strength.

A rather more elegant method of performing this analysis which includes the shift of origin of the theoretical phase amplitude space is however used. A set of values of the quadrature mobility (μ_i) and in phase mobility (μ_r) are used to compute a set of theoretical phase/amplitude points and these are plotted on a phase/amplitude plane with the same scale as the experimental data. Points of common μ_r can be joined, and similarly points of common μ_i can be joined forming a mesh. This mesh is then laid upon the experimental data and moved over it until the zero field experimental (phase/amplitude) point lies under the point on the mobility mesh which is equal to the known zero field mobility. Each remaining experimental (phase amplitude) point may then be read off directly as a mobility using the overlay mobility mesh. The data obtained by this analytic technique is shown in Figures 11 and 12. However, it should be mentioned that considerable difficulty is encountered in obtaining reliable, and reproducible results. This is often associated with specimens failing to load the microstrip, so that the majority of the microwave signal passed round the specimen rather than through it as is indicated in the microstrip analysis.

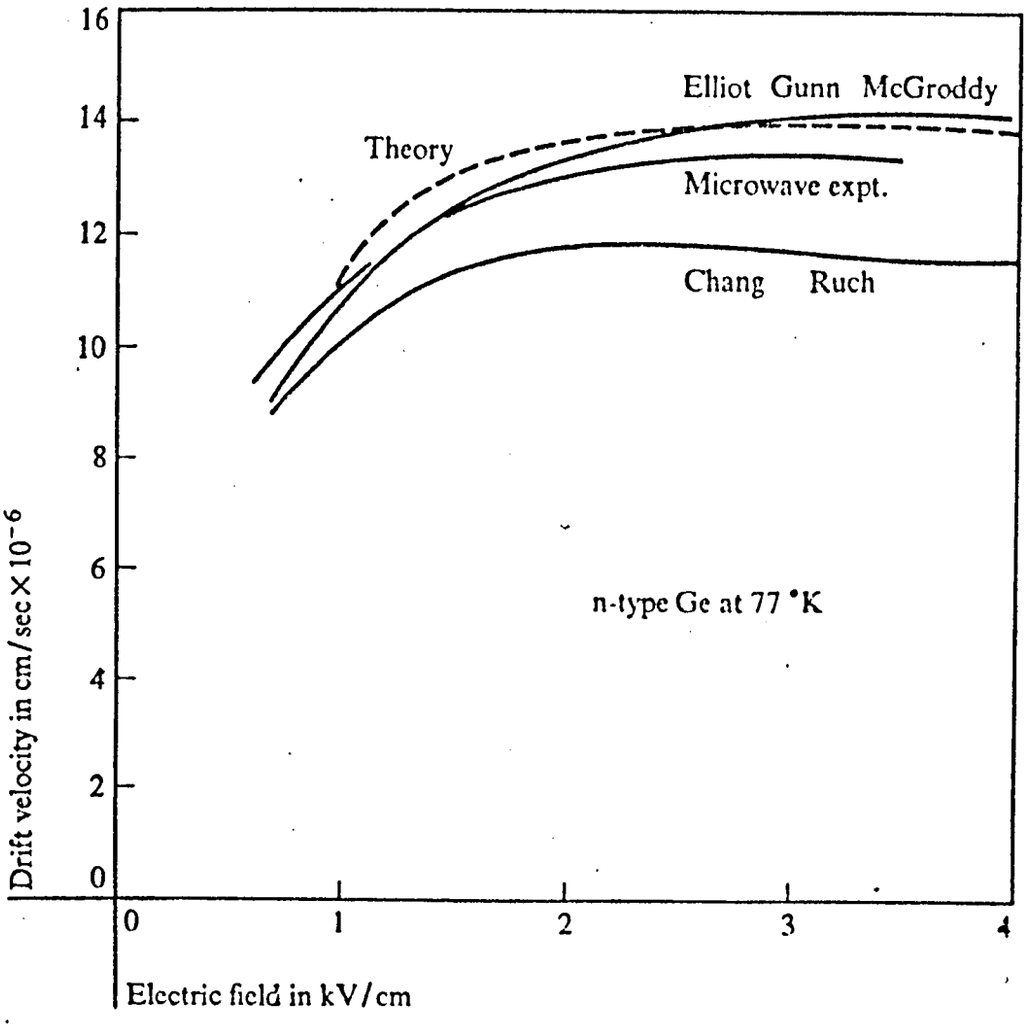

Drift velocity as a function of electric field. The broken curve is obtained by Paige
and the curve labeled "Microwave expt." obtained by integration of the results

Fig 13

TOTAL DIELECTRIC CONSTANT AS A FUNCTION OF ELECTRIC FIELD STRENGTH

N Ge at 77°K

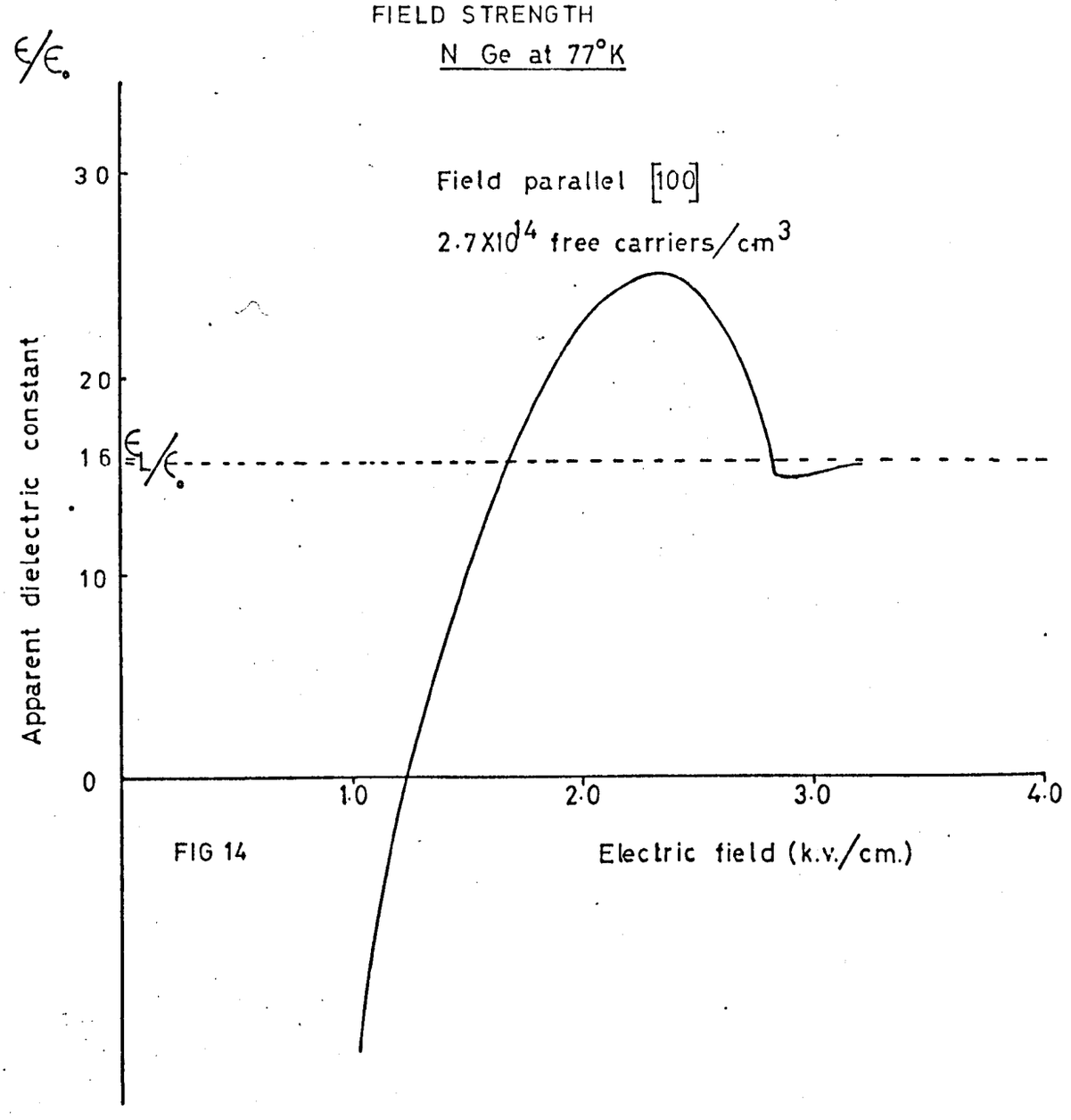

FIG 14

The real part mobility versus field plot shown in Figure 11 may clearly be integrated to provide a velocity field curve. Such an integration has been performed yielding the results shown in Figure 13. Comparison is made here with the theoretical velocity field curve obtained by Paige[11], and other experimentally evaluated velocity field curves. It will be seen that the present experimental data compares well with that of other workers. The theoretical data is fitted to this data and its approximate agreement is not therefore meaningful except in so far as it validates the theoretical work.

The experimental values of μ_r and μ_i can of course be used to evaluate an effective specimen permittivity using the equations of Section 2, see Figure 14. These results indicate not only a falling free carrier contribution to the total dielectric constant, but also significant capacitative free carrier effects. The former effect is to be expected owing to the decreasing momentum relaxation time which accompanies increasing free carrier energy owing to increasing electric field strength.* However, the capacitative behaviour indicates that even lower frequencies should ideally have been employed in this measurement in order to avoid frequency dependent effects. Such frequencies would however introduce further problems of specimen design which are not easily negotiated.

In this section the in phase and quadrature mobilities have been evaluated and a velocity field curve deduced. The measurement has been

---

* The experimental temperature dependence of the mobility has been found to be of order $T^{-1.66}$ for lattice temperatures of 70°K and above. Acoustic phonon scattering may be expected to provide a $T^{-1.5}$ law, which is in fact to be seen in pure material below 70°K [12].

seen to be strictly valid only when the electric field at all points within the specimen is below the threshold field for N.D.C. In the region of greatest interest, it provides only a minimum negative slope mobility of -50 $cm^2/Vsec$. However, the general form of the velocity field curve is seen to be in acceptable agreement with other work, which is not surprising since this curve is dominated by the reliable results obtained below the threshold field rather than those above it. Calculation of the effective dielectric constant reveals that some frequency dependent effects are present in this measurement. This factor together with the problem of arranging for the specimen to adequately load the microstrip transmission line limit the ultimate potential of this technique in the case of n-Ge.

References

1. A. F. Gibson, J. W. Granville, E. G. S. Paige
   J.Phys.Chem.Sol. 19, 198 (1961)

2. J. C. McGroddy and M. I. Nathan
   IBM Jnl. Res. & Dev. 11, 337 (1967)

3. W. Fawcett and E. G. S. Paige
   Elect.Lett. 3, No.11 (Nov. 1967)

   E. G. S. Paige
   IBM, Jnl. Res. & Dev. 13 (1969)

   W. Fawcett and E. G. S. Paige
   J. of Phys. C. 1801 (Sept 1971)

4. H. D. Rees
   IBM Jnl. Res. & Dev. 13 (1969)

5/6. J. N. Morgan and C. E. Kelly
   Proc.Int.Conf.Phys.Semicond. Prague 70 and 151 (1960)

   T. Morgan
   J. Phys.Chem.Sol. 8, 245 (1959)

7. T. Koenig
   Phys.Rev. 118, No.5 (June 1960)

8. J. Zucker, V. Fowler and E. Conwell
   J.Appl.Phys. 32, 2606 (1961)

9. A. F. Harvey
   Proc. IEE 106B , No.26, 129-140 (March 1959)

10. F. Assadourian and E. Rimai
    Proc. I.R.E. 1651-1657 (1952)

11. E. G. S. Paige
    IBM Jnl. Res. Dev. 13, No.5, 562-567 (1969)

12. E. G. S. Paige
    Progress in Semiconductors, 8, 99 (1964)

4. Observation of Emission of T.E.M. Waves Generated within an n-Ge Cavity, and their Diagnostic Potential

In the previous Section, an experimental evaluation of the complex mobility in n -Ge at 77°K with the biasing electric field parallel to the <100> direction, was presented. It provided only a minimum value for the negative slope mobility, owing to problems of spatial non-uniformity of the biasing electric field, and more importantly, it was difficult to make the specimen intercept the incident microwave power effectively, in spite of the care taken to obtain a large microwave filling factor.

One way in which the microwave system may be forced to encounter the specimen, would be for this energy to be generated within the specimen. That is, to dispense with a bridge measurement, increase the N.A. product beyond the threshold for oscillation, and study the emission spectrum. It is intended that the N.L. product be retained below the critical value for domain formation. Thus we deal here with "electromagnetic instability" rather than "space charge instability" or "hybrid instability". (See Section 2).

Such observations still have diagnostic value, for the frequency of oscillation, together with the specimen length, is clearly related to the effective dielectric constant within the specimen. Similarly, if an empirical N.A. product for oscillation is determined, this provides information concerning the rate of growth of T.E.M. waves within the N.D.C. medium. Finally, and of equal importance, such an observation of microwave emission would demonstrate the existence of a new method by which microwave energy may be extracted from a bulk N.D.C.; an alternative to the space charge instability which is usually exploited in the Gunn effect.

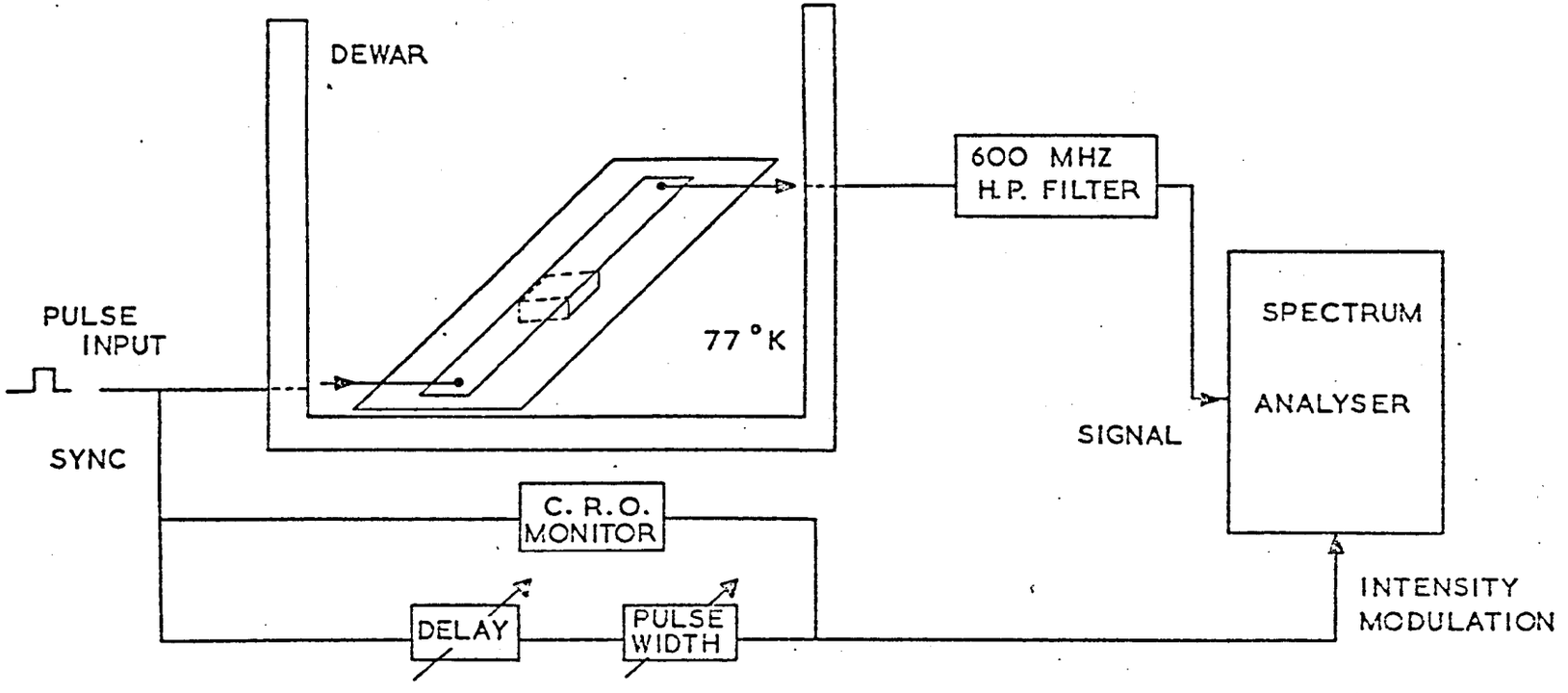

"BRIGHT UP" SYSTEM FOR OBSERVING

EMISSION SPECTRUM DURING A HIGH FIELD PULSE OF SHORT DURATION

FIG 1

4.1 Experimental Concept

In Section 3, computed N.A. products for oscillation were presented in Figure 2. However, in these calculations, the negative mobilities employed are close to the maximum value that may be expected, and are therefore low frequency values. The discussion of experimental constraints placed a value of 3 GHz upon the upper frequency beyond which frequency dependent effects, and thus, presumably, reduction of the N.D.C. is to be expected. Consequently, the value of A. must be such that

$$2A \geqslant \frac{C}{\sqrt{\epsilon_L} \cdot 3 \cdot 10^9}$$

in addition to the constraint placed upon N.A. for oscillation to occur.*

Beyond this consideration, the constraints upon specimen design are such as in the previous section.

The observation envisaged is simply one of the emission spectrum and its dependence upon biasing electric field, free carrier concentration, crystal orientation etc.

4.2 Experimental System - 1

4.2.1 "Bright up" Technique

Initial measurements were made using a simple "bright up" technique, on a Hewlett-Packard spectrum analyser, and photographic recording. The system is shown schematically in Figure 1. A synchronising pre-pulse from the pulse generator was used to drive

---

* The work in Section 3, and theoretical calculations for Gallium Arsenide[1] indicate that any free carrier contribution to the lattice dielectric constant, when biased into N.D.C., is likely to be small or positive.

a monostable multivibrator of variable output pulse width. This was differentiated, clipped, and the trailing edge used to drive a second variable width monostable multivibrator. In this way a pulse which is suitable for intensity modulation of the cathode ray tube of the spectrum analyser, was readily obtained. The width and delay of the intensity modulation pulse was adjusted so that it fell within the high field pulse using the oscilliscope monitor, thus allowing the spectrum analyser to paint the display screen only during the high field pulse. Since a maximum I.F. bandwidth of 1 MHz is provided on the spectrum analyser, a high field pulse duration of about 5 micro-seconds is clearly necessary.

4.2.2 The Measurement and Results

In this measurement some care was necessary in discriminating between spurious and genuine signals. Because of the sensitivity of the spectrum analyser (-80 to -90 d.Bm.) it was particularly susceptible to breakthrough from other microwave generators in the neighbourhood of the laboratory. Thus at each stage a control photograph was taken with no high field pulse applied to the specimen. In this way it was found possible to avoid confusion with signals received from sources outside the immediate experimental gear.

Additional problems were encountered in this measurement which were attributable both to spurious signals originating within the high field pulse rack and to sparking at the specimen. This latter, first became evident when a specimen went open circuit during a measurement, and yet emission was still observed. Subsequently measurements were at all times made of the specimen resistance before and after a run, and dummy runs performed with no specimen in the micro-strip. It will be clear that a degree of integration is possible upon the photographic film, by superposition of many sweeps through the spectrum. The potential of this facility was used to its maximum.

FIGURE 2

Emission spectra from N-Ge at 77°K, with electric field applied in a <100> direction. The dispersion is such as to present 1GHz across the complete spectrum.

The upper photograph shows emission centred upon 3.33GHz, with a biasing pulse of 9 volts.

The centre photograph shows the 3.33GHz emission removed when the high field pulse is switched off.

The lower photograph with the 9 volt field pulse re-applied shows emission in a spectral range centred upon 2.65GHz and with a dispersion of 2GHz across the complete spectrum.

The applied field strength is obtained by multiplying the pulse voltage by 342 cm^{-1}.

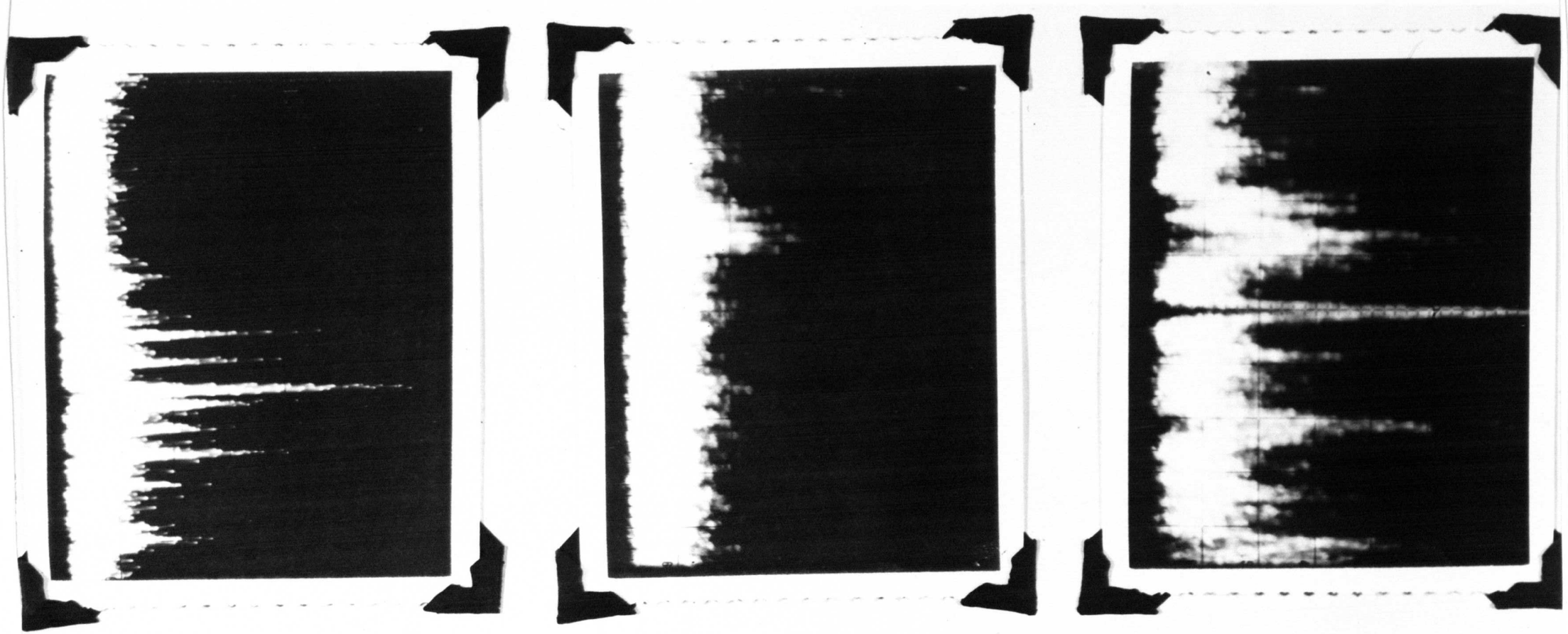

Finally, we comment upon the problems of signal ambiguity which arise with the Hewlett-Packard spectrum analyser. These spring from the use of a local oscillator which, by mixing twice with a high frequency signal can produce a signal which is easily confused with a lower frequency signal which has mixed once with the local oscillator. It is of course the well known problem of image frequencies encountered in radio receivers, and has been solved in all of the work in this and the next section by using a set of suitable filters. At first, a set of waveguide sections, with co-axial to waveguide transformers at each end were fabricated; these providing a crude but convenient series of high pass filters. Subsequently, a set of co-axial band pass filters were obtained and used throughout the remainder of this project.

The photographic recording system was employed successfully as a means of demonstrating the existence of emission from samples of 6 ohm -cm n-Ge at 77^{o}K, and having the electric bias field and wave propagation vectors parallel to $\langle 100 \rangle$ crystallographic axes. Some typical results are shown in Figure 2. A great number of such qualitative observations were made, providing ample evidence of the existence of this new mode of microwave emission proposed in Section 2. However, some improvement in the signal to noise level and method of recording data is clearly desirable. Comments upon the nature of the emission, and conclusions drawn, are therefore postponed until a more suitable experimental technique has been introduced.

4.3 Experimental System - 2

4.3.1 Integrating "Latch and Hold" Detection

In an attempt to increase the ultimate sensitivity of the detection system, relative to noise and to the spurious signal breakthrough level, an integrating latch and hold system was developed. The integrating latch and hold system is now becoming fairly well known[2] and is essentially a pulsed version of a phase sensitive detector. It capitalises upon the fact that the required signal is only occasionally present (i.e. during the high field pulse) and we know when these occasions occur. Thus, provided the unwanted signals are neither always present (C.W. signals) nor locked to the pulse recurrent frequency (P.R.F.) of the experimental system, integration of those signals occuring during the high field pulse must improve the ratio of the real signal to the breakthrough level

In its simplest form the latch and hold circuit is no more than a switch which is closed during prescribed time intervals. When closed the incoming signal is fed into a system which is capable of sensing and storing its amplitude, in a characteristic time known as the "learning time". When the switch is opened, the stored information is lost in a "decay time" which is in general required to be as long as possible, and certainly very much longer than the learning time. The circuit thus "latches onto" an instantaneous voltage and holds it.

If information is likely to vary randomly from pulse to pulse, and the P.R.F. can be made sufficiently high, the latch and hold output signal may be integrated over many pulses providing spurious signal rejection as required. It is in this latter role as an integrating latch and hold system that we perform the present measurements. The circuit which was built is shown in

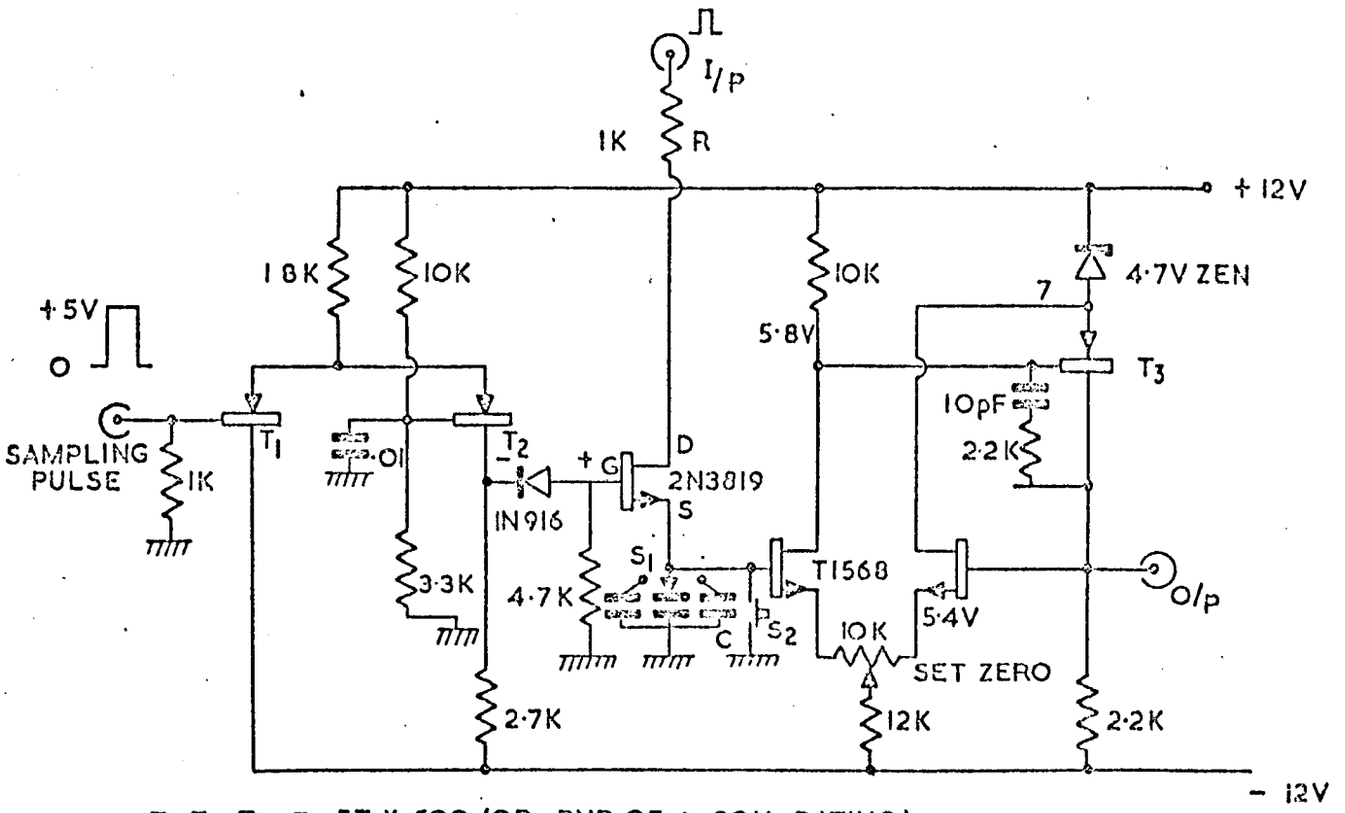

T_1 T_2 T_3 = ZT X 500 (OR PNP OF > 30V RATING)

S_1 = CAPACITOR RANGE SWITCH (2 X 1pGw) R & C TIME CONSTANT

S_2 = PRESS TO MAKE ZERO SET SWITCH

ZT X 500

C B E

D G S

2N3819

SAMPLE AND HOLD CIRCUIT

Fig 3a

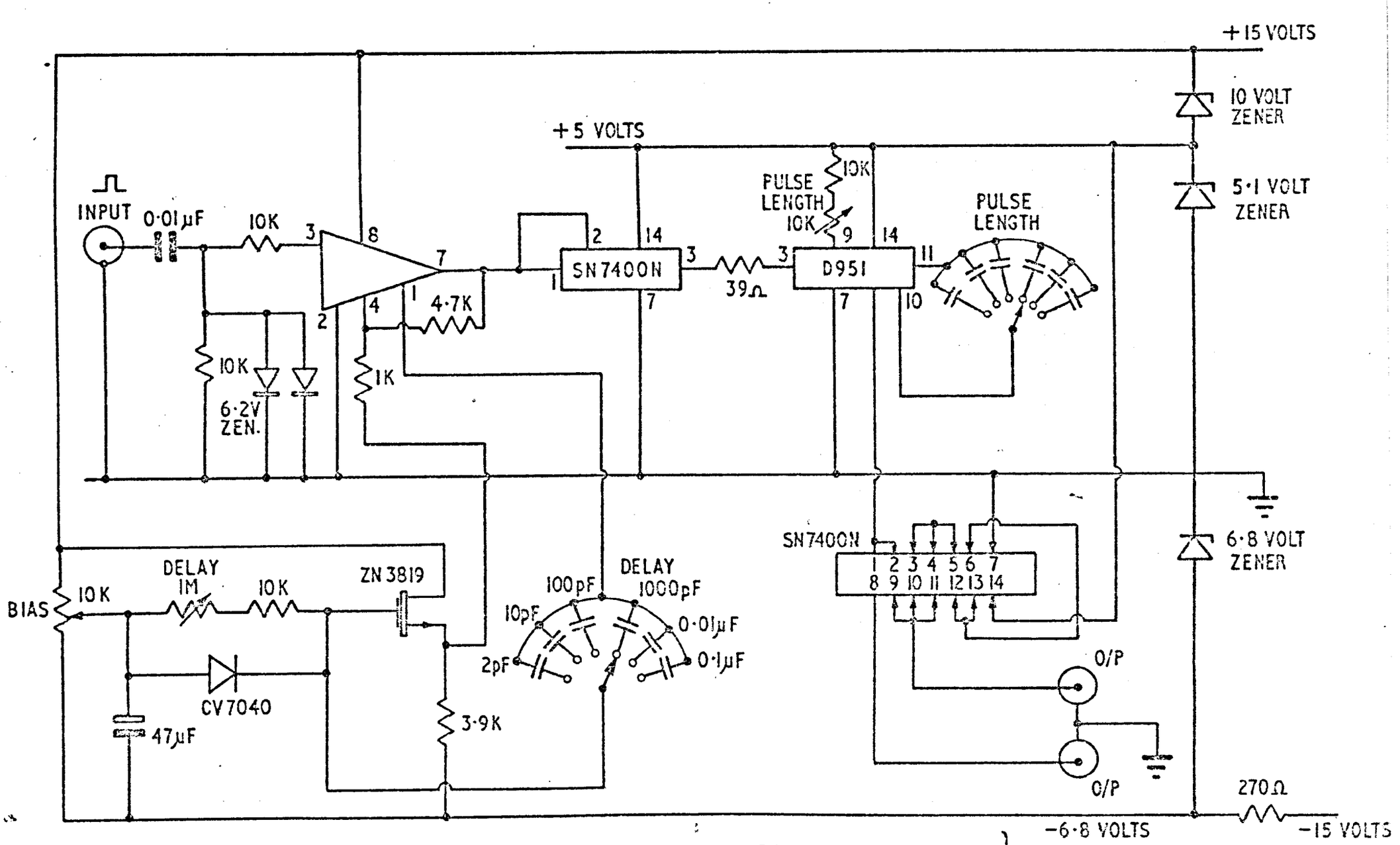

CAPACITANCE VALUES ON PULSE LENGTH SWITCH :- 80pF, 140pF, 300pF, 20pF, 620pF, 1260pF } APPROX.

FIG. 3B

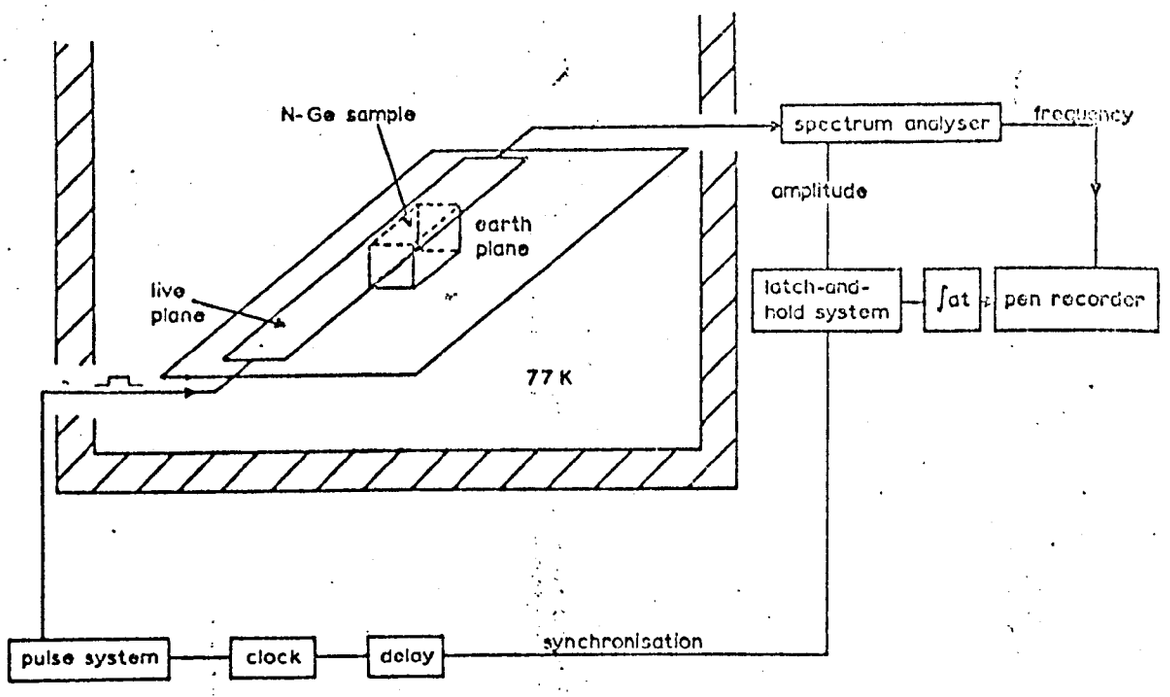

Schematic of experimental system

Fig 4

FIGURE 5

In this figure a latch and hold spectrum is displayed with a photograph of the spectrum analyser screen display inset. In each case low frequencies are to be found on the left of the display and high frequencies on the right. Increasing amplitude of signal is plotted upwards on the spectrum analyser screen but downwards on the latch and hold display.

It is seen that the signal to noise ratio is remarkably improved in the latch and hold display. The signal is a dummy signal centred upon 4GHz, with a 1GHz dispersion across the complete spectrum, in both the latch and hold and the photographic display.

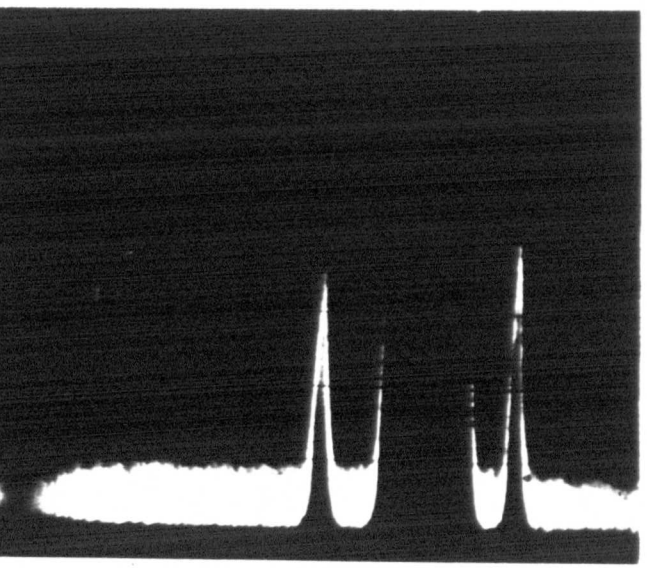

SIGNAL AFTER PROCESSING IN LATCH AND HOLD SYSTEM

FREQUENCY

AMPLITUDE

SYSTEM CHECK USING DUMMY SIGNAL

PHOTOGRAPH OF SPECTRUM ANALYSER DISPLAY

Figures 3a and 3b but is not entirely original work of the present author.

The experimental configuration is shown schematically in Figure 4.

In Figure 5 experimental results indicating the effectiveness of the integrating latch and hold circuit, which was constructed, are provided. The small signal which is only just visible by photographic techniques is shown clearly resolved by the integrating latch and hold system even when, as in this example, a very small integration time constant of 12.2 seconds is used.

Some caution in choice of the rate at which the spectrum is swept relative to the integration time constant is necessary. The criterion governing the sweep rate is clearly that the frequency range swept in one integration time constant should not exceed the spectral resolution of the spectrum analyser. A ready check upon the choice of spectral sweep rate relative to integration time is of course provided by simply repeating the recording in the reverse direction and looking for reproducibility of the spectrum.

4.3.2 The Measurement and Results

Reference has already been made to the fact that a spurious signal having the same P.R.F. as the experimental system, or a C.W. signal, are not rejected by the present system. Thus, it is necessary not only to do control runs with no field applied to the specimen, thus locating spurious external C.W. signals, but also runs in which the same amplitude high field pulse is applied to the micro-strip system without a specimen in it. In the latter observation spurious signals generated by the high field rack have on occasion been discovered. These signals would otherwise have been attributed to the N.D.C. in Ge, since on removing the driving pulse from the

FIGURE 6

The first set of latch and hold spectra show the effect of increasing the biasing electric field strength, applied in the $<100>$ direction to a Ge specimen at $77^{\circ}K$. It will be seen that a spike at the low frequency (left) end of the spectrum is always present.

In the second set of latch and hold spectra the same signal is seen to exist in the absence of any high field pulse, (upper trace) and is therefore spurious. In the lower trace an additional signal is seen when a high field pulse is applied to the empty transmission line. This also is therefore spurious.

Electric field strengths are obtained by multiplying the indicated pulse amplitudes by 666 cm^{-1}.

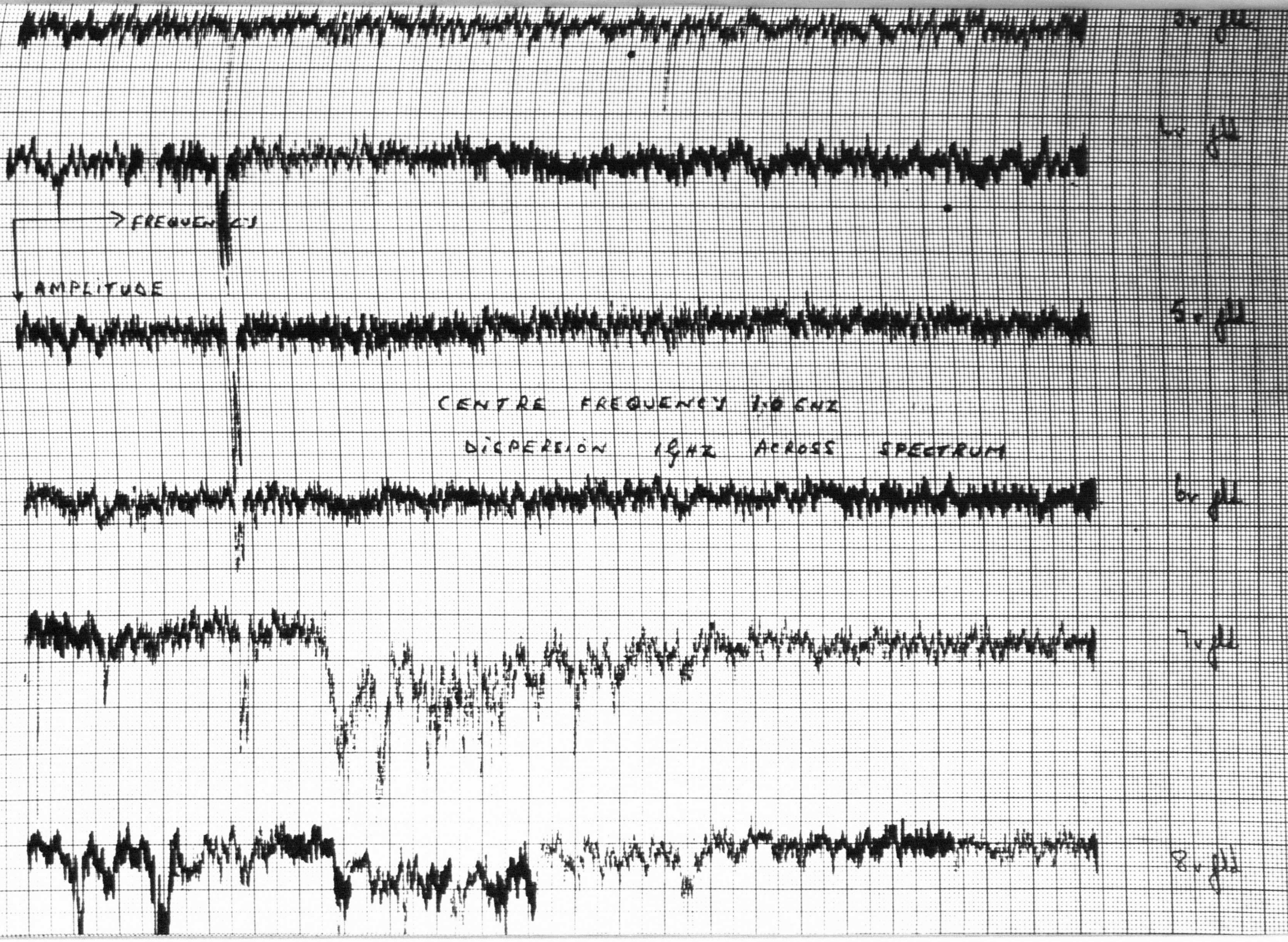
FREQUENCY
AMPLITUDE
CENTRE FREQUENCY 1.0 GHz
DISPERSION 1 GHz ACROSS SPECTRUM


CENTRE FREQUENCY 1.0 GHz
DISPERSION 1 GHz ACROSS SPECTRUM
FREQUENCY
AMPLITUDE

specimen the spurious signals would disappear giving the appearance of a genuine signal rather than a spurious external signal. In the results shown in Figure 6, these two control runs will be seen included. All results presented here are for Ge at 77°K, with electric field parallel to the <100> axis. The specimen geometry is 0.15 cm x 0.45 cm x 0.45 cm. The electric field is parallel to 0.15 cm dimension. Whilst some external spurious signals are clearly evident with zero applied field, an additional signal is also introduced by the high field supply even in the absence of any specimen. High field runs in the presence of a specimen on the other hand have even more emission spectra. However, the obvious immediate conclusion that the remaining spectra are generated by the specimen is not tenable, for evidence of mixing within the specimen was also obtained i.e. the specimen can behave as a microwave mixer, generating new emission frequencies from the incident microwave power, rather than as a microwave generator in its own right. It was, therefore, generally necessary to remove microwave signals generated by the pulse source by suitable screening, slowing down of pulse edges etc. (Similar mixing of external spurious signals was not found to occur presumably because they were picked up directly at the spectrum analyser, in contrast to the spurious signals from the pulse source. These, it can readily be demonstrated, only reach the spectrum analyser by travelling along co-axial leads via the Ge specimen).

Having completely automated this experimental gear, a large number of spectra were readily accumulated (approximately 150 on over a dozen specimens) each of which required ½ to 1 hour of observation time. The specimen fabrication procedure is exactly

FIGURE 7

The four latch and hold spectra are for increasing pulse amplitudes and show emission below the spectral centre frequency of 1GHz. The specimen is of N-Ge at 77°K with the field applied in a <100> direction. (A single very tall spike, present in all spectra, is spurious). The electric field strength is obtained in each case by multiplying the pulse amplitude by 105 cm^{-1}.

freq 1·0 GHz 72 db 100 MHz/cm $\int dt \cdot 12{\cdot}2$ 26·11·69

as for 22.

50 μs

CENTRE FREQUENCY 1 GHz

DISPERSION 1 GHz

→ FREQUENCY

↓ AMPLITUDE

Log 1·0 GHz 72db 100 MHz/cm ∫dt ·12·2 26·11·69

22 with centre 5 cm of Ln in cavity in 5cm bore

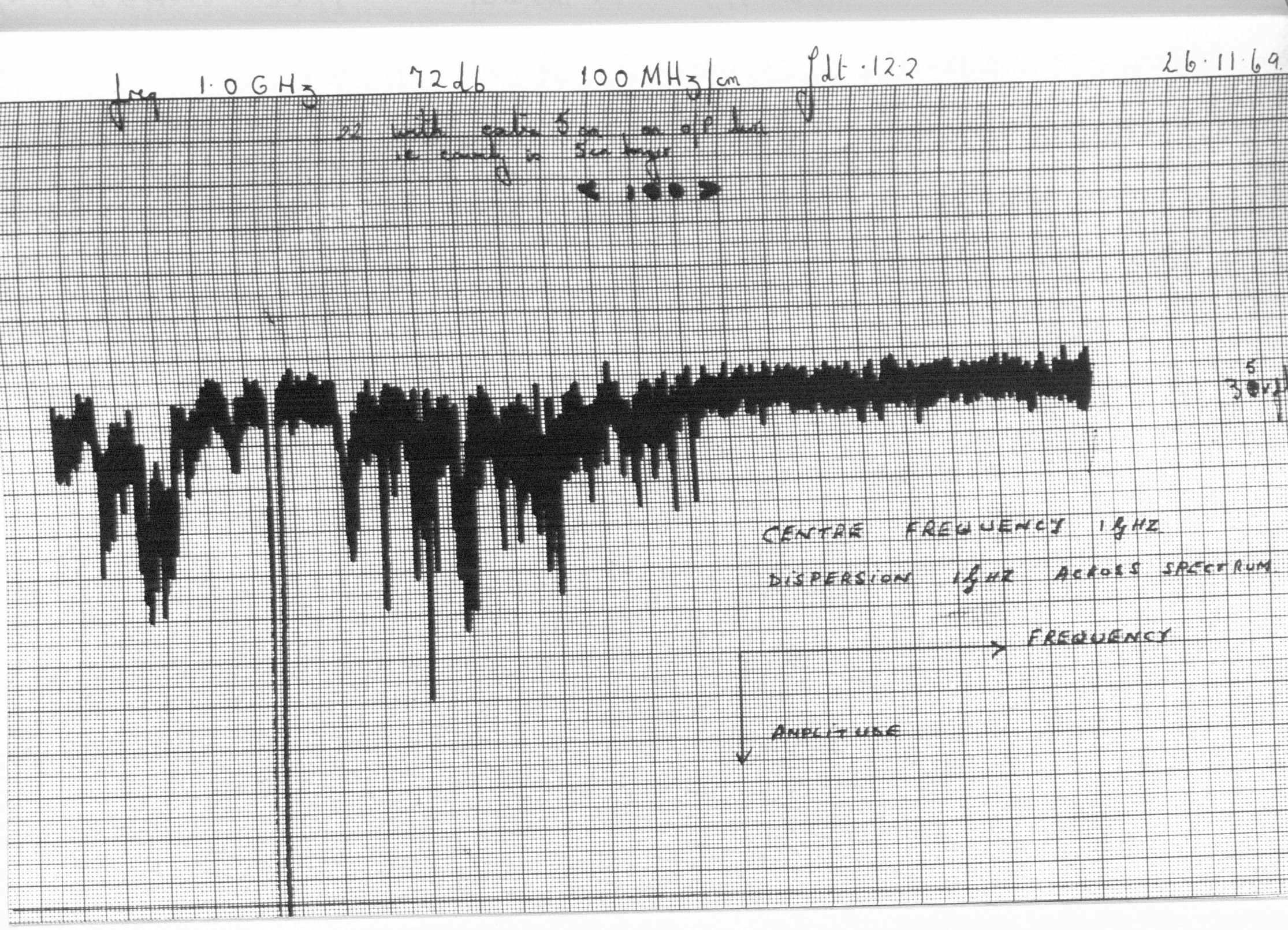

freq 1·0 GHz 72 db 100 MHz/cm $\int dt$ · 12·2 26·11·69

τ for 22

<100>

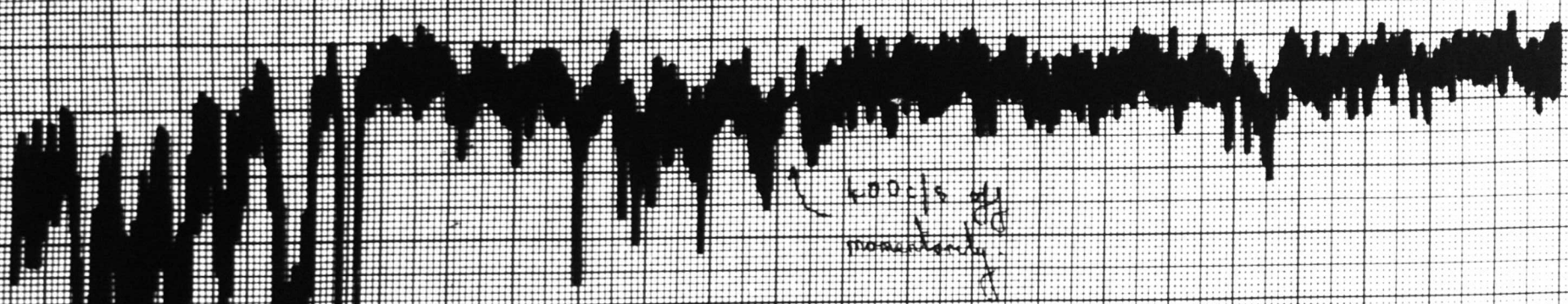

600 c/s dip

CENTRE FREQUENCY 1 GHz

DISPERSION 1 GHz

FREQUENCY

AMPLITUDE

freq 1·0 GHz 72db 100 MHz/cm $\int dt$ · 12·2 26·11·69

∞ for 22

<100>

CENTRE FREQUENCY 1 GHz

DISPERSION 1 GHz

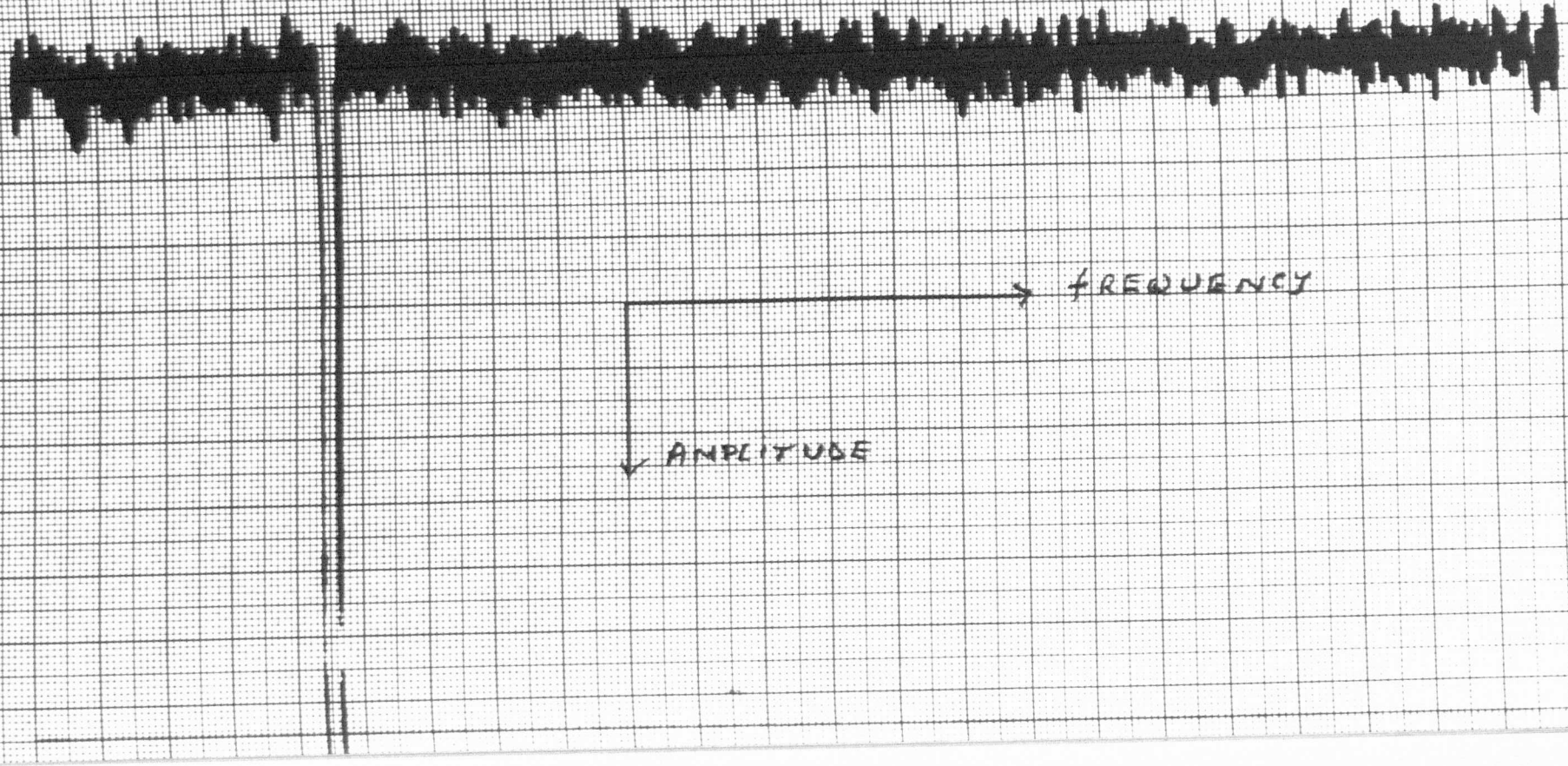

26 v db

as in Section 3.1. All the spectra cannot be included here, rather, we now draw out the salient features of the experimental observations.

Importance of Free Carrier Concentration and Specimen Geometry

Materials having three different free carrier concentrations were employed in the work.

Material "A"

We commence with results obtained in the most heavily doped material which had 2.5×10^{14} free carriers/cc. Emission spectra are presented in Figure 7, for a specimen having all edges parallel to <100> crystallographic directions, and being 0.15 cm in length parallel to the biasing electric field, and 0.45 cm in the remaining two directions. This free carrier concentration and geometry was chosen with the objective of testing the conclusions reached in Section three concerning the range of frequencies over which N.D.C. may be observed; because the free carrier concentration is relatively high, the dimension "A" parallel to the direction of propagation, may be quite short, forcing any emission stemming from electromagnetic instability to a high frequency. The frequency expected from the present specimen would be of order

$$\frac{c}{2.0.5\ \sqrt{\epsilon_L}} \approx 7.5 \text{ GHz}$$

which of course is above the estimated ceiling value for N.D.C., obtained in Section 3, of about 5 GHz.

It will be observed that the emission which was detected was not at 7.5 GHz but near 1 GHz. No amount of matching, mismatching, or general adjustment of the microwave circuit could force the specimen to operate at anything like the 7.5 GHz required by

the specimen geometry. This result will be used at a later stage to confirm our ideas of a ceiling frequency for N.D.C. of around 5 GHz. However, first it is necessary to determine what mode of operation can give rise to emission in the 1 GHz range.

(i) Longitudinal Specimen Stability

The specimen employed in obtaining the fairly typical results of Figure 7, has been sectioned, and the actual effective contact separation, after the alloying process, found to be 0.95 mm. Thus this specimen had an N.L. product of 2.38×10^{13} cm^{-2}, which is to be compared with an empirical N.L. product, obtained by McGroddy et al, which is "well in excess of 2×10^{13} cm^{-2}." This specimen cannot therefore be classified as space charge stable on the basis of these figures.

Evidence that these observations cannot be traced to a simple transit mode of operation may be derived from the frequency of operation. This is clearly in the 700 - 900 MHz range. Now the stable domain velocity is usually slightly less than the electron's saturated drift velocity (1.2×10^7 cm/sec). Recent measurements by McGroddy et al[4] with a capacitative probe, provide a domain velocity of 1.14×10^7 cm/sec at 77°K (taken from the gradient of Figure 8 of this reference), which is thus approximately in keeping with the accepted value of the saturated drift velocity. With a specimen length of 0.95 mm, a transit mode frequency of approximately $\frac{1.14 \times 10^7}{0.095} = 120$ MHz is therefore implied. That is, if the sample were space charge unstable. This frequency is in marked contrast with the observed frequency of emission between 700 and 900 MHz. For the domain mode of operation to be responsible

for such frequencies, one would have to invoke some mechanism of domain quenching, whilst only 1/6th of the way across the sample, and subsequent re-nucleation at the cathode, or the existence of multiple domains.

Domain quenching may occur, as discovered by McGroddy et al[4] owing to impact ionisation across the energy gap. However, as he also points out, this leads to lower rather than higher frequencies of operation since the resultant space charge remains to be extracted before re-nucleation of the domain may proceed. Furthermore, the collapse of such high domain fields is inconsistent with the present extremely low power levels detected. (see below)

Domain quenching by voltage starvation, as in the so called quenched domain mode[6], requires sufficiently high R.F. fields to reduce the mean specimen field well below the threshold field to the minimum sustaining field. (In 3.5 Ohm cm GaAs 0.25 cm long Heeks et al[7] found 0.5 E_T for example). More important than the precise distance below the threshold field at which the minimum sustaining field occurs, is the fact that our mean biasing field is, for example, 1 KV/cm beyond the threshold field. This corresponds to R.F. potential fluctuations of $\pm$ 100 volts on a 50 Ohm line (in a circuit which apparently has a low Q) about the pulsed biasing potential of 400 volts. This R.F. power of 200 watts is to be compared with the present observations in which the noise level is at -80 to 90 dBm, and signals are perhaps 10 dB up on this level. Domain quenching by either mechanism is thus unlikely.

ii) Transverse Specimen Stability

Having demonstrated that a simple domain mode of operation is unlikely but not impossible, we compare the present

FIGURE 8

The observation here is as for figure 7 but for the removal of 5 cm of open circuited co-axial line from one end of the specimen transmission line. The same large spurious signal spike is seen at low frequencies together with one additional one which is labelled. However in spite of the use of similar fields, no strong emission is now seen in this frequency range.

freq 1·0 GHz 72 db 100 MHz/cm $\int dt = 12 \cdot 2$ 26 11 6

<100>

CENTRE FREQUENCY 1 GHZ

DISPERSION 1 GHZ

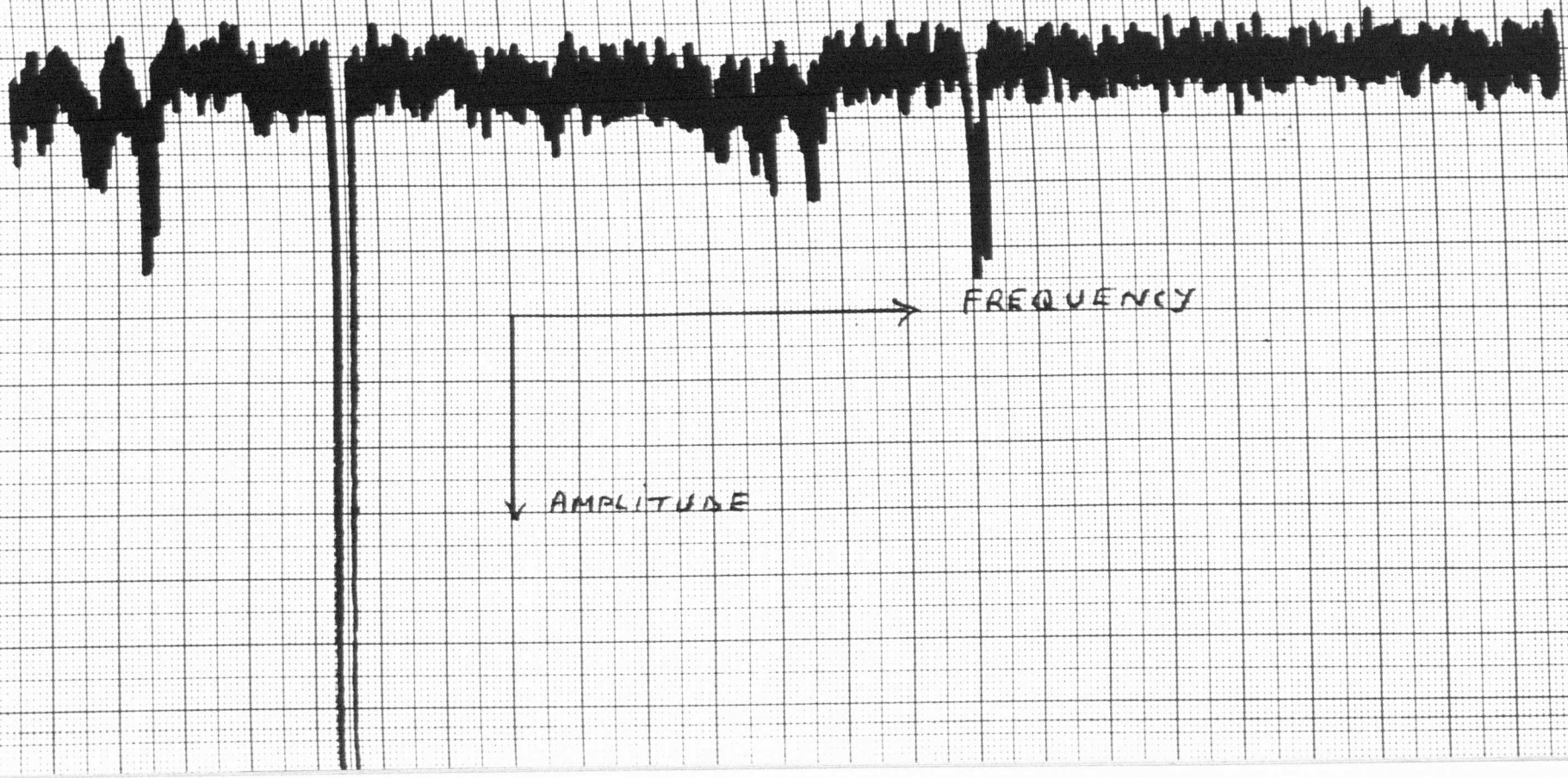

30 v

freq 1.0 GHz 72db 100 MHz/cm $\int dt \cdot 12.2$. 26.11.69.

<100>

CENTRE FREQUENCY 1 GHZ

DISPERSION 1 GHZ

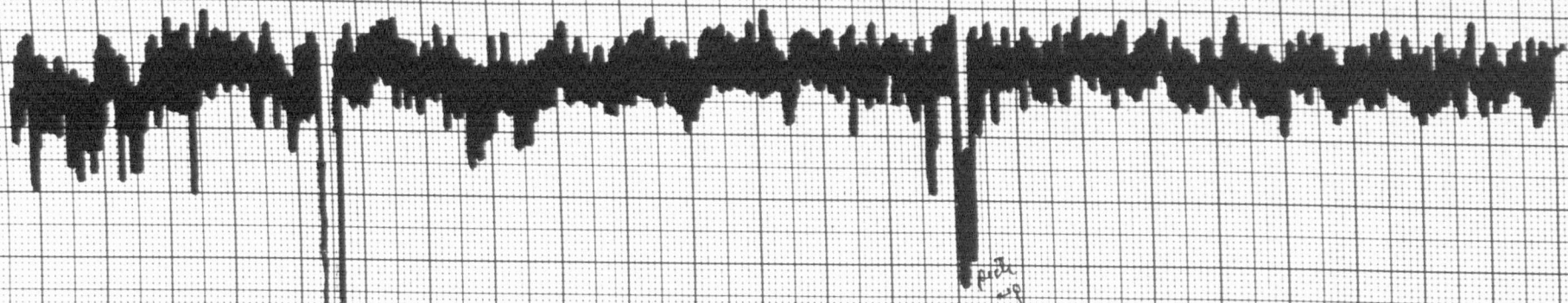

35v. pk

FREQUENCY

AMPLITUDE

results with the requirements for electromagnetic instability. An approximate theoretical N.A. product of 2.2×10^{14} cm^{-2} has been introduced in Section 3 as the threshold of electromagnetic instability. In the present experiment the N.A. product is $2.5 \times 10^{14} \times 0.5$ cm $= 1.25 \times 10^{14}$ cm^{-2}, thus to the accuracy of the theory, the specimen is on the threshold of electromagnetic instability. However, the calculation does assume that microwave reflection occurs at germanium/air boundaries, whilst in the experiment this is clearly not the case, for the frequency of observed emission (700 - 900 MHz) does not correspond with a cavity dimensional resonance expected at approximately

$$\frac{c}{\sqrt{\epsilon_L}\, 2.0.5} = 7.5 \text{ GHz}$$

It is apparent that having failed to become unstable between its own boundaries at 8.3 GHz, the specimen has found one or more, distant mismatches which provide sufficiently large reflection coefficients for round trip gain to occur at a lower frequency. In the results of Figure 7 the location of the mismatch is readily found. "Looking" from the specimen towards the spectrum analyser each item presents a guaranteed 50 ohm load. Looking away from the spectrum analyser, however, we see an open circuit; which is thus, not only the most likely source of an external mismatch reflection, but the only possible source apart from coupling to the high field pulse line, which should be minimal.

This conclusion is confirmed by the data of Figure 8 in which the cavity is shortened by removing 5 cm of open circuited co-axial line which was attached to the open circuited end of the micro strip transmission line. We note that the emission pattern is entirely changed.

At 0.8 GHz the wavelength in co-axial line is approximately 20 cms. Bearing in mind that we are concerned with round trip effects, the cavity of interest which includes the specimen, has therefore been shortened from approximately 10 cms to 5cms in effective length in co-axial line. Thus, consistent with the observations, we expect emission to have been moved to higher frequencies beyond the present spectral range. Not only can this observation be regarded ~~as confirming~~ CONSISTENT WITH the foregoing description of the mode of operation, but it also emphasises the fact that adequate mismatches can be produced outside the specimen for low frequency operation. Our failure to move this emission frequency beyond 2.3 GHz however clearly indicates that these higher frequencies (5 - 7.5 GHz) do lie in the range where frequency dependent effects have produced major reductions in the strength of the N.D.C. if not annihilated it.

To summarise, the foregoing discussion of material A thus indicates

1) That the mode of emission is one in which the specimen is a significant part (10%) of a larger microwave cavity, where round trip gain occurs for T.E.M. waves.*

---

* The present mode of operation is in many ways mid-way between work done by Thim[8] on low N.L. product amplifiers, and the initial objective of producing electromagnetic instability within the sample boundaries. In the work of Thim a sample of GaAs having N.L. below the critical value for domain formation behaves as a LOCALISED negative resistance circuit element, with the microwave flux flowing around the sample rather than through it. Here the microwave flux is partially within the sample and partially outside it; the sample is certainly not insignificant in proportion relative to a wavelength of radiation. (In practise of course, further contrast exists in that in the present work, OSCILLATION (not amplification) is achieved with N.L. below its critical value, and this is in germanium rather than gallium arsenide).

FIGURE 9

Latch and hold emission spectrum from N-Ge at $77^{\circ}K$, in which a spurious signal spike occurs at the extreme left of the spectrum. The remaining spikes are genuine. The electric field strength is found by multiplying the indicated pulse voltage by 143 cm^{-1}.

freq 3·0 GHz 72 db 100 MHz/cm $\int dt = 12.2$ 3·12·69

WR 3 <100>

CENTRE FREQUENCY 3·0 GHz

DISPERSION 1·0 GHz

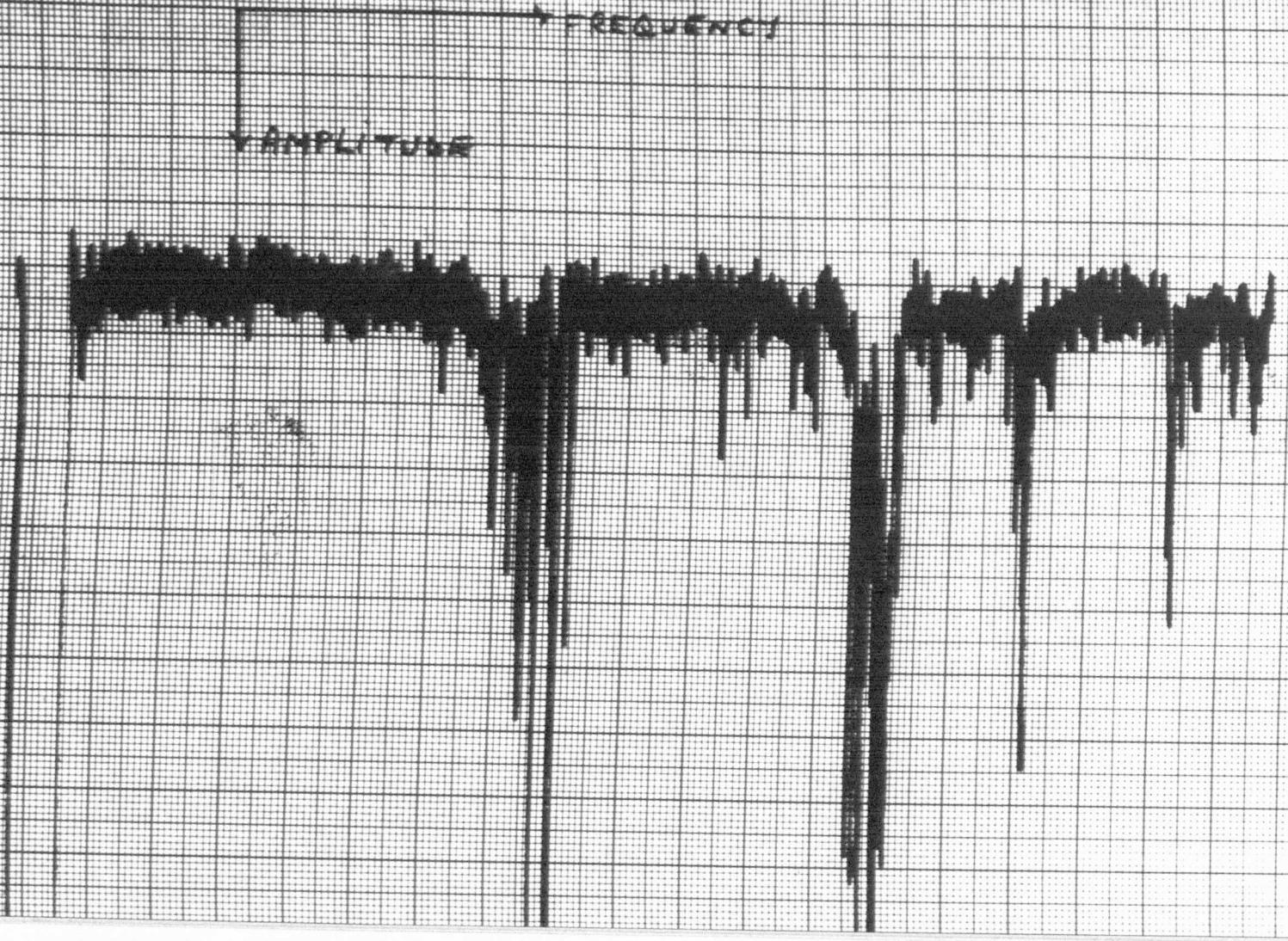

35 v

2) There is no detectable N.D.C. at 8 GHz. If an N.D.C. does exist at this frequency it is certainly much weaker than that existing at lower frequencies. Thus the broad predictions concerning the frequency dependence of this N.D.C. are confirmed.

Subsequent work by Professor Meyer[5] has similarly failed to detect any N.D.C. in such material at 9 GHz, in the $<100>$ field direction and at $77^{\circ}K$.

Material "B"

We now describe further work in which the mode of operation is forced into the regime of electromagnetic instability, by suitable choice of sample length in the propagation direction and choice of free carrier concentration. To this end, we increase the "A" dimension of the sample to allow a lower frequency of operation, and reduce the conductivity of the sample material in order to establish space charge stability. The work under "B" is upon 10 ohms cm material (at $300^{\circ}K$) having an impurity concentration of 1.5×10^{14} cm^{-3}. An emission spectrum for a sample of 1.175 cms in the propagation and $<100>$ directions and 0.07 cms in the $<100>$ direction parallel to the applied biasing electric field is shown in Figure 9. The N.L. product for this specimen is 1.05×10^{13} cm^{-2}, and it should thus now be stable against domain formation. Its N.A. product is 1.76×10^{14} cm^{-2} which is in the estimated region of threshold for electromagnetic instability. Moreover, the frequency of the observed emission 3.0 to 3.2 GHz is consistent with this mode of operation which would require a frequency of approximately

$$\frac{c}{\sqrt{\epsilon_L}\ 2 \times 1.176} = 3.19 \text{ GHz}$$

FIGURE 10

Latch and hold spectrum which has one spurious spike at 3.5 GHz. Results are as for figure 9, but with the specimen shortened as described in the text.

10·12·69

key 3·75 72db 100 MHz/cm ∫dt · 12·2

Envelope + Log 1 GHz LP filter

<100>

CENTRE FREQUENCY 3·75 ½ MHz

DISPERSION 1·0 ½ MHz

→ FREQUENCY

↓ AMPLITUDE

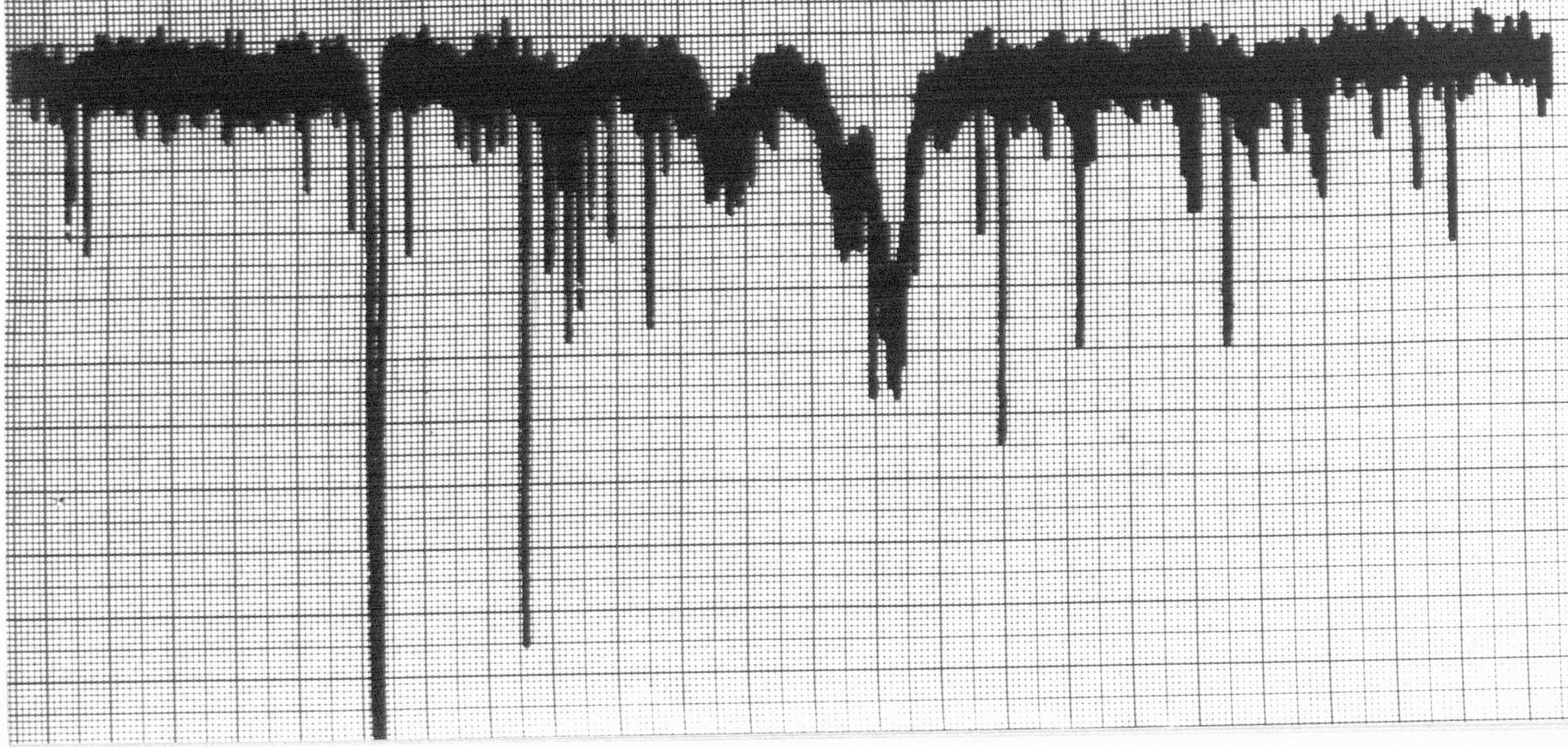

30v

This implication that the emission observed springs from an electromagnetic instability is confirmed by shortening the specimen to 1 cm in the propagation direction "A". The emission then observed is shown in Figure 10, where emission occurs primarily in the spectral range 3.6 to 3.8 GHz. (The large spike at 3.5 GHz is shown by the zero field control run to be an external spurious break through signal) and emission is to be expected at

$$\frac{c}{\sqrt{\epsilon_L}\ 2 \times 1.0} = 3.75 \text{ GHz}$$

At this stage the specimen had an N.A. product of 1.5×10^{14} and was oscillating in the required fashion. With the sample further shortened to 4.5 mm in the propagation direction no emission was observed.

These observations establish an empirical N.A. product for oscillation which is very close to the estimated value, and in turn therefore confirms the value of the negative slope mobility (300 $cm^2/V.sec$) used in deriving that estimate. The uncertainties of the precise form of the effective microwave circuit, degree of carrier accumulation throughout the region of N.D.C., validity of the uniform medium model etc. render any attempt to press precise quantitative conclusions from this data a little unwise. Rather, we point out that this result for the slope mobility in the region of N.D.C. was, when obtained, four times greater than the accepted value of 80 $cm^2/V.sec$. Since this data was obtained and published, Neukerman[3] has obtained precisely this value of 300 $cm^2/V.sec$ for the negative slope mobility. Finally, these observations on the 10 Ohm cm material constitute the first clear cut observation of the form of electromagnetic instability initially postulated, in which

the round trip gain path for a T.E.M. wave lies entirely within the cavity formed by the specimen boundaries.

Material "C"

The third material from which specimens were fabricated was 20 Ohm cm n-Ge. No emission could be detected from any specimens made out of this material. However, since these specimens were limited to 0.5 cm in the "A" dimension, providing an N.A. product of 3.37×10^{13} cm^{-2} this merely confirms that N.A. must be greater than this value for electromagnetic instability to occur. (The data obtained on the 10 Ohm cm material places an even higher threshold upon N.A.)

Having discussed the data obtained through studying the importance of free carrier concentration and specimen geometry, we now introduce some other conclusions provided by the experimental data already introduced.

Threshold Electric Field

In Figure 7 a typical electric field dependence of emission is demonstrated. A clear threshold field for emission is evident. Sectioning of the specimen revealed that the effective contact separation was 0.95 mm indicating a threshold field for emission of between 2.75 KV/cm, and 3.15 KV/cm. The consensus of many measurements indicate a threshold field for emission of 3.1 KV/cm $\pm$ 0.15 KV/cm. It is evident from Figure 7 that the power of the emission increases with field. Thus specimens which were only marginally unstable would need biasing well beyond the threshold field for N.D.C. before the emission would exceed our finite detection threshold. We therefore conclude that the threshold electric field for N.D.C. is $\lesssim$ 2.95 KV/cm. This result is consistent with the previous section and is to be compared with

other measurements of the threshold electric field for N.D.C. which are already published[10] and which range from 2.2 KV/cm to 3 KV/cm (no limits of accuracy given). It should also be compared with a more recent careful measurement by Neukerman and Kino[3] in which a threshold field of 3.35 KV/cm at 80°K is obtained. (This latter work was carried out after the publication[9] of the results given here.)

Temperature Dependence

No emission was observed when specimens were studied at 300°K. Other temperatures were not studied owing to the associated cryogenic requirements which could not be met by the present experimental system.

Crystallographic Orientation Dependence

One specimen was made from 10 Ohm cm material in which the field could be applied parallel to a <111> crystallographic direction, but no emission was observed either between specimen boundaries in the desired mode of operation, or employing microwave mismatches external to the specimen.

In summary, the work described in this section upon microwave emission from n-Ge at 77°K has, first of all, demonstrated the existence of the proposed mode of electromagnetic instability. It has also provided values of :

i) the threshold electric field for N.D.C. (2.95 KV/cm)

ii) the negative slope mobility (300 cm^2/V sec.)

iii) the N.A. product for oscillation (1.10^{14} cm^{-2})

The absence of an N.D.C. for biasing electric fields parallel to a <111> direction has been confirmed; that is, in so far as the absence of any phenomenon can be conclusively affirmed. Finally, the frequency ceiling at which the N.D.C. was expected to become weaker and eventually disappear (5 GHz) has also been substantially confirmed. Conclusions (i) and (ii) above, have recently been reproduced by Neukerman et al,[3] whilst the frequency dependence of the N.D.C. has, in a measure, received corroboration from work carried out by Professor Meyer in which he failed to find any N.D.C. in Ge at 9 GHz[5].

References

1. H. D. Rees

   IBM. Jnl. Res. Dev. 13 (1969)

2. J. W. Hodby

   J.Phys. (E) Scientific Instruments 3, 229-233 (1970)

3. A. P. Neukerman and G. S. Kino

   10th International Conf.Phys. of Semicond. 40-45 (1970)

4. See Figure 8 of J. C. McGroddy, M. I. Nathan and J. E. Smith Jnr.

   IBM.Jnl.Res. Dev. 543-561, 13, No.5 (1969)

5. Private Communication, Prof. Meyer.

   He has tried to observe NDC in n-Ge at 77°K

   and 10 GHz and failed.

6. I. B. Bott and W. Fawcett

   Advances in Microwaves, 3, (1968)

7. J. S. Heeks, A. D. Woode and C. P. Sandbank

   Proc. IEEE correspondence 53, 554-555 (1965)

8. H. W. Thim, M. R. Barber, B. W. Hakki, S. Knight and M. Uenohara

   Appl. Phys. Lett. 7, 167 (1965)

9. A. C. Baynham

   Elect. Lett. 6, No.10 (May 1970)

10. See Section 1.

5. Observation of Emission of T.E.M. Waves Generated within a GaAs Cavity and some Characteristics of the Emission Spectrum

In this section, the new mode of microwave emission introduced in Section 2 and demonstrated experimentally in Section 4 is further examined. In Section 4, the emphasis was upon the demonstration of a new phenomenon, and the diagnostic value which such work may have. Here, the emphasis is upon the mode of microwave emission itself; its potential power, its spectral distribution etc. We employ GaAs both in order that the emission may be more powerful and because of its importance as the current vehicle for Gunn device fabrication.

In Section 5.1, the criteria which govern a successful experiment in GaAs are considered. In Section 5.2 experimental evidence of the existence of this mode of microwave emission in GaAs is presented when N.L. is smaller than the critical value for domain formation. Estimates of the microwave power, and some observations concerning the width of spectral emission are included, together with other basic characteristics of the emission process.

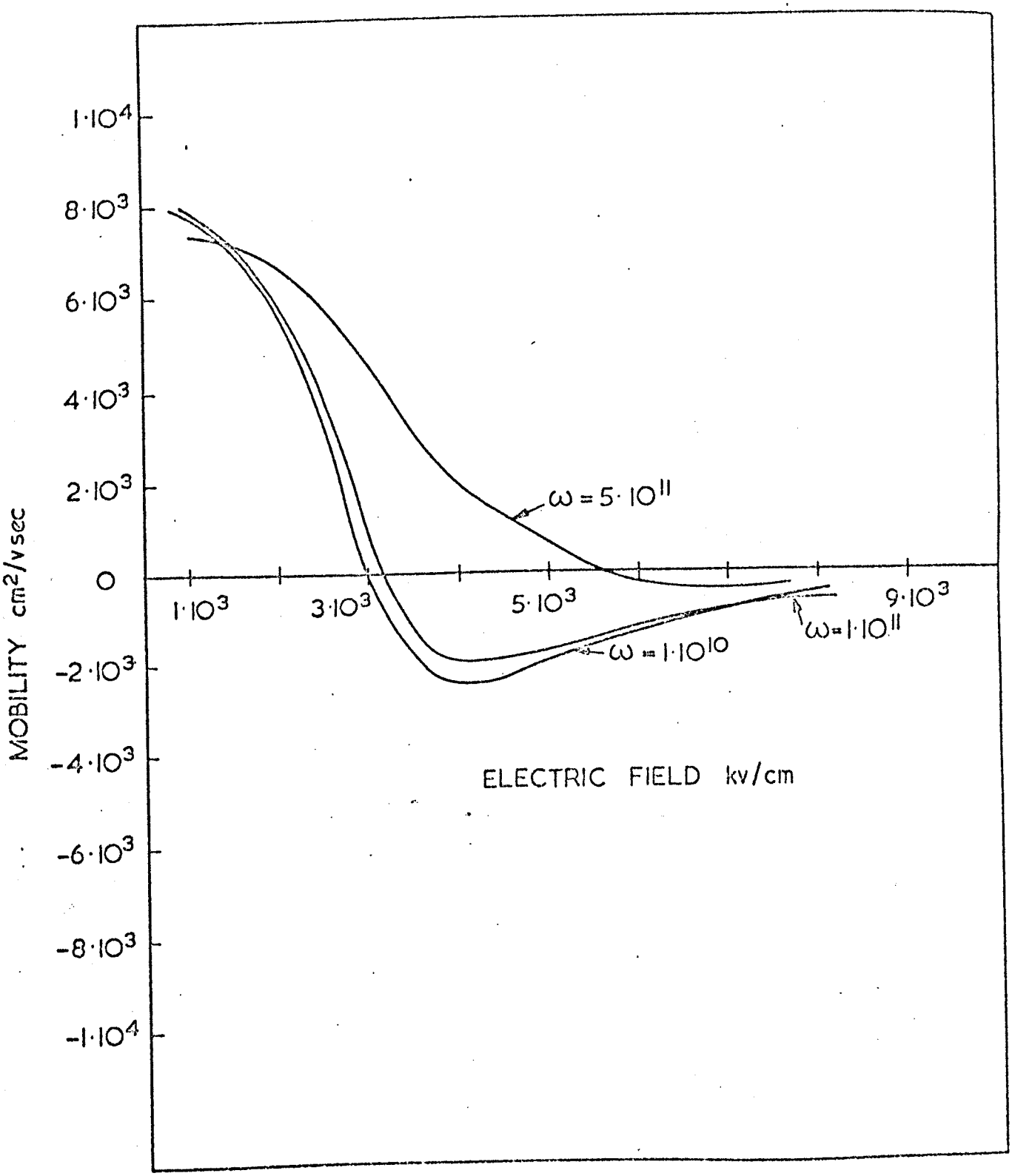

REAL MOBILITY AS A FUNCTION OF ELECTRIC FIELD FOR GaAs AT 300°K AT A VARIETY OF ANGULAR FREQUENCIES

Fig 1

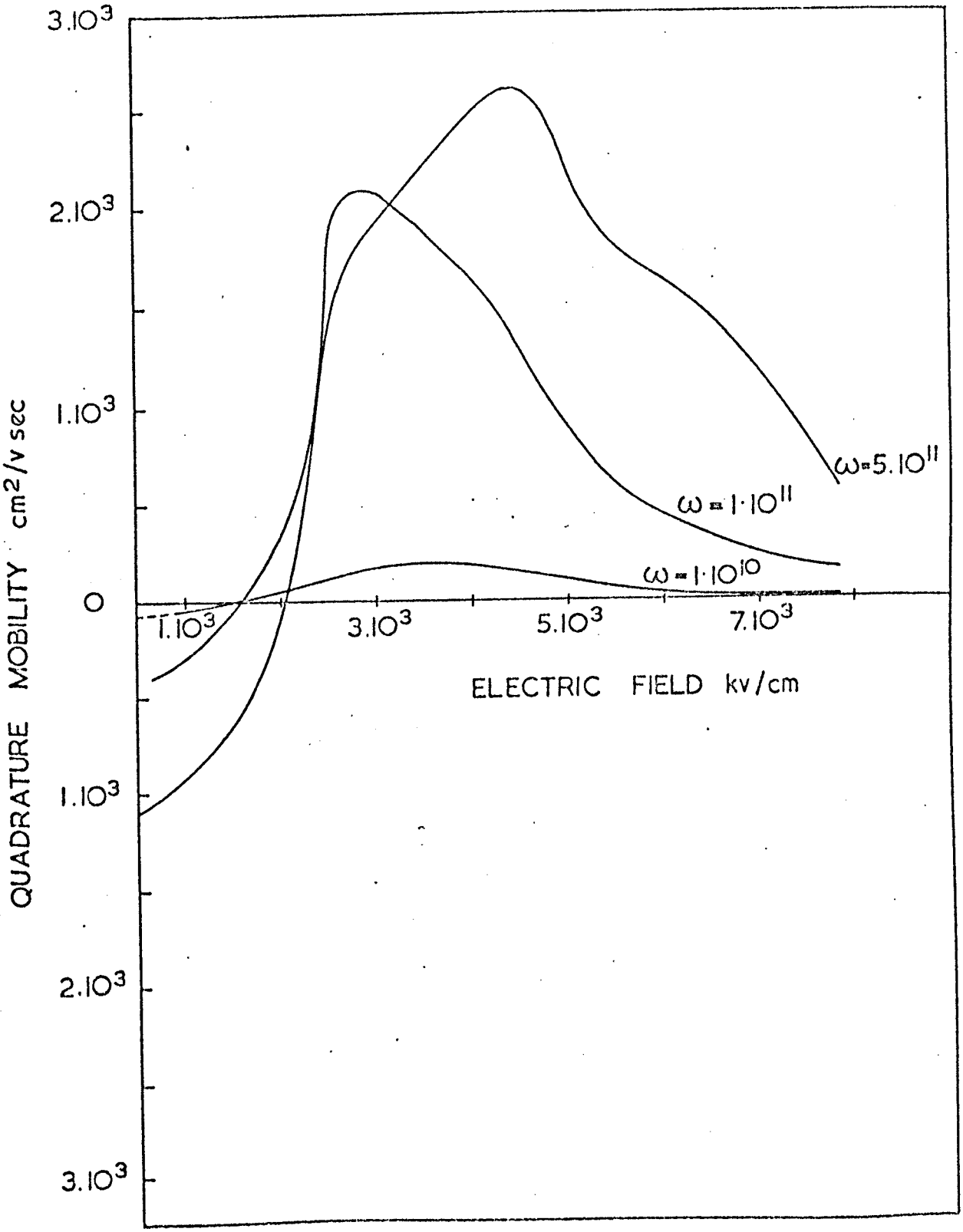

QUADRATURE MOBILITY AS A FUNCTION OF ELECTRIC FIELD FOR GaAs. AT 300°K AT A VARIETY OF ANGULAR FREQUENCIES

Fig 2

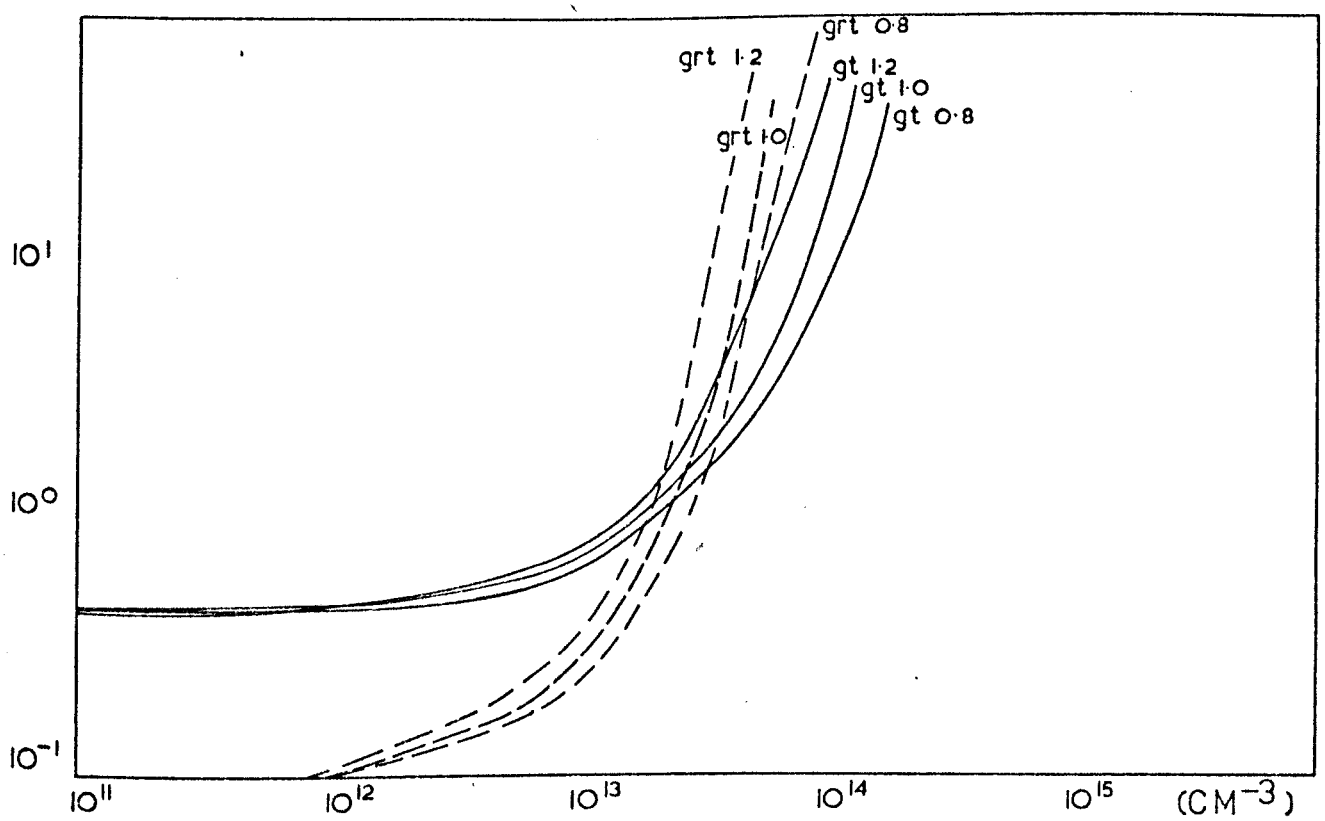

COMPUTED TRANSMISSION GAIN (gt) AND ROUND TRIP GAIN (grt) IN Ga As AT 300°K AS A FUNCTION OF FREE CARRIER CONCENTRATION USING THE FOLLOWING DATA:

LATTICE DIELECTRIC CONSTANT 12
MOBILITY = −2260 −419 i cm^2/v sec
FREQUENCY $2{\cdot}5.10^{10}$ rad/sec
ELECTRIC FIELD 3·65 kv/cm

THE SUFFIXES ON (gt) AND (grt) INDICATE THE SPECIMEN LENGTH IN THE PROPAGATION DIRECTION

Fig 3

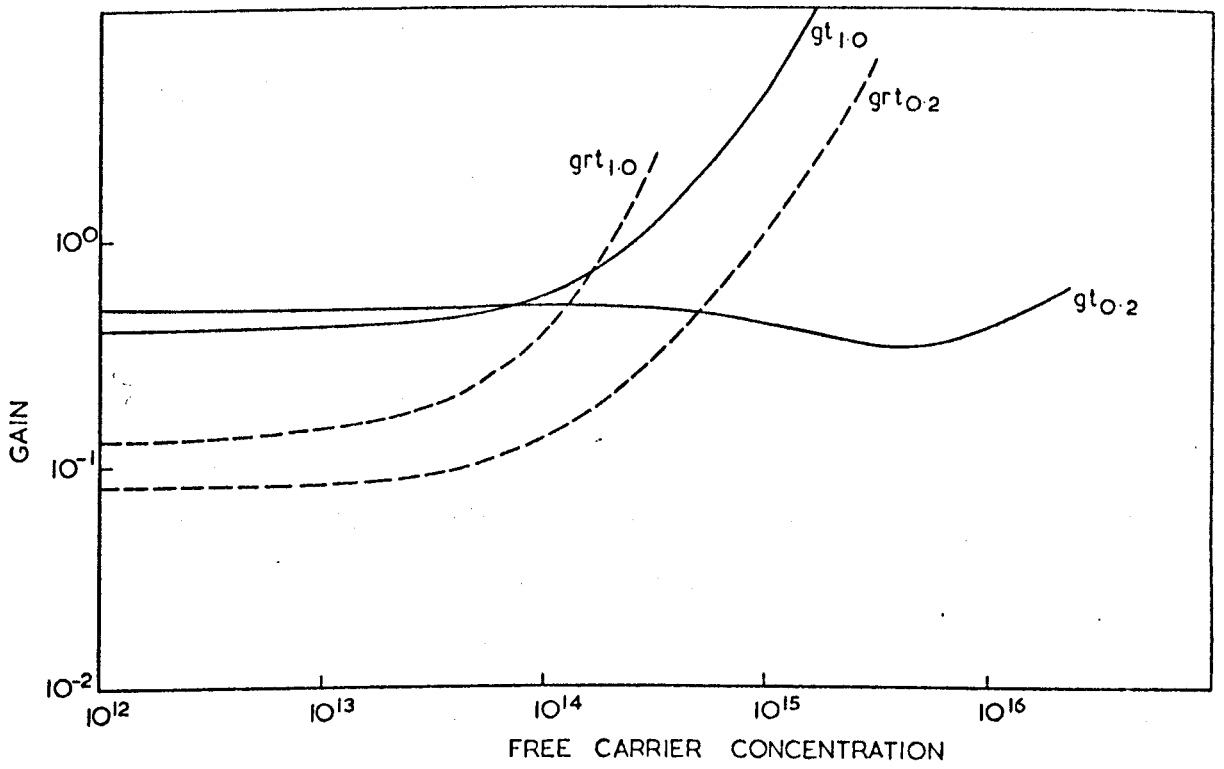

COMPUTED TRANSMISSION GAIN (gt) AND ROUND TRIP GAIN (grt) IN GaAs AT 300°K AS A FUNCTION OF FREE CARRIER CONCENTRATION USING THE FOLLOWING DATA.

MOBILITY = $-1600 - 2000i\ cm^2 / v\ sec$

FREQUENCY = $1{\cdot}45\ 10^{11}$ rad / sec

LATTICE DIELECTRIC CONSTANT = 12

ELECTRIC FIELD 3·65 kv/cm

THE SUFFIXES ON (gt) AND (grt) INDICATE THE LENGTH OF THE SPECIMAN IN THE PROPAGATION DIRECTION.(CMS)

FIG 4

5.1 Choice of Experimental Regime

In Section 2, some of the constraints which govern the choice of an experimental regime were enumerated. We now consider them in the context of a proposed experiment in GaAs.

5.1.1 Specimen Stability

Initial work was carried out using specimens which were capable of electromagnetic instability only; thus requiring

$$N.L. < 5 \times 10^{11} \text{ cm}^{-2}$$

$$N.A. > 2 \times 10^{13} \text{ cm}^{-2}$$

The former value is obtained from Bott et al[1]. The value of the N.A. product is obtained using the uniform medium equations of Section 2, and computed* mobility data of Rees et al[2] shown in Figures 1 and 2. Figure 3 shows the predicted dependence of round trip and insertion gain upon free carrier concentration at a frequency of 4 GHz for a number of specimen lengths. (see Section 2) The qualitative behaviour of these curves is just the same as for n-Ge and will therefore not be laboured. Similar curves are shown in Figure 4 for a higher frequency of 23 GHz, again derived using the Figures 1 and 2. In both Figures 3 and 4 a surface reflection co-efficient defined by the effective permittivity of the GaAs relative to that of air is employed.

---

* No experimental information concerning the quadrature mobility was available, whilst this computed in phase mobility was in fair agreement with experiment[7]

The foregoing stability requirements imply a specimen aspect ratio of

$$\frac{L}{A} < 10^{-2}$$

This stands in contrast to the aspect ratio obtained for n-Ge. The slope mobilities which have been used for n-Ge and GaAs differ by only a factor of 10, thus rendering the N.A. products computed for the two materials which also differ by a factor of 10, consistent.

It is the N.L. products which differ by a factor of 100 and which are therefore inconsistent with the slope mobilities employed here. However, both the slope mobilities and the N.L. products are emperimental values for both materials. The resolution of this conflict may lie in the fact that observations of emission as a function of N.L. product can clearly only place a maximum value upon the N.L. product, beyond which oscillation can occur, ie. observations of emission are incontrovertible, whilst observations of no emission do not prove the impossibility of emission at such lower N.L. products. Consistency may be achieved only therefore by reducing the N.L. product for n-Ge, and not by increasing the N.L. product for GaAs. The work reported in Section 4, in which stability of an n-Ge specimen was achieved by shortening it in the "A" dimension would however tend to confirm the accepted value of $N.L._{Ge}$.

A reduction in the mobility of n-Ge or an increase of the slope mobility in GaAs would again introduce consistency. Again however, these quantities are by now well known for GaAs[3], and in the case of n-Ge receive confirmation in the present work and subsequent work of Neukerman[4].

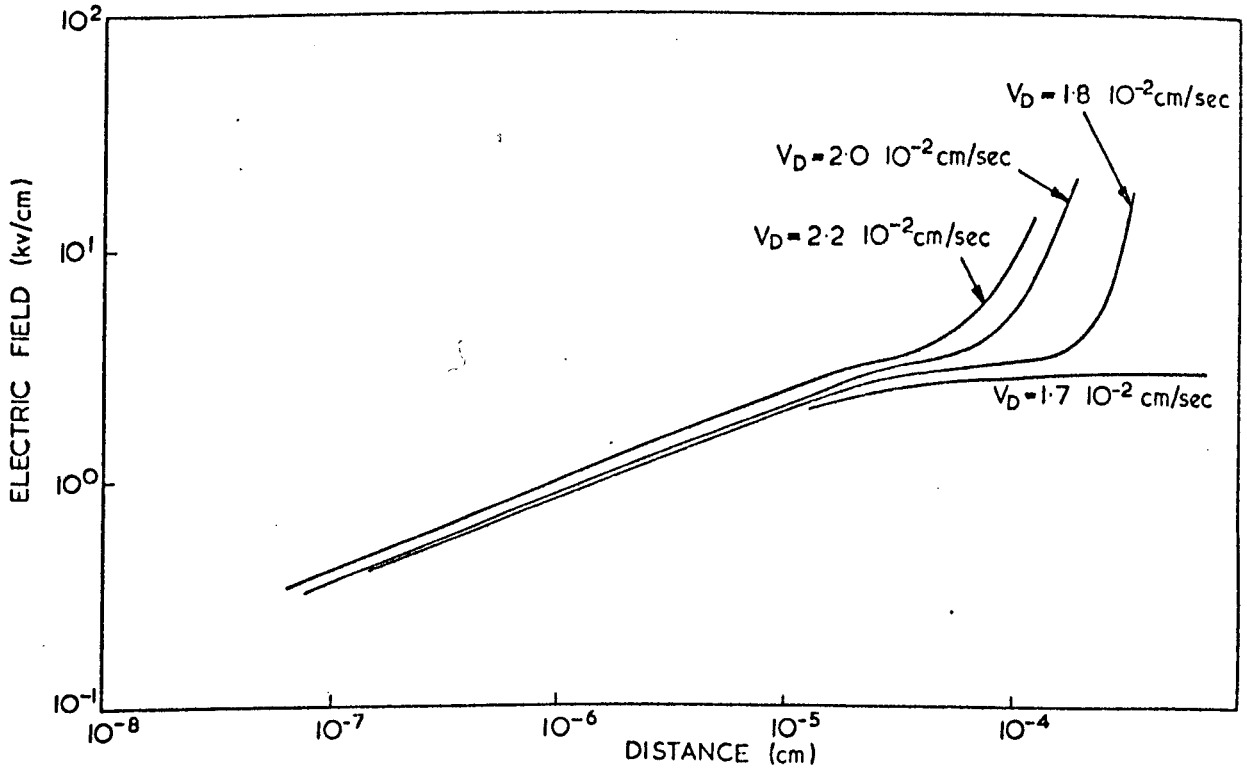

SPATIAL DISTRIBUTION OF ELECTRIC FIELD IN Ga As AT 300° K COMPUTED USING THE VELOCITY FIELD CURVE OF RUCH AND KINO AND THE FOLLOWING DATA :-

FREE CARRIER CONCENTRATION = $8.0\ 10^{14}/cm^3$
(ZERO APPLIED FIELD)
LATTICE DIELECTRIC CONSTANT = 12
THRESHOLD FIELD = 3·5 kv/cm

RESULTS ARE SHOWN FOR A SERIES OF DIFFERENT ELECTRON DRIFT VELOCITIES (CURRENT DENSITY IN ARBITARY UNITS) IN THE CONTACT REGION, THE LOWEST ONE BEING SUCH THAT THE SAMPLE NEVER ENTERS THE REGION OF N.D.C.

FIG 5

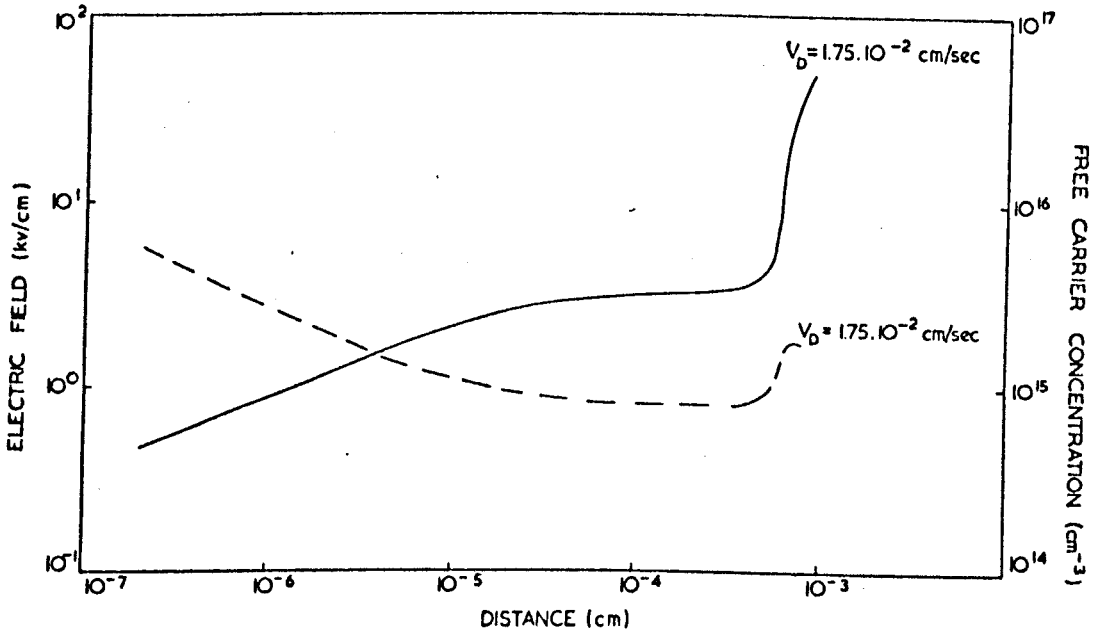

SPATIAL DISTRIBUTION OF FIELD (SOLID LINE) AND FREE ELECTRON CONCENTRATION (BROKEN LINE) IN GaAs AT 300° K CALCULATED USING THE VELOCITY FIELD CURVE OF KINO AND RUCH AND THE FOLLOWING DATA

DRIFT VELOCITY IN CONTACT AREA = $1.75\ 10^{-2}$ cm/sec
FREE CARRIER CONCENTRATION = 8.10^{14} /cc in THE ABSENCE OF APPLIED ELECTRIC FIELD
LATTICE DIELECTRIC CONSTANT = 12
THRESHOLD FIELD = 3·5 kv/cm

FIG 6

A third avenue towards consistency may lie in the diffusion constants. If these constants were very different in the two materials then in spite of their relative mobilities, the N.L. products could remain remarkably different. We accept both the figures for the N.L. product and the slope mobility in the following work upon GaAs.

5.1.2 Non-uniformity of Biasing Electric Field

We have seen in Section 2 that a spatially non-uniform biasing electric field is to be expected in samples which are stable against space charge fluctuations. Using the equations of Section 2, the results shown in Figure 5 were obtained with the following data

i) Free carrier concentration = 8. 0. $10^{14}/cm^3$ (zero field)

ii) Lattice dielectric constant = 12

iii) Threshold electric field = 3.5 KV/cm

iv) The velocity field curve obtained by Ruch and Kino[3]

The results are qualitatively similar to those obtained for n-Ge (Section 3, Figure 2) and therefore no comments are made concerning its form. The results are in good agreement with similar calculations by, for example, Mahrous and Robinson[5]. However, no publication has appeared in which the accompanying free carrier distribution is included. In Figure 6, the accompanying distribution of space charge within the specimen is presented for a particular biasing electric field strength.

It will be seen that the space charge accumulation in GaAs is very much greater than that predicted in n-Ge (Section 3,Figure 3). This result emphasises the superiority of n-Ge as a material in which to attempt diagnostic measurements directed at the underlying transport process. It also serves to highlight the care which

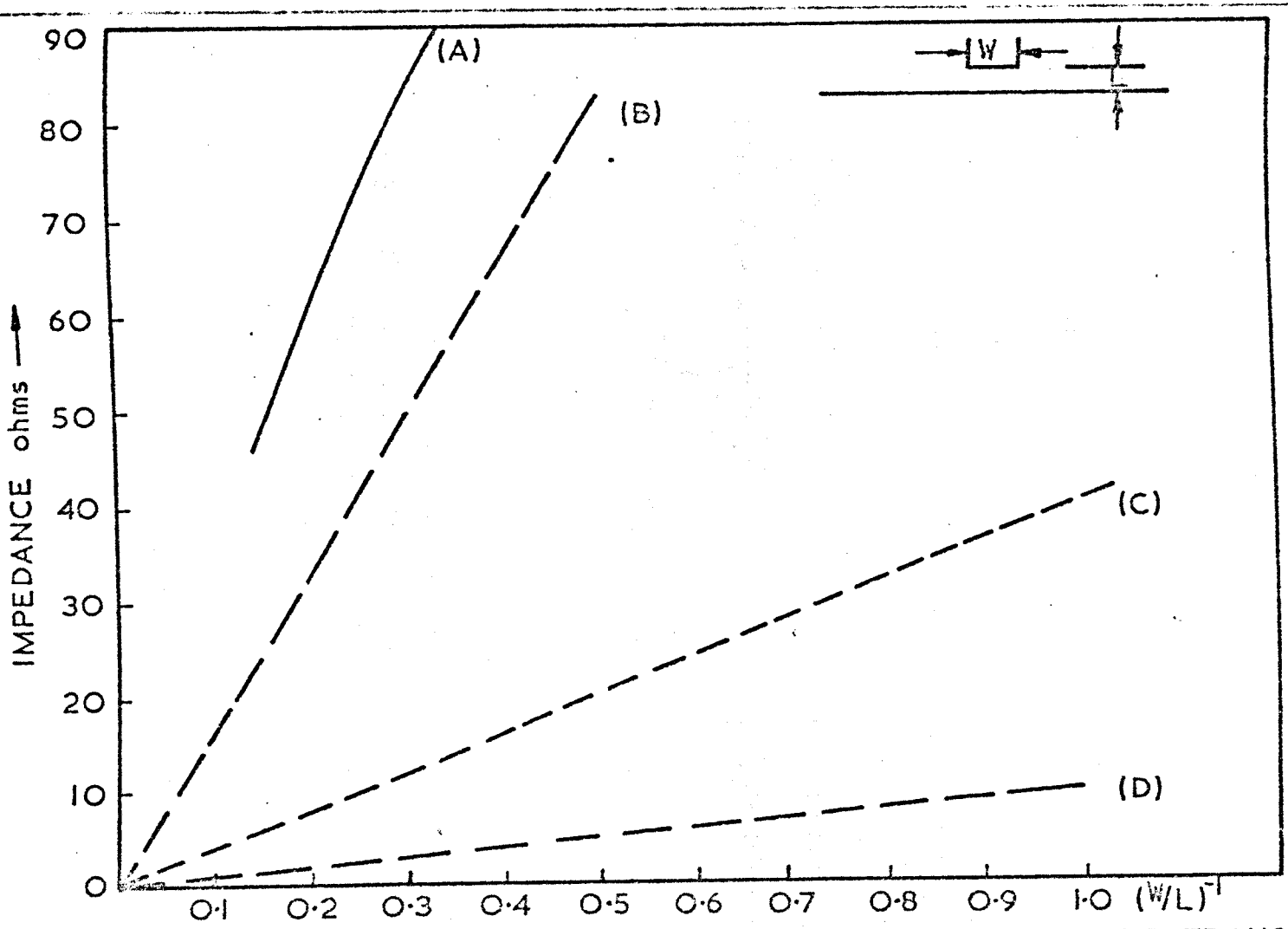

THEORETICAL MICROSTRIP IMPEDANCE AS A FUNCTION OF TRANSMISSION LINE ASPECT RATIO $(W/L)^{-1}$ FOR A UNIFORM AIR DIELECTRIC IN CASE 'A'. CURVES B, C AND D OF SPECIMEN IMPEDANCE WITH NA PRODUCTS OF $8\,10^{12}$ $2\,10^{13}$ AND $8\,10^{13}$ RESPECTIVELY. IN EACH CASE THE SPECIMEN OCCUPIES THE SPACE BELOW THE LIVE PLANE ONLY.

FIG. 7.

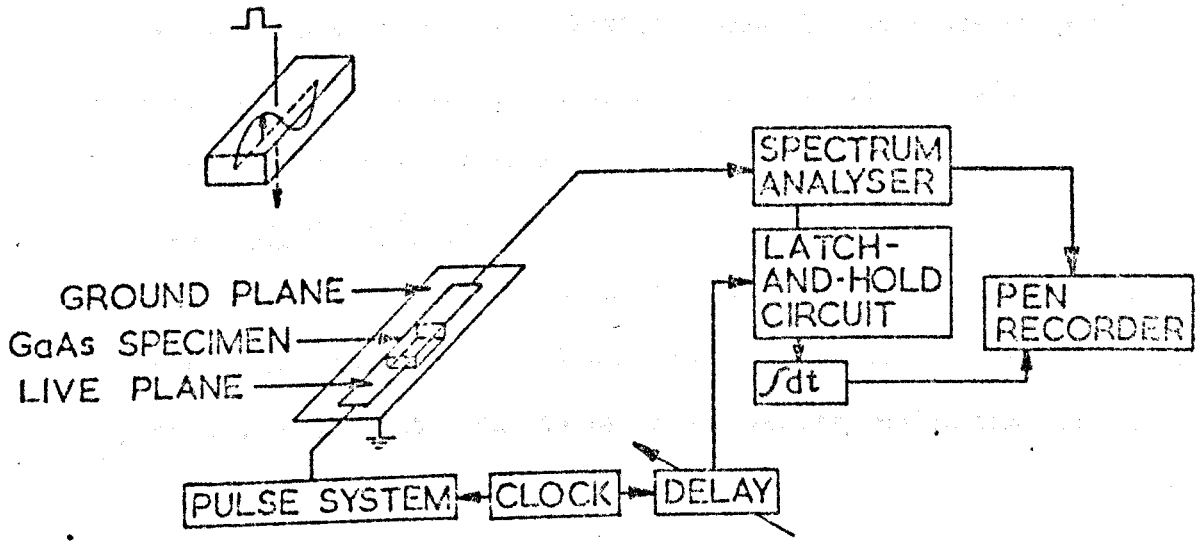

FIG. 8

SCHEMATIC OF EXPERIMENTAL SYSTEM
THE INSERT SHOWS THE RELATIVE ORIENTATION OF THE MICROWAVE AND D.C. ELECTRIC FIELDS.

must be exercised in using the uniform medium calculations already discussed. These lead to the "N.A." product evaluated in Section 5.1.1. However, here we show that "N" may vary by hundreds of percent within a sample of GaAs which is stable against small space charge fluctuations.

5.1.3 Frequency Limit

Observations of microwave emission from a GaAs sample have been made up to 10 GHz with little change in the power output[6]. Thus, at all lower frequencies, no reduction of the N.D.C. is assumed in the present work.

5.1.4 Specimen Impedance

The micro-strip transmission line system is retained in the experiments to be described here. This microwave environment places a constraint upon the specimen geometry which has already been described in Section 3. Thus the consequent specimen impedance, transmission line impedance and geometry are related as shown in Figure 7 when the aspect ratio of Section 5.1.1 is assumed. In spite of the larger aspect ratio, the impedance of the GaAs specimen is seen to remain acceptible. This is a consequence of the Lower N.L. product, and lower CHORD mobility in GaAs at 300°K than that in n-Ge at 77°K.

5.2 Observations of Microwave Emission from GaAs

In the previous section a latch and hold system was described which was developed in order to study the emission from n-Ge. The GaAs work described here uses that same experimental system and the same experimental safeguards to prevent observation of spurious signals. However, the observations are now made at room temperature rather than at 77°K as in the case of n-Ge (See Figure 8)

FIGURE 9

Latch and hold emission spectrum obtained from GaAs at 300°K. All spikes are genuine. The electric field strength is obtained by multiplying by 125 cm^{-1}.

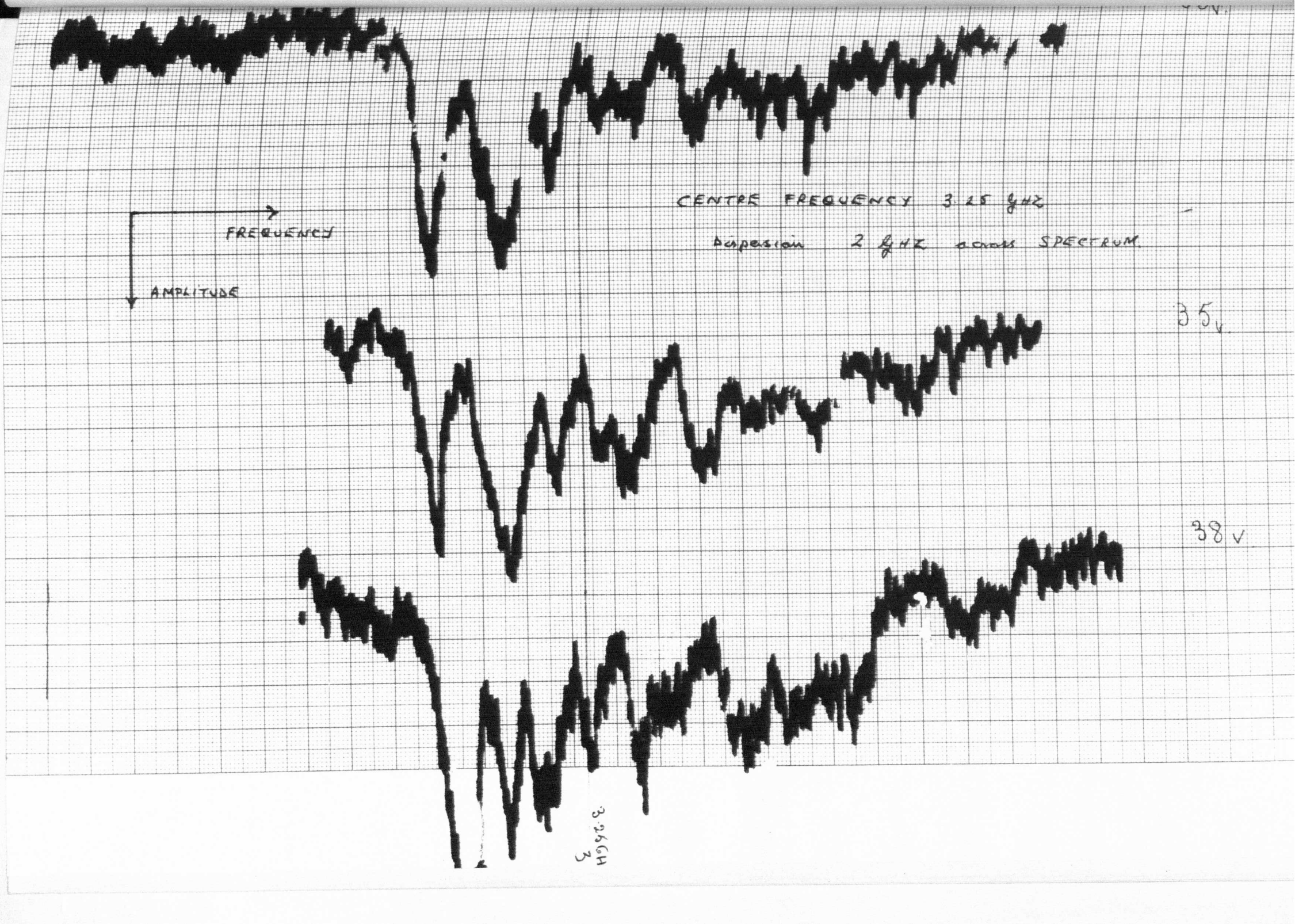
FREQUENCY
AMPLITUDE
CENTRE FREQUENCY 3.25 GHz
Dispersion 2 GHz across SPECTRUM.
35 v
38 v
3.25GHz

The semi-insulating substrate of a slice of epitaxial GaAs was polished off, and silver tin contacts made to both faces of the remaining material by alloying at a temperature of 350°C. The material was then cut into long needle like specimens, and gold ribbon compression bonded to one face, whilst the other was attached to the earth plane of the transmission line with a low melting point solder.

The first specimens studied had N.L. below the critical value for domain formation, the free carrier concentration being 1.7×10^{13} cm^{-3}, and L, the specimen length parallel to the biasing electric field, being 80 microns. Results shown in Figure 9 were obtained with a sample of 1.225 cm length in the propagation, "A", direction, providing an N.A. product of 2.08×10^{13} cm^{-2}. We shall use these results to demonstrate the characteristics of the emission observed from a range of different samples.

Electric Field Dependence

For each of the emission spectra shown, the mean biasing electric field is well in excess of the threshold field for N.D.C. in GaAs. Increasing the bias field appears to have very little effect upon the distribution of energy within the emission spectrum, though the general level of power emitted increases. Reduction of the electric field, on the other hand, reveals a sharp threshold field below which there is no observable emission.

Mode of Operation

The sample employed in the results of Figure 9 was shortened to 0.915 cm in the A direction, and at this stage no clear evidence of emission could be obtained. Thus, it is clear that it is the "A" dimension rather than the "L" dimension which is crucial in allowing instability. The empirical requirement for this electromagnetic instability is therefore

$$1.55 \times 10^{13} < \text{N.A.} < 2.08 \times 10^{13} \text{ cm}^{-2}$$

which compares well with the estimate of Section 5.1.1.

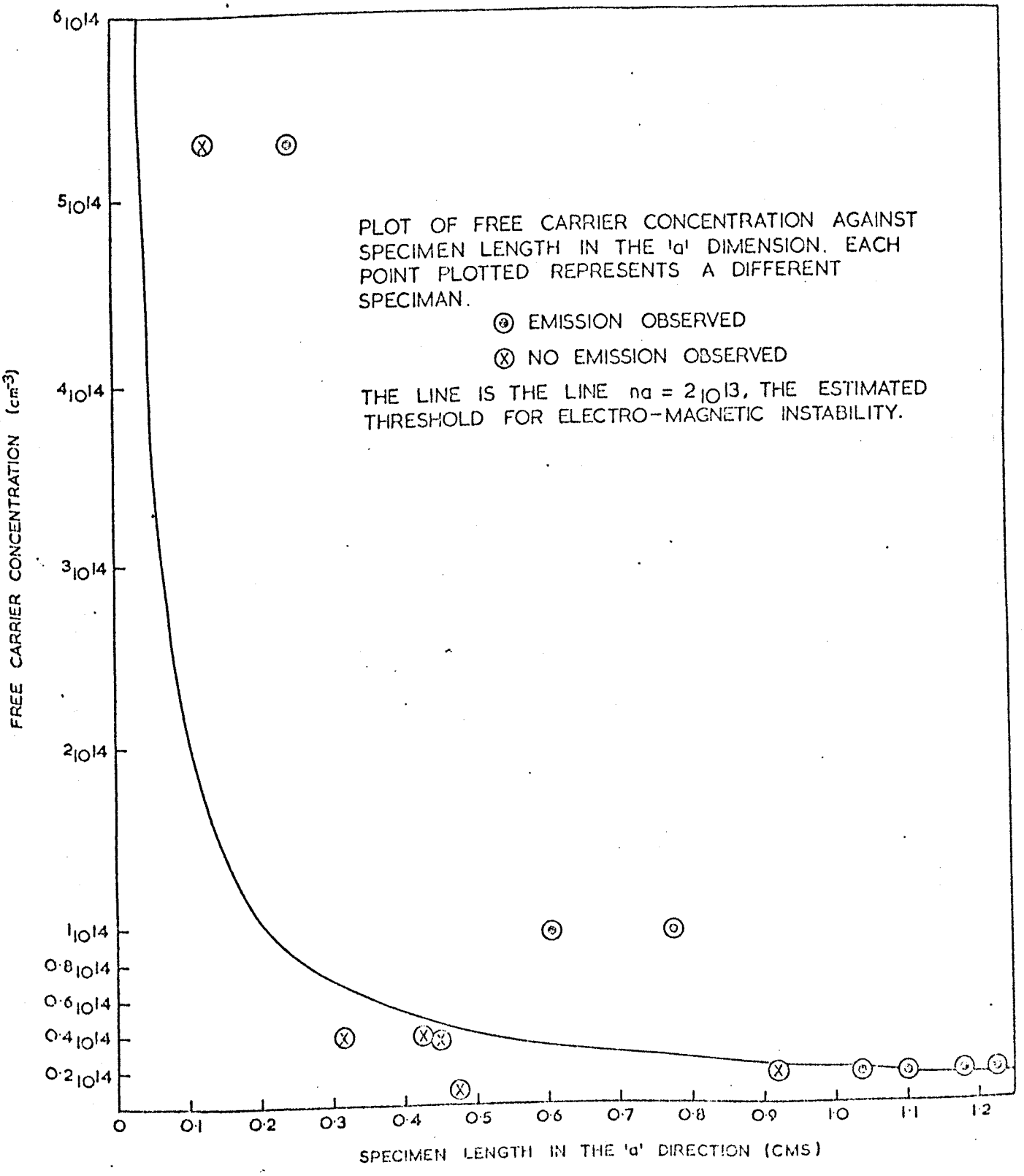
PLOT OF FREE CARRIER CONCENTRATION AGAINST SPECIMEN LENGTH IN THE 'a' DIMENSION. EACH POINT PLOTTED REPRESENTS A DIFFERENT SPECIMAN.
EMISSION OBSERVED
NO EMISSION OBSERVED
THE LINE IS THE LINE na = 2 10 13, THE ESTIMATED THRESHOLD FOR ELECTRO-MAGNETIC INSTABILITY.
FREE CARRIER CONCENTRATION (cm-3)
6 10 14
5 10 14
4 10 14
3 10 14
2 10 14
1 10 14
0·8 10 14
0·6 10 14
0·4 10 14
0·2 10 14
0
0·1
0·2
0·3
0·4
0·5
0·6
0·7
0·8
0·9
1·0
1·1
1·2
SPECIMEN LENGTH IN THE 'a' DIRECTION (CMS)

Fig 10

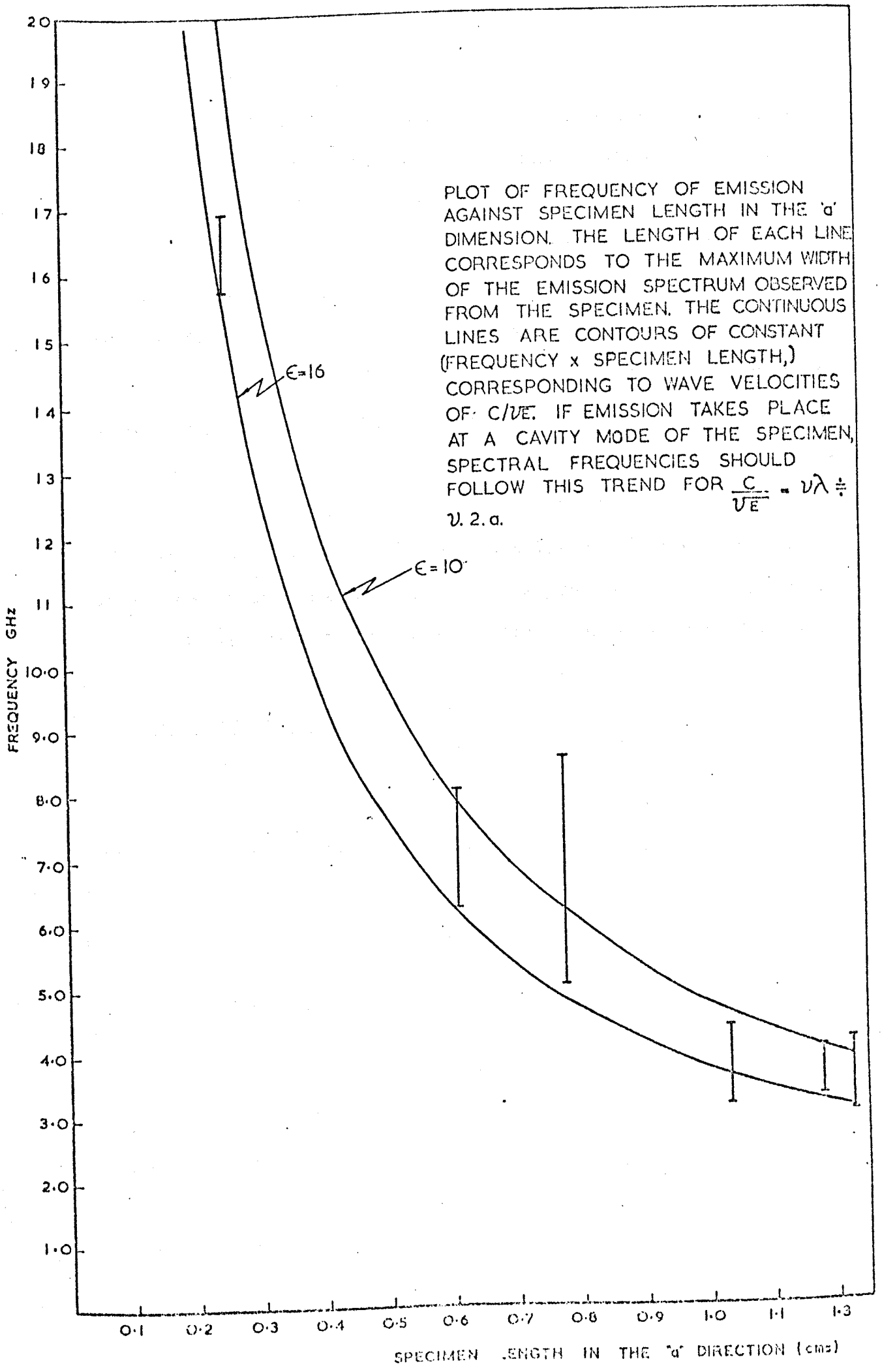
PLOT OF FREQUENCY OF EMISSION AGAINST SPECIMEN LENGTH IN THE 'a' DIMENSION. THE LENGTH OF EACH LINE CORRESPONDS TO THE MAXIMUM WIDTH OF THE EMISSION SPECTRUM OBSERVED FROM THE SPECIMEN. THE CONTINUOUS LINES ARE CONTOURS OF CONSTANT (FREQUENCY x SPECIMEN LENGTH,) CORRESPONDING TO WAVE VELOCITIES OF C/√ε. IF EMISSION TAKES PLACE AT A CAVITY MODE OF THE SPECIMEN, SPECTRAL FREQUENCIES SHOULD FOLLOW THIS TREND FOR $\frac{c}{v\sqrt{\varepsilon}} = \nu\lambda \div \nu.2.a.$
ε=16
ε=10
FREQUENCY GHz
20
19
18
17
16
15
14
13
12
11
10·0
9·0
8·0
7·0
6·0
5·0
4·0
3·0
2·0
1·0
0·1
0·2
0·3
0·4
0·5
0·6
0·7
0·8
0·9
1·0
1·1
1·3
SPECIMEN LENGTH IN THE "a" DIRECTION (cms)

Fig 11

Free Carrier Concentration

In Figure 10 each specimen from which emission was observed is plotted as a function of its free carrier concentration and length in the "A" direction. For reference the rectangular hyperbola formed by the stability condition N.A. = 2×10^{13} is also plotted. It will be seen that in all cases emission is observed only from those specimens having an "N.A" product which is greater than this critical value.

In one case emission is not observed when N.A. exceeds the critical value. This is at a small value of A, and therefore would have been a high frequency sample, where the mobility has possibly decreased, requiring a longer N.A. for oscillation. Such a conclusion is supported by the fact that a rather longer sample (in the A dimension) of the same free carrier concentration material is seen in Figure 10 to have oscillated.

(A similar graph could not be plotted for n-Ge owing to the low frequency range of operation available to this material).

Frequency of Emission

In Figure 11 the observed frequencies of emission are plotted as a function of the specimen length in the "A" direction. Because of the characteristic breadth of the emission spectrum each specimen is represented by a line whose length indicates the breadth of the spectrum. For reference purposes, the line defined by

$$f = \frac{c}{\sqrt{\epsilon}} \cdot \frac{1}{2A}$$

is also shown for which an effective permittivity of 16 is used. Whilst the general trend of these results seems in keeping with the mode of operation already suggested, the breadth of the spectrum is more reminiscent of a noise amplifier than of a cavity in which there is a strong negative resistance. Similar, though less marked spectral characteristics were

also evident in the emission from n-Ge. An understanding of this characteristic feature of the emission is thus clearly essential to the present work.

At this stage we point out that because of the mode of experimental observation, (latch and hold followed by integration) the spectral width is uncertain. There are three sources of such spectral uncertainty in this measurement. The first springs from the fact that this is a pulsed measurement. Thus because the source is only switched on for 5 μ sec no spectral line of less than 1/5 MHz can exist or be resolved by the system.

The second limitation arises because of the role played by the spectrum analyser. This instrument makes observations of the signal found within the I.F. bandwidth, then moves to an adjacent frequency and makes a similar observation. Thus each frequency is observed in turn, and the rate at which the frequency spectrum is swept is so slow that there is negligable change in the frequency of observation during a high field pulse. Since the spectrum analyser sweep is not synchronised to the high field pulse, and integration takes place over many pulses, the whole spectrum is interrogated after a suitable period of time. However, within any one pulse only one frequency channel having a width equal to the I.F. bandwidth of 1 MHz can be studied, owing to the slow sweep rate. Thus a more stringent limitation upon the frequency resolution than that imposed by the pulse length is introduced by the spectrum analyser. A limit which on the one hand implies that no structure narrower than 1 MHz can now be resolved, and on the other hand requires 1 μ Sec for a signal in a given frequency channel to be properly observed. Any signal which is present in a frequency channel for a shorter period is of course still observed, but with a reduced sensitivity, energy having been spread into the adjacent

spectral range to be observed when, in subsequent pulses the analyser interrogates those frequencies. Consequently in the present observation the broad spectrum observed could be derived either from a set of independent oscillators throughout the frequency range each switched on for the duration of the high field pulse. Alternatively one oscillator sweeping across the 1 GHz range during the 5 μ Sec high field pulse would produce a signal in each 1 MHz frequency gate, and therefore also produce a broad spectrum. The two are indistinguishable because of the instrumental response time.

Finally, because of the pulse to pulse integration which is necessary it is impossible to tell if a given 1 MHz frequency gate receives a signal in each high field pulse, indicating pulse to pulse reproducibility. The alternative possibility is of course that the device produces a different frequency with each high field pulse. In summary therefore, it could be that

a) All the frequencies, shown in Figure 9 for example, are simultaneously present throughout the high field pulse.

b) The emission spectrum is the same from pulse to pulse, but changes with time during each high field pulse.

c) The emission is different from pulse to pulse.

These three possibilities will be examined in the following section using a series of experiments specifically designed to distinguish between them. They will be referred to as spectra of type a), b) or c) as they are considered, and the emphasis will be upon evaluating the "short term spectral width" *

---

* The phrase "short term spectral width" is not of course intended to imply a measurement of a frequency in anything approaching zero time. Rather to focus attention upon the importance of progressively more rapid

observations. (made with a system having an appropriately increased bandwidth). In the case of spectrum a),the observed band width would not change. (in the time domain signals at a given frequency would occur at all points within the field pulse). In the second case the spectrum would get narrower. (and a given frequency would occur at a certain time or times within the field pulse). Spectrum c)would present a different spectrum for each pulse. (a given frequency being observed from some pulses and not others). Finally of course as observation times of 10^{-9} secs and less are approached the observed spectrum must undergo instrumental broadening.

The term will be used frequently in this sense throughout the remainder of this thesis.

Power Emitted

A crude estimate of the power emitted is possible, knowing the sensitivity of the spectrum analyser. This is obtained by using a continuous source of a similar frequency which is fed into the spectrum analyser and latch and hold systems, via a variable attenuator. The dummy signal was attenuated until it produced a displacement upon the pen recorder of the same magnitude as that obtained from the actual device. Finally, the signal is reduced by further attenuation to become commensurate with noise upon the spectrum analyser screen. The attenuation necessary at this final stage is equal to the number of dB by which the detected signal exceeds the known noise level of the spectrum analyser. This procedure produced an estimated peak power of 1 micro watt per megaoycle bandwidth.

Two comments are necessary regarding this estimate. They refer first to the units employed in the measurement, and second, to the comparison of a continuous dummy signal with a pulsed real signal.

The argument is closely allied to that of the previous paragraphs. However, we now examine its impact upon measurements of power.

The units of power per unit bandwidth are necessary because of the role played by the spectrum analyser. As we have seen this instrument makes an observation of the signal received within a certain region of the spectrum defined by the I.F. band width. (1 MHz in the present observation). Then, it moves to the adjacent region and makes a similar observation there. Such a system cannot therefore distinguish the following two situations :

1) Two 1 micro watt oscillators continually present one in each spectral range, corresponding to an I.F. bandwidth. Total power is then 1 micro watt plus 1 micro watt equals 2 micro-watt. (cf. Spectrum of type a) defined earlier in this sub-section)

2) A frequency agile 1 micro watt source which happens to be in the lower spectral I.F. range when the spectrum analyser is observing it, and also happens to be in the upper spectral I.F. range when that is being monitored. Total power 1 micro-watt NOT 2 micro-watt. We conclude therefore that the spectrum analyser can only measure the power within the band width of its observation, in this case 1 MHz.

The second of the two possibilities cited above is lifted from the plane of the improbable by the fact that the spectrum analyser is followed by a latch and hold circuit which integrates throughout the high field pulse and indeed over many high field pulses. It would therefore "catch" any signal sweeping through the I.F. band width whenever it occurred during the pulse (C.F. spectrum of type two in previous sub section). Equally, if the emission frequency varied from pulse to pulse, because of the latch

and hold integration over many pulses, a signal could be observed in any band width currently being monitored by the spectrum analyser. (C.F. spectrum of type 3 in previous sub section).

Thus an observation of powers of order 1 micro watt per MHz band width is fundamental to the observational system. It may not be multiplied by the total frequency range over which emission is seen to occur, namely 1 GHz, to give a total apparent power of 1 milli-watt. This latter power is in fact the maximum power which this observation could imply if emission at all the spectral frequencies co-existed throughout each high field pulse. The actual power depends upon the correlation of the adjacent MHz band widths, or, the real time dependence of the power spectrum.

A second qualification is necessary regarding this estimate of the power emitted. This follows from one of the foregoing possibilities namely of an emission frequency which changes during the high field pulse. The high field pulse of 5 micro sec duration has been chosen to be somewhat longer than $^{1}/$(I.F. band width) in order that the spectrum analyser may respond to incoming signals. However, if a narrow ($\delta f \ll 1$ MHz) spectral line is sweeping linearly across the 1 GHz spectral range shown in Figure 9 in 5 micro sec, then the time spent in any 1 MHz frequency range is only 5×10^{-9} sec. Thus any signal detected by the spectrum analyser is detected with a much reduced sensitivity. An estimate of this reduction is readily obtained if the spectrum analyser is likened to a tuned circuit of centre frequency 3 GHz and band pass half width of 1 MHz. The objective is then to calculate the response of such a circuit to an input oscillatory function which it "sees" for only 5×10^{-9} seconds.

The proposed equivalent circuit is shown in Figure 12.

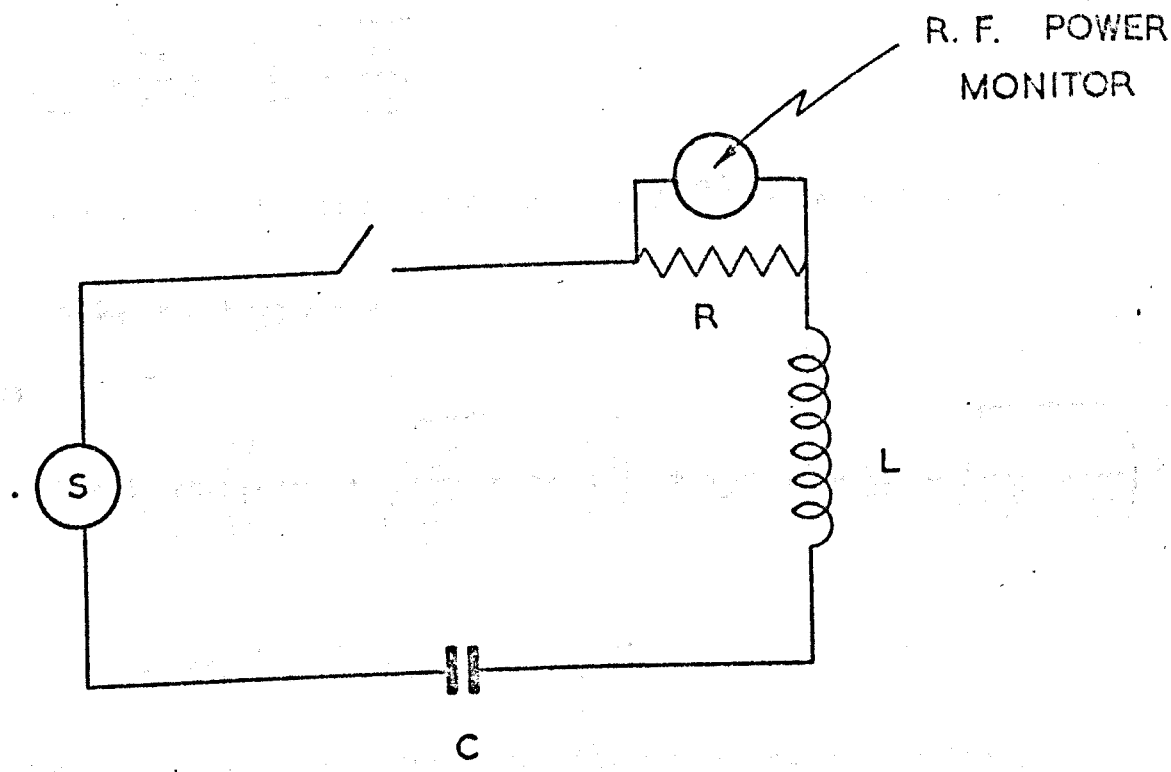

PROPOSED EQUIVALENT CIRCUIT OF SPECTRUM ANALYSER

FIG 12

Taking the emf as $E_o e^{i\omega t}$ gives

$$L\frac{dI}{dt} + RI + \frac{1}{C}\int I dt = E_o\, e^{i\omega t}$$

This equation has a "particular integral", $I = I_o\, e^{i\omega t}$

where

$$I_o = E_o/(i\omega L + R - i/C\omega)$$

$$= -\,i\,E_o\omega\,/L(\omega-\omega_+)\,(\omega-\omega_-)$$

$$\omega_{\pm} = \frac{Ri}{2L} \pm \sqrt{\frac{1}{LC} - \frac{R^2}{4L^2}}$$

The complementary function is of the form $Ae^{\alpha t}$ where α is given by

$$A\left(L\alpha + R + \frac{1}{C\alpha}\right) = 0$$

Thus

$$I = A_+ \exp\left(\left(-\frac{R}{2L} + \sqrt{\frac{R^2}{4L^2} - \frac{1}{LC}}\right)t\right) + A_-\exp\left(\left(-\frac{R}{2L} - \sqrt{\frac{R^2}{4L^2} - \frac{1}{LC}}\right)t\right)$$

$$= A_+ \exp(\theta_+ t) + A_- \exp(\theta_- T)$$

Combining the particular integral and the complementary function we obtain the general solution

$$I = A_+ \exp(\theta_+ t) + A_- \exp(\theta_- t)$$

$$-\frac{i\,E_o\,\omega\,\exp(i\omega t)}{L\,(\omega-\omega_+)\,(\omega-\omega_-)}$$

Boundary conditions of zero current and stored charge at zero time applied to this equation for the current and its integral for the charge give

$$A_+ + A_- = \frac{i\ E_o \omega}{L\,(\omega - \omega_+)(\omega - \omega_-)}$$

$$\frac{A_+}{\theta_+} + \frac{A_-}{\theta_-} = \frac{E_o}{L\,(\omega - \omega_+)(\omega - \omega_-)}$$

After some manipulation the solution is thus

$$I = \text{R.P.}\ \frac{E_o}{L}\left(\frac{-i\omega_-\ \exp i\omega_- t}{(\omega_- - \omega)(\omega_- - \omega_+)} - \frac{i\omega_+\ \exp i\omega_+ t}{(\omega_+ - \omega_-)(\omega_+ - \omega)}\right.$$

$$\left. - \frac{i\omega \exp\ i\omega t}{(\omega - \omega_+)(\omega - \omega_-)}\right)$$

Writing $\omega_\pm = \pm\ \omega_o + i\delta$ we obtain

$$I = -\ \frac{\text{R.P.}\ i\ E_o \left[i\ e^{-\delta t}\ \text{Sin}\omega_o t\right.}{\left[(\omega + \omega_o)^2 + \delta^2\right]\ \left[(\omega - \omega_o)^2 + \delta^2\right]\omega_o L}\ \left\{\omega_o^4 + \delta^4 + 2\omega_o^2\delta^2\right.$$

$$\left. - i\omega_o^2\omega\delta - \omega^3 i\delta - \omega i\delta^3 + \omega^2\delta^2 - \omega^2\omega_o^2\right\} + e^{-\delta t}\ \text{Cos}\ \omega_o t\ \left\{\right.$$

$$\left.-\omega^3\omega_o + \omega\omega_o^3 + \omega\omega_o\delta^2 - 2\omega^2\omega_o\, i\delta\right\} + \omega e^{i\omega t}\omega_o\ \left\{\omega^2 - \omega_o^2 - \delta^2 + 2\omega i\delta\right\}$$

The non-oscillatory power in the resistor at infinite time is given by

$$R\ I\ I^* = \frac{E_o^2\omega^2 R}{L^2}\Big/\ \left[(\omega + \omega_o)^2 + \delta^2\right]\ \left[(\omega - \omega_o)^2 + \delta^2\right]$$

Which is readily shown to be a maximum when

$$\omega^2 = \omega_o^2 + \delta^2$$

and to fall to half maximum power when

$$\omega = \omega_o \pm \delta$$

Thus since the spectrum analyser represented by the tuned circuit of Figure 12 has a centre frequency of 3GHz and band-width of 1 MHz

$$\delta = 0.5 \times 10^6$$
$$\omega_0 = 3 \times 10^9$$

The power absorbed by the resistor at a time t such that $\omega_0 >> t^{-1} >> \delta$ is found to be

$$\left[|I|^2 R\right]_t \approx \left[|I|^2 R\right]_{t \to \infty} \cdot 2\delta t$$

Thus with the assumption that a narrow spectral line sweeps over the 1 GHz range of spectral emission shown in Figure 9 in 5×10^{-6} secs. (i.e. the high field pulse duration) "t", the time spent in any 1 MHz bandwidth is 5×10^{-9} secs. Therefore the observed power in a 1 MHz bandwidth of 1 micro-watt implies an actual power of approaching 1 milli-watt per MHz bandwidth. If however, the frequency emitted during each pulse is constant, but varies from pulse to pulse (spectrum of type 3) the actual power is 1 micro-watt.

Finally, if all frequencies are simultaneously present in each pulse, (spectrum type 1) then the power is again of order 1 mill-watt.

5.3 Concluding Comments

In this section observations of microwave emission from GaAs have been described, which are demonstrated to be a consequence of amplification of T.E.M. waves within the specimen cavity. Characteristic threshold electric fields, and N.A. products occur as expected. However, the short term spectral width and in consequence the power emitted remain uncertain. If the spectra presented thus far represent the short term spectral width (i.e. if the spectral width observed with an observational time of say 10^{-8} secs instead of 5×10^{-6} secs is identical) then, as we shall show in the

next section, some alternative explanation of the mechanism of microwave generation is necessary. The following section is therefore devoted to an examination of the spectral width and power, and, in turn to achieving an understanding of the mechanism of microwave generation.

References

1. I. B. Bott and W. Fawcett

   Advances in Microwaves, 3, (1968)

2. H. D. Rees

   Privately communicated mobility data related

   to that shown in IBM, Jnl. of Res. Dev. 13, (1969)

3. See for example J. G. Ruch and G. S. Kino

   Appl. Phys. Lett. 10, 40-42, (1967)

   or

   W. Fawcett, A. D. Boardman and S. Swain

   J. Phys. Chem. Sol. 31, 1963-1990 (1970)

4. A. P. Neukerman and G. S. Kino

   10th Int. Conf. Phys. of Semicond. 40-45 (1970)

5. S. M. Mahrous and P. N. Robson

   Elect. Lett. 2, 107-108 (1966)

6. See Reference 1, p.285.

7. H. D. Rees

   Sol.Stat. Comm. 7, 267-269 (1969)

6. The Mechanism of Microwave Generation : The Form of the Emission Spectrum

Foregoing sections have employed the concept of an active "Fabry Pérot" etalon in which emission stems from round trip gain of noise within a cavity, We now have to relate the spectrum to be expected from such a system to that observed experimentally. This problem is tackled from a theoretical standpoint initially. As a result of this work, the relationship between the spectral power and spectral width will emerge as of fundamental importance to an understanding of the mechanism of microwave generation. In the latter half of this Section experiments specifically designed to evaluate the short term spectral width and power will be described. The three basic forms of emission spectrum, which it has been pointed out in Section 5 cannot be distinguished by the latch and hold equipment, will be distinguished experimentally.

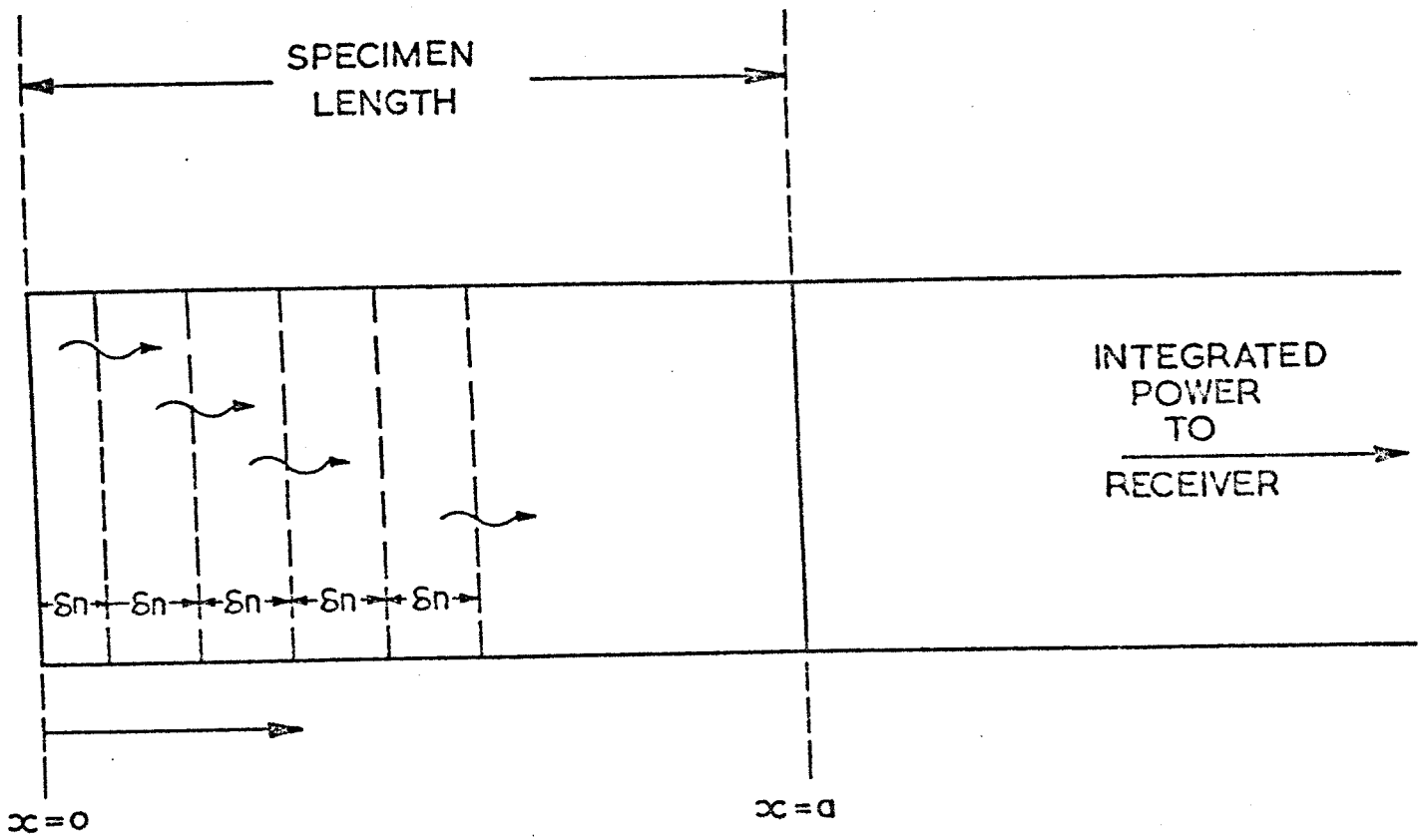

A SPECIMEN DIVIDED INTO A LINEAR ARRAY OF NOISE SOURCES, ALONG THE DIRECTION OF WAVE PROPAGATION.

FIG. 1

6.1 Theoretical Relationship of Spectral Width and Power

In Section 2 we used a rather simple argument to predict a very narrow emission spectrum from a Fabry Pérot etalon, having round trip gain. The observations of emission from both n-Ge and GaAs have however been of anything but a narrow emission spectrum. Indeed, the spectrum is much more reminiscent of amplified noise than of a well defined spectral line. We are therefore forced to consider the possibility of the observed emission arising from a cavity filled with noise sources, but not having round trip gain.

In this Section we first discuss the expected emission spectrum from a linear array of elemental noise sources within a cavity. It will be shown that the expected spectral width is not incompatible with that observed experimentally particularly in the case of GaAs. However when the power expected from such a system is calculated, this will be shown to be incompatible with the experimental results. This Section concludes that if :

i) The actual spectral power were much lower than previous observations suggested then the emission could come from a noise amplifying cavity.

ii) The spectral width were much smaller than previous observations suggested then the emission could come from a cavity oscillator i.e. a cavity having internal round trip gain.

6.1.1 Emission Spectrum from a Linear Array of Noise Sources within a Cavity

We consider the emission from a linear array of uncorrelated elemental noise sources within a cavity. The cavity is assumed not to have round trip gain. The noise sources are arrayed along the device as shown in Figure 1. We avoid the complexity of the non-uniformity parallel to the applied electric field by assuming a net resultant noise emission from the whole elemental height of the sample.

A source of radiation of amplitude A_o is assumed, where the temporal dependence is implicit, and may be regarded as being carried in A_o. Then for a source at a point x along the cavity the emitted signal in the positive x direction is

$$A = A_o \exp(i\,k(a-x)\,).\ T.\ (1 + r\,e^{i\,k\,a}\,r\,e^{i\,k\,a}\ )$$

where k is the wave number of waves propagating through the N.D.C. medium and T and r are the electromagnetic surface transmission and reflection co-efficients. Assuming that no frequency has round trip gain this becomes

$$= A_o\,e^{i\,k(a-x)}\,T\left(\frac{1}{1 - r^2\,e^{2\,i\,k\,a}}\right)$$

The total power emitted must be obtained by adding the powers rather than amplitude of the uncorrelated elemental noise sources along the x axis. The non oscillatory power emerging along + x from an element δx

$$= \frac{P_o\,e^{-2\,k_i(a-x)}\ T\,T^*\,\delta x}{(1 - r^2\,e^{2\,i\,k\,a})(1 - r^2\,e^{2\,i\,k\,a})^*}$$

After some manipulation this can be shown to reduce to

$$A\,A^*\,dx = P_o\,\xi\,e^{-\,2\,k_i(a-x)}\,dx$$

where

$$\xi = 4(k_R^2 + k_i^2)\ \left[(k_R + k_o)^2 + k_i^2\right]\ \Big/\ \Big[(1 + \alpha^2)\,(A_1^2 + B^2 + C^2 + D^2) + 2(1 - \alpha^2)(A_1 B + CD) + 2\alpha\left[(B^2 - A_1^2 + D^2 - C^2)\,\mathrm{Cos}\,\phi + 2\,\mathrm{Sin}\,\phi\ (BC - A_1 D)\right]\Big]$$

where T and R have been expressed in terms of k_R

k_i and k_o and

$$A_1 = k_R^2 - k_i^2 + k_o^2$$

$$B = 2 k_R k_o$$

$$C = 2 k_i k_R$$

$$D = 2 k_i k_o$$

$$\alpha = e^{-2 k_i a}$$

The total power from this array of sources is then

$$P = \int_o^A A A^* \, dx = P_o \xi \int_o^a e^{-2k_i (a-x)} \, dx$$

$$= \frac{P_o \xi}{2k_i} \left(1 - e^{-2k_i a} \right)$$

providing there is no round trip gain within the cavity. We assume k_i is frequency independent and set $e^{-2k_i a} = 1$ as a typical value. The fairly characteristic values of k_R, a, and k_o, implied by the results of Figure 9 of Section 5 at the centre of the spectrum then yield a predicted spectral width of

$$\frac{\delta f}{f} \approx \frac{1}{2.7}$$

This result is very similar to the results obtained experimentally, particularly when GaAs specimens are employed. It would, in itself, seem to indicate that the emission observed is much more likely to be associated with this type of noise amplification process than with a round trip gain process. However, there is a fundamental limit upon the amount of gain possible within the cavity before the onset of round trip gain i.e.

$$e^{i2k_i a} < \frac{1}{r^2} \approx 3$$

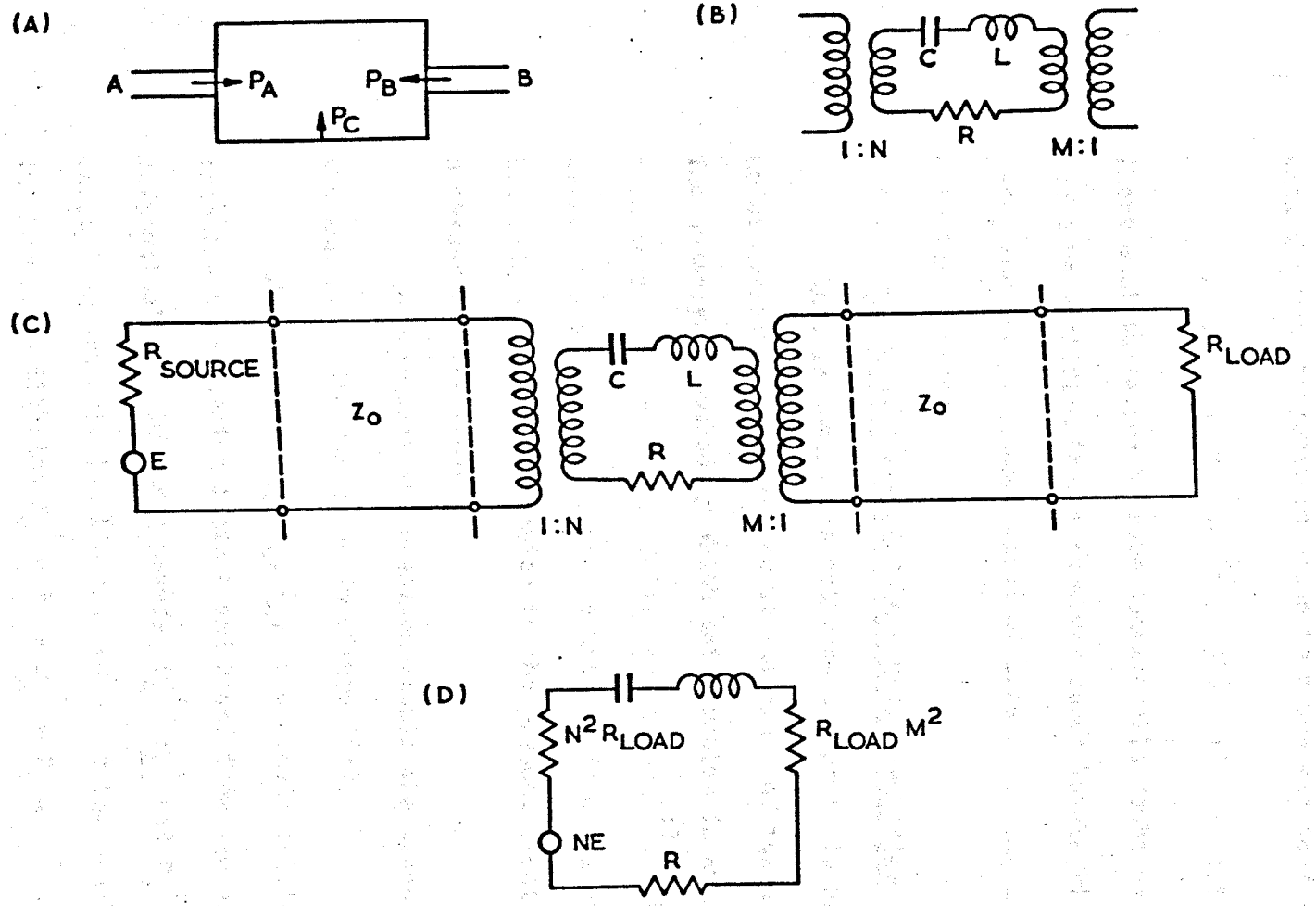

EQUIVALENT CIRCUITS OF A TWO PORT CAVITY NOISE AMPLIFIER

FIG. 2

In contrast, thermal noise is at a very much lower power level than those power levels at which the present signals are observed; thus we may contrast the 1 micro watt per MHz band width observed with the room temperature noise in a one MHz band width of

$$KT \delta f = 1.37 \quad 10^{-23} \cdot 300 \quad 10^{6} = 4.1 \quad 10^{-15} \text{ watt}$$

There must therefore be some considerable doubt as to whether noise could be amplified to the observed power levels without round trip gain, and the consequent onset of line narrowing in the emission spectrum.

6.1.2 The Power Spectrum from a Noise Amplifier

In this Section we estimate the power to be expected from a noise amplifier, in relation to the width of the associated spectrum. The underlying method by which this problem is approached is derived from some work by Gordon, Zeiger and Townes[1]. However, the derivation of the fundamental equations is considerably simpler, and the mode of their application to the present problem is of course necessarily different.

We represent the specimen within the transmission line by the schematic diagram shown in Figure 2(a).

Noise powers P_a, P_b, P_c, are considered to enter the cavity from the transmission lines a and b and from the cavity walls c respectively. Similarly powers P_a' P_b' and P_c' leave the cavity for transmission lines a and b and the cavity wall c respectively. In thermal equilibrium $P_b' - P_b = P_a' - P_a = P_c' - P_c = 0$

Philosophy of the Analysis

When the system is not in equilibrium, having a negative resistance medium within the cavity, the same noise is generated in a, b, and c, and powers P_{a_a}, P_{b_a}, and P_{c_a} enter the cavity. However, the powers leaving the cavity, P_{a_a}', P_{b_a}' and P_{c_a}' have now clearly increased. The power leaving the cavity for transmission line b, P_{b_a}' is clearly derived from P_{a_a} and P_{c_a}, providing that the switch to negative resistance has added no new noise source*. Then

$$P_{b_a}' = P_{a_a} \cdot T_{b_a} + P_{c_a} \cdot T_{b_c}$$

where T_{b_a} and T_{b_c} are the microwave transmission co-efficient for energy entering the cavity from a or c and leaving along b. These transmission coefficients will be calculated in terms of various Qs of the system. Since the emergent power is measured and the noise power is known, it is possible to evaluate the systems Q. Thus the emission spectral width is obtained as a function of the emission power, as required.

Calculation of Transmission Coefficients

We may clearly write

$$P_{b_a}' - P_{b_a} = P_{a_a} \cdot T_{b_a} + P_{c_a} \quad T_{b_c} - P_{b_a}$$

$$= P_{a_a} \cdot \frac{\text{Loss of power to b}}{\text{Loss of power to b and c}} + P_{c_a} \cdot$$

$$\frac{\text{Loss of power to b}}{\text{Loss of power to b and a}} - P_{b_a}$$

---

* We shall return to this assumption at a later stage. We also assume that after entry no power is reflected back along its port of entry.

since power entering the cavity from a, P_{a_a} must finally leave the cavity via ports b or c. Thus

$$P_{b_a}' - P_{b_a} = P_{a_a} \cdot \frac{Q_{La}^{\,a}}{Q_b} + P_{c_a} \frac{Q_{La}^{\,c}}{Q_b} - P_{b_a} \qquad \ldots (1)$$

where $Q_a = 2\pi$ Stored energy in cavity/energy lost to port α per cycle, Q_L is the loaded cavity Q in the absence of the negative resistance, i.e. $\frac{1}{Q_L} = \frac{1}{Q_a} + \frac{1}{Q_b} + \frac{1}{Q_c}$,

$Q_L^{\,x}$ is the loaded Q, neglecting any power loss to port x, e.g.

$$\frac{1}{Q_L^{\,a}} = \frac{1}{Q_b} + \frac{1}{Q_c}$$

and $Q_{L_a}^{\,x}$ is the loaded Q, neglecting any loss of power to port x when the cavity has a negative resistance medium within it.

It now remains to calculate the powers entering the cavity from the respective ports. We employ an equivalent circuit for this purpose which is shown in Figure 2b.

In Figure 2c we include the source of amplitude E, a source impedance R_s, transmission lines of impedance Z_o to the specimen cavity and away from it and a load impedance R_L. The system would in practise be matched and we therefore set $R_L = R_s = Z_o$. This complete equivalent circuit is now readily transformed into equivalent elements which all lie within the cavity as shown in Figure 2d thus simplifying the problem.

In equilibrium the net power entering the cavity from the source, P_{source} is equal to that dissipated in the cavity and load,

$$P_{source} = \frac{I I^*}{2} \cdot \left\{ R + M^2 Z_o \right\}$$

$$= \left| \frac{N E}{(N^2 Z_o + R + M^2 Z_o) + j(\omega L - \frac{1}{\omega C})} \right|^2 \left\{ \frac{R + M^2 Z_o}{2} \right\}$$

remembering that $R_s = R_L = Z_o$.

A maximum power of $P_o = \frac{|E|^2}{2.4\ Z_o}$ is available from the source when matched. $\left[\frac{E^2}{2\ Z_o}\right.$ is delivered to the source plus matched load but only a half of this is available to the load.$\left.\right]$ Thus the fraction of power entering the cavity is

$$\frac{P_{source}}{P_o} = \left| \frac{N\,E}{(N^2Z_o + R + M^2Z_o) + j(\omega L - \frac{1}{\omega C})} \right|^2 \left\{ R + M^2Z_o \right\} \frac{4Z_o}{|E|^2}$$

$$= \frac{4\,N^2Z_o\,(R + M^2Z_o)}{(N^2Z_o + R + M^2Z_o)^2 + (\omega L - \frac{1}{\omega C})^2}$$

Now the unloaded Q is $Q_u = \frac{\omega_o L}{R} = \frac{1}{\omega_o CR}$

and loaded Q is $$Q_L = \frac{\omega_o L}{(N^2Z_o + R + M^2Z_o)}$$

and external Qs are $Q_{load} = \frac{\omega_o L}{M^2Z_o}$

$$Q_{source} = \frac{\omega_o L}{N^2Z_o}$$

Thus after some algebra

$$\frac{P_{source}}{P_o} = \frac{1/\left(Q_{source} \cdot Q_L^{source}\right)}{\left(1/(2Q_L)\right)^2 + \frac{1}{4}\left(\frac{\omega}{\omega_o} - \frac{\omega_o}{\omega}\right)^2} \qquad \ldots \quad (2)$$

So long as this system does not oscillate, equation 2 remains valid even if the dissipation within the cavity is negative. Thus when the cavity has a negative resistance element within it we have

$$\frac{P_{source}}{P_o} = \frac{1/\left(Q_{source} \cdot Q_{L_A}^{source}\right)}{\left(\frac{1}{2Q_{L_A}}\right)^2 + \frac{1}{4}\left(\frac{\omega}{\omega_{o_A}} - \frac{\omega_{o_A}}{\omega}\right)^2}$$

since the Q of the source has clearly not been changed though looking in at the port used by the source the remaining Q, Q_L^{source} certainly appears to have changed to some new value $Q_{L_a}^{source}$.

In the terms of the circuit of Figure 2(a) therefore

$$\frac{P_{c_A}}{P_o} = \frac{1/\left(Q_c \cdot Q_{L_A}^{c}\right)}{\left(\frac{1}{2Q_{L_A}}\right)^2 + \frac{1}{4}\left(\frac{\omega}{\omega_{o_A}} - \frac{\omega_{o_A}}{\omega}\right)^2} \quad \ldots (3)$$

and

$$\frac{P_{a_A}}{P_o} = \frac{1/\left(Q_a \cdot Q_{L_A}^{a}\right)}{\left(\frac{1}{2Q_{L_A}}\right)^2 + \frac{1}{4}\left(\frac{\omega}{\omega_{o_A}} - \frac{\omega_{o_A}}{\omega}\right)^2} \quad \ldots (4)$$

$$\frac{P_{b_A}}{P_o} = \frac{1/\left(Q_b \cdot Q_{L_A}^{b}\right)}{\left(\frac{1}{2Q_{L_A}}\right)^2 + \frac{1}{4}\left(\frac{\omega}{\omega_{o_A}} - \frac{\omega_{o_a}}{\omega}\right)^2} \quad \ldots (5)$$

substituting (3), (4) and (5) in Equation (1) therefore,

$$P_{b_A}' - P_{b_A} = \delta P = \frac{KT}{Q_b}\left\{\frac{1/Q_L^{b} - 1/Q_{L_A}^{b}}{\left(\frac{1}{2Q_{L_a}}\right)^2 + \frac{1}{4}\left(\frac{\omega}{\omega_{o_a}} - \frac{\omega_{o_a}}{\omega}\right)^2}\right\} \quad \ldots (6)$$

where P_o has been set equal to the thermal noise of KT per unit bandwidth. Consequently all powers "P" are hereafter in units of noise power per unit bandwidth.

We note that :

(1) If $Q_L^b = Q_{L_a}^b$ there is no net noise exchange between the cavity and the transmission line b, which is of course correct.

(2) If $Q_L^a \rightarrow \infty$ then at the frequency $\omega = \omega_{o_a}$ infinite power is emitted. This is of course the threshold for oscillation at a cavity mode, and the theory becomes invalid at this point.

(3) Equation 6 is equalent to equation 29 in Reference 1.

This equation relates the spectral power output and spectral bandwidth as required; the second point above is of course just one extreme of this relationship.

In order to remove some of the unknown terms in Equation 6 we integrate over frequency to find the power in a certain bandwidth, $2D_1$. If we consider operation below, say, 10 GHz, the slope mobility of GaAs is largely frequency independent as shown by Figure 1 and 2 of Section 5. Thus we assume no suppressed frequency dependence in Equation 6, and further that the power of interest is close to the cavity resonance, so that

$$\int_{\omega_{o_A} - D_1}^{\omega_{o_A} + D_1} \delta P \, d\nu = \frac{KT}{Q_b} \left\{ \frac{1}{Q_L^b} - \frac{1}{Q_{L_A}^b} \right\} \left[\frac{2\omega_{o_A}}{Q_{L_A}^{-1}} \tan^{-1} \left\{ \frac{\omega - \omega_{o_A}}{\omega_{o_A} \left(\frac{1}{2Q_{L_A}} \right)} \right\} \right]_{\omega_{o_A} - D_1}^{\omega_{o_A} + D_1}$$

where $\left(\frac{\omega}{\omega_{o_A}} - \frac{\omega_{o_A}}{\omega}\right) \doteq \frac{2(\omega - \omega_{o_A})}{\omega_{o_A}}$ has been used. Hence

$$\int_{\omega_{o_A} - D_1}^{\omega_{o_A} + D_1} \delta P \, d\nu = \frac{KT}{Q_B} \left\{\frac{1}{Q_L^b} - \frac{1}{Q_{L_A}^b}\right\} \left\{\tan^{-1}\left(\frac{2Q_{L_A} D_1}{\omega_{o_A}}\right) - \tan^{-1}\left(\frac{-2Q_{L_A} D_1}{\omega_{o_A}}\right)\right\} 2Q_{L_A} \omega_{o_A} \quad \ldots (7)$$

Having an experimental observation of one micro-watt of microwave power per MHz bandwidth from GaAs, we now calculate for comparison the power predicted in such a bandwidth. For a 1 MHz bandwidth we have $10^6 = D_1 \ll \omega_{o_A} = 3 \times 10^9$. Thus expanding the inverse tangent function, (for Q_{L_a} is known from the same experimental observation to be small)

we have

$$\int_{3\text{ GHz} - 10^{+6}}^{3\text{ GHz} + 10^{+6}} \delta P \, d\nu = 2 \frac{Q_{L_A}}{Q_b} \omega_{o_A} KT\pi \left\{\frac{1}{Q_L^B} - \frac{1}{Q_{L_A}^B}\right\}$$

Writing $\frac{1}{Q_{L_A}^b} = \frac{1}{Q_L^b} - \frac{1}{\beta}$ we have

$$\delta P = \int_{3\text{ GHz} - 10^{-6}}^{3\text{ GHz} + 10^{-6}} \delta P \, d\nu = \frac{2\omega_{o_A} KT\pi\beta Q_L}{Q_b \beta (\beta - Q_L)} \quad \ldots (8)$$

From Equation 6, the spectral half power points occur when

$$\left(\frac{1}{2Q_{L_a}}\right)^2 = \left(\frac{\omega - \omega_{o_A}}{\omega_{o_A}}\right)^2$$

Thus the spectral width

$$\Delta\gamma = \frac{\omega_{o_A}}{Q_{L_A}} = \omega_{o_A}\left(\frac{\beta - Q_L}{\beta\, Q_L}\right) \qquad \ldots (9)$$

and with Equation 8

$$\delta P_{1\ MHz} = \frac{2\omega_{o_A}\, KT\pi\, (\omega_{o_a} - Q_L \Delta\gamma)}{Q_b\, \Delta\gamma\ \ Q_L} \qquad \ldots (10)$$

On the basis of the reflection co-efficient of a GaAs/air surface, Q_b may be estimated as $\dot{\approx}$ 3, and from the experimental work (Section 5), the overall spectral width when the power was estimated was $\dot{\approx}$ 1 GHz, whilst ω_{o_A} was $\dot{\approx}$ 3×10^9 Hz.

Thus

$$P'_{B_{A_{1\ MHz}}} - P_{B_{A_{1\ MHz}}} = \delta P_{1\ MHz} \leq \frac{2\ KT\pi\ (3 \times 10^9)^2}{3 \times 10^9\ Q_L} \qquad \ldots (10a)$$

$$= \frac{7.75 \times 10^{-11}}{Q_L} \text{ Watt}$$

Now $P_{b_{a_{1\ MHz}}}$ cannot be larger than the total noise power generated in transmission line b in a 1 MHz bandwidth which is $1.37 \times 10^{-23} \cdot 300 \times 10^6 \dot{\approx} 4 \cdot 10^{-15}$ watt and is therefore negligible.

Clearly then, from (10a), powers of 1 micro-watt cannot be predicted on the basis of this noise amplifier model, and an overall spectral bandwidth of 1 GHz. Nor can any refuge be found in questioning the earlier assumption that the negative resistance process is noise free, for even if a huge electron noise temperature

of 30,000°K is assumed and attributed to all noise generators in the system, adequate powers are still not predicted.*

We now reverse the computational procedure, and assume that the power in equation (10) is to be 10^{-6} watts as observed with a spectrum analyser having a resolution of 1 MHz. The magnitude of Q_b indicates that Q_L is $\gtrsim$ 3

Thus, with Equation 10,

$$\delta\gamma \gtrsim \omega_{o_A} \frac{1.8 10^{-5}}{Q_L} \gtrsim 6 \times 10^4 \text{ Hz} \quad \ldots (11)$$

in contrast with the experimental value of 10^9 Hz. (For future reference we note in passing that a power of 1 mill-watt would imply a line width of 60 Hz).

We conclude that the spectral breadth and power cannot be simultaneously accounted for by the noise amplifier model. Equally however, the Fabry Perot oscillator seems incompatible with the very broad observed spectra. On the other hand, the experimental data is beyond reproach. The only loop-hole lies in the uncertainties introduced in Section 5 concerning the interpretation of the latch and hold observation. We now therefore proceed to further experimental work; work which is specifically intended to distinguish between the three forms of spectra which, as pointed out in Section 5, could not be resolved by the latch and hold system.

---

* A second method of derivation is possible in which the power of Equation 6 is integrated over a wider spectrum range and this total emitted microwave power equated to the power generated within the sample volume $\int \sigma_{-ve} E_{RF}^2 \, d(vol)$ Here σ_{-ve} is the negative slope conductivity, and E_{RF}, the microwave field amplitude, is set equal to 1 KV/cm. This latter figure is intended to represent a reasonable estimate of the possible fluctuation amplitude. On calculating the spectral line width, again a result which is incompatible with experiment is obtained.

FIGURE 3

Emission spectra with biasing pulse amplitudes of 9.5 volts (top) 10 volts (middle) and 11.5 volts (lower). The centre frequency is 16.9 GHz, and the dispersion 1 GHz across the screen. Vertical (logarithmic) sensitivity of 5 dB/cm.

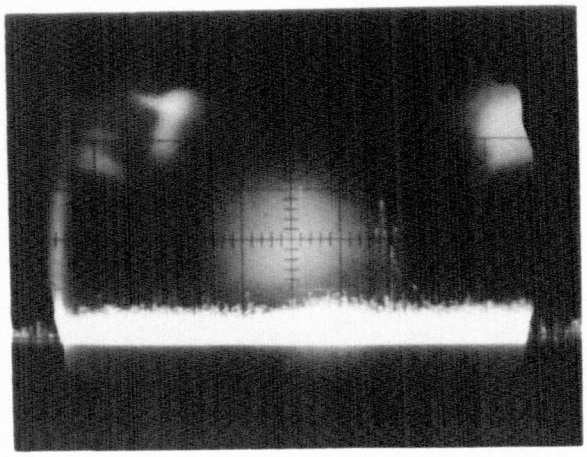

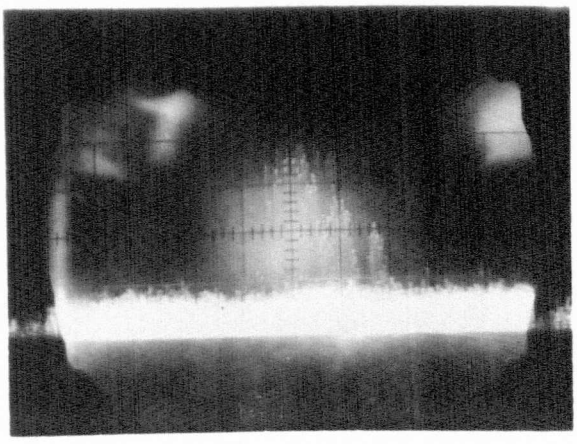

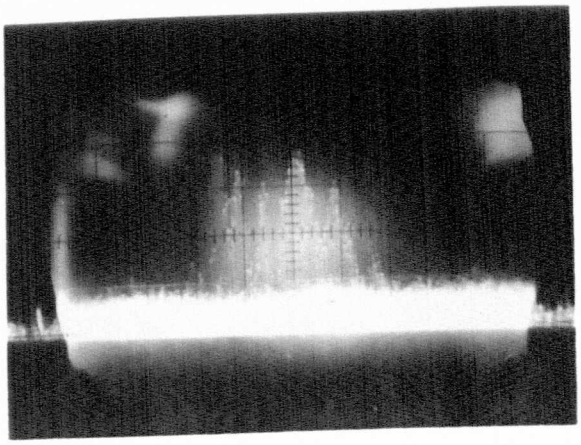

6.2 Experimental Investigation of the Nature of the Emission Spectrum

Interest in this Section is once again confined to specimens having N.L. below the critical value for domain formation.

6.2.1 Demonstration of Electric Field Dependence of Emission Frequency

We first exploit the higher powers available from GaAs than n-Ge by using a less sensitive form of receiver; a panoramic receiver. This receiver has a major advantage over the very sensitive Hewlett Packard spectrum analyser employed thus far, in that it has no local oscillator and intermediate frequency stages. Thus, it does not have the usual problem of spurious image frequencies. Furthermore, because it employs a YIG filter pre-selector any pulse break-through inadvertently allowed merely saturates the filter and no signal is observed rather than spurious responses being produced.

The disadvantage of this equipment is that outputs cannot be taken away to a pen recorder, nor can "bright up" pulses be applied. Instead, photographic integration of the display at low ambient screen intensity, has to be employed. In consequence the photographs presented here are poor, the general glow from the tube phosphor having built up during the photographic display. The remaining high field pulse source and specimen mounting in microstrip transmission line remains unchanged from the previous systems described.

In Figure 3 some emission spectra are shown from a specimen of 5.3×10^{14} free carriers/cc. 2.45 mm in the "A" dimension and 8 microns in the "L" dimension. A number of shorter test samples from the same epitaxial layer and therefore also 8 microns thick gave no emission. Thus the sample may certainly be regarded as

space charge stable. It will be seen that the present longer sample not only oscillates, but provides evidence of an increasing spectral breadth with an increasing amplitude of high field pulse.

This observation demonstrates the electric field dependence of the emission frequency and/or spectral width. If the voltage pulse is not flat, as is indeed the case, these two conclusions reduce to one and the same, namely that the emission frequency is electric field dependent. Equally, if there is a variation of the biasing electric field from pulse to pulse, these two again reduce to a simple electric field dependence of the emission frequency. Since the voltage swept out by the biasing pulse is much greater than any pulse to pulse irreproducibility the former case is favoured.

The source of the electric field dependence of the emission frequency is readily located, for the effective dielectric constant is known to be electric field dependent. (See results of Gibson et al[2] or Sections 2 and 3, or Figures 1 and 2 of Section 5). Thus the "optical length" of the cavity will vary during a high field pulse of varying amplitude, sweeping the normal modes of the cavity across the frequency spectrum.

Other less direct sources of this observed electric field dependence of the emission frequency are for example sample heating, or the formation of a carrier accumulation layer. Furthermore, the existence of both of these mechanisms cannot be denied, nor can they be proved insignificant. However, each of these mechanisms must finally effect the emission frequency through the permittivity. In the case of lattice heating through repurcussions upon the relaxation times, and therefore the electron distribution function, whilst in the case of the accumulation layer through local variations in the plasma frequency.

FIGURE 4

Current and voltage pulses. The upper voltage pulse is displayed with a sensitivity of 5V/cM, on a time scale of 200 n-sec/cm. The current pulse is obtained with a sensitivity of 10 amp/cm.

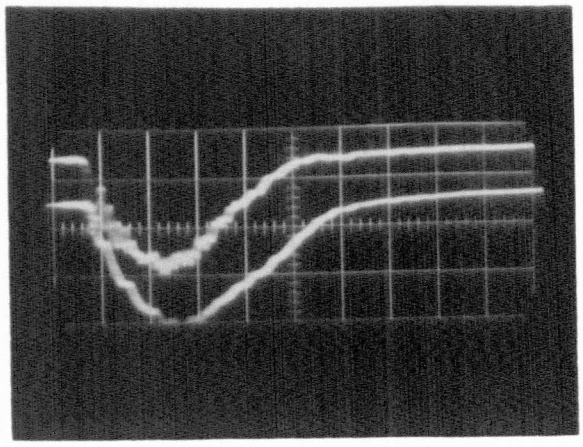

The fact that no such effect has been observed when using the latch and hold system is possibly attributable to the small range of electric field strengths over which this effect is to be seen. At higher field strengths, the spectrum appears uniformly broad irrespective of the precise magnitude of the high field pulse.

An alternative reason is to be found in the difference between the two observational systems. If the present low brightness/ photographic integration system is, as one would expect, very slow to respond, it would favour the flat portions of the pulse where little frequency sweeping is occurring. As the high field pulse is then increased in amplitude the displacement of the emission spectrum may be more readily discovered. Certainly differing response speeds could account for different apparent spectral widths. The major conclusion of this section has been demonstrated, namely that the emission spectral breadth is electric field dependent, and a mechanism provided. Some further supporting data which is of considerable interest, proving qualitative support for these ideas is presented in the remainder of this section 6.2.1.

It will be recalled that at an earlier stage it was found necessary to use slow rising and falling edges on the high field pulses to prevent spurious signal generation. This feature, though essential when employing the highly sensitive latch and hold system does, never the less, provide an ideal high field pulse, see Figure 4 for such spectral broadening to occur. It remains however to show conclusively that this is the source of the present spectral width, that is, to distinguish between frequency sweeping and pulse to pulse irreproducibility of the spectrum.

In order to improve the high field pulse rather more than was possible merely by removing the slowing circuits already discussed,

FIGURE 5

Voltage pulse at sensitivity of 5V/cm and 200 nsec/cm.

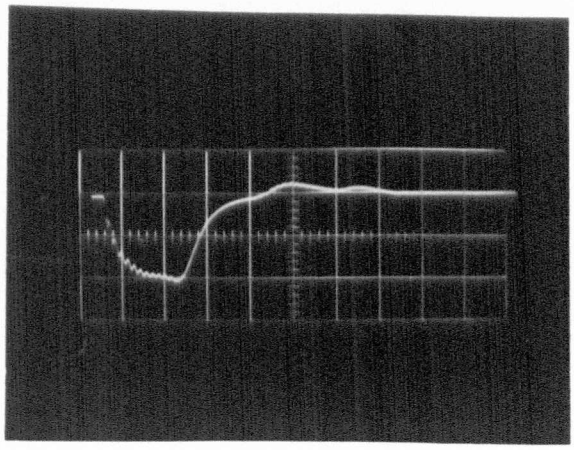

FIGURE 6

Upper (A) and lower (C) photographs are of the emission spectrum. It is masked to make photography possible, thus only the horizontal axis contains information relating to the frequency of emission. The Upper photograph (A) has a dispersion of 4.3 GHz across the screen and centre frequency of 16.1 GHz. In the Lower case (C) the dispersion is reduced to 0.1 GHz.

The centre picture (B) is of the panoramic receiver's sweep waveform. It is recorded on a time scale of 10 milli sec/cm.

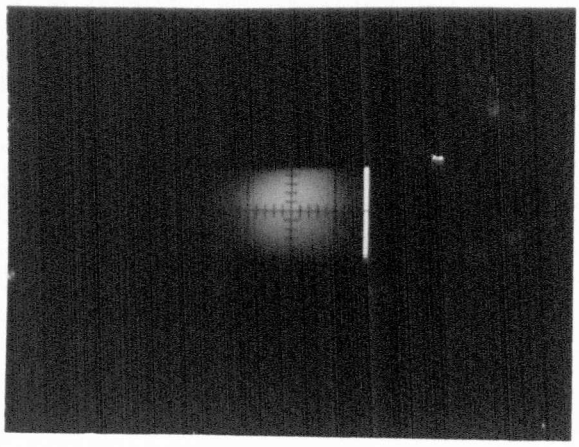

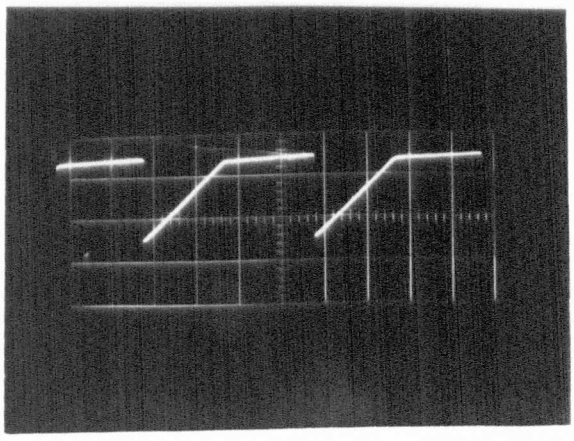

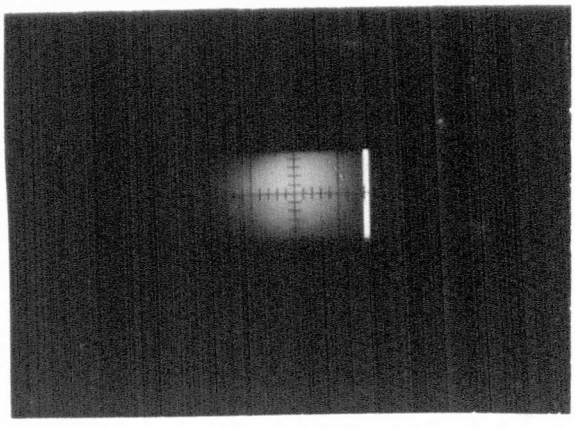

a mercury wetted relay was introduced. This system operates upon precisely similar principles of pulse formation, by reflection of voltage steps within transmission lines, as those used in the earlier pulse generator. It has the advantage of a higher speed pulse, see Figure 5, but the disadvantage of a low, highly irregular, P.R.F.

Using the mercury wetted relay pulse generator similar but somewhat narrower emission spectra were obtained. The low P.R.F. of this device made these spectra very difficult to photograph. However, the qualitative trend to a narrower spectrum would again seem to favour a frequency sweeping mechanism during each high field pulse.

The irregular P.R.F. from this relay was found to be associated with the transistorised flip flop used to drive the solenoid which moves the reed. It was found that, by driving this relay from the 50 cps supply through a variac, this irregularity was drastically reduced, (by some 10^3 times in mean pulse to pulse jitter). Having made this step forward, the emission spectrum shown in Figure 6(a) was obtained under the same conditions as in Figure 4, but synchronising the panoramic receiver sweep to a 50 cps pulse from a mercury wetted relay.

The apparent conclusion that the spectrum is momentarily very narrow, and being swept by the high field pulse cannot, however, be drawn from this result alone. The reason is that the sweep ramp (Figure 6(b)) of the panoramic receiver is very slow and is synchronised to the high field pulse. Thus on the time scale of the high field pulse, the panoramic receiver sweep is essentially stationary and samples only one frequency window, and the same one in each successive pulse. (A window of width equal to the I.F. bandwidth). Consequently any signal occurring WITHIN THE PULSE

DURATION AND AT THIS FREQUENCY is superimposed upon the C.R.T. display each time a pulse occurs. Hence the very bright and very narrow emission spectrum. This explanation is confirmed by Figure 6(c) in which a line of about 1 mm breadth corresponds to a signal line width of $\frac{1}{2}$ MHz resolved using a system having a video band-width of 3 MHz. This is of course impossible.

What this observation does do, is once again lend support to the growing conviction that there is a high degree of pulse to pulse reproducibility of the emission spectral frequencies. Such observations would all therefore seem to support a conclusion that frequency sweeping is occurring within the high field pulse. It remains however to demonstrate this unequivocally, and then to measure the short term spectral line width.

6.2.2 Demonstration of Frequency Sweeping within a High Field Pulse, and Power Measurement

The spectrum analyser is an instrument which is specifically designed to provide high frequency resolution, and does so at the expense of its time resolution. Hence, the spectrum analyser is not the ideal instrument with which to discover the time dependance of the present emission spectrum.

The frequency distribution within a high field pulse of a micro-second total duration is required. It is therefore necessary to make time measurements with an accuracy of perhaps 10^{-7} secs. implying that a spectral resolution down to 10 MHz is to be sought. A device which can be arranged to provide such an admixture of resolutions in the time and frequency domains is the balanced mixer.*

---

* Of course there is no fundamental difference between this device and a spectrum analyser with no frequency sweeping facility.

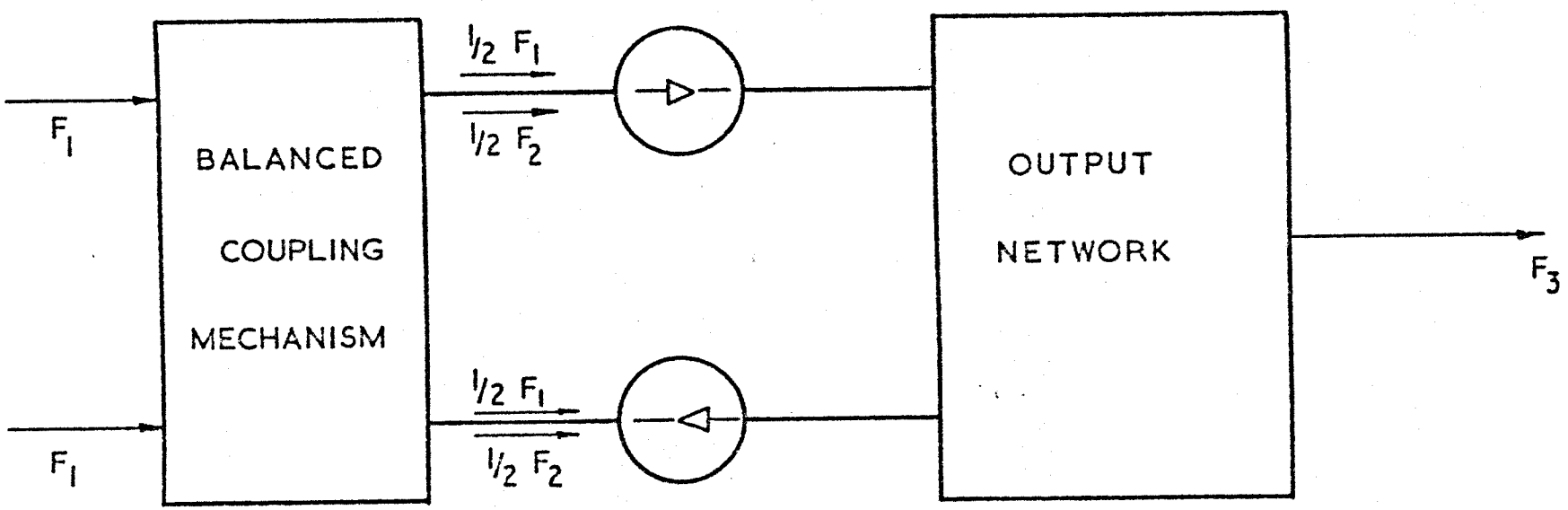

FIG. 7.

SCHEMATIC DIAGRAM OF BALANCED MIXER

PLATE 1

X Band Mixer

Balancing a pair of mixers is simply a technique for discriminating against (local oscillator) noise. The incoming signal is divided in half by a balanced coupling device such as a 3 dB coupler (Figure 7). Outgoing signals from such a device are then 90° out of phase. When mixed with the local oscillator signal, I.F. signals are developed which are 180° out of phase. Local oscillator noise in each channel is however in phase. By using diodes of opposite polarities in the two channels, outputs are developed which may be added to provide noise rejection and I.F. signal retention.

A suitable choice of the head amplifier bandwidth is then made to allow the necessary time resolution of 10^{-7} secs.

Balanced Mixer systems were assembled for operation at both X-band, 8 - 12 GHz, and J-band, 12 - 18 GHz. The X-band system is shown in Plate 1. In each case a manually tunable klystron was used as the local oscillator, and an I.F. amplifier of centre frequency 60 MHz and bandwidth 10 MHz.

The observation consists merely of viewing the output from the balanced mixer and head amplifier when local oscillator and unknown signals are fed into the mixer. The system has in addition a wave guide switching facility allowing a signal from a dummy source to be mixed with the local oscillator in place of the real signal Both the dummy source and the local oscillator are continuous wave devices, although the dummy source can be 100% modulated. Thus, it is possible not only to make observations of emission signals with an improved time resolution, but also to make power measurements by the following substitutional technique.

FIGURE 8

X Band Balanced mixer output as a function of time. Local oscillator frequency of 10.18 GHz I.F. amplifier centre frequency of 60 MHz. Biasing pulse amplitude of 37 volts where threshold occurs at 25 volts.

TIME BASE 0·2 μ sec/cm

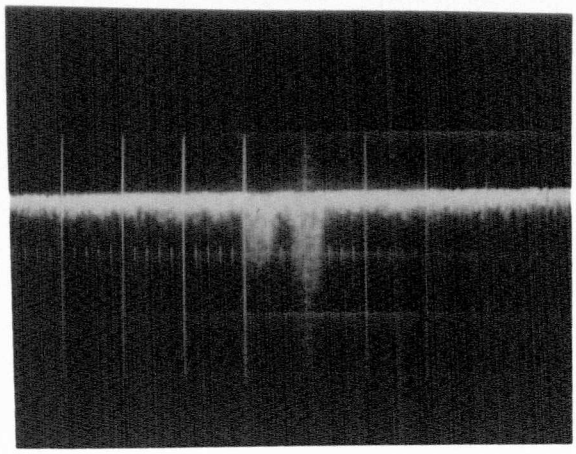

With the switch in "position 1", the pulsed signal from the sample is mixed with the continuous wave local oscillator and the amplitude of the detected signal measured. Meanwhile any power from the dummy source is entering the power meter at this time. Putting the wave guide switch into its second position, a signal is again detected as a result of mixing the 100% modulated dummy source signal with the local oscillator. The dummy signal is adjusted to give the same detected amplitude as the real signal gave. Finally, on switching back to position 1, and switching off the 100% modulation of the dummy sourse, a power measurement is made. This is of course equal to the peak power delivered by the device.

Similarly, by reducing the dummy signal pulse power whilst the wave guide switch was in its second position until detection was only just possible, then switching back to position one, the ultimate system sensitivity could be obtained. Both systems had sensitivities of -75 to -80 dBm.

X-Band Results

Using a specimen of GaAs having 9.6×10^{13} carriers/cc 0.775 cm long in the "A" dimension and 50 microns in the "l" dimension, the signal shown in Figure 8 was detected. This sample had already been shown to oscillate in the required mode using the latch and hold system. The results here are of amplitude as a function of real time. It will be seen that twice during the high field pulse an emission signal is obtained of frequency $f_{klystron}$ -60 MHz = 10.12 GHz the signal at $f_{klystron}$ + 60 MHz being suppressed by the appropriately tuned wave-meter. By adjusting the local oscillator frequency this pair of signals could be moved in time, and finally caused to merge near the centre of the high field pulse. Clearly,

FIGURE 9

In this series of photographs results are shown in pairs. At each local oscillator frequency, a photograph of the panoramic receiver frequency spectrum (right) and one of the mixer output in real time (left) is provided. The former provides an indication of the relative values of the signal and local oscillator frequencies, whilst the latter shows any mixer signal output (single side-band operation) which occurs during the high field pulse. The panoramic receiver is on line sync. centre frequency 16.53 GHz dispersion 3 GHz across screen.

It will be seen that as the local oscillator is moved progressively across the frequency spectrum the time at which a mixer signal occurs within the high field pulse is changed.

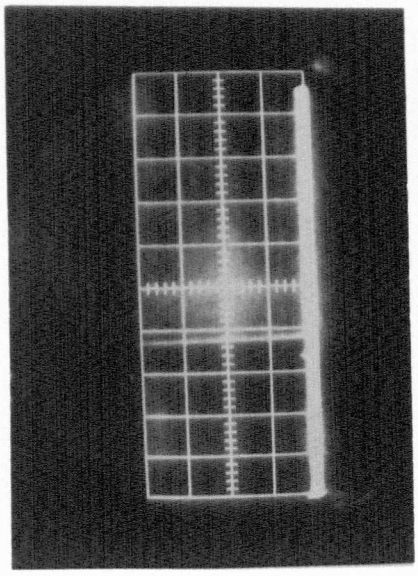

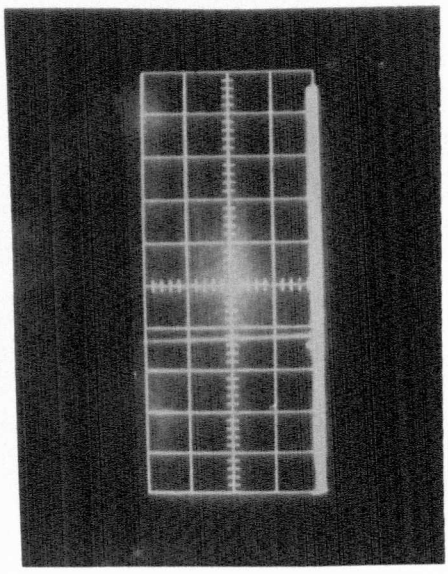

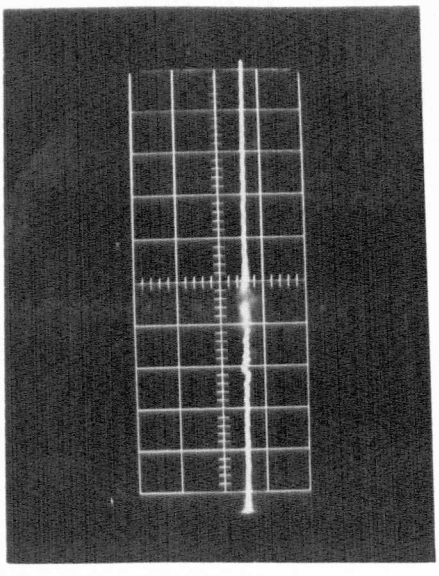

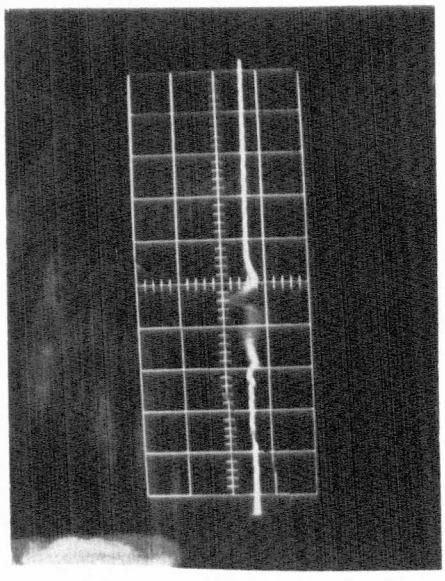

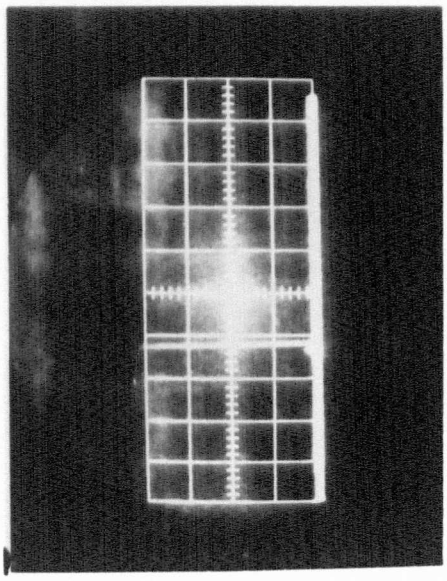

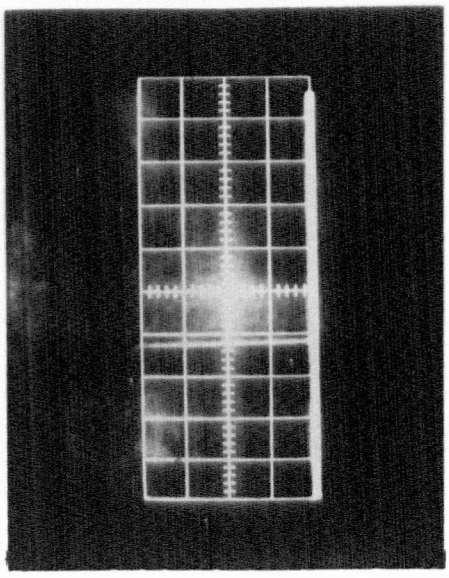

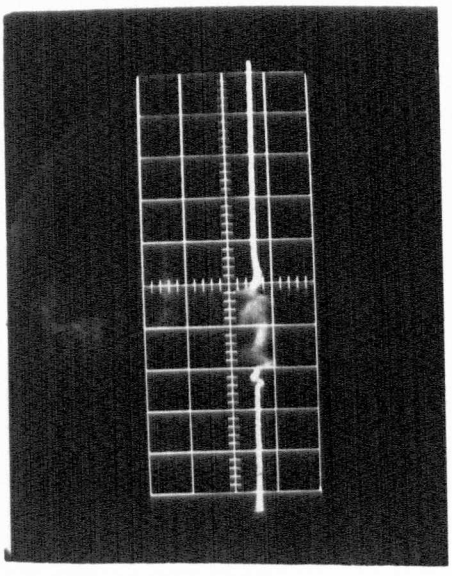

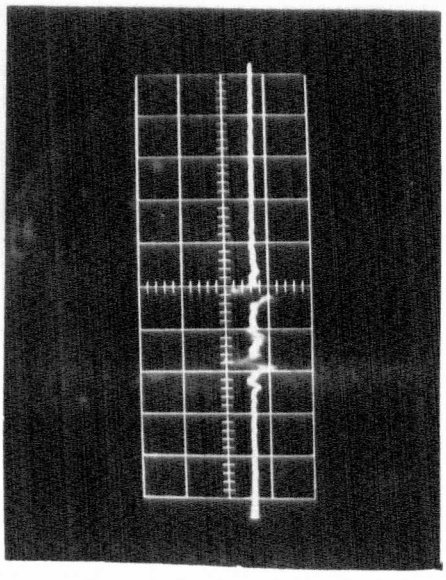

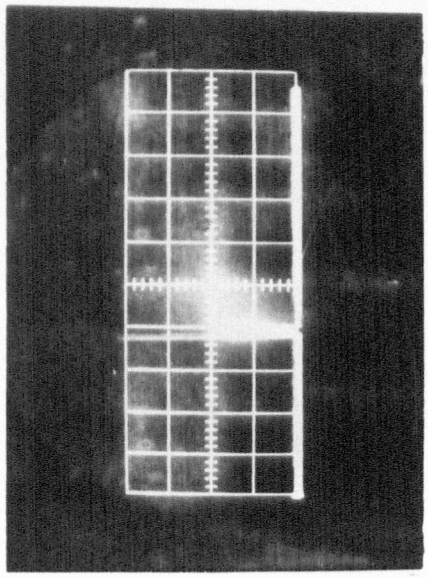

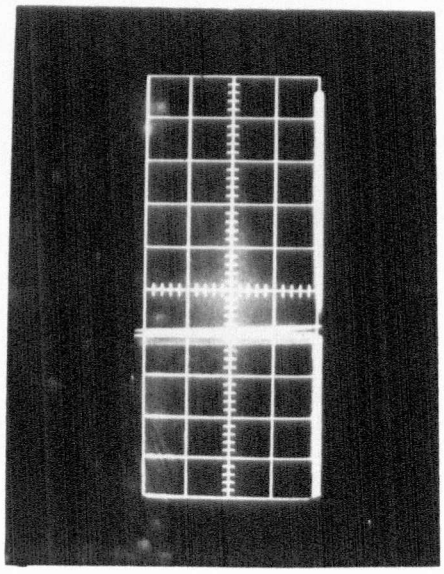

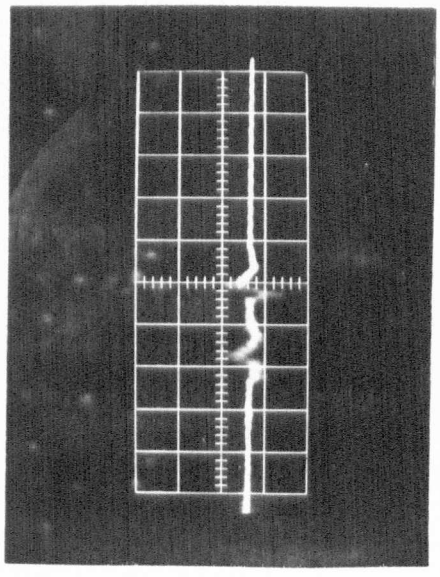

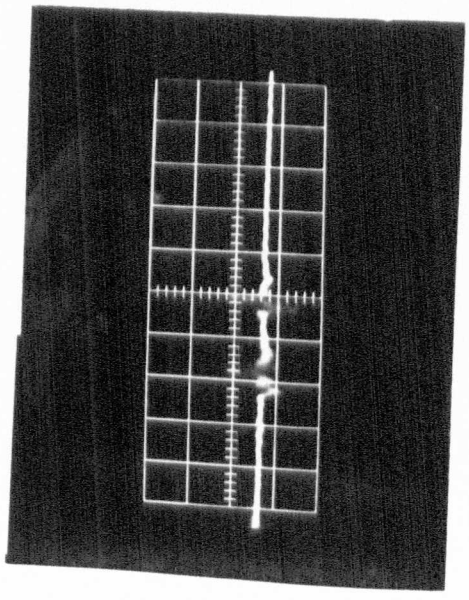

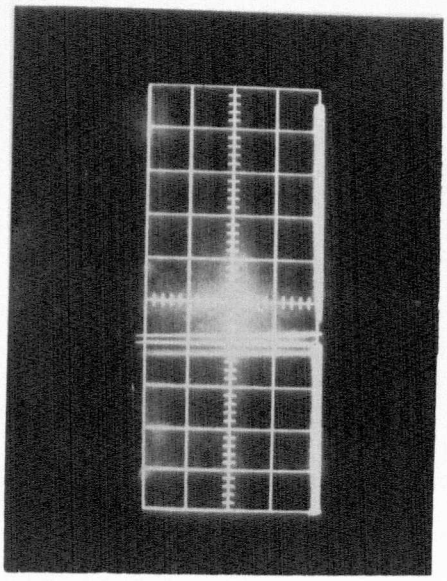

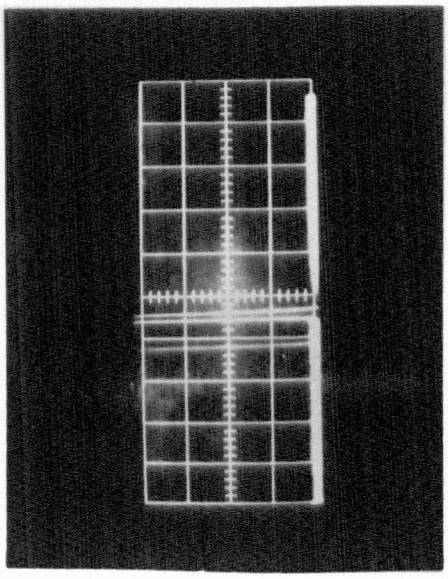

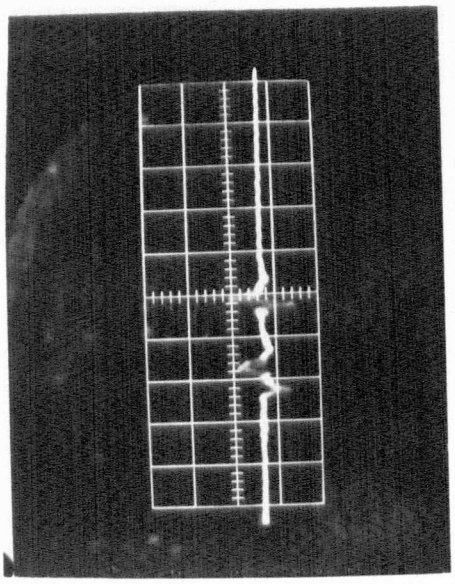

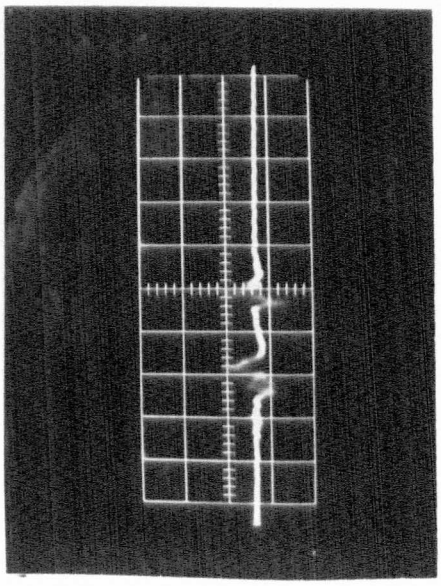

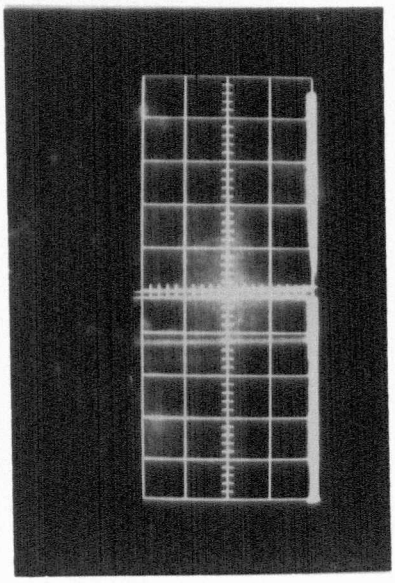

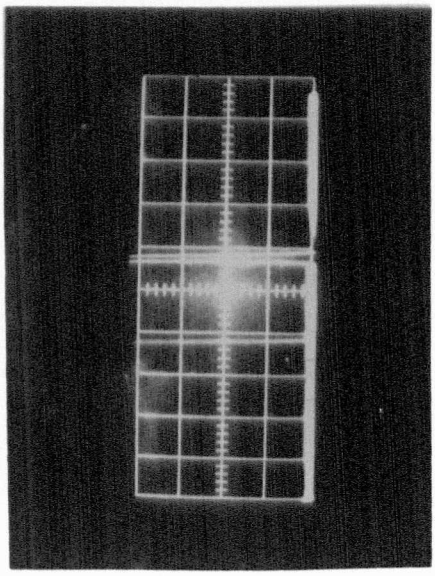

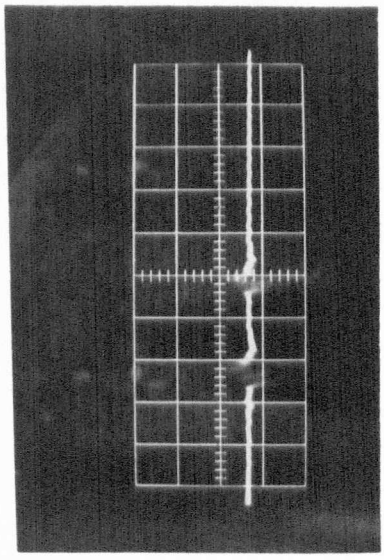

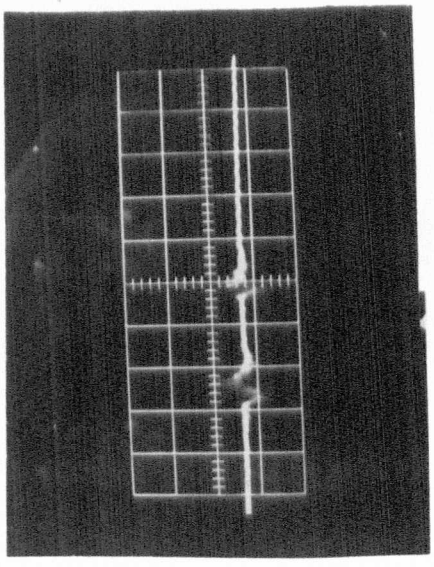

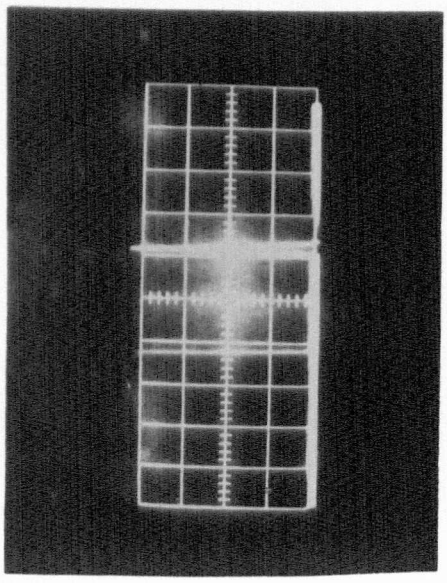

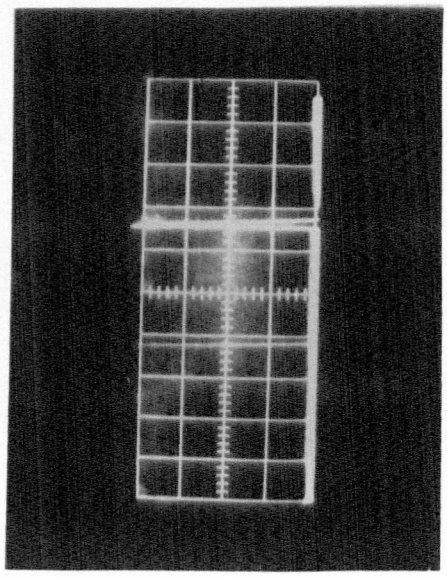

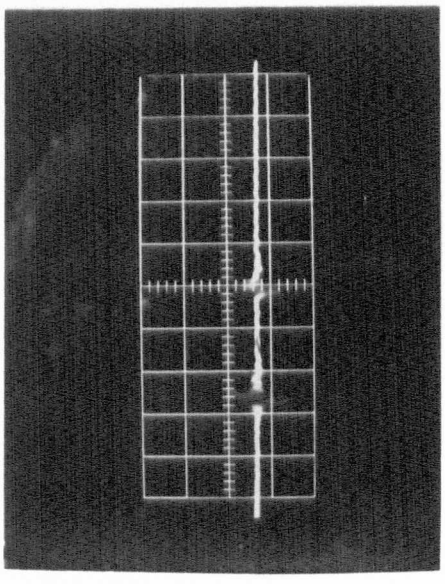

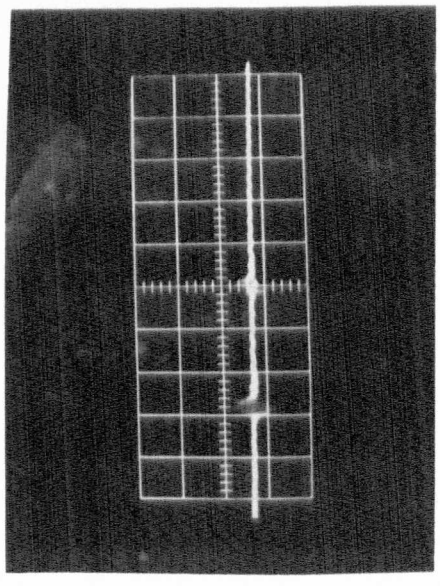

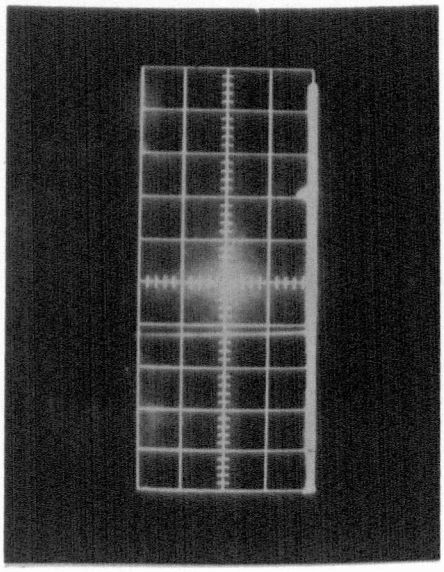

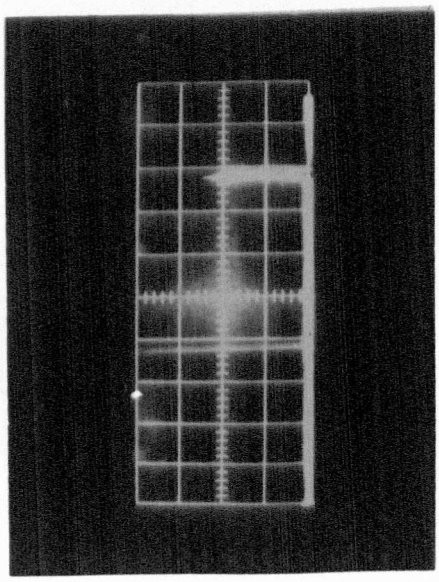

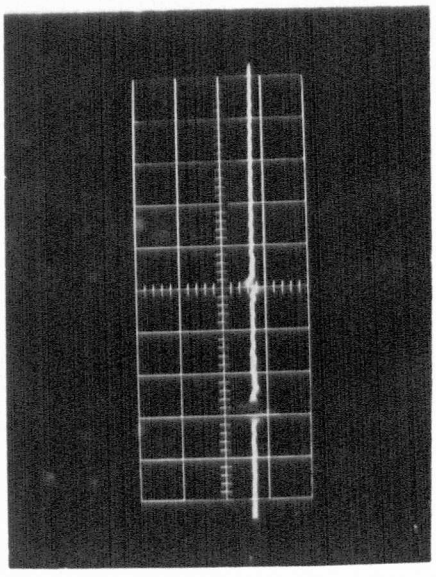

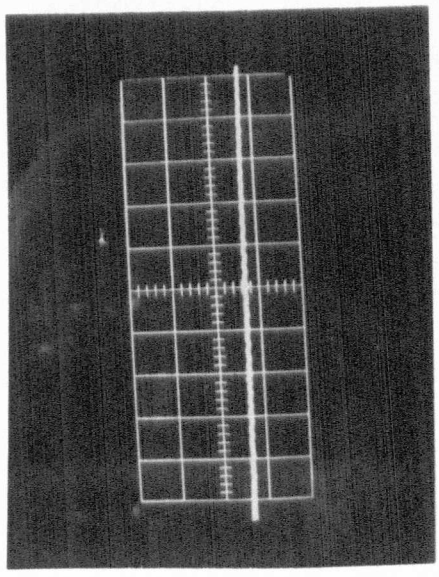

FIGURE 10

Voltage bias pulse on sensitivity of 5V/cm and at a speed of 100 nsec/cm.

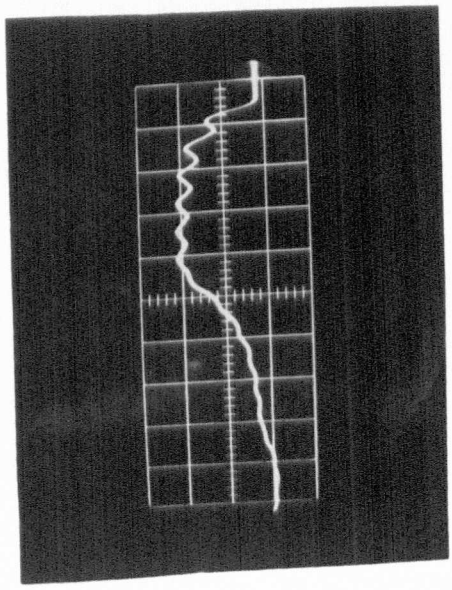

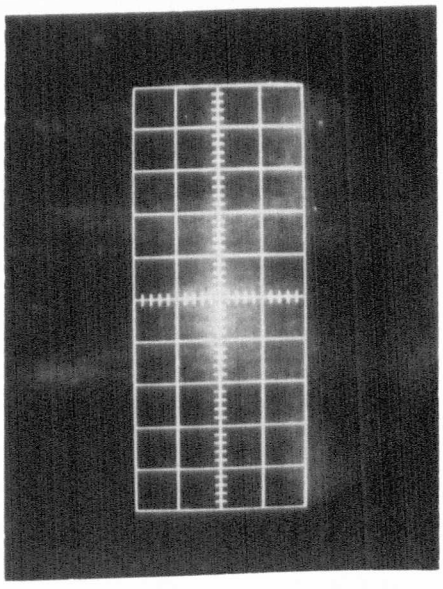

therefore, the frequency of emission changes during the high field pulse, rather than from high field pulse to high field pulse. It is therefore a spectrum of type 2 according to the terminology introduced in Section 5. The apparent duration of the signal at $f_{klystron}$ - 60 MHz is not of any significance because of its proximity to the limit of temporal resolution for this system (approx. 1/I.F. bandwidth). The peak pulse power measured was 300 micro-watts on several rather poor specimens. This figure is very close to the power estimated in Section 5.2 after taking account of the effects of frequency sweeping upon the spectrum analyser sensitivity.

J-Band Results

Using a sample of GaAs, having a free carrier concentration of 5.3×10^{14}/cc, 'a' dimension 2.45 mms and 'l' dimension 8 microns, and known to oscillate in the required mode, the photographs shown in Figures 9 and 10 were obtained. Once again these show a pair of emission signals in real time, occurring during the high field pulse. Each picture of emission is paired with a panoramic receiver spectrum, in which the more powerful line is the local oscillator line. The other line is the apparently steady emission line from the sample, which as has already been mentioned (Section 6.2.1) can be obtained by using the line synchronized facility. It provides a useful marker with which to relate the local oscillator frequency and approximate sample emission frequency. In the series of photographs shown, the local oscillator has been moved across the frequency range in which the sample emission spectrum occurs. The progressive merger of the two emission signals, already described in the X-band results, is clearly shown, as the local oscillator frequency is adjusted. Furthermore, the frequency range over which

the local oscillator must be moved in order to sweep the detected signal through the high field pulse, is quite as large as any emission spectrum observed using the latch and hold system. Thus this frequency sweeping effect not only exists but can account for the magnitude of the spectral width observed earlier.

The motion of the emission peaks indicates that the lowest frequencies occur at the centre of the pulse, and therefore at the highest voltages. This is consistent with the earlier observations shown in Figure 3 of Section 6.2.1 where it will be seen that the emission spectrum is extended towards lower frequencies as the high field pulse amplitude is increased. It implies that as the electric field strength rises the average effective dielectric contant increases. It has already been pointed out that the high electric field may affect the dielectric constant either directly through the hot carrier effects or indirectly through accumulation*, or through lattice heating, and its repercussions upon the carrier "temperature". Of these mechanisms, the former provides a positive contribution to the dielectric constant which, in theory decreases with increasing electric field[2, 3]. (See Figure 2, Section 5). The second mechanism provides a local dielectric constant which increases with the biasing electric field strength, owing to increasing carrier accumulation. The final mechanism is neglected, on the basis that no dependence of the spectral width upon pulse duration was observed even when the pulses were much shorter than an estimated thermal relaxation time. Thus, it is clear that providing no unforseen mechanism is important, it is the effects of carrier accumulation

---

* Reference to Equation 1 of Section 2 will show how these terms occur in the expression for the effective permittivity.

rather than hot electron effects which dominate the electric field dependence of the mean effective dielectric constant.

The plots of frequency as a function of specimen length in Section 5 (Figure 11) indicate that the emission spectrum usually tends to lie in a spectral range which implies effective dielectric constants in excess of the lattice value as predicted by theory[3]. It is important that the effective dielectric constant should be in excess of the lattice value for consistancy with the foregoing comments; if there were a negative free carrier contribution to the effective dielectric constant, no amount of carrier accumulation could have explained the results of the previous paragraph. The increasing accumulation accompanying increasing electric fields would have increased the negative contribution to the dielectric constant from the free carriers, so reducing the total dielectric constant.

The dependence of the mean dielectric constant upon electric field in GaAs is evidently not the same as that in n-Ge. (See the results of the bridge measurements of effective dielectric constant in n-Ge. Section 3). However, if the foregoing conclusion is correct, that carrier accumulation is the dominant process in this material, then the disparity is not surprising, accumulation effects having been shown to be much weaker in n-Ge than GaAs (See Figure 3a in Section 3 and Figure 6 in Section 5).

Finally, the peak pulse power measured using the J-Band mixer was 4 milli-watts.

We conclude that the emission frequency is being swept during the high field pulse, (type 2 spectrum) and that this effect is sufficiently large to account for the spectral breadths observed using the latch and hold system. Discussion of the form of the electric field dependence of the emission frequency has shown that

the dominant effect is the electric field dependence of the accumulation layer, and that the free carrier contribution to the dielectric constant is capacitative in accordance with theory and the results of Section 5. Finally, the peak pulse powers observed by X- and J-Band systems are of the order of 1 milli-watt, and therefore consistent with the estimates made in Section 5.2 when the reduced sensitivity of the spectrum analyser to Type 2 spectra was accounted for.

6.2.3 Intrinsic Spectral Line Width

We have concluded that the spectrum is being swept by the applied high field pulse, consequently the intrinsic line width remains uncertain. To measure this we use a modification of the J-band balanced mixer system already described. In this observation we mix the signal from the device with itself in one channel only. In so doing, the sum and difference frequencies are generated by all those signals reaching the mixer diodes simultaneously (with the approximation that the diode is infinitely fast). The mixer diode is then followed not by a head amplifier, as before, but by a spectrum analyser. Use of this latter instrument is possible in spite of the foregoing remarks concerning the interrelation between bandwidth and time resolution. This is because the self-mixing process effectively provides the "instantaneous" nature of the measurement. What the spectrum analyser cannot see of course is any variations in this mixing line width during the high field pulse, since it has a band width of 1 MHz. It should also be noticed that the line width determined here does not define the frequency of operation to the accuracy of that line width. It defines the line width of a rapidly changing frequency whose actual value is not determined at any time during the high field pulse.

This measurement showed a low frequency self mixed signal extending up to 125 MHz when a spectrum analyser of -80 dBm sensitivity was used. Self-mixed signals were however very weak throughout the observable spectral range from 10 to 125 MHz. At the low frequency end of the spectrum the signal was perhaps 10 dB above the noise level of the spectrum analyser, and it decreased uniformly as high frequencies were approached, where it finally fell below the noise level.

Even if a mixer efficiency of only 1% is assumed, the present down converted power of approximately 10^{-11} watts at 10 MHz would imply that the mixing signals are well out in the "skirts" of the 4 milli-watts observed from this device at J-band. Thus we conclude that the line width is much smaller than 50 MHz.

6.3 Summary of the Form of the Emission Spectrum

In Section 6.1 theoretical arguments were used to show the inadequacy of a noise amplifier model to explain the power and spectral width, measured in Section 5 using the latch and hold system. In consequence it became necessary to make a further careful examination of the emission spectrum with particular emphasis upon its width and power. The following experimental work of Section 6.2.1 showed first that the observed spectral width was electric field dependent, and that this was related to the electric field dependence of the free carrier dielectric constant. Following this, further measurements with a mixer system (6.2.2) demonstrated the variation of the emission frequency during a high field pulse, and revealed peak power levels in the region of 1 milli-watt. The detailed behaviour of the frequency as a function of electric field allowed the following conclusions to be drawn. The free carrier accumulation is an important mechanism in determining the electric field

dependence of the spectral frequency and the free carriers are behaving capacitatively. Finally, in Section 6.2.3 a first attempt has been made to measure the intrinsic emission line-width. It has been shown to be very much less than 50 MHz. Since this measurement was made upon a fundamental frequency of $\simeq$ 15 GHz a fractional line width of 1/300 is clearly established. However in the absence of a true line width, no comparison can yet be made with the line width of 60 MHz predicted (Section 6.1.2) for a noise amplifier operating at a power level of 1 milli-watt per MHz bandwidth. For such a line width to be observed the device would of course have to be operated continuously rather than pulsed.

References

1. J. P. Gordon, H. J. Zeiger and C. H. Townes
Phys,Rev. 99, No.4, 1264-1274 (Aug 15, 1955).

2. A. F. Gibson, J. W. Granville and E. G. S. Paige
J.Phys.Chem. Sol. 19, 198 (1961).

3. H. D. Rees
IBM. Jnl. Res. Dev. 13, (1969).

7. Observations of Microwave Emission from GaAs Samples which are Space Charge and Electromagnetically Unstable

In this section we present some observations of the microwave emission from GaAs when both electromagnetic and space charge systems are unstable. The work in this area is, however, not persued at length because Ono[1] and co-workers have recently reported some measurements which fall into this category and because of the similarity which we find between this region and the low N.L. region already described. We therefore report here those initial measurements which have been made, for the sake of completeness.

FIGURE 1

Emission spectrum with vertical amplitude masked to make photography possible. The (horizontal) centre frequency is 4 GHz and dispersion 8 GHz across the screen.

Biasing pulse amplitudes of 45 volts, 48 volts, 50 volts are employed, commencing at the lower photograph of the page.

On the second page, biasing pulse amplitudes are 52 volts, 55 volts and 56 volts, again commencing at the lower photograph of the page.

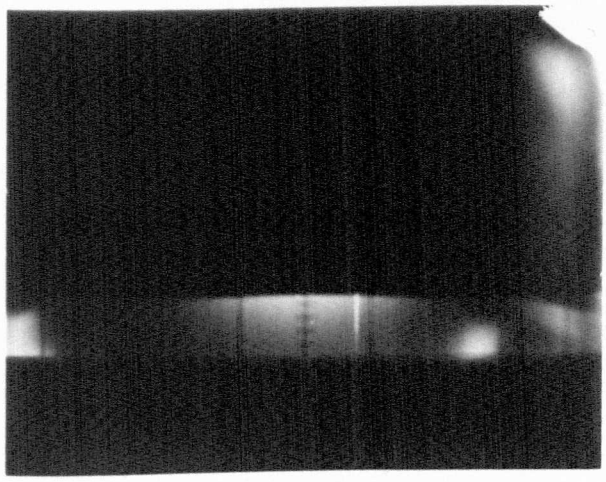

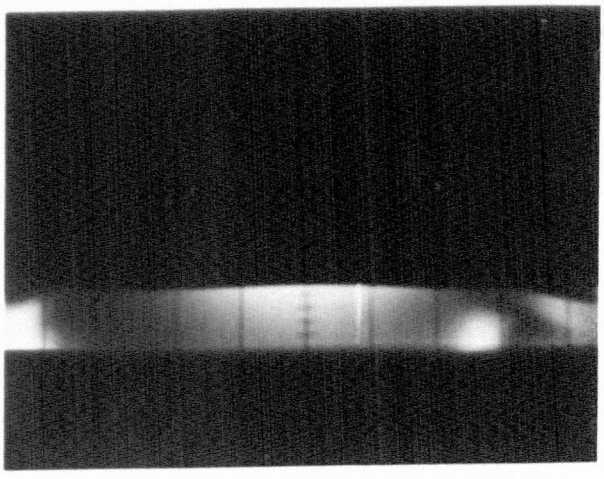

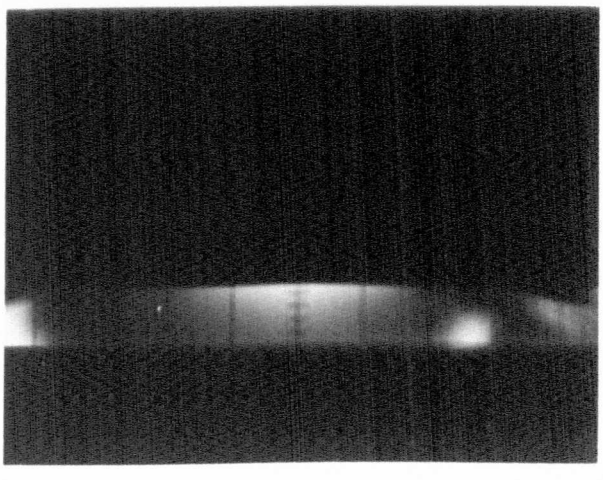

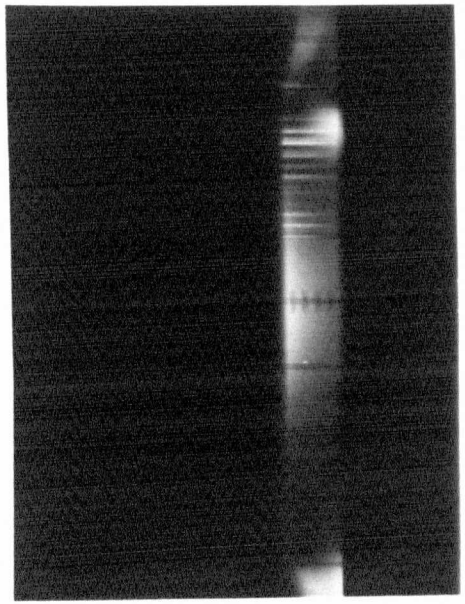
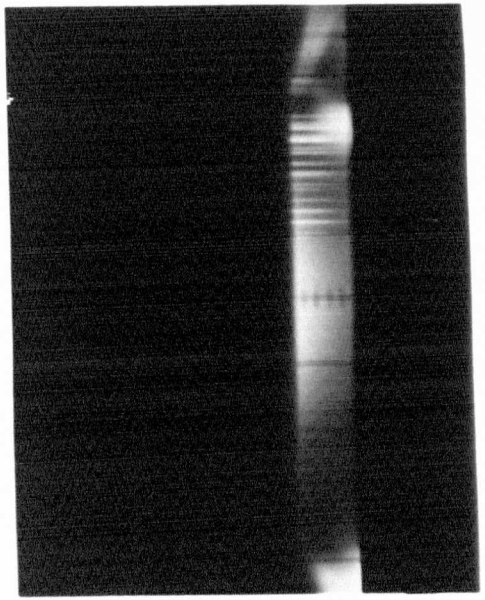
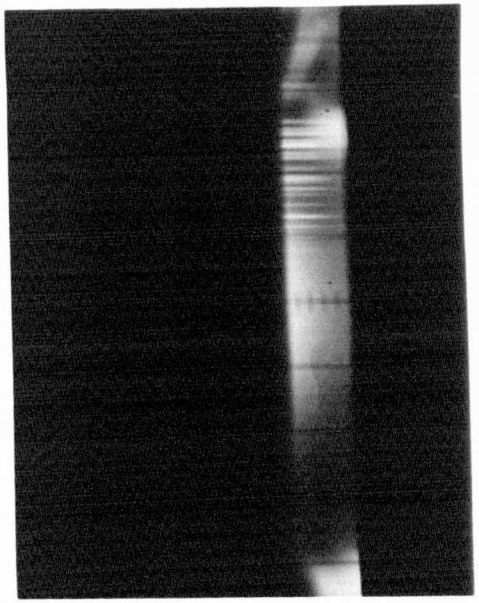

7.1 Experimental Technique and Results

The specimen is fabricated in the usual way, apart from the live plane bonding proceedure. When alloyed contacts were made to these specimens, it was found that the material cleaved, owing to residual strain within the crystal. The specimen was therefore mounted between live and earth planes under pressure applied through a layer of fairly uniform sorbo rubber.

The observational system is identical to that described in Section 6.2.1 using a Panoramic receiver. Results are shown in Figure 1 for a specimen having 1×10^{15} carriers/cc an "A" dimension of 0.2844 cm, and an "L" dimension of 250 microns. The products NA and NL are therefore both in excess of the critical values for their respective modes of instability.

It will be seen that, like the results of Section 6 where N.L. is less than the critical value for domain formation, frequencies are moved downwards with increasing biasing electric field. (In the photographs only the positions, and not the amplitudes of the spectral lines are visible since it was found necessary to mask a large part of the cathode ray tube screen in order to make any observation), This result is consistent with the only ~~qualitative~~ quantitative result included in the abstract already mentioned[1]; this is that a biasing voltage change from 24 to 40 volts produced a change of emission frequency from 8.8 GHz to 7.2 GHz.

It is pointed out that in this observation the frequency is much higher than would be expected from a sample, 250 microns long, undergoing a simple domain mode instability. On the other hand the frequency is much lower than would have been expected from a specimen of only 0.284 cm in the A dimension on the basis of the results summarised in Figure 11 of Section 5 which relate to electromagnetic instability. However, since

the ambient free carrier concentration is now almost two orders of magnitude greater, the effective dielectric constant must be expected to be very much greater too.[2] We therefore regard this rather low frequency of emission for such a short specimen as not inconsistent with an electromagnetic instability and with the foregoing data, which indicates that the free carrier contribution to the dielectric constant is capacitative. Beyond this the emission is seen to have very similar characteristics to those already described in Sections 5 and 6 in some detail. Thus we conclude that the mode of operation is complicated, neither space charge or electromagnetic instability alone being readily capable of accounting for the observed frequency of emission. In fact, just the behaviour which might be expected in the hybrid range of instability. Clearly however, a definitive experiment identifying the mode of operation and its characteristics has yet to be performed.

References

1. Shoichi Ono, Kuniyoshi Yokko and Yukio Shibata
Proc. Moga. Conf. Paper 6.2 (1970)

2. See arguments of Section 6.2.2 concerning the role of free carriers.
See also theoretical calculations of H. D. Rees IBM. Jnl. Res. Dev. 13, No.5, 537-542 (1969) which evaluates a maximum total dielectric constant of 45 for material having 10^{15} carriers/cc

8. Concluding Remarks

The work which has been described here commences with the idea that suitably polarised T.E.M. waves would exhibit amplification in negative resistance materials. After devising experiments by which this concept may be examined, experimental work upon n-Ge and GaAs was undertaken and has been described. The work upon n-Ge was directed primarily towards a diagnostic evaluation of some of the unknown parameters of the N.D.C. process in that material, though during the course of this work the first observations of the predicted electromagnetic instability were made. Observations which confirm the existence of travelling (T.E.M.) wave amplification in suitably biased negative differential conductivity media.

The diagnostic measurements made upon n-Ge, though imperfect for many reasons, have been proved substantially correct by subsequent publications of other workers. In particular the velocity field curve, Figure 13 of Section 3, indicates very good agreement between the integrated results of the present experiment and other contemporary data. The more demanding measurement is of course that of the slope mobility. In Section 3 the maximum negative slope mobility was found to be in excess of 50 cm^2 volt sec whilst in Section 4 an alternative technique of measurement indicate that the maximum negative mobility was 300 $cm^2/Vsec.$ at $77^oK.$ The latter figure has subsequently been confirmed by the work of Neukerman. A threshold electric field of 2.95 KV/cm in the $\langle 100 \rangle$ direction, a frequency ceiling for NDC of 5 GHz, and the absence of NDC in the $\langle 111 \rangle$ direction have also been indicated for n-Ge at 77^oK during the course of this work.

In gallium arsenide more powerful microwave emission was achieved, and consequently a series of tests were undertaken which were designed to elucidate some of the fundamental characteristics of the emission spectrum. Although the breadth of the emission spectrum seemed to imply that amplified noise was being observed, this conclusion was not substantiated when the observed power was compared with that to be expected from a noise amplifier. More detailed examination of the spectrum revealed that the emission spectrum was in fact more powerful and narrower than initial measurements had indicated. Peak power levels in excess of a milli-watt and line widths of less than 50 MHz were finally detected. Further work is, however, necessary in order to measure the actual line-width. This having been done, some comparison of power and line width is required using both the theoretical approach introduced in Section 6 and a theoretical description of the device when behaving as a saturated oscillator. The latter theory would be formidable owing to problems of both non-uniformity and non-linearity and has yet to be undertaken.

Finally we would mention the device aspects of the present work, It was expected that the electromagnetic instability would have some advantages over the space charge instability as a mechanism by which to extract microwave energy from suitably biased NDC media. These thoughts were based upon the fact that at a given frequency of operation, the space-charge unstable device is long in a direction parallel to the biasing electric field. The electromagnetic unstable device however is thinly spread over a large contact area. The latter device therefore has immediate advantages from the point of view of heat dissipation. Never-the-less the microwave emission which has been obtained from GaAs is not competitive with that obtained from space charge unstable Gunn oscillators either in terms of peak power or efficiency. This could

well be overlooked since the present work is at a much earlier stage of development than is the conventional Gunn oscillator. However, the extreme sensitivity of the emission frequency to the biasing electric field strength, which has been discovered, does not lead one to expect that the device would be easy to use in an operational system.

The possibility of using the present T.E.M. wave amplification process as a travelling wave amplifier at high frequencies (35 GHz) has not yet been examined. This possibility opens up a whole field of work which could be particularly rewarding since there is a demand for a solid state amplifier operating in this frequency range. Such an application also presents a further attractive problem; that of rendering the present reciprocal amplification process non reciprocal. Unless this can be achieved,* a pulse entering the amplifier will produce an infinite train of amplifying echoes whenever presented with a significant missmatch. That is, it will oscillate. More careful matching may prevent oscillation, but still cause amplified signals to appear at the input port, which is an undesirable feature.

Clearly there is a considerable body of work yet to be done upon this novel amplification process.

---

* It is possible that a solution is to be found in the similarity of the present device to the maser which has already been exploited once. (Section 6). In that device the identical problem has been encountered and solved.

APPENDIX I

Programme for calculation of the insertion gain of a biased sample of NDC material. The programming language is a modified version of Algol 60.

```
    acb optimise

algol
test

begin
real mur,mui,n,l,w,epsl,alfa,alfa1,alfa2,alfa3,beta,beta1,gt,
beta2,beta3,t12,g,gt,r,wdi,wdr,b,d,kr,ki,n2,diff1,diff2;

exact read(l,epsl,mur,mui,alfa1,alfa2,alfa3,beta1,beta2,beta3);
print5(¢ optimisation of carrier concentration in order that
 surface reflection losses are not too high,yet single transit
amplifying gain is still of significant proportian


specimen length = ¾,l,¢
lattice dielectric constant = ¾,epsl,¢
mobility = ¾,mur,¢+i¾,mui,¢

  frequency = ¾,w,¢
carrier density   surface transmission   wave growth power   gain ¤:
*);

  layout(6,10,40);
for beta ← beta1:beta2:beta3 do;
for alfa ← alfa1:alfa2:alfa3 do;
begin
n ← alfa*10↑beta;
wdr ← 1.8*n*mur/(epsl*10↑6);

wdi ←-1.8*n*mui/(epsl*10↑6);
  b ←1+wdi/w;
```

```
diff1 ← (wdr/(w*b))**2;
if diff1<0.05 then
begin
     d ← abs(b)*(1+0.5*diff1);
     kr ← 0.236₁₀-10*w*n2*sqrt(b+d);
    diff2 ← abs(b)-b;
    ki ←0.236₁₀-10*w*n2*mur/abs(mur)*sqrt(0.5*abs(b)*diff1+diff2);
end
else
begin
     d ← sqrt(b**2+(wdr/w)**2);
    kr ← 0.236₁₀-10*w*n2*sqrt(b+d);
    ki ← 0.236₁₀-10*w*n2*mur/abs(mur)*sqrt(d-b);
end
end
else
begin
      d ← sqrt(b**2+(wdr/w)**2);
      kr ← 0.236₁₀-10*w*n2*sqrt(b+d);
      ki ← 0.236₁₀-10*w*n2*mur/abs(mur)*sqrt(d-b);
end;

kr← kr/(w*0.33₁₀-10);
ki ← ki/(w*0.33₁₀-10);
t12 ← 1-(kr*kr+ki*ki)/((kr+1)**2+ki*ki)**2;

r ← ((kr-1)**2+ki*ki)/((kr+1)**2+ki*ki);
g ← exp(-2*ki*l);
grt ← g*r*g*r;
gt ← g*t12;
print(r,t12,g,gt,grt,r);

end
end
finish
>>>>>>
```

APPENDIX II

Programme for the calculation of the spatial distribution of electric field and free electron concentration within a biased sample. The programming language is a modified version of Algol 60.

```
  acb geom e v x
a
b
  b in i,k,step;
    r no,vdo,jo,div e,eps,dx,de,v,grad,elim,xlim,et,beta,arrlim,n1,t,ev
h0,theta,rata,alpha,j,w,r step,damp;
    exact read(step,no,vdo,eps,xlim,elim,et,k,n1,t,arrlim,h0,theta,
              rata,alpha,beta,damp,ev);
    print5(¢
array points at temp.      = ¢,t,¢degrees kelvin
electron density at x=0    = ¢,no,¢/c.c.
electron density for ge    = ¢,n1,¢/c.c.
drift velocityat x=0       = ¢,vdo,¢cm/sec
dielectric constant        = ¢,eps,¢
limit on distance          = ¢,xlim,¢cms.
limit on field strength    = ¢,elim,¢kv/cm.
transition field           = ¢, et,¢kv/cm.
step on transition field   = ¢,step,¢
angle of taper             = ¢,theta,¢
width at step              = ¢,h0,¢cms
valley field               = ¢,ev,¢kv/cm.

field (kv/cm)   distance (cm)   electron density (/c.c.) ¢,
¢  dx(cm)    grad (kv/cm/cm)    integrated voltage
¢);

  b arr e,x,n,pd[1:arrlim],vd,field[1:k];
    exact read(e[1]);
    for j←1:1:k do
    b exact read(field[j],vd[j]);
    comm field is read in kv per cm, and drift velocity in units of
         ten to the seventh cm per second;
      vd[j]←vd[j]*10↑7;
    en;
    i←1;
    jo←no*vdo;
    n[i]←no;
 x[1]←0;
 pd[1]←0;

    r step ← step*damp↑4.1;


if i<2 then
      begin
          v←alpha*vdo;
    for j←1,j+1 while vd[j]<v do;
grad←(vd[j]-vd[j-1])/(field[j]-field[j-1]);
de←e[j-1]+(v-vd[j-1])/grad;
e[i]←e[i]+de;
j←1.81↑-9;
n[i]←(j*h0*(v*no+v*eps*de*tan(theta)/h0+jo*rata)+
    sqrt((j*h0*(v*no+jo*rata+v*eps*de*tan(theta)/h0))↑2-4*j*j*h0*h0*
    jo*no*rata))/(2*j*h0*v);
x[i]←de/(n[i]-no)/1.81↑-9*eps;
goto l1;
end;
```

```
l: div e←(n[i-1]-n1)/eps*1.81₁₀-9;
  comm a conversion factor is included hebe  to put e in kv per cm;
l2:  for j←0,j+1 wh et/step< abs (div e)*10*(-j) do ;
  dx←10*(-j);
  de←dx*div e;
  e[i]←e[(i i=1 th 1 e i-1)]+de;
  x[i]←x[(i i=1 th 1 e i-1)]+dx;
i e[i]>elim  th g ll;
  i  x[i]>xlim  th g ll;
  for j←1,j+1 wh field[j]<e[i] do ;
  grad←(vd[j]-vd[j-1])/(field[j]-field[j-1]);
  v←grad*(e[i]-field[j])+vd[j];
  n[i] ← jo*rata/(1-x[i-1]/h0*tan(theta))/v;


  if step< r step then
  begin
  if(n[i]-n1)*(n[i-1]-n1)<0 then
  begin
  step ← step*damp;
  g l2;
  end;end;

  if abs((n[i]-n1)/n1)<2₁₀-6 then
  begin
  step ← step*2.0;
  g l2;
  end;
  step ← r step/(damp*4.1);

if i>10 th b
          if abs((n[i]-n[i-10])/n[i])<1₁₀-5 and e[i-1]<et
            th b

  if e[i-1]<et/2 then de ← et*beta else
 de←(et-e[i])*beta;
                e[i]←e[i]+de;
            for j←1,j+1 wh field[j]<e[i] do ;
              grad←(vd[j]-vd[j-1])/(field[j]-field[j-1]);
                w←grad*(e[i]-field[j])+vd[j];
                dx←(h0/tan(theta)-x[i])*(1-v/w);
                x[i]←x[i]+dx;
              en;
            en;

if abs(ln(e[i])+ln(dx))<50
  then b  pd[i]←pd[i-1]+dx*(e[i]-de/2); en
  else b  pd[i]←pd[i-1];en;

l1:  punch(59);
   print5(e[i],x[i],n[i],dx,(de/dx),pd[i]);
  i lines>50 th punch(60);
  i←i+1;
  g l;
ll:
en
en
finish
>>>>>>>>>
.........
```

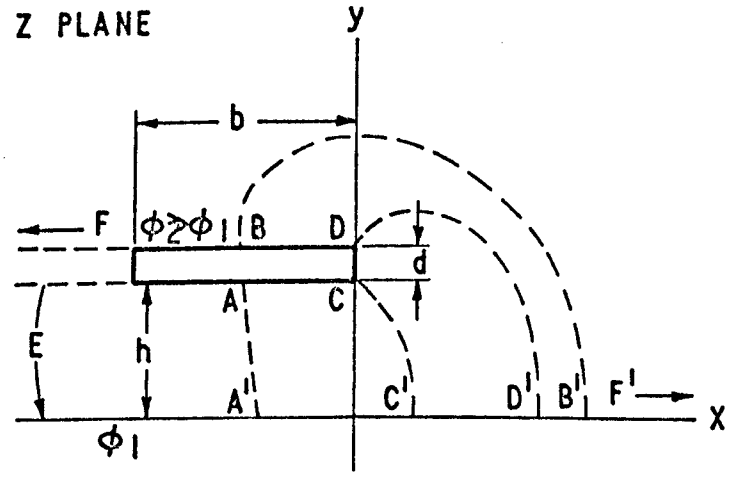

FIG. 1a

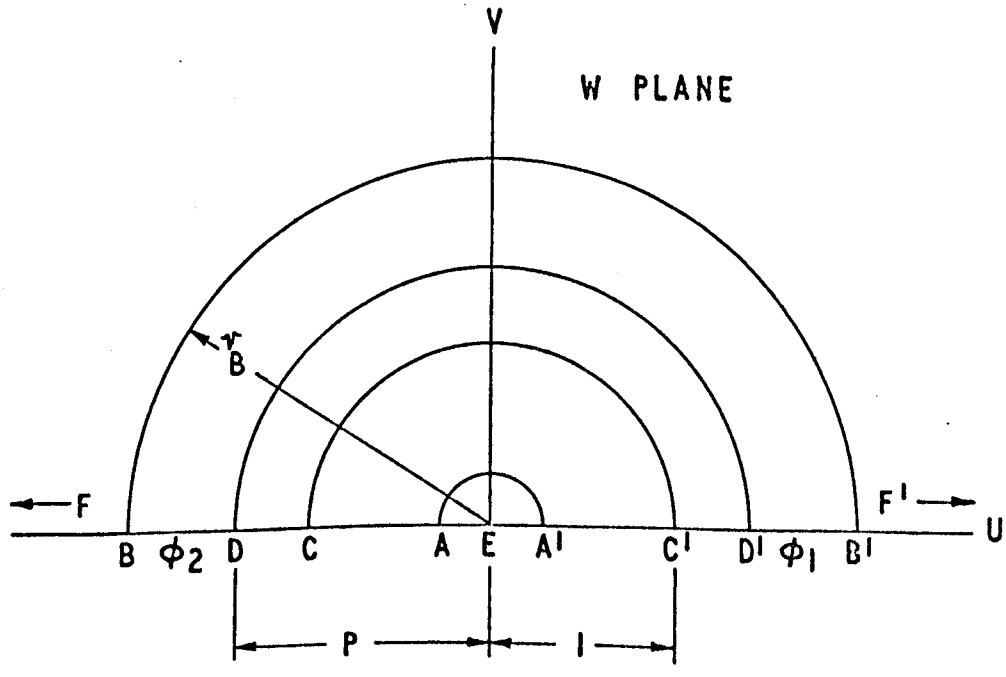

FIG. 1b

CONFORMAL MAPPING OF THE MICROSTRIP HALF WIDTH OF FIG. 1a INTO W SPACE IN FIG. 1b.

APPENDIX III

Heterogeneously Loaded Microstrip Transmission Line

It has already been pointed out that no analysis which deals with the present dielectric geometry within a microstrip transmission line is known to the author. The following analysis is based largely upon work by Assadourian and Rimai[1], but includes some additional features which are necessary in order to deal with this heterogeneous dielectric.

The technique employed is quite standard. Calculation of the line impedance is reduced to the problem of calculating the line capacity per unit length "C". Now this is just one of a class of two dimensional potential problems which may be solved by transformation into a new, more convenient, co-ordinate system. The complex potential function F(W) is transformed into a new co-ordinate space in which the problem is simplified. The solution is then expressed in terms of the new space co-ordinates and then transformed back.

We consider a strip of zero thickness width "b" and height "h" above an infinite ground plane. The plane through the transmission line normal to the direction of propagation is divided in half about the symmetry axis A, A' see Figure 1a. Following Assadourian[1] et al a conformal mapping

$$\frac{\pi z}{h} = 1 + W + \text{Log}\,(W) \qquad \ldots (1a)$$

i.e.

$$\left.\begin{aligned} \frac{\pi x}{h} &= 1 + u + \tfrac{1}{2}\,\text{Log}_e\,(u^2 + v^2) \\ \frac{\pi y}{h} &= v + \text{Tan}^{-1}\left(\frac{v}{u}\right) \end{aligned}\right\} \qquad \ldots (1b)$$

is used which transforms the z half plane in which the transmission line exists into the W plane as shown in Figure 1b.

The real potential at any point in the W plane is clearly

$$\phi(W) = \phi_1 + \frac{\phi_2 - \phi_1}{\pi r} \cdot r\theta = \phi_1 + \frac{\phi_2 - \phi_1}{\pi} \mathrm{Tan}^{-1} \frac{V}{U} \quad \ldots \quad (2)$$

where r and θ are the co-ordinates in the W plane, and ϕ_1 and ϕ_2 are the potentials of the lines A' B' and AB respectively.

The complex potential function corresponding to (2) is

$$F(W) = \phi_1 + j\left(\frac{\phi_2 - \phi_1}{\pi}\right) \mathrm{Log}\ (U^2 + V^2)^{\frac{1}{2}} = \phi_1 + j\left(\frac{\phi_2 - \phi_1}{\pi}\right) \mathrm{Log}\ r$$

$= \phi + j\psi$ where ψ is the function conjugate to ϕ and r is the radius of a flux line in W space.

In the case of a homogeneously loaded transmission line Assadourian evaluates the charge between A and B, Q_{AB} by taking ϵ times the change in ψ over a circuit of a conductor boundary. This may be justified as follows.

The flux of electric field per unit length of a surface S perpendicular to the UV plane is

$$-\int \underline{E} \cdot d\underline{S} = \int -\nabla\phi \cdot d\underline{S} = -\int \left(\frac{\partial\phi}{\partial U}\,\underline{i} + \frac{\partial\phi}{\partial V}\,j\right) \cdot d\underline{S} = \frac{Q}{\epsilon\epsilon_0}$$

by Gauss theorem, where $\underline{i}$ $\underline{j}$ and $\underline{k}$ are unit vector $\underline{i}$ and $\underline{j}$ being parallel $\underline{U}$ and $\underline{V}$ and Q is the charge per unit length enclosed by S.
Now ϕ and ψ must satisfy the Cauchy Rieman equations so long as ϕ and ψ are analytic.

$$\frac{\partial\psi}{\partial U} = -\frac{\partial\phi}{\partial V}$$

$$\frac{\partial\psi}{\partial V} = \frac{\partial\phi}{\partial U}$$

Thus
$$4\pi Q = -\int\left(\frac{\partial\psi}{\partial V}\underline{i} - \frac{\partial\psi}{\partial U}\underline{i}\right)\cdot d\underline{S}$$
$$= -\int(\nabla\psi\wedge\underline{k})\cdot d\underline{S}$$
$$= -\int\nabla\psi\cdot(\underline{k}\wedge d\underline{S})$$
$$= -\int\underline{\nabla}\psi\ d\underline{t}$$
$$= \psi_1 - \psi_2$$

where dt is a vector along the equipotential contour of unit height.

Hence
$$Q_{AB} = \epsilon\epsilon_o\frac{(\phi_2 - \phi_1)}{\pi}(\text{Log } r_B - \text{Log } r_a)$$
$$= \frac{\epsilon\epsilon_o hE_o}{\pi}\text{Log}\,(r_B/r_a) \qquad \text{as required}$$

where
$$E_o = \frac{\phi_2 - \phi_1}{h}$$

In the case of heterogeneous loading of the transmission line we assume that the specimen boundary lies along a flux line $r = r_{spec}$. Then E_{tang} is continuous across the specimen boundary, the flux lines remain undistorted, and we may therefore define two independent systems in the region of W space for which $r < r_{spec}$ and $r > r_{spec}$. An empirical argument has led Schwartzmann[2] to the same conclusion. In dealing with his form of hetrogeneously loaded microstrip he also divides the area around the live plane into two separate capacitors one with dielectric and one without.

The total charge is now, remembering that only half the transmission line has been considered,

$$2 \cdot Q_{AB} = 2\epsilon_{spec}\,\epsilon_o \frac{(\phi_2 - \phi_1)}{\pi} \operatorname{Log}\left(\frac{r_{spec}}{r_a}\right)$$

$$+ 2\epsilon_{air}\,\epsilon_o \frac{(\phi_2 - \phi_1)}{\pi} \operatorname{Log}\,(r_B/r_{spec})$$

$$= 2\frac{h\,E_o\,\epsilon_o}{\pi}\left[\operatorname{Log} r_B - \epsilon_{spec} \operatorname{Log} r_a + (\epsilon_{spec} - 1)\operatorname{Log} r_{spec}\right]$$

if $\epsilon_{air} = 1$

Now if B/h large

$$\operatorname{Ln} R_a \doteqdot -\frac{\pi B}{2h} - 1; \quad R_B \doteqdot 1 + \frac{\pi B}{2h}$$

Thus $\operatorname{Ln} \frac{R_B}{R_a} \doteqdot 1 + \frac{\pi B}{2h} + \operatorname{Ln}\left(1 + \frac{\pi B}{2h}\right)$

Thus

$$\text{Total charge} = \frac{2h\,E_o\,\epsilon_o}{\pi}\left[1 + \frac{\pi b}{2h} + \operatorname{Ln}\left(1 + \frac{\pi B}{2h}\right)\right.$$

$$\left. + (\epsilon_{spec} - 1)\operatorname{Ln}\left(\frac{r_{spec}}{r_a}\right)\right] \qquad \cdots \quad (3)$$

With equation 1b we see that if

$$x = o, \quad y = h, \quad \text{then } U = -1, \; V = 0$$

With $r_{spec} = 1$, the expression for the total charge becomes

$$2\,Q_{AB} = \frac{2hE_o\,\epsilon_o}{\pi}\left[1 + \frac{\pi b}{2h} + \operatorname{Ln}\left(1 + \frac{\pi b}{2h}\right)\right.$$

$$\left.(\epsilon_{spec} - 1)\operatorname{Ln}\left(\frac{1}{r_a}\right)\right]$$

$$= \frac{2hE_o\,\epsilon_o}{\pi}\left[1 + \frac{\pi b}{2h} + \operatorname{Ln}\left(1 + \frac{\pi b}{2h}\right)\right.$$

$$\left.(\epsilon_{spec} - 1)\left(\frac{\pi B}{2h} + 1\right)\right]$$

$$= \frac{2hE_o \epsilon_o}{\pi} \left[\left(1 + \frac{\pi b}{2h}\right) \epsilon_{spec} + \text{Ln} \left(1 + \frac{\pi b}{2h}\right) \right]$$

Now the capacitance per unit length, $C_a = 2Q_{AB} / (Q_2 - Q_1)$

The characteristic impedance of the loaded transmission line is then

$$Z_o = \frac{(\mu\epsilon)^{\frac{1}{2}}}{C_a} = \frac{(\mu\epsilon)^{\frac{1}{2}} (\phi_2 - \phi_1)}{\frac{2hE_o \epsilon_o}{\pi} \left[\left(1 + \frac{\pi b}{2h}\right) \epsilon_{spec} + \text{Ln} \left(1 + \frac{\pi b}{2h}\right) \right]}$$

$$Z_o = \frac{\pi (\mu\epsilon)^{\frac{1}{2}}}{2\epsilon_o} \cdot \Bigg/ \left[\left(1 + \frac{\pi b}{2h}\right) \epsilon_{spec} + \text{Ln} \left(1 + \frac{\pi b}{2h}\right) \right]$$

This is the required equation, expressing the loaded microstrip transmission line impedance in terms of the specimen and microstrip dimensions, and the complex specimen dielectric constant. It holds for the case where the specimen boundary lies along $r_{spec} = 1$.*

The final expression contains a bracket $(\mu\epsilon)^{\frac{1}{2}}$, the inverse of the velocity of the electromagnetic wave in this hetrogeneously loaded transmission line. This of course is unknown. However precisely this

---

* In fact an $r_{spec} = 0.368$ was found to provide a good "match" between the specimen boundary and the flux lines. The characteristic impedance is then slightly modified and substitution in equation 3 then yields

$$Z_o = \frac{\pi (\mu\epsilon)^{\frac{1}{2}}}{2\epsilon_o} \Bigg/ \left[1 + \frac{\pi b}{2h} \epsilon_{spec} + \text{Ln} \left(1 + \frac{\pi b}{2h}\right) \right]$$

this problem has been discussed[2] in the literature and a factor K is used to adjust the free space velocity c. Thus

$$\frac{1}{(\mu \epsilon)^{\frac{1}{2}}} = c\,K = c\,\sqrt{\frac{1}{\ell + \ell^2 (\epsilon_{speo} - 1)}}$$

where ℓ relates the hetrogeneous air/dielectric capacitances to the capacitances that would occur if the air were replaced with the substrate dielectric. The loaded transmission line impedance may now therefore be readily evaluated.

References

1. F. Assadourian and E. Rimai,

Proc. IRE, (1952), pp 1651 - 1657.

2. A. Schwartzmann,

Electronics, (Oct 2, 1967) pp. 109 - 112.